Electron Transfer in Ruthenium-Modified Recombinant Cytochromes and Myoglobins

A Thesis

Submitted by

Danilo Riguera Casimiro

In Partial Fulfillment of the Requirements

for the Degree of Doctor of Philosophy in Chemistry

Division of Chemistry and Chemical Engineering

California Institute of Technology

Pasadena, California

1994

September 17, 1993

to Joyce and our families

to my "lola" and "lolo"

Acknowledgements

My deepest thanks to ...

to Joyce and our families for their unending love and support;

to Harry and Jack for taking in this rather inexperienced foreign student and believing in him, for the stimulating discussions, for encouraging participation at numerous scientific meetings, and for the warmth and support they have extended during all the ups and downs in the past years ... You are the greatest!!

to Jay Winkler for those insightful discussions and for keeping science in the group as exciting and challenging as can be;

to I-Jy Chang for her assistance with the laser experiments, for placing our meal orders at every dimsum run, for introducing us to her wonderful family, and whose awakening voice never fails to transform the seemingly gloomy BI sub-basement into a "happening" place;

to Luet-lok Wong for being an excellent mentor and for hosting our stay at Oxford;

to Yi Lu, who has been very inspiring to watch and work with, and who has shown that there are still more to learn in molecular biology;

to Jorge Colón, Andreas Muheim, Mike Hill, Kara Bren, Robert Todd, and Frances Arnold for those very productive collaborations;

to Claire Slutter, Ralf Langen, Dave Long, Diane Hollenbaugh, Tom Chang, Yun Sun, Juris Germanas, Wonwha Cho, Clyde Rodriguez, Todd Richmond, Cindy Kiser, Neil Farrow, Mike Emerling, Phoebe Ray, and Herman Hesen for their long-standing friendship, the occasional Thursday lunches, and the company at third floor Braun;

to members of the Bio group, namely Gary Mines, Jack Mizoguchi, Morten Bjerrum, Zhong Huang, Torbjorn Pascher, Raymond Verhaert, Tim Karpishin, Mark McCleskey, Jeff Chang, Don Low, Deborah Wuttke, Jens Duus, and Mark Grinstaff for very stimulating discussions, the laughs, and the fun;

to the Gray group for sharing those moments in the lab, during our biweekly welcome/farewell parties, and during out-of-town trips;

to Max Bachrach for keeping the nanosecond laser system in excellent condition for my measurements and for retrieving at the last minute certain lost files that were critical to the preparation of this thesis;

to Steve Mayo, Bruce Bowler, and Judith Campbell for their valuable contributions during the initial stages of the cytochrome *c* project;

to Michael Smith for the gift of the cytochrome *c* expression system and Gary Brayer, Albert Berghuis, and Terence Lo for providing information on the crystal structures of the protein and various mutants;

to Steve Boxer, Wayne Hendrickson, and David Lambright for providing us the human myoglobin gene and information on the crystal structure of the protein;

to David Beratan, Jose Onuchic, Prabha Siddarth, and Rudy Marcus for the helpful insights on the mechanisms of biological ET;

to Thomas Sutherland for performing the large-scale fermentation runs at UCLA and to Lynn Williams, John Racs, and Keith Herman for the microchemical analyses;

to Alto Benedicto, Vicente Reyes, Jude Socrates, Marissa La Madrid, and that dynamic, charming pair, Tess and Belen, for their friendship and for keeping me "in touch" with what I left on the other end of the Pacific;

to Eva, Catherine, Cat, and Virginia for organizing such an elegant farewell party for me and Joyce (thanks too, Harry); and

to Paul Saltman for his help paving the way to a splendid post-doctoral position.

Abstract

The aim of the work described in Chapters 2-4 is to elucidate the role of the protein matrix in determining the distant electronic couplings for intramolecular electron-transfer (ET) reactions. The study focuses on two paradigmatic proteins - myoglobin, a non-ET molecule, and cytochrome *c*, a mitochondrial electron carrier. Site-directed mutants of human myoglobin were constructed each having a single surface histidine for ruthenium labeling. These histidines are at various distances from the heme center (9.5, His70; 12.7, His48; 15.5 Å, His83). Each mutant was derivatized with a pentaammineruthenium complex and the heme was substituted with a photoexcitable zinc mesoporphyrin. The rates of photoinduced and back ET between the histidine-bound Ru complex and the porphyrin were measured via a laser flash technique. The experimentally derived electronic couplings were found to decay exponentially with the intersite separation.

Three site-directed mutants (Glu66His, Glu66His/Tyr67Phe, and Leu58His) of yeast iso-1-cytochrome *c* were constructed in order to examine whether intervening aromatic side chains affect the rates of intramolecular ET to a significant extent. The crystal structure of the wild-type protein indicates that the ET pathways involve aromatic side chains - a bridging tryptophan at position 59 (in the case of His58) or a tyrosine at 67 (for His66). Incorporation of the Tyr67Phe mutation in the His66 mutant modifies the ET path in a well defined manner. The rates of intramolecular ET from the ferroheme to ruthenium polypyridine complexes bound to the surface histidines were measured using a laser flash-quench technique. Comparison of the experimentally derived donor-acceptor couplings with those of other previously studied cytochromes does not indicate any significant rate enhancement in the presence of bridging aromatic side chains.

Furthermore, the rates correlate reasonably well with the predictions of a σ-tunneling pathway model.

The electronic couplings in these myoglobins and cytochromes were analyzed in the context of current theoretical models. The data on cytochrome *c* strongly support the presence of specific routes for ET to and from the heme. In contrast, myoglobin provides a homogeneous barrier for ET. A comprehensive analysis of the data on both proteins, however, suggests that the apparent square-barrier nature of the polypeptide matrix of myoglobin is symptomatic of the presence of several competing pathways that effectively cause the electronic couplings to scale with direct intersite separations. These results suggest that more complex factors such as stereoelectronic effects and multiple pathways can contribute significantly to the coupling through a structurally heterogeneous medium such as that of a protein.

In Chapter 5, we have extended the use of a substitution-inert ruthenium polypyridine complex in introducing stabilizing intramolecular crosslinks in a protein. We found a dramatic increase in thermal stability of a yeast iso-1-cytochrome *c* mutant upon crosslinking two adjacent histidines (His39 and His58) on opposite strands of a β-sheet with bis(2,2'-bipyridine)ruthenium complex. The melting point of the Ru-modified cytochrome (72.8 °C) is 23.2 °C higher than that of the unmodified protein. Comparison with another Ru-modified di-histidine mutant suggests that the extent of the effect is largely dependent on the size of the loop generated by the crosslink. The technique should be readily applicable to stabilizing proteins with β-sheets.

Chapter 6 describes a novel strategy for the expression and purification of a recombinant, nonfunctional axial-ligand mutant of iso-1-cytochrome *c* (Met80→Ala) in *S. cerevisiae*. It involves coexpressing in the same plasmid (YEp213) the nonfunctional gene with a functional gene copy for complementation on a nonfermentable carbon medium. The functional gene encodes a product with an engineered metal-chelating site

(His39 and His58) that enables efficient separation of the two isoforms by immobilized metal-affinity chromatography. The purified Met80→Ala protein, which possesses a binding site for dioxygen and other exogenous ligands, was produced in quantities sufficient for extensive biophysical characterization. Absorption spectra of several derivatives of this mutant show striking similarities to those of the corresponding derivatives of horseradish peroxidase, myoglobin, and cytochrome P-450. The new method greatly expands the possible structural changes that can be incorporated into this paradigmatic protein.

Table of Contents

List of Figures

Chapter 4

Chapter 5

List of Tables

Chapter 1

Electron Transfer In Biological Systems

BACKGROUND

Electron-transfer (ET) reactions are key steps in numerous biological processes such as photosynthesis,[1,2] oxidative phosporylation,[3,4] metabolism,[5] and nitrogen fixation.[6] These reactions occur between redox-active centers (metal complexes or organic cofactors) that are physically bound within protein matrices. In most cases, the redox sites are sufficiently embedded in the protein that direct contact between the exchange partners is impossible; hence, ET has to occur over long distances (>10 Å) and across the polypeptide matrix. Despite the noncollisional distances that electrons have to transverse, ET reactions can be remarkably fast and proceed with high specificity. These properties of biological ET have fascinated theorists and experimentalists alike; it is not surprising therefore that our understanding of these processes has greatly advanced over the past decade.

The efficacies of the energy-harvesting apparatus inside the cell depend on the precise sequence of ET events between the redox components. Nature has cleverly devised ways of controlling these ET reactions in both temporal and spatial manner. One of the control mechanisms lies in placing redox centers in the order of their reduction potentials so that the flow is often downhill in free energy. Such design is evident in both the mitochondrial respiratory chain (Figure 1.1) and photosynthesis (Figure 1.2). In the mitochondrial ET chain,[3] electrons are transferred from nicotinamide adenine dinucleotide (NADH) or flavin adenine dinucleotide ($FADH_2$) to molecular oxygen (O_2) through a series of membrane-bound enzyme complexes (NADH-Q reductase, cytochrome reductase, cytochrome oxidase) linked by mobile electron carriers (ubiquinone, cytochrome *c*). This sequence of ET reactions results in an overall free energy release of 1.4 volts (53 kcal) that is utilized to drive ATP synthesis via a transmembrane proton-electrical gradient.[7]

In photosynthesis, a similar yet more complicated sequence of reactions is observed. The process depends on the interplay of two transmembrane assemblies, photosystems (PS) I and II. PSII, which consists of an oxygen-evolving center, a light-harvesting complex, and a reaction center, catalyzes the transfer of electrons from water to plastoquinone (Q).[8] Because the electrons in the reduced plastoquinone (QH_2) are at a higher potential than those in water, PSII utilizes the free energy of light to drive the reaction thermodynamically uphill. In particular, light is absorbed, creating both a strong oxidant and a strong reductant. The former drives the oxidation of water by the manganese cluster, while the latter initiates a series of ET events in the reaction center. As in the mitochondrial respiratory chain, ET to plastoquinone within the PSII reaction center is downhill in free energy. Two independent carriers (cytochrome *bf*, plastocyanin) mediate the transfer of electrons from PSII to PSI. As with PSII, PSI drives the thermodynamically uphill $NADP^+$-dependent ($NADP^+$ = nicotinamide adenine dinucleotide phosphate) oxidation of plastocyanin by harvesting light energy; the free energy of excited-state electron is subsequently relayed along a string of lower potential-energy states leading to the formation of NADPH.[9]

In both the mitochondrial electron-transport chain and photosynthesis, electrons are transferred down a series of carriers for which the potentials between exchange partners do not differ significantly. This is essential in order for the overall free energy change to be efficiently converted to work and not dissipated as heat. How does nature preserve this delicate stepwise flow of electrons and prevent the transfer from occurring directly from the high-potential state to the final low-potential state? The known structures of bacterial reaction centers (RC) from *Rhodopseudomonas viridis*[1] and *Rhodobacter sphaeroides*,[10,11] considered homologous to that in PSII, provide a clue as to how directional ET is achieved. The redox centers are assembled at fixed positions within the RC such that the sequence of intramolecular ET reactions[12-14] ($BChl_2$ dimer $\rightarrow$

$BChl_A \rightarrow BPh_A \rightarrow Q_A \rightarrow Q_B$) parallels the organization of these redox centers along the length of the molecule (Figure 1.3). This vectorial arrangement ascertains that (1) ET from initial charge-separated species $BChl_2^+BChl_A^-$ occurs exclusively to BPh_A and not to Q_A and (2) Q_A^- reduces Q_B instead of unproductively reacting with the more distant and weakly coupled $BChl_2^+$ dimer. While the reactions in RC are clearly intramolecular, a large number of biological ET reactions involve two redox centers that must undergo diffusional collision (e.g., cytochrome *c*-cytochrome *c* oxidase, cytochrome *bf*-plastocyanin, cytochrome *c* reductase-cytochrome *c*). For such reactions, the direction of electron flow is determined by the specificity of the interactions between redox partners.[15] Complementarity between protein surfaces (in terms of contour and charges) provides a higher probability of ET than that arising from mere random collisions.

In summary, the combination of tuning the reaction driving force, long-range couplings between donor (D) and acceptor (A) sites, and factors that dictate molecular recognition appears to ensure that a "reaction occurs at the right time and place."

OVERVIEW OF ELECTRON-TRANSFER THEORY

Electron transfer in proteins may be classified as either intramolecular or intermolecular. In the latter, a diffusion event is first invoked leading to the formation of the precursor complex. Electron transfer occurs within this complex followed by product dissociation. Scheme 1 describes this overall process;

Scheme I

$$D + A \underset{}{\overset{K_p}{\rightleftharpoons}} D/A \xrightarrow{k_{ET}} D^+/A^- \underset{K_s}{\rightleftharpoons} D^+ + A^-$$

K_p and K_s are the formation constants for the precursor and successor complexes, respectively, whereas k_{ET} is the rate constant for ET within the complex. The rate of

intramolecular ET will depend only on those factors that influence k_{ET}. Intermolecular reactions however are controlled by factors that determine formation of the precursor complex. Thus, diffusion rates (either in two or three dimensions) and electrostatic effects will contribute to the overall ET rate in intermolecular reactions. There are several excellent reviews that discuss these effects on selected protein-protein ET reactions.[20,21]

The factors that affect k_{ET} were presented by Rudolph Marcus in an elegantly simple quantitative model, very much known today as the Marcus theory.[22] For this, the Royal Swedish Academy of Science has bestowed Professor Marcus the 1992 Nobel Prize in Chemistry.[23] Consider a unimolecular $D/A \rightarrow D^+/A^-$ conversion for which $-\Delta G^o = 0$; the free energy profile in a one-dimensional reaction coordinate is shown in Figure 1.4. Curve R represents the potential energy of the reactant state D/A and curve P corresponds to that of the product D^+/A^-. Transition-state theory suggests that for ET to occur, the reactant state must distort along the reaction coordinate from its equilibrium position **a** to position **b**, the transition state. ET occurs at this point and the system can then relax to equilibrium product position **c**.

The classical Marcus theory predicts that the first-order rate constant for ET between a donor and acceptor site can be partitioned into a product of three terms: a frequency factor (ν_N), an electronic factor (κ_{EL}), and a nuclear term (κ_N).

$$k_{ET} = \nu_N \kappa_{EL} \kappa_N \qquad (1)$$

ν_N reflects the frequency of nuclear passage through the transition state. The electronic factor (κ_{EL}) depends on the coupling strength between the initial and final states. When this coupling is strong ($\kappa_{EL} = 1$), ET occurs every time the system passes through the transition state and the reaction is said to be adiabatic. When this coupling is weak ($\kappa_{EL} << 1$) or in case of a nonadiabatic reaction, the transition state must be reached several

times before ET can occur; under this condition, the k_{ET} becomes independent of the nuclear frequency and $\kappa_{EL}\nu_N$ term approaches the electron-hopping frequency at the transition state (ν_{EL}). ν_{EL} is a function of the the electronic coupling matrix element H_{AB} and the reorganization energy λ (eq 2).

$$\nu_{EL} = \frac{2H_{AB}^2}{h}\left(\frac{\pi^3}{\lambda kT}\right)^{1/2} \qquad (2)$$

In Figure 1.4, H_{AB} measures the energy gap between the mixed and split potential energy curves and λ is defined as the free energy required for isoergonic ET reaction ($\Delta G^o = 0$) to occur without initial displacement from the reactants' equilibrium configuration [a].

The nuclear term (κ_N) is a measure of the activation barrier ΔG^*, the free energy difference between the reactant equilibrium state and the transition state (eq 3). The activation energy involves an interplay of the reaction free energy (ΔG^o) and the reorganization free energy (eq 4).

$$\kappa_N = \exp(-\Delta G^*/kT) \qquad (3)$$

$$\Delta G^* = \frac{(\Delta G^o + \lambda)^2}{4\lambda} \qquad (4)$$

Figure 1.5 illustrates the effect of varying the reaction free energy on the activation energy for ET. For an isoergonic reaction ($\Delta G^o = 0$), it follows from the properties of the parabola that $\Delta G^* = \lambda/4$. As the reaction driving force increases, the energy barrier is reduced and k_{ET} increases accordingly. At the point $-\Delta G^o = \lambda$, the barrier for ET disappears and the reaction rate is said to have reach its maximum or activationless value (k_{max}). As the reaction becomes ever more exothermic, the intersection point of the R and P surfaces moves to the left of reactant equilibrium configuration, thereby resulting in the development of an energy barrier. Thus, k_{ET} decreases as the $-\Delta G^o$ exceeds λ in what has been regarded as the Marcus inverted effect. This classical view predicts a gaussian

behavior of log k_{ET} vs. $-\Delta G^{o}$ (Figure 1.6, curve a). The breath of the gaussian is proportional to the $(2\lambda kT)^{1/2}$, where kT is the Boltzmann thermal energy. But when the effective frequency (ω) of the oscillators is large and $h\omega/2\pi$ is greater than kT, a quantum correction must be introduced. Under these conditions, nuclear tunneling from the lowest vibrational R state to the P surface is quite significant; according to Siders and Marcus,[24] the falloff in k_{ET} in the inverted region becomes approximately linear in $-\Delta G^{o}$ rather than quadratic and hence, is less dramatic (Figure 1.6, curves b-d).

To summarize, the classical Marcus theory predicts that the rate constant for the non-adiabatic ET reaction is expressed as the following (eq 5):

$$k_{ET} = \left\{ \frac{4\pi^3}{h^2 \lambda kT} \right\}^{1/2} (H_{AB})^2 \exp\left\{ \frac{-(\Delta G^{o} + \lambda)^2}{4\lambda kT} \right\} \qquad (5)$$

The point at which a reaction is to be classified as adiabatic or nonadiabatic varies with the system. However, Newton and Sutin[25] indicate that for typical transition-metal redox reactions, the demarcation point is $H_{AB} \sim 0.25$ eV (200 cm^{-1}).

ET REACTIONS IN SYNTHETIC D-A MOLECULES

Nuclear and Electronic Control

A great deal of our understanding of long-range ET was established through studies of exchange reactions in synthetic, low-molecular-weight D-A systems; such studies were in fact the first to demonstrate the validity of the Marcus theory. The first observations of the inverted region were made in 1984 by Miller and coworkers on intermolecular charge-shift reactions between the biphenyl radical anion and various acceptors in a rigid low-temperature glass[26] as well as on intramolecular ET reactions in biphenyl-acceptor couples separated by hydrocarbon linkage.[27] Since then, evidences for inverted region have been reported in numerous other systems: Ir dimer-pyridinium

couples,[28] geminate radical ion pairs,[29-32] and porphyrins capped with organic acceptors.[33] Most of these cases warrant a quantum-mechanical interpretation of the inverted effect.

Other factors that may contribute to the nuclear term have also been examined in considerable detail. The role of solvent reorganization in limiting k_{ET} for strongly coupled systems has been treated both theoretically[34-36] and experimentally.[37] Analyses of metal-metal charge transitions in polyene-bridged mixed-valence complexes[38] and thermal ET reactions in oligoproline-bridged Os^{2+}-Ru^{3+} couples[39] have raised the possible dependence of κ_N on the intersite distances.

Studies of bridged D-A systems have provided some fundamental insights into the effect of the electronic couplings on the first-order rate of intramolecular ET. Quantitative analyses of the distance dependence of k_{ET} were made possible using rigid D-A complexes wherein the linker length was systematically varied. They include porphyrin-quinone couples separated with spirocyclobutane[40] (**1**) or phenyl-bicyclooctane fragments[41] (**2**), biphenyl-acceptor couples with steroid and fused ring systems[42] (**3**), and dimethoxynaphthalene-dicyanoethylene systems with rigid, nonconjugate ring spacers[43] (**4**). Results from these studies agree that ET rates drop monotonically with increasing length of the linker. A simple quantitative model to accomodate these observations assumes that the medium is a homogenous barrier and as such, the rate should drop exponentially with distance (eq 6).

$$H_{AB} = H_{AB}^{o} \exp \{-\beta/2 (d - d_o)\} \qquad (6)$$

The data on systems **1-4** correlate well with the predictions of this model and values for β of 0.85-0.95 $Å^{-1}$ have been derived.

Another plausible mechanism by which electron tunnels through the intervening medium makes use of the wavefunction of the spacer itself to propagate the DA

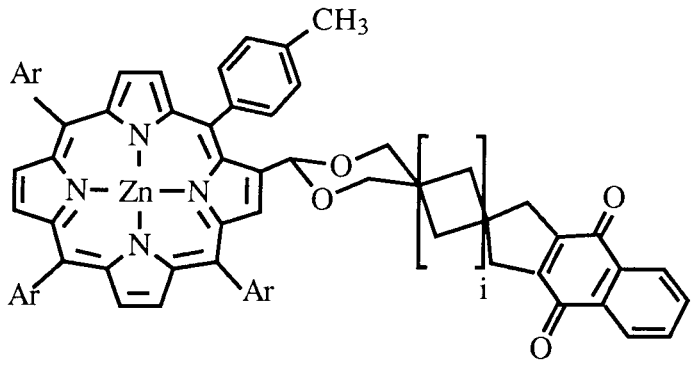

1

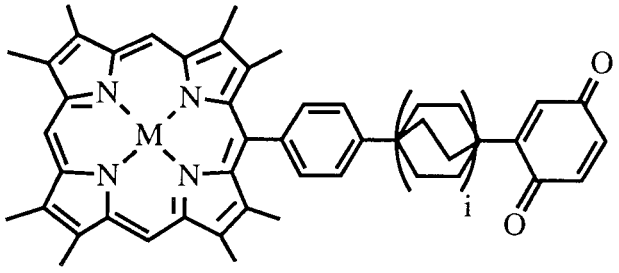

2

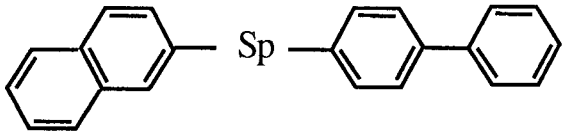

3

Sp =

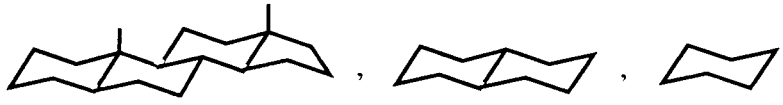

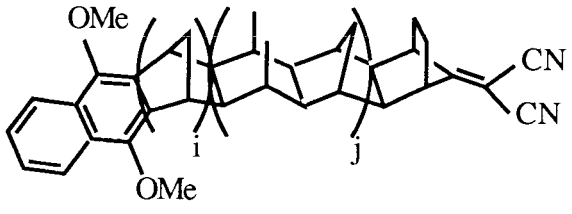

4

interaction.[44-46] The simplest interpretation of this model assumes that the electronic contributions from each of the bonds in the intervening medium are equivalent and as such, the D-A electronic coupling decays exponentially with increasing number of bonds (n) in the spacer. On the basis of this argument, eq 6 can be reformulated into eq 7,

$$H_{AB} = H_{AB}^{o} \exp\{-\beta' n/2\} \quad (7)$$

where β' is the electronic transmission coefficient per covalent bond. Data for **1-4** can be reasonably described by eq 7 with β' = 0.8 to 0.9 $Å^{-1}$. Since the number of bonds in these synthetic D-A systems parallel the distance that separates the donor and acceptor moieties, their studies generally do not allow us to distinguish between through-bond and through-space mechanism.

Perhaps the only direct evidence for through-bond ET mechanism arises from comparison of rates in stereoisomeric decalin-bridged biphenyl-naphthalene molecules (**5** and **6**) having the same number of bonds yet different intersite distances.[47] The center-to-center distances in **5** and **6** are 12.5 and 6.5 Å, respectively, yet the ET rates are almost the same (58, **5**, vs. 63 s^{-1}, **6**).

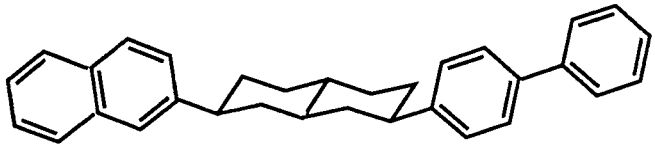

5

6

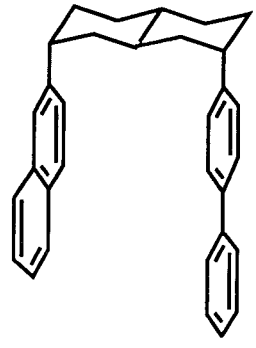

Biomimetic D-A Systems

Intense interest in protein-mediated ET has stimulated numerous kinetic studies of D-A systems with peptide spacers. The groups of Klapper[48] and Meyer[49] have investigated the reactions in polypeptide-bridged organic radicals and transition-metal complexes, respectively, but the most prominent biomimetic molecules are those that utilize oligoproline spacers. While most other polypeptide spacers assume very little structure in solution, polyprolines are unique in that they can adopt a rigid extended (all *trans*) or a left-handed helical (all *cis*) structure depending on the solvent polarity and chain length;[50] such property makes them very appropriate for studies of long-range ET. Isied and coworkers have studied the high-driving-force $Ru^{1+} \rightarrow Co^{3+}$ ET across $(proline)_n$ spacers (n = 1-6); the first-order rate constants were consistent with helical formation at n

≥ 4.[51] While considerable efforts are recently directed at constructing D-A systems based on supramolecular assemblies (e.g., helix bundles[52,53]), it is still apparent that synthetic D-A systems cannot adequately cover the multitude of structural elements that characterize the larger biological counterparts.

ET REACTIONS IN METALLOPROTEINS

Metalloprotein Systems

One of the earliest evidences that long-range ET can occur across a protein medium was provided in 1982 by Gray and coworkers in a flash photolysis experiment involving the intramolecular reduction of cytochrome *c* heme by a covalently bound pentaaminеruthenium(II) complex at His33 *ca.* 11 Å away (Figure 1.7).[54] The reaction has a $-\Delta G^{o}$ of *ca.* 180 mV and a rate constant of 30 s^{-1}. Since then, Ru-ammine derivatives of other naturally occurring metalloproteins (e.g., blue copper proteins,[55-57] iron-sulfur proteins,[58] heme proteins[59-61]) have been prepared and ET reactions at distances as far as 13 Å have been observed. These experiments rely on a bimolecular induction step: the electron is injected or removed from the D-A complex via a bimolecular reaction with a photolytically or radiolytically generated reductant or oxidant. A small fraction of the D^{+}/A^{-} species is usually formed, and the system relaxes to the thermodynamically stable D/A state. These schemes however suffer from the low exergonicity of the intracomplex reactions involved, which often required low protein concentrations to avoid intercomplex ET and hence reduce the signal size. With heme proteins, the problem is partially reconciled by using photoexcitable, metal-substituted porphyrins (e.g., Zn, Mg, Pt, Pd, Cd);[62,63] the enhanced exergonicity of the reactions to and from the surface Ru sites has extended the upper limit of D-A distances for which k_{ET} is measurable to as far as 20 Å.

Recent work has however revolutionized the manner in which long-range ET in proteins are studied. Our group and those of Millett and Durham have adopted a general approach wherein photoexcitable Ru complexes are used instead as secondary redox sites on the surface of a metalloprotein. The approach provides reaction driving forces comparable to those with luminescent porphyrins, but has the advantage of retaining the native metal center of the protein. As such, it is applicable to nearly all classes of proteins. Millett, Durham, and coworkers have functionalized surface cysteine[64,65] (**7**) and lysine residues[66] (**8**) of several hemeproteins with tris(bipyridine)ruthenium complexes. Our group has reported the intramolecular oxidation of horse heart cytochrome *c* by a bis(bipyridine)imidazoleruthenium complex (**9**) attached to a surface histidine.[67] In terms of selectivity, histidines and cysteines are particularly attractive targets because of their low occurrence on most proteins. The reactions are typically initiated via laser excitation to generate a strong Ru^{2+*} reductant. In the case of an oxidized protein, direct ET to the protein center can occur, followed by a thermal back reaction. The latter can be blocked by filling the hole in the surface Ru with a reductive quencher (e.g., aniline). In an alternative scheme involving reduced proteins, the Ru^{2+*} state can be oxidized with an exogenous quencher, creating a hole on the surface Ru that is then filled by ET from the protein center. A comprehensive review of ET reactions in ruthenium-modified metalloproteins was published recently by Winkler and Gray.[68]

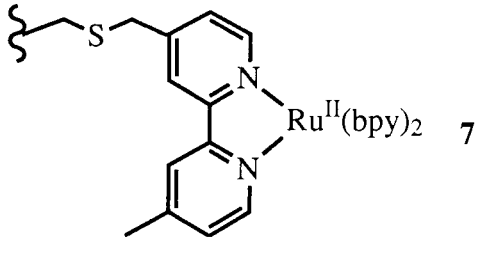

7

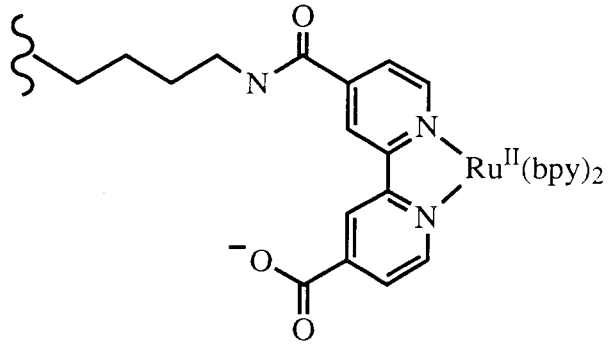

8

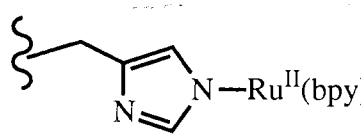

9

Two other classes of biological ET reactions have attracted tremendous attention in the last few years. A tier above in complexity to small molecule-protein complexes are the intramolecular exchange reactions in multisite proteins. Examples include photoinitiated reactions in metal-substituted hemoglobins[69] and the bacterial reaction centers,[1,10-17] and the reduction of blue-copper site in azurin by an artificially generated protein radical (RSSR$^{\bullet}$).[70] The next class of redox reactions involves those between weakly interacting metalloproteins capable of forming stable transient complexes. The most widely characterized set of reactions comprise those of cytochrome *c* with its physiological (e.g., cytochrome *c* peroxidase,[64,71,72] cytochrome *c* oxidase,[73,74] cytochrome b_2,[75,76] cytochrome *c* reductase[77,78]) as well as nonphysiological partners (e.g., plastocyanin,[79,80] cytochrome b_5[81-86]). The advent of ultra-fast kinetic techniques has spurred the development of methods that allow us to monitor the reaction far beyond the diffusional limit and extract the microscopic first-order ET rate constant (k_{ET}) in the preformed complex. The kinetic schemes utilized thus far rely on rapid *in situ* generation (either photochemically or by pulse-radiolysis) of a powerful reductant, which can either be the donor protein (e.g., metal-substituted heme proteins),[71,82] an exogenous reagent (e.g., excited-state porphyrins,[73] organic radicals,[74,80,83,85] hydrated electrons[82]), or an artificial redox tag (e.g., ruthenium polypyridine complexes)[64,72,84] on the surface of the donor protein. The reductant either transfers an electron(s) directly to the acceptor protein (i.e., when metal-substituted heme proteins are employed) or to the donor half of the complex (i.e., in the case of exogenous or covalently bound reagents), that subsequently reduces the other protein. Generally, the observed redox kinetics are partitioned into a first-order component arising from ET within specific complexes

present at the instance the reductant is produced, and a concentration-dependent component arising from typical Stern-Volmer quenching. It is interesting that intracomplex ET proceeds at rates (10^4-10^5 s^{-1}) several orders of magnitude above the diffusional limit. This raises the possible existence of an optimal interaction configuration that provides an efficient path for ET between the two metal centers.

Nuclear and Electronic Control

While numerous studies have shown that k_{ET} increases with the exergonicity of the reaction, there have been only two observations of the inverted Marcus behavior in metalloprotein-mediated ET reactions. McLendon and coworkers have measured the ET rates in cytochrome *c*-cytochrome b_5 complexes with native as well as metal-substituted cytochrome b_5 and found that the rates begin to decline at driving forces beyond 0.8 eV (λ).[83] Durham and coworkers have examined the intramolecular photoinduced ET and thermal recombinations rates in cytochrome b_5 functionalized at a genetically engineered surface cysteine with different tris(bipyridine)ruthenium complexes.[65] Their studies show that the more exergonic thermal back reactions are highly inverted, whereas the rates of the excited-state ET reactions lie on the normal region. In both cases, the experimentally derived λs roughly approximate those predicted by the Marcus cross relation from the individual self-exchange kinetics.[22,87]

Analysis of the nuclear control in an extensive number of biological ET reactions has revealed certain distinguishing properties of different classes of proteins. It has been suggested that electron-carrier proteins differ from non-ET proteins in the ability of the former to minimize the nuclear reorganization energy. For example, a majority of the cytochromes (*c*- and *b*-type) retain the same spin state at different oxidation states and do not undergo any ligand exchange reactions with redox change. Single-site λ of 0.3 to 0.6 eV have been estimated for these proteins from self-exchange measurements as well as intramolecular ET measurements.[87] Even more impressive are the first three reactions in

the photosynthetic reaction center, whose λs are between 0.3-0.5 eV.[88] In contrast, myoglobin, a non-ET protein, undergoes ligand displacement upon heme reduction (high-spin Fe^{3+}-H_2O to five-coordinate, high spin Fe^{2+}).[89] The rates at which the protein is reduced (either in a self-exchange reaction, by exogenous reagents, or by covalently bound redox group) are greatly accelerated when ligand binding is blocked by derivatizing the distal histidine with cyanogen bromide (i.e., five-coordinate Fe^{2+} and Fe^{3+} forms); the rate increase is partially accounted for by a 0.2 eV drop in reorganization energy.[59c,68,90]

Metalloprotein ET presents a far more complicated problem when dealing with the intersite electronic coupling. This is largely due to the structural intricacies of the protein medium. It is not surprising that the electronic control in biological ET remains to be the subject of intense debate; the issue of through-space vs. through-bond mechanism has drawn considerable attention in the last few years. In a detailed account, Dutton and coworkers[88,91] have examined ET reactions in systems such as the photosynthetic reaction center and chemically modified proteins, and suggested that the activationless rates correlate with a homogeneous-decay model, where $\beta = 1.4$ Å^{-1} and an adiabatic rate limit of 10^{13} s^{-1} (d = 3Å). However, the authors noted that β for synthetic, low-molecular-weight D-A systems is significantly lower (0.9 Å^{-1}), indicating that a covalent bridge provides a far better electron-tunneling medium than a protein matrix.

The faster decay-with-distance of k_{max} in protein-mediated ET processes relative to that with covalent systems is symptomatic of more tortuous ET paths than what the through-space intersite distances normally predict. Several experiments have however eliminated the possibility of a purely covalent ET route along the polypeptide chain.[68,92] Beratan and Onuchic have proposed that electrons can tunnel through noncovalent interactions such as hydrogen bonds and van der Waals contact, although less efficiently than through σ bonds.[93] The ability of hydrogen bonds to mediate ET has been

demonstrated in small ET systems consisting of weakly interacting donor and acceptor groups (**10**[94] and **11**[95]). These studies indicate that hydrogen-bonded ET pathways can

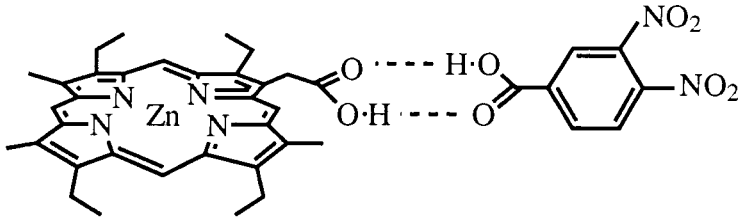

10

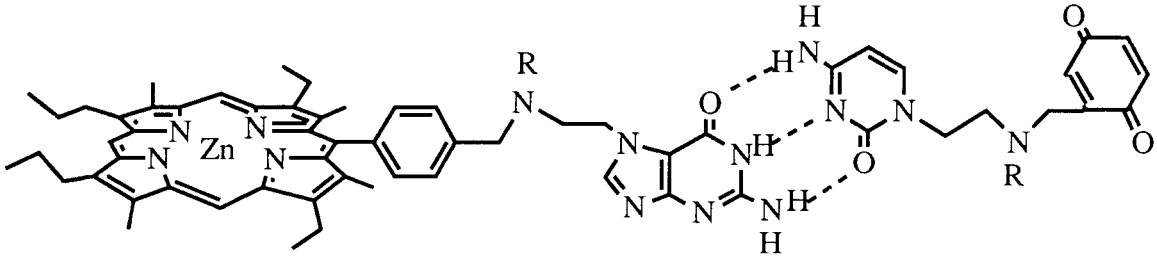

11

be competitive to covalent routes. Other theoretical approaches to the problem of distant electronic couplings in proteins have been reported. Siddarth and Marcus have utilized an artificial-intelligence procedure to search for the relevant amino acids in the bridge and from these fragments, determined the electronic coupling matrix element using extended Hückel calculations.[96] Gruschus and Kuki have developed an *inhomogeneous aperiodic lattice* theory for calculating the electronic coupling matrix using experimental ionization potentials.[97]

The ET reactions in four different bis(2,2-bipyridine)imidazoleruthenium(II) derivatives of cytochrome *c*[98] (His72 and His33 of horse heart protein, His39 of *Candida krusei* protein, and His62 of yeast iso-1-cytochrome *c*) have been investigated and the calculated activationless rates were found to correlate well with the predictions of the σ-tunneling model of Beratan and Onuchic than a homogenous barrier formalism. Considerable agreement was also reported with the predictions of Gruschus-Kuki and Siddarth-Marcus models.

There are still several important questions that need to be addressed regarding how the protein affects the distant electronic couplings for ET. For example, can electron tunneling occur through π-conjugated systems of aromatic residues and if so, how does this affect the rates of exchange? How do defined structural features such as β-strands and helices influence the D-A couplings? Significant differences in electronic transmission properties of these secondary structures have been proposed[93b] but a direct, systematic investigation of the matter has not yet been carried out. Aside from the nuclear control, do ET and non-ET proteins differ in their abilities to modulate the electronic couplings to the native metal centers?

Brief Overview of the Thesis Projects

In the succeeding chapter, studies of intramolecular ET reactions in ruthenium-modified site-directed mutants of myoglobins aimed at understanding the manner in which this highly α-helical protein modulate the electronic couplings to the metal center will be presented. In these experiments, the heme in each myoglobin is replaced with luminescent porphyrins and photoinitiated ET reactions with surface Ru-ammine sites are examined. Metal-substituted porphyrins were chosen to avoid certain complications associated with the native iron site. It is general knowledge that reduction of the metmyoglobin leads to dissociation of the bound water ligand; the reverse reaction is accompanied by water ligation. The question of whether ET and ligand exchange proceed in a concerted or stepwise fashion remains unsettled. However, recent electrochemical[99] and low-temperature spectroscopic studies[100] of horse myoglobin have suggested that the initial product of metmyoglobin reduction is a low-spin Fe^{2+}-H_2O species and the ligand dissociates at a very slow rate (~1 s^{-1} at ambient temperature). Scheme II outlines how such reduction/ligand dissociation and oxidation/ligand complexation processes (solid arrows for two-step mechanism, dashed arrows for the

concerted processes) may influence the intramolecular ET kinetics to and from a photoexcitable ruthenium tag.

Scheme II

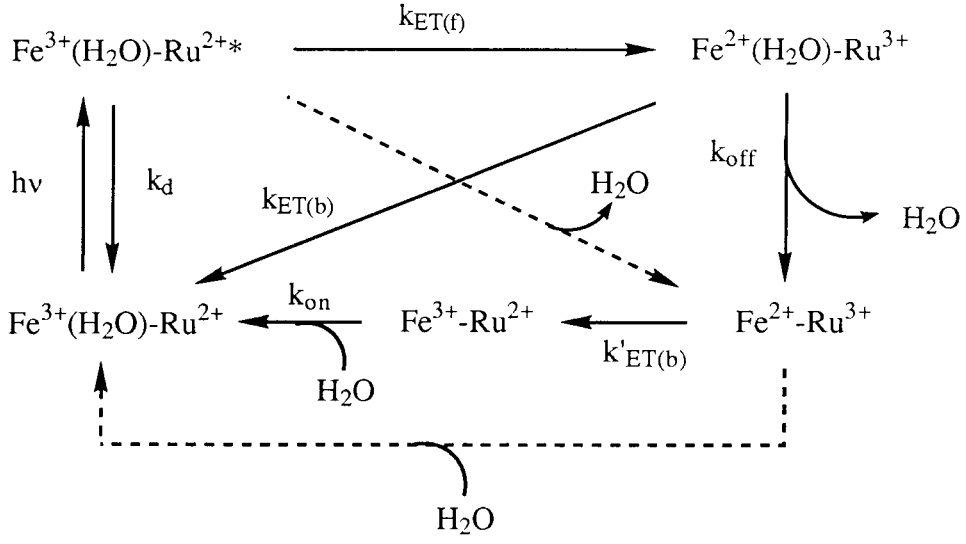

For a strongly coupled Ru-heme system, the forward and back ET can proceed without dissociation of the bound water ($k_{ET(b)} >> k_{off}$); unfortunately, very little is known regarding the nuclear activation parameters of such reactions, thereby complicating the extraction of intersite electronic couplings. In contrast, the kinetic scheme is greatly simplified when a closed-shell metal porphyrin is used (Scheme III).

Scheme III

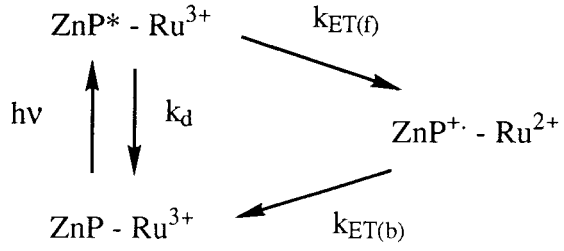

It should be pointed out that we do not undermine the significance of this ligand binding/rebinding process in native myoglobin. In fact, the protein may well be the best model system for understanding such ET-coupled processes; a rapid electron-injection

system such as that afforded by covalent attachment of photoexcitable ruthenium complexes should permit both detection and characterization of the transient species involved.

In Chapter 3, we address one of the oldest questions in biological ET - does the presence of intervening aromatic residues enhance the rates of ET between a donor and an acceptor site? Site-directed variants of yeast iso-1-cytochrome *c* were constructed where, in each case, a histidine was incorporated at a surface position for which the bridging medium to the heme contains an aromatic side chain. The surface histidines were modified with photoexcitable ruthenium polypyridine complexes and the $Fe^{2+} \rightarrow Ru^{3+}$ ET reactions were monitored following a laser flash-quench technique. The experimentally derived Ru-heme couplings are compared to those of other previously studied Ru-modified cytochromes for which the intervening media are largely aliphatic in composition. In Chapter 4, the results on the myoglobin and cytochrome *c* systems are analyzed in the context of current electron-tunneling models.

In Chapter 5, I digress from the mainstream of the previous chapters and present results from our recent efforts in collaboration with Professor Frances H. Arnold and her group to develop general strategies for stabilizing the folded structure of proteins. For the first time, we show that modification of genetically engineered metal-chelating sites with substitution-inert Ru complexes can introduce stabilizing covalent crosslinks on the surface of a protein (in this case, yeast iso-1-cytochrome *c*). The approach is far more promising than most other covalent crosslinking techniques, owing to such factors as inertness of the crosslink to reducing conditions and low stringency of design requirements.

Chapter 6 discusses the development of an gene expression strategy for generating axial-ligand mutants of yeast iso-1-cytochrome *c*. Prior to this work, ligand mutagenesis of Class I cytochromes *c* has only been possible through semisynthetic techniques;

previous expression systems prohibit alteration of the ligands because of the requirement of *in vivo* function. Our approach combines the use of a dual-gene plasmid and metal-affinity separation; its utility is demonstrated by expressing a novel ligand-binding mutant (Met80Ala) of cytochrome *c*. The methodology provides the opportunity of employing this paradigmatic protein as a mimetic tool to understand numerous heme-mediated processes of key biological significance (e.g., oxygen activation).

REFERENCES

1. Deisenhofer, J.; Epp, O.; Miki, K.; Huber, R.; Michel, H. *Nature* **1985**, *318*, 618.
2. Blankenship, R. E.; Prince, R. C. *Trends Biochem. Sci.* **1985**, *10*, 383.
3. Hatefi, Y. *Annu. Rev. Biochem.* **1985**, *54*, 1015.
4. Wikstrom, M.; Saraste, M. *Bioenergetics*; Ernster, L., Ed.; Elsevier: New York, 1984; pp. 49-94.
5. Numa, S., Ed. *Fatty Acid Metabolism and Its Regulation*; Elsevier: New York, 1984.
6. (a) Kim, J. S.; Rees, D. C. *Nature* **1992**, *360*, 553. (b) Kim, J. S.; Rees, D. C. *Science* **1992**, *257*, 1677. (c) Georgiadis, M. M.; Komiya, H.; Chakrabarti, P.; Woo, D. Kornuc, J. J.; Rees, D. C. *Science* **1992**, *257*, 1653.
7. Mitchell, P. *Science* **1979**, *206*, 1148.
8. Holzenburg, A.; Bewley, M. C.; Wilson, F. H.; Nicholson, W. V.; Ford, R. C. *Nature* **1993**, *363*, 470.
9. (a) Krauss, H. *et al. Nature* **1993**, *361*, 326. (b) Boettcher, B.; Graber, P.; Boekema, E. J. *Biochim. Biophys. Acta* **1992**, *1100*, 125.
10. (a) Allen, J. P.; Feher, G.; Yeates, T. O.; Rees, D. C.; Deisenhofer, J.; Michel, H.; Huber, R. *Proc. Natl. Acad. Sci. USA* **1986**, *83*, 8589. (b) Allen, J. P.; Feher, G.; Yeates, T. O.; Komiya, H.; Rees, D. C. *Proc. Natl. Acad. Sci. USA* **1987**, 84, 5730. (c) Allen, J. P.; Feher, G.; Yeates, T. O.; Komiya, H.; Rees, D. C. *Proc. Natl. Acad. Sci. USA* **1987**, 84, 6162. (d) Yeates, T. O.; Komiya, H.; Rees, D. C.; Allen, J. P.; Feher, G. *Proc. Natl. Acad. Sci. USA* **1987**, 84, 6438. (e) Yeates, T. O.; Komiya, H.; Chirino, A.; Rees, D. C.; Allen, J. P.; Feher, G. *Proc. Natl. Acad. Sci. USA* **1987**, 84, 6438. (f) Allen, J. P.; Feher, G.; Yeates, T. O.; Komiya, H.; Rees, D. C. *Proc. Natl. Acad. Sci. USA* **1988**, 85, 8487. (g) Komiya, H.; Yeates, T. O.; Rees, D. C.; Allen, J. P.; Feher, G. *Proc. Natl. Acad. Sci. USA* **1988**, 85, 9012.

11. (a) Chang, C.-H.; Schiffer, M.; Tiede, D.; Smith, U.; Norris, J. *J. Mol. Biol.* **1985**, *186*, 201. (b) Chang, C.-H.; Tiede, D.; Tang, J.; Smith, U.; Norris, J.; Schiffer, M. *FEBS Lett.* **1986**, *205*, 82.

12. (a) Holzapfel, W.; Finkele, U.; Kaiser, W.; Oesterhelt, D.; Scheer, H.; Stilz, H. U.; Zinth, W. *Chem. Phys. Lett.* **1989**, *160*, 1. (b) Holzapfel, W.; Finkele, U.; Kaiser, W.; Oesterhelt, D.; Scheer, H.; Stilz, H. U.; Zinth, W. *Proc. Natl. Acad. Sci. USA* **1990**, *87*, 5168.

13. Kirmaier, C.; Holten, D. *Photosynth. Res.* **1987**, *13*, 225.

14. Feher, G.; Allen, J. P.; Okamura, M. Y.; Rees, D. C. *Nature* **1989**, *339*, 111.

15. Shopes, R. J.; Wraight, C. A. *Biochim. Biophys. Acta* **1985**, *806*, 348.

16. Gunner, M. R.; Dutton, P. L. *J. Am. Chem. Soc.* **1989**, *111*, 3400.

17. Takahashi, E.; Wraight, C. A. *FEBS Lett.* **1991**, *283*, 140.

18. Pelletier, H.; Kraut, J. *Science* **1992**, *258*, 1748.

19. Chen, Y. L. *et al. Biochemistry* **1992**, *31*, 4959.

20. McLendon, G.; Hake, R. *Chem. Rev.* **1992**, *92*, 481.

21. Kostic, N. *Metal Ions in Biological Systems*; Sigel, H., Ed.; M. Dekker: New York, 1990; Vol. 27, pp. 129-182.

22. Marcus, R. A.; Sutin, N. *Biochim. Biophys. Acta* **1985**, *811*, 265.

23. Marcus, R. A. *Angew. Chem.* **1993**, *32*, 1111.

24. Siders, P.; Marcus, R. A. *J. Am. Chem. Soc.* **1981**, *103*, 748.

25. Newton, M. D.; Sutin, N. *Annu. Rev. Phys. Chem.* **1984**, *35*, 437.

26. Miller, J. R.; Beitz, J. V.; Hudelston, R. K. *J. Am. Chem. Soc.* **1984**, *106*, 5057.

27. Miller, J. R.; Calcaterra, L. T.; Closs, G. L. *J. Am. Chem. Soc.* **1984**, *106*, 3047.

28. (a) McCleskey, T. M.; Winkler, J. R.; Gray, H. B. *J. Am. Chem. Soc.* **1992**, *114*, 6935. (b) Fox, L. S.; Kozik, M.; Winkler, J. R.; Gray, H. B. *Science* **1990**, *247*, 1069.

29. Gould, I. R.; Ege, D.; Mattes, S. L.; Farid, S. *J. Am. Chem. Soc.* **1987**, *109*, 3794.

30. Vauthey, E.; Suppan, P.; Haselbach, E. *Helv. Chim. Acta* **1988**, *71*, 93.

31. Levin, P. P.; Pluzhnikov, P. F.; Kuzmin, V. A. *Chem. Phys. Lett.* **1988**, *147*, 283.

32. Ohno, T.; Yoshimura, A.; Mataga, N. *J. Phys. Chem.* **1986**, *90*, 3295.

33. Irvine, M. P.; Harrison, R. J.; Beddard, G. S.; Leighton, P.; Sanders, J. K. M. *Chem. Phys.* **1986**, *104*, 315.

34. Zusman, L. D. *Chem. Phys.* **1980**, *49*, 295.

35. Calef, D. F.; Wolynes, P. G. *J. Phys. Chem.* **1983**, *87*, 3387.

36. Sumi, H.; Marcus, R. A. *J. Chem. Phys.* **1986**, *84*, 4894.

37. Barbara, P. F.; Walker, G. C.; Smith, T. P. *Science* **1992**, *256*, 975.

38. Sutin, N. *Advances in Chemistry Series*; Bolton, J. R., Mataga, N., McLendon, G., Eds.; American Chemical Society:Washington, DC, 1991; Vol. 228, pp. 25-44.

39. Isied, S. S.; Vassilian, A.; Wishart, J. F.; Creutz, C.; Schwarz, H. A.; Sutin, N. *J. Am. Chem. Soc.* **1988**, *110*, 635.

40. Knapp, S.; Dhar, T. G. M.; Albaneze, J.; Gentemann, S.; Potenza, J. A.; Holten, D.; Schugar, H. J. *J. Am. Chem. Soc.* **1991**, *113*, 4010.

41. (a) Leland, B. A.; Joran, A. D.; Felker, P. M.; Hopfield, J. J.; Zewail, A. H.; Dervan, P. B. *J. Phys. Chem.* **1985**, *89*, 5571. (b) Joran, A. D.; Leland, B. A.; Felker, P. M.; Zewail, A. H.; Hopfield, J. J.; Dervan, P. B. *Nature* **1987**, *327*, 508.

42. Closs, G. L.; Miller, J. R. *Science* **1988**, *240*, 440.

43. Oevering, H.; Paddon-Row, M. N.; Heppener, M.; Oliver, A. M.; Cotsaris, E.; Verhoeven, J. W.; Hush, N. S. *J. Am. Chem. Soc.* **1987**, *109*, 3258.

44. McConnell, H. M. *J. Chem. Phys.* **1961**, *35*, 508.

45. Halpern, J.; Orgel, L. E. *Discuss. Faraday Soc.* **1960**, *29*, 32.

46. Anderson, P. W. *Phys. Rev.* **1950**, *79*, 350.

47. Closs, G. L.; Calcaterra, L. T.; Green, N. J.; Penfield, K. W.; Miller, J. R. *J. Phys. Chem.* **1986**, *90*, 3673.

48. (a) DeFelippis, M. R.; Faraggi, M.; Klapper, M. H. *J. Am. Chem. Soc.* **1990**, *112*, 5640. (b) Faraggi, M.; DeFelippis, M. R.; Klapper, M. H. *J. Am. Chem. Soc.* **1989**, *111*, 5141.

49. Mecklenburg, S. L.; Peek, B. M.; Schoonover, J. R.; McCafferty, D. G.; Wall, C. G.; Erickson, B. W.; Meyer, T. J. *J. Am. Chem. Soc.* **1993**, *115*, 5479.

50. Stryer, L.; Haugland, R. P. *Proc. Natl. Acad. Sci. USA* **1967**, *58*, 719.

51. Isied, S. S. *Advances in Chemistry Series*; Bolton, J. R., Mataga, N., McLendon, G., Eds.; American Chemical Society: Washington, DC, 1991; Vol. 228, pp. 229-246.

52. Ghadiri, M. R.; Case, M. A., submitted. A three-helix bundle structure stabilized by designed Ru^{2+} and type-II Cu^{2+} binding sites on opposite termini has been constructed. Attempt to measure the photochemical reduction of the copper site by the ruthenium complex was however unproductive due to the weak electronic coupling between the sites (McCleskey, T. M.; Winkler, J. R., personal communication).

53. Akerfeldt, K. S.; Kim, R. M.; Camac, D.; Groves, J. T.; Lear, J. D.; DeGrado, W. F. *J. Am. Chem. Soc.* **1992**, *114*, 9656.

54. (a) Winkler, J. R.; Nocera, D. G.; Yocom. K. M.; Bordignon, E.; Gray, H. B. *J. Am. Chem. Soc.* **1982**, *104*, 5798. (b) Nocera, D. G.; Winkler, J. R.; Yocom. K. M.; Bordignon, E.; Gray, H. B. *J. Am. Chem. Soc.* **1984**, *106*, 5145.

55. Jackman, M. P.; McGinnis, J.; Powls, R.; Salmon, G. A.; Sykes, A. G. *J. Am. Chem. Soc.* **1988**, *110*, 5880.

56. Farver, O.; Pecht, I. *Proc. Natl. Acad. Sci. USA* **1989**, *86*, 6968.

57. Kostic, N. M.; Margalit, R.; Che, C.-M.; Gray, H. B. *J. Am. Chem. Soc.* **1983**, *105*, 7765.

58. Jackman, M. P.; Lim, M.-C.; Sykes, A. G. Salmon, G. A. *J. Chem. Soc., Dalton Trans.* **1988**, 2843.

59. (a) Lieber, C. M.; Karas, J. L.; Gray, H. B. *J. Am. Chem. Soc.* **1987**, *109*, 3779. (b) Crutchley, R. J.; Ellis, W. R.; Gray, H. B. *J. Am. Chem. Soc.* **1985**, *107*, 5002. (c) Zewert, T. E. Ph.D. Thesis, California Institute of Technology, Pasadena, CA, 1990.

60. Jacobs, B. A.; Mauk, M. R.; Funk, W. D.; MacGillivray, R. T. A.; Mauk, A. G.; Gray, H. B. *J. Am. Chem. Soc.* **1991**, *113*, 4390.

61. Osvath, P.; Salmon, G. A.; Sykes, A. G. *J. Am. Chem. Soc.* **1988**, *110*, 7114.

62. (a) Meade, T. J.; Gray, H. B.; Winkler, J. R. *J. Am. Chem. Soc.* **1989**, *111*, 4353. (b) Elias, H.; Chou, M. H.; Winkler, J. R. *J. Am. Chem. Soc.* **1988**, *110*, 429. (c) Therien, M. J.; Selman, M. A.; Gray, H. B.; Chang, I.-J.; Winkler, J. R. *J. Am. Chem. Soc.* **1990**, *112*, 2420.

63. (a) Axup, A. W.; Albin, M.; Mayo, S. L.; Crutchley, R. J.; Gray, H. B. *J. Am. Chem. Soc.* **1988**, *110*, 599. (b) Cowan, J. A.; Upmacis, R. K.; Beratan, D. N.; Onuchic, J. N.; Gray, H. B. *Annu. N. Y. Acad. Sci.* **1989**, *550*, 68.

64. Geren, L.; Durham, B.; Millett, F. *Biochemistry* **1991**, *30*, 9450.

65. Scott, J. R.; Willie, A.; McLean, M.; Stayton, P. S.; Sligar, S. L.; Durham, B.; Millett, F. *J. Am. Chem. Soc.* **1993**, *115*, 6820.

66. Durham, B.; Pan, L. P.; Long, J. E.; Millett, F. *Biochemistry* **1989**, *28*, 8659.

67. Chang, I.-J.; Gray, H. B.; Winkler, J. R. *J. Am. Chem. Soc.* **1991**, *113*, 7056.

68. Winkler, J. R.; Gray, H. B. *Chem. Rev.* **1992**, *92*, 369.

69. (a) Peterson-Kennedy, S. E.; McGourty, J. L.; Hoffman, B. M. *J. Am. Chem. Soc.* **1984**, *106*, 5010. (b) Peterson-Kennedy, S. E.; McGourty, J. L.; Kalweit, J. A.; Hoffman, B. M. *J. Am. Chem. Soc.* **1986**, *108*, 1739. (c) McGourty, J. L.; Peterson-Kennedy, S. E.; Ruo, W. Y.; Hoffamn, B. M. *Biochemistry* **1987**, *26*, 8302. (d) Natan, M. J.; Hoffman, B. M. *J. Am. Chem. Soc.* **1989**, *111*, 6468.

70. (a) Farver, O.; Pecht, I. J. *J. Am. Chem. Soc.* **1992**, *114*, 5764. (b) Farver, O.; Skov, L. K.; Pascher, T.; Karlsson, B. G.; Nordling, M.; Lundberg, L. G.; Vanngard, T.; Pecht, I. *Biochemistry* **1993**, 32, 7317.

71. (a) Everest, A. M.; Wallin, S. A.; Stemp, E. D. A.; Nocek, J. M.; Mauk, A. G.; Hoffman, B. M. *J. Am. Chem. Soc.* **1991**, *113*, 4337. (b) Liang, N.; Pielak, G.; Mauk, A. G.; Hoffman, B. M. *Proc. Natl. Acad. Sci. USA* **1987**, *84*, 1249.

72. Hahm, S.; Durham, B.; Millett, F. *Biochemistry* **1992**, *31*, 3472.

73. Larsen, R. W.; Winkler, J. R.; Chan, S. I. *J. Phys. Chem.* **1992**, *96*, 8023.

74. Hazzard, J. T.; Mauk, A. G.; Tollin, G. *Arch. Biochem. Biophys.* **1992**, *298*, 91.

75. Capaillere-Blandin, C.; Iwatsubo, M.; Testylier, O.; Labeyrie, F. *Flavins and Flavoproteins: 6th International Symposium*; Science Society Press: Japan, 1980; pp. 617-630.

76. McLendon, G. L.; Pardue, K.; Bak, P. *J. Am. Chem. Soc.* **1987**, *109*, 7540.

77. Yu, C.-A.; Yu, L.; King, T. E. *J. Biol. Chem.* **1973**, *248*, 528

78. König, B. W.; Wilms, J.; van Gelder, B. F. *Biochim. Biophys. Acta* **1981**, *636*, 9.

79. Geren, L. M.; Stonehuerner, J.; Davis, J. D.; Millett, F. *Biochim. Biophys. Acta* **1983**, *724*, 62.

80. Peerey, L. M.; Brothers, H. M.; Hazzard, J. T.; Tollin, G.; Kostic, N. M. *Biochemistry* **1991**, *30*, 9297.

81. (a) Wendeloski, J. J.; Matthew, J. B.; Weber, P. C.; Salemme, F. R. *Science* **1987**, *238*, 794. (b) Salemme, F. R. *J. Mol. Biol.* **1976**, *102*, 563.

82. McLendon, G.; Miller, J. R. *J. Am. Chem. Soc.* **1985**, *107*, 7811.

83. Qin, L.; Rodgers, K. K.; Sligar, S. G. *Mol. Cryst. Liq. Cryst.* **1991**, *194*, 311.

84. Willie, A.; Stayton, P. S.; Sligar, S. G.; Durham, B.; Millett, F. *Biochemistry* **1992**, *31*, 7237.

85. Meyer, T. E.; Rivera, M.; Walker, F. A.; Mauk, M. R.; Mauk, A. G.; Cusanovich, M. A.; Tollin, G. *Biochemistry* **1993**, *32*, 622.

86. Eltis, L. D.; Herbert, R. G.; Barker, P. D.; Mauk, A. G.; Northrup, S. H. *Biochemistry* **1991**, *30*, 3663.

87. Dixon, D. W.; Hong, X.; Woehler, S.; Mauk, A. G.; Sishta, B. P. *J. Am. Chem. Soc.* **1990**, *202*, 543.

88. Moser, C. C.; Keske, J. M.; Warncke, K.; Farid, R. S.; Dutton, P. L. *Nature* **1992**, *355*, 796.

89. (a) Takano, T. *J. Mol. Biol.* **1977**, *110*, 537. (b) Takano, T. *J. Mol. Biol.* **1977**, *110*, 569.

90. Tsukahara, K. *J. Am. Chem. Soc.* **1989**, *111*, 2040.

91. Farid, R. S.; Moser, C. C.; Dutton, P. L. *Curr. Opin. Struct. Biol.* **1993**, *3*, 225.

92. Mayo, S. L.; Ellis, W. R.; Crutchley, R. J.; Gray, H. B. *Science* **1986**, *233*, 948.

93. (a) Onuchic, J. N.; Beratan, D. N.; Winkler, J. R.; Gray, H. B. *Annu. Rev. Biophys. Biomol. Struct.* **1992**, *21*, 349. (b) Beratan, D. N.; Betts, J. N.; Onuchic, J. N. *Science* **1991**, *252*, 1285. (c) Betts, J. N.; Beratan, D. N.; Onuchic, J. N. *J. Am. Chem. Soc.* **1992**, *114*, 4043.

94. Turro, C.; Chang, C. K.; Leroi, G. E.; Cukier, R. I.; Nocera, G. E. *J. Am. Chem. Soc.* **1992**, *114*, 4013.

95. Harriman, A.; Kubo, Y.; Sessler, J. L. *J. Am. Chem. Soc.* **1992**, *114*, 388.

96. (a) Siddarth, P.; Marcus, R. A. *J. Phys. Chem.* **1990**, *94*, 8430. (b) Siddarth, P.; Marcus, R. A. *J. Phys. Chem.* **1992**, *96*, 3213. (c) Siddarth, P.; Marcus, R. A. *J. Phys. Chem.* **1993**, *97*, 2400. (d) Siddarth, P.; Marcus, R. A. *J. Phys. Chem.* **1993**, *97*, 6111. (e) Siddarth, P.; Marcus, R. A. *J. Phys. Chem.* **1993**, in press.

97. Gruschus, J. M.; Kuki, A. *J. Phys. Chem.* **1993**, *97*, 5581.

98. Wuttke, D. S.; Bjerrum, M. J.; Winkler, J. R.; Gray, H. B. *Science* **1992**, *256*, 1007.

99. King, B. C.; Hawkridge, F. M.; Hoffman, B. M. *J. Am. Chem. Soc.* **1992**, *114*, 10603.

100. Gasyna, Z. *Biochim. Biophys. Acta* **1979**, *577*, 207.

Figure 1.1. The ET events in the mitochondrial respiratory chain. NADH, reduced nicotinamide adenine dinucleotide; $FADH_2$, reduced flavin adenine dinucleotide; FMN, flavin mononucleotide; Fe-S, iron-sulfur proteins; Q, ubiquinone.

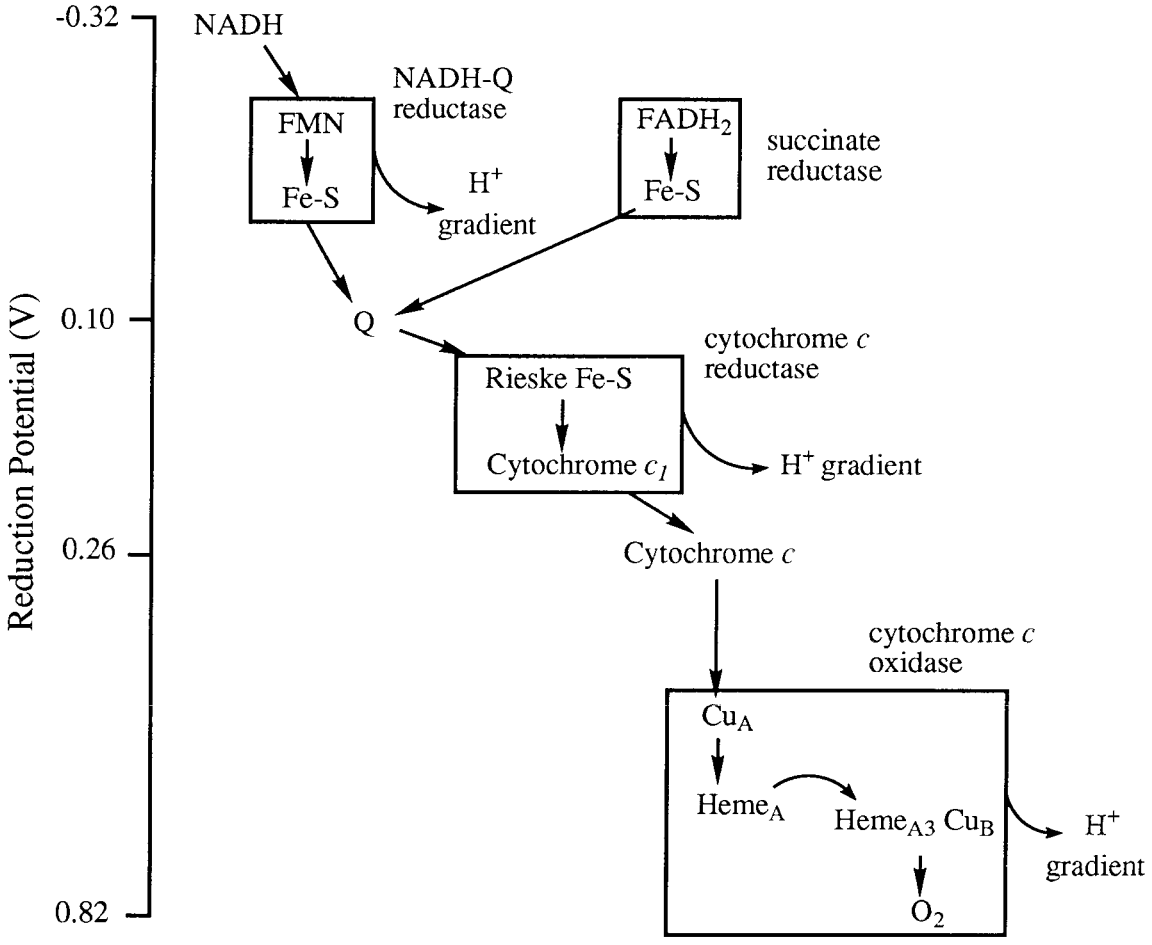
-0.32
0.10
0.26
0.82
Reduction Potential (V)
NADH
NADH-Q reductase
FMN
Fe-S
H+ gradient
FADH2
Fe-S
succinate reductase
Q
cytochrome c reductase
Rieske Fe-S
Cytochrome c1
H+ gradient
Cytochrome c
cytochrome c oxidase
CuA
HemeA
HemeA3 CuB
O2
H+ gradient

Figure 1.2. Pathway of electron flow in photosynthesis. P680, light-harvesting complex of PSII; P700, light-harvesting complex of PSI; Ph, pheophytin; Q_A and Q_B, plastoquinone-binding proteins; QH_2, reduced plastoquinone; PC, plastocyanin; A_0 and A_1, acceptors; Fp, flavoprotein; $NADP^+$, nicotinamide adenine dinucleotide phosphate.

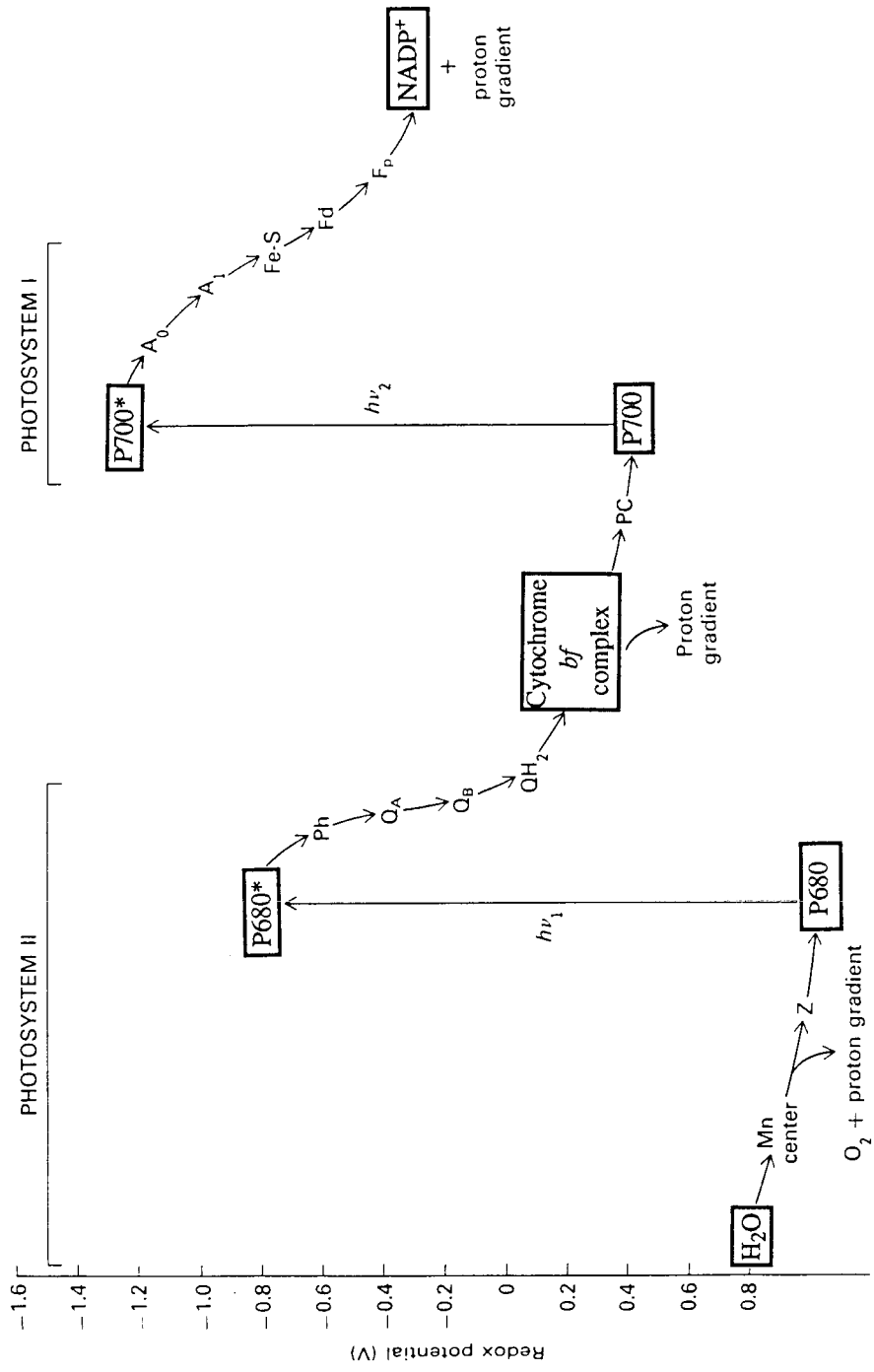
PHOTOSYSTEM II
PHOTOSYSTEM I
Redox potential (V)
−1.6
−1.4
−1.2
−1.0
−0.8
−0.6
−0.4
−0.2
0
0.2
0.4
0.6
0.8
H2O
Mn center
Z
P680
P680*
Ph
QA
QB
QH2
Cytochrome bf complex
Proton gradient
PC
P700
P700*
A0
A1
Fe-S
Fd
Fp
NADP+
+ proton gradient
hν1
hν2
O2 + proton gradient

Figure 1.3. Spatial arrangement of the prosthetic groups in the transmembrane bacterial photosynthetic reaction center. The rates of ET reactions between these sites are indicated. $BChl_2$, bacteriochlorophyll *b* dimer; $BChl_A$, bacteriochlorophyll *b*; BPh_A, bacteriopheophytin; Q_A and Q_B, quinones.

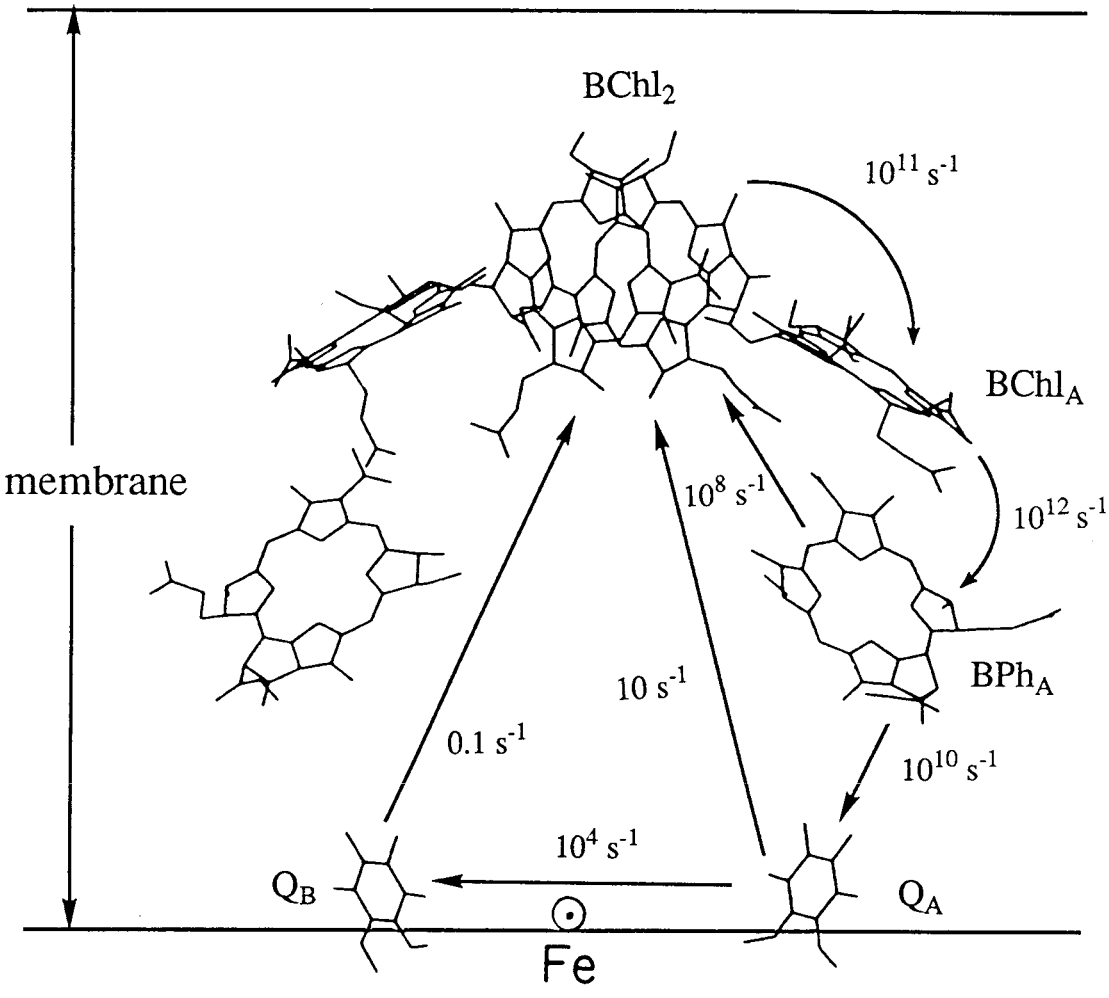
BChl2
10^11 s^-1
BChlA
membrane
10^8 s^-1
10^12 s^-1
BPhA
10 s^-1
0.1 s^-1
10^10 s^-1
10^4 s^-1
QB
QA
Fe

Figure 1.4. The role of nuclear motion in ET. Free energies of the reactants (R) and products (P) as a function of the nuclear coordinates for an electron-exchange reaction with $\Delta G^o = 0$.

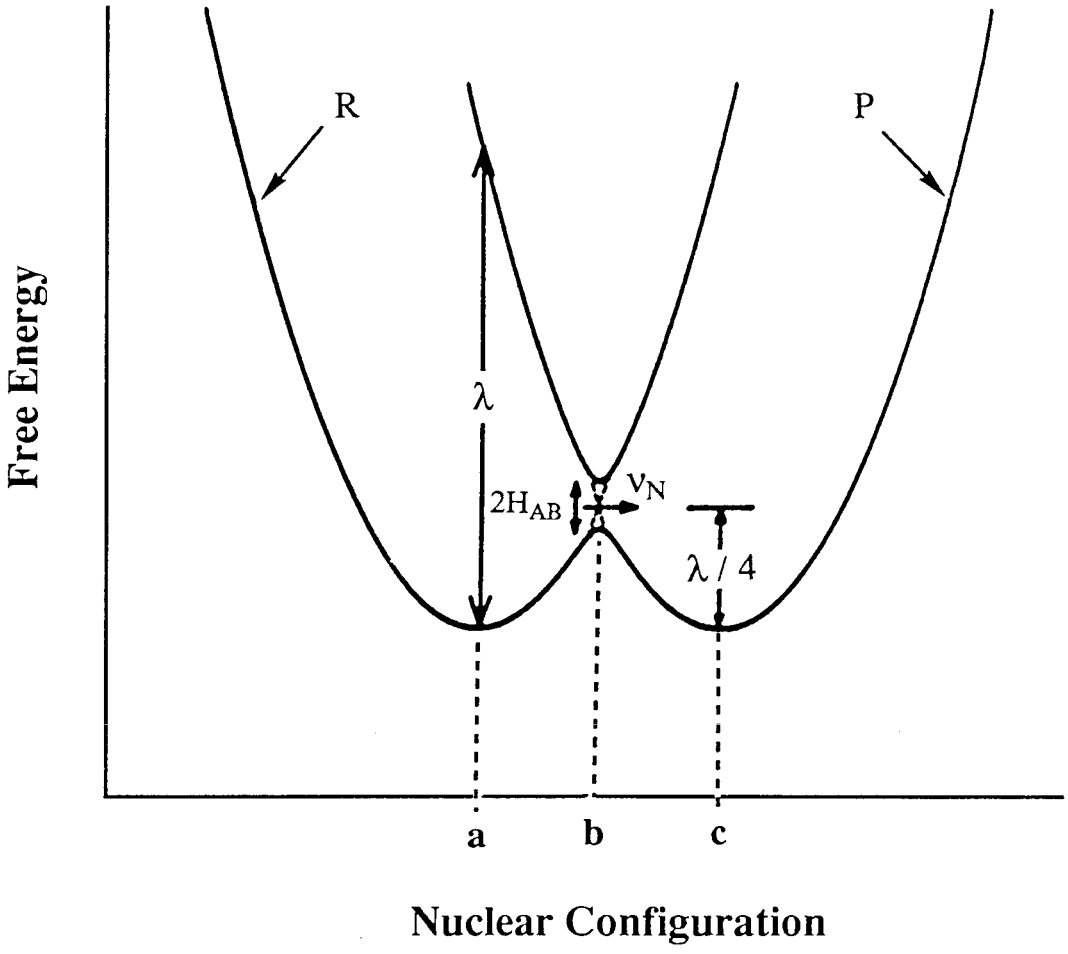
R
P
λ
2H_AB
ν_N
λ / 4
a
b
c
Free Energy
Nuclear Configuration

Figure 1.5. Free energy diagrams for ET reactions of varying driving forces: (**A**) an isoergonic reaction, (**B**) the normal region where $0 \leq \Delta G^{o} \leq \lambda$, (**C**) $-\Delta G^{o} = \lambda$, and (**D**) the inverted region where $-\Delta G^{o} > \lambda$.

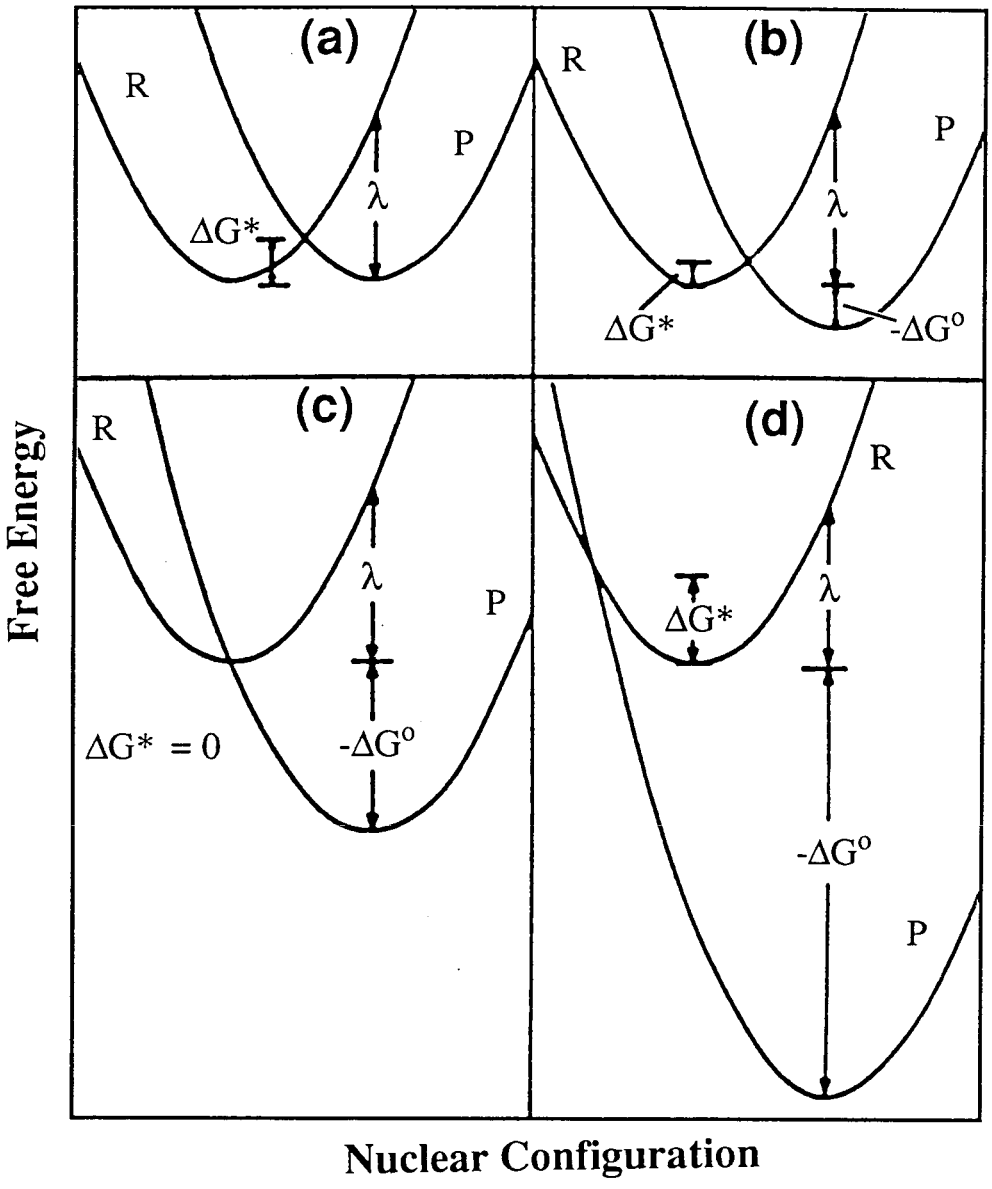
(a)
R
P
λ
ΔG*
(b)
R
P
λ
ΔG*
-ΔG°
(c)
R
P
λ
ΔG* = 0
-ΔG°
(d)
R
ΔG*
λ
-ΔG°
P
Free Energy
Nuclear Configuration

Figure 1.6. Log k_{ET} as a function of $-\Delta G^{o}$. Curve **a** depicts a classical Marcus inverted effect; curves **b-d** were determined with increasing values for the oscillator frequency (ω).

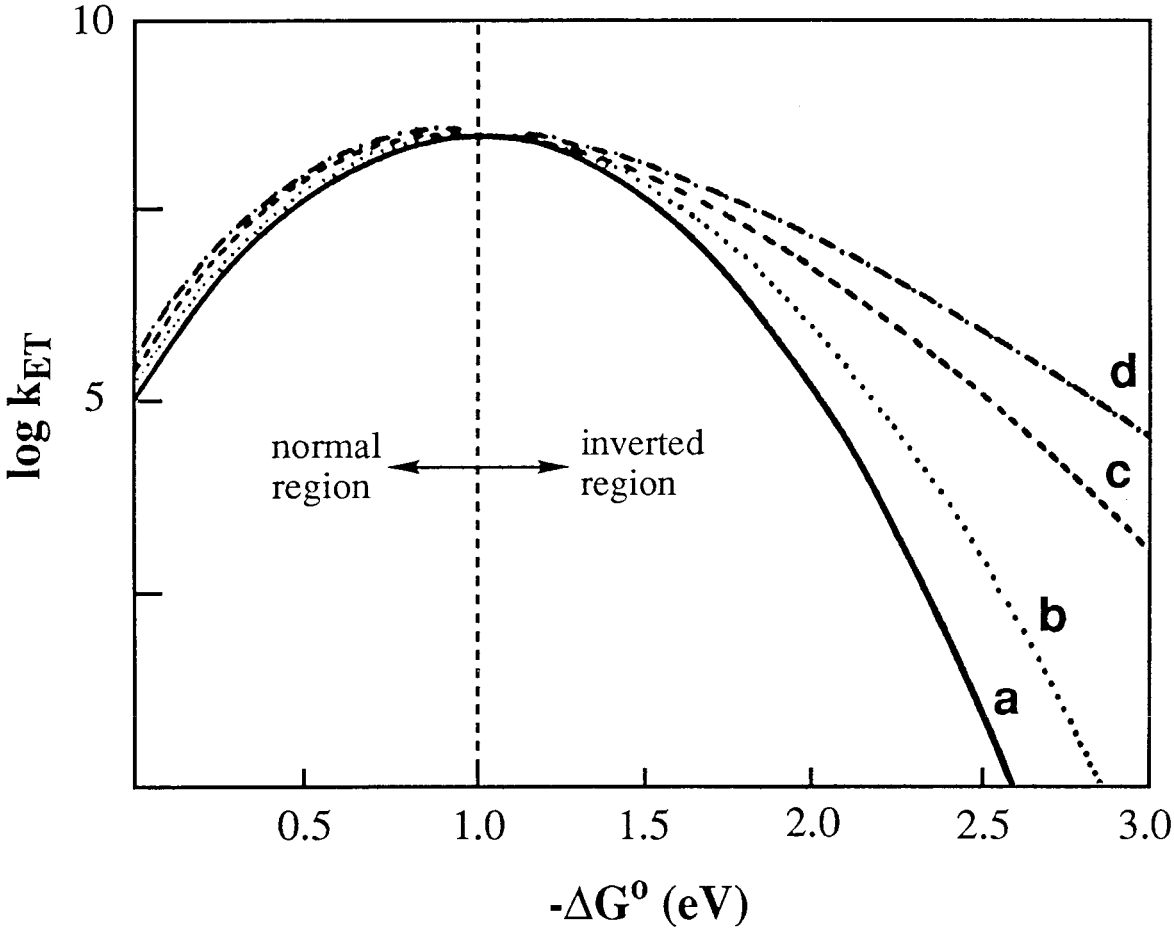
10
5
log k_{ET}
normal region
inverted region
a
b
c
d
0.5
1.0
1.5
2.0
2.5
3.0
$-\Delta G^o$ (eV)

Figure 1.7. Pentaammineruthenium-modified His33 of horse heart cytochrome *c*. On the right is a space-filling model of those residues that lie between the surface Ru site and the heme. Reproduced from reference 92.

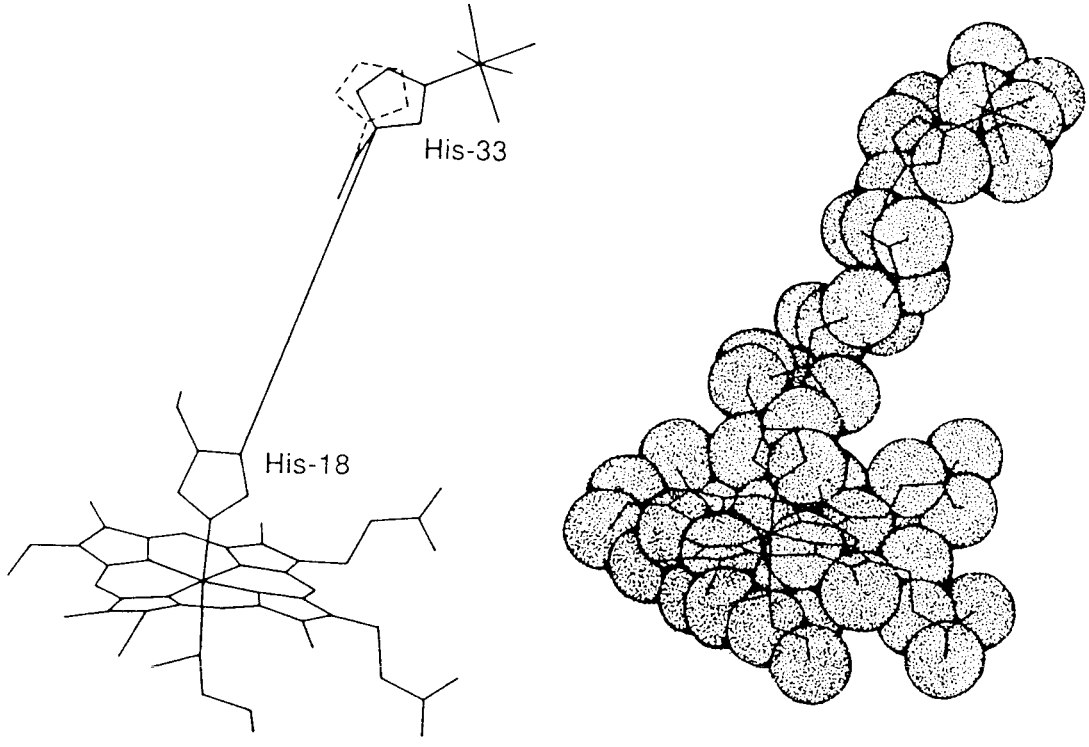
His-33
His-18

Chapter 2

Intramolecular Electron Transfer in Zinc Porphyrin/Ruthenium-Modified Recombinant Human Myoglobins

[This work is described in D. R. Casimiro, L.-L. Wong, J. L. Colon, T. E. Zewert, J. H. Richards, I.-J. Chang, J. R. Winkler, & H. B. Gray, *J. Am. Chem. Soc.*, **1993**, *115*, 1485.]

INTRODUCTION

The simplest model that describes the effect of the bridging medium on the rates of electron transfer (ET) between two redox sites assumes that the medium provides a homogeneous barrier; as such, the rates are predicted to decay exponentially with increasing distance.[1] Whether this model is generally applicable to protein ET processes has stimulated numerous investigations in the past decade. Most of these involve studies of ET in semisynthetic donor-acceptor (D-A) systems wherein artificial redox groups are covalently attached to different sites on the surface of a metalloprotein and at different distances from the protein center. These chemically modified proteins range from those arising from attachment of Ru complexes to histidine,[2] cysteine,[3] or lysine residues[4] to those involving functionalization of side-chain carboxylates with cobalt cage complexes.[5]

One of the earliest attempts to address the distance dependence of ET processes in a metalloprotein involved a study of photoinduced ET reactions in ZnP-substituted sperm whale myoglobins (ZnP = zinc porphyrin) each with a Ru ammine complex attached at one of four different surface histidines.[2a] Porphyrins with closed-shell metal ions (e.g., Zn^{2+}, Mg^{2+}, Pd^{2+}) have long-lived triplet excited states that are highly reducing species.[6] Sperm whale myoglobin has four native surface-accessible histidines (at positions 48, 81, 116, and 12) at different distances from the heme (edge-edge separations of 12.7, 19.3, 20.1, and 22.0 Å, respectively). The activationless $^3ZnP^* \rightarrow Ru^{3+}$ ET rates are: 3.1×10^5, His48; 3.8×10^2, His81, 4.0×10^2, His116; and 4.4×10^2 s^{-1}, His12. Analysis of these results, however, raises certain confusion regarding the influence of the intervening medium on ET rates. First, while the rates decrease initially in a monotonic manner with increasing distance, they level off at longer D-A separations. The faster-than-predicted rate in His12 was originally interpreted as a consequence of having an intervening tryptophan (at position 14), but theoretical analysis[7] of this system using ET path integrals found no special role for the said conjugated ring system. Secondly,

extrapolation of the best fit line to the log k_{max} *vs.* distance plot suggests an adiabatic rate (k_{max} at d = 3) of 10^9 s^{-1}, four orders of magnitude lower than the theoretical value[1] and those obtained with synthetic donor-acceptor (D-A) molecules.[8]

To resolve the discrepancies described above, it became apparent that ET reactions at distances (d < 10 Å, 13 Å < d < 18 Å) which had not been sampled earlier must be examined. Construction of D-A complexes in myoglobin with such intersite distances requires that non-native histidines that will serve as anchors for the ruthenium probes be introduced at appropriate surface positions. In the work that will be described, we resort to the use of human myoglobin (HuMb) as the model system. The gene for HuMb has been cloned and expressed in high yields in *Escherichia coli*.[9] The crystal structure of a pseudo-wild-type Lys45→Arg/Cys110→Ala mutant has been solved and refined to 1.6-Å resolution (Figure 2.1);[10] this should facilitate the design of surface histidines on the molecule.

HuMb is 84 % (by identity) homologous to sperm whale protein[11] with no deleted nor inserted sequences; the three-dimensional structure is virtually superimposable with that of sperm whale myoglobin.[12] It contains two (His48 and His81) of the four surface histidines found in sperm whale myoglobin. Our group has constructed HuMb mutants that have only one of the two histidines and a Cys110→Ala.[13] The rates of photoinduced $^3ZnP^*\rightarrow Ru^{3+}$ ET ($k_{ET(f)}$) and subsequent charge-recombination reaction ($k_{ET(cr)}$) in a_5Ru(His48)/ZnP-modified human myoglobin (a = NH_3) have been measured (7.2×10^4 and 1.1×10^5 s^{-1}, respectively). These rates are very close to those of the analogous sperm whale derivative, suggesting the absence of any significant species-dependent factor that may obscure comparison with sperm whale myoglobin. On the other hand, direct quenching of the $^3ZnP^*$ via intramolecular ET to a_5Ru(His81) in human myoglobin could not be detected.[14] At very low protein concentrations (< 1 μM), the excited-state lifetime in a_5Ru(His81)/ZnP human myoglobin is equal to that of free ZnP and hence,

$k_{ET(f)}$ can be no more than ~5 s^{-1}. This raises the question of whether the rates reported for the equivalent sperm whale myoglobin derivative as well as those for Ru-modified His12 and His116 contain bimolecular components and do not represent the true first-order intramolecular reactions.

In this chapter, the construction of two site-directed mutants of human myoglobin each containing a single histidine (at position 70 or 83) on the protein surface for Ru labelling will be described. Both proteins were modified with pentaammineruthenium(III) and the hemes replaced with zinc mesoporphyrin IX. The intramolecular ET rates in both systems were measured and will be analyzed in the context of previous data on sperm whale and other human myoglobin systems.

MATERIALS AND METHODS

Design of Histidine Mutants

The crystal coordinates of human myoglobin were graciously provided by David Lambright, Steve Hubbard, and Wayne Hendrickson (Columbia University).[10] The structure was displayed and analyzed on an Evans and Sutherland PS390 using BIOGRAF software (Molecular Simulations, Inc.). The surface sites for histidine incorporation were selected with the following criteria in mind: (1) the appropriate distance of the C_α to the heme edge; (2) high sequence variability in the phylogenetic series;[11] (3) absence of any aromatic residue in the path to the heme; and (4) low thermal flexibility of local backbone atoms. Because the issue concerning the possible effect of intervening aromatic side chain(s) on ET rates was largely unclear at the start of this project, we chose to probe ET only through aliphatic polypeptide matrices. The fourth requirement reduces any fluctuation in the D-A distance that may be attributed to thermal motions; for this reason, sites located at turns were avoided. All 55 surface-accessible

sites on HuMb were evaluated on the basis of these requirements and two target sites were selected - positions 70 (edge-to-edge d = 9.5 Å) and 83 (d = 15.5 Å).

Gene for Base Protein

HuMb contains a single buried cysteine (position 110) that sometimes complicates the purification of genetically engineered apoproteins.[9] All of our proteins incorporate a Cys110→Ala mutation to prevent dimer formation during purification. Removal of the native surface histidines (His48 and His81) should greatly simplify the purification of the protein modified at the novel histidine site; the His48→Gln/His81→Gln/Cys110→Ala mutant is referred to as the base protein. An M13mp19 vector harboring the gene for the base HuMb protein was constructed in the following manner. Three separate restriction reactions were run at 37 °C for 3 h. In one, 10 μg of pLcIIFXHuMb-H48Q/C110A (pLcII vector with 0.7-kb *Bam*HI/*Hin*dIII insert containing the factor X_a sequence and the His48→Gln/Cys110→Ala HuMb gene[13]) was digested with 4 μL *Bam*HI (10 units/μL) and 4 μL *Afl*II (10 units/μL) in 80 μL 1 × B (low magnesium) buffer (Boehringer Mannheim). In the second, 10 μg of pLcIIFXHuMb-H48Q/C110A (pLcII vector with 0.7-kb *Bam*HI/*Hin*dIII insert containing the factor X_a sequence and the His81→Gln/Cys110→Ala HuMb gene[13]) were digested with 4 μL *Afl*II (10 units/μL) and 4 μL *Hin*dIII (10 units/μL) in 80 μL 1 × B buffer. In the third Eppendorf tube, 5 μg of M13mp19 replicative form (RF) were digested with 4 μL *Bam*HI (10 units/μL) and 4 μL *Hin*dIII (10 units/μL) in 80 μL 1 × B buffer.

Upon completion of the reactions, the volume was reduced to 50 μL by solvent evacuation in a Speed Vac; the solution was loaded into 1.4% low-melting-point agarose (NuSieve GTG, FMC). The gel was run at 4 °C until the bands were fully resolved. The bands containing the 243-bp *Bam*HI/*Afl*II restriction fragment of pLcIIFXHuMb-H48Q/C110A, 505-bp *Afl*II/*Hin*dIII fragment of pLcIIFXHuMb-H48Q/C110A, and the cut M13mp19 RF vector were excised from the gel and melted at 65 °C prior to the

cloning experiment. Ligation was performed with a 5:5:1 insert:insert:vector molar ratio (10 μg/μL total DNA concentration) at 16 °C for 20 h. 300 μL of competent *E. coli* TG1 (*supE hsdΔ5 thi Δ(lac-proAB)* F'[*traD36 proAB*$^+$ *lacI*^{q} *lacZΔM15*]) cells, prepared following the TFB-based method,[15] were transformed with varying amounts of the reaction mixture and plated on an IPTG/Xgal-supplemented (IPTG = isopropyl-β-D-thiogalactopyranoside; Xgal = 5-bromo-4-chloro-3-indolyl-β-D-galactoside) H medium. Because the polylinker site is located in the *lacZ* gene, fragment insertion at this site leads to a β-galactosidase product that is unable to hydrolyze the chromogenic Xgal substrate. Large-scale preparation of the plasmid from a selected clear plaque was performed and the presence of the HuMb insert was confirmed by restriction analysis.

A uracil-containing single-strand copy of M13mp19FXHuMb-H48Q/H81Q/C110A was prepared according to the procedure described by Kunkel.[16a] 50 mL 2 × YT supplemented with 30 μg/mL chloramphenicol, 20 μg/mL thymidine, and 100 μg/mL 2-deoxyadenosine were inoculated with overnight culture of *E. coli* CJ236 (*dut1 ung1 thi1 relA1*/pCJ105 (Cm^r)). The cells were grown at 37 °C to an OD_{550} of 0.4-0.5, pelleted by centrifugation (5k rpm, SS34 rotor, 15 min, 4 °C), and resuspended in 50 mL 2 × YT supplemented with 0.25 uridine. 5 μL of phage stock in TE (equivalent to 1 mL supernate of fully infected cells) were added; the resulting multiplicity of infection (phage per cell) is less than 1. The culture was incubated at 37 °C overnight (> 12 h). At the same time, a 200 mL culture of fresh CJ236 grown to an OD_{550} of 0.4-0.5 was prepared for a second round of infection in the same manner as the original 50 mL culture. The culture from the first round of infection was pelleted and 5 mL of the supernate were used to infect the 200 mL log-phase CJ236 culture. The procedure was repeated with another fresh 200 mL culture of CJ236 for a third round of infection. Multiple infections ensure high uracil incorporation on the single-stranded template. Efficiency of uracil incorporation was determined by titering the phage particles against

TG1 and CJ236. Because TG1 strain encodes an active uracil N-glycosylase that releases uracil from DNA and creates apyrimidic sites, transfection of this strain by a uracil-containing DNA is inhibited. Thus, the ratio of transfected TG1:CJ236 cells for a fixed amount of phage particles reflects the efficiency of uracil incorporation as well as the expected efficiency of oligonucleotide-directed mutagenesis. Three rounds of infection typically gave ~10^5 uracil-containing templates for every normal single-stranded DNA. The phage particles were concentrated by polyethylene glycol extraction[16b] from the culture supernate; the uracil-containing template was isolated from the phage material by phenol extraction of viral coat protein.[16b]

Site-Directed Mutagenesis

Site-directed mutagenesis experiments follow the procedure developed by Kunkel;[16] the Muta-Gene kit from Bio-Rad customized for these experiments was used. The base sequence of the wild-type HuMb gene can be found in Appendix A. The mutagenic primers used for ACC→CAT conversion at codon 70 and GAG→CAT at codon 83 were synthesized at the Caltech Microchemical Facility and are listed below.

Thr70→His	5'- A C T G T G C T C C A T G C C C T G G G T -3'
Glu83→His	5'- G G G C A A C A T C A T G C A G A G A T T A -3'

The primers were phosphorylated with T4 polynucleotide kinase for 1 h at 37 °C using the following recipe: 200 pmol, primer; 3 μL, 1 M Tris (pH 8.0), 3 μL, 100 mM $MgCl_2$; 1.5 μL, 100 mM dithiothreitol; 1.5 μL, 10 mM ATP; 2 μL, kinase (10 units/μL); and ddH_2O to make 30 μL. The reaction was quenched by heating to 65 °C, 5 min. The solution was diluted to 60 μL (~3 pmol/μL). 1 μL of the phosphorylated primer was mixed with 0.1 pmol of the uracil-containing template, 1 μL 10 × annealing buffer and the solution diluted to 10 μL with ddH_2O. The solution was heated to 70 °C for 5 min and cooled slowly to room temperature. To the solution, 1 μL T4 DNA polymerase (1 unit), 1

μL T4 DNA ligase (3 units), and 1 μL 10 × synthesis buffer were added. The solution was incubated at 37 °C for 2 h. Competent *E. coli* MV1190 (*supE thi Δ(lac-proAB) Δ(srl-recA)306*:Tn*10*(tet^r) F'[*traD36 proAB lacI*^{q} *lacZΔM15*]) cells were transformed with the aliquots of the reaction mixture and the plated on H agar. TG1 strain can be used as an alternative to MV1190. The plates were incubated overnight at 37 °C; the resulting plaques were picked and used to infect 2 mL of log-phase MV1190. Preliminary screening for the mutant constructs were conducted by dot-blot hybridization with the P^{32}-labelled mutagenic primer.[17] Single-stranded circular DNA copies and replicative forms of the positive clones were prepared from 200 mL of infected TG1 following standard protocols.[16,18] Complete DNA sequences of the mutated HuMb genes in the single-stranded templates were obtained by the Sanger dideoxy method (Sequenase kit, USB).[19]

Gene Expression

pLcII vector was cut with *Bam*HI and *Hin*dIII. The digests were run on a 1.4% low-melting-point agarose (NuSieve GTG, FMC) at 4 °C and the cut pLcII band was excised. 18 μg of M13mp19FXHuMb RF were digested with 4 μL *Bam*HI (10 units/μL), 4 μL *Hin*dIII (10 units/μL), and 4 μL *Cla*I (10 units/μL) in 80 μL 1 × B buffer. The restriction enzymes were extracted from the aqueous solution 2× with TE-equilibrated phenol and 3× with 1:1 $CHCl_3$:phenol. Dissolved organic materials were extracted with ether, which was then removed with the use of a pipet; remaining traces of ether were removed by heating the solution at 55 °C for 1 min. To the DNA solution, 3 μL 3M sodium acetate (pH 5.2) and 200 μL ethanol were added and the solution incubated overnight at -20 °C. The DNA was pelleted by microcentrifugation at 4 °C for 30 min and redissolved in 10 μL 1/10 TE. The 0.7-bp HuMb-containing fragment was cloned into pLcII using the following recipe: 0.7 μg cut pLcII (in gel); 3.1 μg

M13mp19F*X*HuMb digests; 4 μL 10 × ligase buffer; 2 μL ligase (1 unit/μL); and double-distilled H_2O (ddH_2O) to make 40 μL. Fragment ligation was carried out at 16 °C, 16 h.

The ligation mixture was used to transform competent *E. coli* AR68 (*lac*^{amber} *pho*^{amber} *sub*^{cts} *Str*^{r} *hdpr galE*::Tn*10*(λcI857 Δ*Bam* Δ*H I bio uvrB*) *tet*^{r}) by electroporation.[20] The cells were prepared in the following manner. 250 mL *E. coli* AR68 in L medium were grown at 30 °C to an OD_{600} of 0.7 at 30 °C. The cells were spun down at 4k rpm, 15 min, 4 °C, and the supernate discarded. The cells were resuspended in 250 mL ice-cold ddH_2O and spun down as before. The cells were washed another time with 125 mL ice-cold ddH_2O and resuspended in 5 mL 10% glycerol. The cells were centrifuged in a 50-mL sterile tube at 3k rpm, 15 min, 4 °C. The supernate was discarded and the cells resuspended in 0.75 mL 10% glycerol. The ligation mixture was desalted by applying the drop on a 0.025-μm membrane that was made to float on ddH_2O. The drop was carefully collected after 45 min of equilibration. To 40-μL aliquots of the cells, varying amounts of the desalted ligation mixture (< 20 μL) were added and each cell/DNA mixture transferred to a 0.2-cm electroporation cuvettes (Bio-Rad). An exponentially decaying electrical pulse was applied (2.5 kV, 25 μF, 200 Ω) to each mixture using a Bio-Rad Gene Pulser apparatus. The mixture was immediately cooled by adding 1 mL ice-cold L broth. The culture was transferred into a 15-mL disposable sterile tube and incubated at 30 °C for 1 h. Aliquots of differing amounts were plated on L agar supplemented with 50 μg/mL ampicillin.

Clones were analyzed for HuMb expression by SDS/PAGE. Colonies were picked and used to inoculate 1 mL of L broth. The culture were grown overnight at 30 °C. A 0.5-mL aliquot was collected and stored at -70 °C in 15% glycerol. 40 μL of the remaining culture were used to inoculate 2 mL of fresh L broth at 30 °C, 3-4 h. HuMb expression was induced by transferring the cultures into 42 °C bath where they were swirled for 2 h. The cells were spun down using a microcentrifuge and resuspended in

100 μL Laemmli buffer.[21] The cells were lysed by boiling the suspension for 5 min. 15-μL aliquots were loaded and run on a 12% SDS/polyacrylamide gel. A recombinant clone was identified by the appearance of an overexpressed 21-kDa protein. For a large-scale preparation of the protein, the mutant clone was grown to saturation at 30 °C in 4 L 2 × YT broth supplemented with ampicillin. The culture was used to inoculate 170 L broth (fermentation facility at UCLA Molecular Biology Institute). The cells were grown at 30 °C to an OD_{550} of 0.6-1.0, at which time, the temperature was raised to 42 °C (jump time of no more than 5 min) where it was maintained for 2 h. The cells were collected; the apoproteins were isolated and the heme reconstituted following the procedures described by Varadarajan *et al.*[9] The purity of the protein was verified by SDS/PAGE. All proteins isolated using this protocol were in the stable metaquo form.

Preparation of Pentaammineruthenium/Zinc Porphyrin Derivatives

The myoglobin mutants were first modified at the sites of the surface histidine with a_5Ru^{3+}. Pentaammineaquoruthenium(II) ($a_5Ru(OH_2)^{2+}$) was freshly prepared by reducing pentaamminechlororuthenium(III) chloride (a_5RuCl_3, Strem Chemicals, Inc.) with zinc amalgam. 20 g of the zinc metal were treated with 100 mL 0.1 N HCl; the mixture was swirled and left standing for 10 min. The zinc metal was washed repeatedly with ddH_2O and wiped dry. 5 mL concentrated HCl was added to the metal. While swirling, 0.6 g mercuric oxide (Sigma) was added to the system which was then left for 20 min. The metal became shiny as amalgamation proceeded. The metal was wiped dry and transferred into a septum bottle. a_5RuCl_3 that would give 25-fold molar excess relative to the protein was weighed out and poured into the septum bottle containing the dried, amalgamated metal strips. The bottle was degassed and purged with purified argon on a dual-manifold vacuum/argon line incorporating a manganese oxide scrubbing column to remove residual oxygen. In a separate septum bottle, *ca.* 5 ml of 100 mM HEPES (4-(2-hydroxyethyl)-1-piperazineethanesulfonic acid), pH 7.5, was likewise

degassed and the atmosphere exchanged to argon. The buffer was transferred into the septum bottle containing the zinc strips via a canula connecting the two containers. Reduction of the Ru complex by the amalgam was complete in *ca.* 30 min. In another septum bottle, 15 mL 2 mg/mL mutant myoglobin in 100 mM HEPES, pH 7.5, was degassed and equilibrated under argon. The $a_5Ru(OH_2)^{2+}$ solution was delivered to the protein solution via a canula. The solution turned red indicative of a reduced heme and kept under anaerobic conditions. The reaction was quenched at a predetermined time by oxidation with $Co(phen)_3^{3+}$ (phen = 1,10-phenanthroline) and desalting through Sephadex G-25 pre-equilibrated with μ 100 mM sodium phosphate (NaP_i) buffer, pH 7.0. The reaction time was determined by running the reaction at a smaller scale, collecting aliquots at hourly intervals, and analyzing the products chromatographically. The 1:1 Ru:protein product was isolated by loading the protein mixture into a Mono-S 16/10 cation-exchange column fitted to a Pharmacia FPLC apparatus. A combined pH and salt gradient was developed using μ 50 mM NaP_i buffer, pH 5.5, as loading buffer and 1 M NaCl, 50 mM NaP_i, pH 6.5, as the eluent. The Ru-modified myoglobin solution was exchanged to μ 100 mM NaP_i, pH 7.0, by ultrafiltration.

The heme was extracted following established procedures.[22] The Ru-modified myoglobin was concentrated to 1-2 mg/mL and cooled on ice as the pH was adjusted slowly to 2.3 with ice-cold 0.1 M HCl. The heme was extracted several times with equal volumes of ice-cold butanone until the aqueous layer was colorless. The organic layer was discarded and the protein solution was dialyzed twice against 1 L 10 mM $NaHCO_3$ for at least 6 h each time to remove trace butanone. The dialysis tubing was dialyzed three times against 1 L μ 100 mM NaP_i buffer, pH 7.0. Protein concentration was determined spectroscopically (ε_{280} = 15,800 M^{-1} cm^{-1}). To 2 mg/mL solution of Ru-modified apoprotein, 3 equivalents of Zn-mesoporphyrin IX (ZnP) solution (prepared by adding 10 drops of 0.1 N NaOH for every 3 mg of porphyrin and diluting to 1.5 mg/mL

with μ 100 mM NaP_i, pH 7.0) were added dropwise and the mixture was stirred gently for 18 h at 4 °C. All manipulations involving ZnP were done in the dark. Excess ZnP was removed by running the solution through Sephadex G-25 and washing it with μ 100 mM NaP_i, pH 7.0. The protein band was collected into an Amicon ultrafiltraion unit where it was concentrated. The a_5Ru/ZnP-substituted myoglobin was purified chromatographically in the same manner as the a_5Ru-modified metmyoglobin. Sample purity was confirmed by a A_{414}/A_{280} of *ca.* 16 (ε_{414} = 250 mM^{-1} cm^{-1}).

ET Rate Measurements

Fully oxidized protein samples (0.5-10 μM) in μ 100 mM NaP_i, pH 7.0, were transferred into vacuum cells with 1-cm cuvette side arms. The samples were degassed and purged with purified argon. At least 10 vacuum/fill cycles were performed to deoxygenate the samples, taking care not to denature the proteins by bubbling. The deoxygenated samples were excited with pulses from the second harmonic of a Q-switched Nd:YAG laser (532 nm, 10-ns fwhm). ZnP triplet-state (^{3}ZnP*) decay kinetics were monitored by transient absorption measurements at 450 nm. Charge-recombination kinetics were monitored by following the porphyrin cation radical ($ZnP^{+\cdot}$) at 380 nm. The samples were deoxygenated with additional vacuum/fill cycles and the laser experiments repeated until the ^{3}ZnP* decay kinetics has not changed from the previous measurement. The kinetic traces were analyzed using the software KINFIT.

RESULTS AND DISCUSSION

Design of Histidine Mutants

On the basis of the criteria outlined in the previous section, two target surface sites were selected - positions 70 and 83. A histidine at position 70 has an edge-to-edge distance of 9.5 Å (Figure 2.2); a threonine and serine residue have been found at this site

in all known myoglobin sequences. A histidine at position 83 has an edge-to-edge distance of 15.5 Å (Figure 2.2). There is one other existing fact that reinforces the choice of His83 mutation. The inability to resolve ^{3}ZnP*→a_5Ru(His81)$^{3+}$ ET from the intrinsic excited-state decay suggests that moving the probe closer to the heme along the same helix is likely to provide a measurable rate. Combined with His48, His70 and His83 should allow us to redefine the distance dependence of the rates of ET across a predominantly aliphatic medium in myoglobin.

Site-Directed Mutagenesis

Human myoglobin has two naturally occurring surface histidines - His48 and His81. Removal of both histidines should greatly improve the reaction yield at a new surface site and simplify purification of the corresponding modified product. To achieve this, a hybrid M13mp19FXHuMb plasmid was constructed from the *Bam*HI/*Afl*II His48→Gln HuMb fragment and the *Afl*II/*Hin*dIII His81→Gln HuMb fragment (Figure 2.3); a uracil-containing single-stranded DNA copy of this vector was used for oligonucleotide-directed mutagenesis. The M13mp19 shuttle vector was employed instead of the original amber-containing M13mp11 construct of Varadarajan *et al.*[9] because the *E. coli* strains commonly available are non-suppressors.

The mutagenesis experiments followed the procedure developed by Kunkel.[16] The method uses a DNA template containing a small number of uracil residues in place of thymine. This DNA is produced by transfecting an *E. coli dut*$^-$ *ung*$^-$ strain with the M13 vector. *dut*$^-$ mutants lack the enzyme dUTP pyrophosphatase and therefore contain elevated levels of dUTP, which can compete with dTTP for incorporation into the DNA. *ung*$^-$ mutants lack a uracil N-glycosylase that excises uracil from the DNA. Thus, an M13 vector can be propagated in a *dut*$^-$ *ung*$^-$ strain to generate uracil-containing single-stranded DNA templates. A mutagenic primer is annealed to the uracil-containing template; the new strand is then extended and the ends ligated. The heteroduplex is

introduced into a *dut*$^+$ *ung*$^+$ strain, which selects against the wild-type uracil-containing template. This *in vivo* selection technique has the advantage of having considerably less number of steps than most *in vitro* selection protocols and being highly efficient.

For the Thr70→His mutagenesis, 5 of 5 chosen tested positive on the dot-blot hybridization screen; for the Glu83→His substitution, the efficiency is 90% (18 of 20). The mutant constructs were further confirmed by dideoxy sequencing. Figure 2.4 shows a representative nucleotide sequence, which is that of Thr70→His myoglobin. Full gene sequences of the mutants revealed no other base alterations aside from those at codons 110, 48, 81, 70, and 83. The 0.7-kb HuMb fragment was introduced into pLcII and the ligation mixture was used to transform the AR68 expression host. The gene products were primarily expressed as 21-kDa fusion protein consisting of a 31 amino-terminal residues of λ *c*II, the factor X_a (F*X*), and the HuMb apoprotein (Figure 2.5A).[9,23] Overexpression of the fusion product was induced by raising the growth temperature to 42 °C, thereby deactivating the temperature-sensitive *c*II repressor specific for the plasmid promoter. Positive clones were identified by their ability to express the 21-kDa protein (Figure 2.5B).

Pentaammineruthenium/Zinc Porphyrin-Modified Myoglobins

The mutant metmyoglobins were isolated and purified from a large-scale fermentation batch following established protocols.[9] The mutants were first modified with $a_5Ru(OH_2)^{2+}$ and the 1:1 products were purified by cation-exchange chromatography (Figure 2.6). For each of the mutant proteins, the reaction with the Ru complex were highly specific, showing only one major product. The retention volumes of the unmodified and modified proteins correlate with the overall charge on the protein surface. In each chromatogram, the unmodified protein eluted first followed by the more positively charged modified protein. The a_5Ru(His70) HuMb derivative eluted earlier in

the gradient than a_5Ru(His83) HuMb; His70 HuMb incorporates a threonine-to-histidine mutation whereas the His83 muatnt involves the loss of a surface glutamate.

ET Kinetics

ET in the a_5Ru/ZnP-substituted HuMbs was initiated by pulsed-laser excitation of the ZnP (Figure 2.7). The ^{3}ZnP* excited state is long-lived (20 ms) and highly reducing (E^o ~ -0.74 eV *vs.* NHE).[2a] In addition to its usual deactivation processes, ^{3}ZnP* can decay by electron transfer to a surface Ru^{3+}. The subsequent electron-hole recombination reaction ($Ru^{2+} \rightarrow ZnP^{+\cdot}$ ET) regenerates the ground-state species. The reactions were monitored at wavelengths where the transient absorption arises mainly from ^{3}ZnP* (450 nm) or $ZnP^{+\cdot}$ π-cation radical (380 nm).

The kinetics observed at 450 nm monitor the deactivation of the ^{3}ZnP* excited state; the first-order rate constant of the kinetics at this wavelength is taken as the sum of k_d and $k_{ET(f)}$ (eq 1; $C_o > 0$).

$$[^3ZnP^*]_t = C_o \exp\{-(k_d + k_{ET(f)})t\} \qquad (1)$$

That these processes are unimolecular were verified by varying the protein concentration. Figure 2.8 shows the transient absorbances at 450 nm for a_5Ru(His70) and a_5Ru(His83) HuMb after applying a 10-ns, 532-nm laser pulse. The fit to the data a_5Ru(His70) HuMb has a first-order rate constant (~$k_{ET(f)}$) of $1.6(2) \times 10^7$ s^{-1}. The fit to the data for a_5Ru(His83) HuMb has a rate constant of $4.5(4) \times 10^2$ s^{-1}; thus, $k_{ET(f)} = 4.0(4) \times 10^2$ s^{-1}.

Because the back reactions in a_5Ru/ZnP-substituted HuMbs are inherently faster than the forward ET reactions due to a larger driving force, the kinetics at 380 nm ($ZnP^{+\cdot}$) will be described by eq 2 (C_1, $C_2 > 0$).[24]

$$[ZnP^{+\cdot}]_t = -C_1 \exp\{-k_{ET(cr)}t\} + C_2 \exp\{-(k_d + k_{ET(f)})t\} \qquad (2)$$

The first part of the trace which involves a build up in signal has a rate constant equal to that of the charge-recombination process ($k_{ET(cr)}$); this is followed by a decay in absorbance with a rate constant of ($k_d + k_{ET(f)}$). The latter should be identical to that observed at 450 nm and as such, confirms that the deactivation of ^{3}ZnP* is partly due to intramolecular ET. Figure 2.9 shows the ET kinetics monitored at 380 nm for a_5Ru(His70) and a_5Ru(His83) HuMb. Unfortunately, the charge-recombination signal was too fast to be resolved from the instrument response; the rate constant for the decaying signal equals that of the forward ET reaction as deduced from that transient absorbances at 450 nm. For a_5Ru(His83) HuMb, the kinetics at 380 nm is described by $k_{ET(cr)} = 7.3(7) \times 10^2\ s^{-1}$ and $k_{ET(f)} + k_d = 4.5(4) \times 10^2\ s^{-1}$.

D-A Couplings in Ruthenium-Modified Myoglobins

According to semiclassical ET theory,[1] the rates of long-range nonadiabatic electron transfer depend upon reaction driving force ($-\Delta G^o$), the extent of nuclear reorientation accompanying electron transfer (λ), and an electronic matrix element (H_{AB}) coupling reactants and products at the transition state (eq 3). The exponential term represents the nuclear factor; when $-\Delta G^o = \lambda$, the reaction is activationless and is limited by the electronic term.

$$k_{ET} = \left\{\frac{4\pi^3}{h^2\lambda RT}\right\}^{1/2} (H_{AB}^2) \exp\left\{\frac{-(\Delta G^o + \lambda)^2}{4\lambda RT}\right\} \qquad (3)$$

Thus, in order to compare the electronic couplings in the Ru-modified myoglobins, the nuclear term must be factored from the observed intramolecular ET rates. The driving force for the ^{3}ZnP*$\rightarrow$Ru^{3+} ET is 0.82 eV. A study of the driving-force dependence of the ET rates in metal-substituted Ru-modified His48 sperm whale myoglobin indicates that the reorganization in these processes is ~1.3 eV.[2b] The equivalent reactions in a_5Ru(His48) HuMb has been examined previously; $k_{ET(f)}$ and

$k_{ET(cr)}$ values were determined to be $7.2(7) \times 10^4$ and $1.1(1) \times 10^5$ s^{-1}, respectively.[13] Assuming a similar value of λ for the Ru-modified human myoglobins, values of k_{max} can be extracted using eq 1: 7.2×10^7 (His70, d = 9.5); 3.3×10^5 (His48, d = 12.7); and 1.8×10^3 s^{-1} (His83, d = 15.5 Å).

A plot of log k_{max} *vs.* d for the Ru-modified human and sperm whale myoglobins is shown in Figure 2.10. The best fit line through the sperm whale myoglobin data[2a,b] suggests an adiabatic rate limit (k_{max} at d = 3 Å) of 4.2×10^8 s^{-1} and a β (-2.303 × slope) of 0.79 $Å^{-1}$. In contrast, a fit through the HuMb data reveals a much higher value for β (1.7 $Å^{-1}$) and an adiabatic rate limit (6.7×10^{12} s^{-1}) close to theoretical predictions. This does not imply a difference in electronic properties between these two proteins. Instead, it is very likely that the sperm whale myoglobin data at long distances contain bimolecular contributions; recent kinetic measurements at very low protein concentration indicate that the intramolecular rates are indeed much lower than these reported values.[25] An upper limit of ~5 s^{-1} for the photoinduced ET rate in a_5Ru(His81)/ZnP HuMb would be consistent with the prediction of the best fit line through the HuMb data (Figure 2.10).[14]

A β of 1.7 $Å^{-1}$ for human myoglobins is significantly higher than those observed in synthetic D-A molecules[8] (0.85-0.9 $Å^{-1}$) indicating that the presence of non-covalent interactions lowers the electronic coupling through the medium. Beratan, Betts, and Onuchic[26] have surveyed a number of representative metalloproteins and proposed that the nature of the secondary and tertiary structures can dramatically influence the electronic transmission properties of these proteins. The decay-with-distance coefficient in the highly helical myoglobin was found to be one of the highest among the systems examined; a β comparable to the experimentally derived value (1.4 $Å^{-1}$) was suggested. A more comprehensive analysis of the D-A electronic couplings in these myoglobins as well as those in other proteins will be presented in Chapter 4.

CONCLUSION

We have successfully combined the use of site-directed mutaganesis and ruthenium modification to construct novel donor-acceptor complexes that will allow us to examine in a systematic manner the role of the protein in mediating the distant electronic couplings in a metalloprotein such as myoglobin. The pentaammineruthenium/zinc porphyrin derivatives of three recombinant myoglobins (His48, His70, and His83 HuMb) were prepared and the rate of photoinduced ET and thermal back reactions were measured by transient absorption spectroscopy. A β higher than those observed in covalent D-A molecules was obtained strongly indicative of reduced electronic coupling through non-covalent interactions within the protein medium.

REFERENCES

1. Marcus, R. A.; Sutin, N. *Biochim. Biophys. Acta* **1985**, *811*, 265.
2. (a) Axup, A. W.; Albin, M.; Mayo, S. L.; Crutchley, R. J.; Gray, H. B. *J. Am. Chem. Soc.* **1988**, *355*, 796. (b) Cowan, J. A.; Upmacis, R. K.; Beratan, D. N.; Onuchic, J. N.; Gray, H. B. *Ann. N. Y. Acad. Sci.* **1989**, *550*, 68. (c) Winkler, J. R.; Gray, H. B. *Chem. Rev.* **1992**, *92*, 369. (d) Wuttke, D. S.; Bjerrum, M. J.; Winkler, J. R.; Gray, H. B. *Science* **1992**, *256*, 1007. (e) Wuttke, D. S.; Bjerrum, M. J.; Chang, I.-J.; Winkler, J. R.; Gray, H. B. *Biochim. Biophys. Acta* **1992**, *1101*, 168.
3. (a) Geren, L.; Hahm, S.; Durham, B.; Millett, F. *Biochemistry* **1992**, *30*, 9450. (b) Willie, A.; Stayton, P. S.; Sligar, S. G.; Durham, B.; Millett, F. *Biochemistry* **1992**, *31*, 7237. (c) Scott, J. R.; Willie, A.; McLean, M.; Stayton, P. S.; Sligar, S. G.; Durham, B.; Millett, F. *J. Am. Chem. Soc.* **1993**, *115*, 6820.
4. (a) Durham, B.; Pan, L. P.; Long, J. E.; Millett, F. *Biochemistry* **1989**, *28*, 8659. (b) Hahm, S.; Durham, B.; Millett, F. *Biochemistry* **1992**, *31*, 3472.
5. Conrad, D. W.; Zhang, H.; Stewart, D. E.; Scott, R. A. *J. Am. Chem. Soc.* **1992**, *114*, 9909.
6. Cowan, J. A.; Gray, H. B. *Inorg. Chem.* **1989**, *28*, 2074.
7. Kuki, A.; Wolynes, P. G. *Science* **1987**, *236*, 1647.
8. (a) Moser, C. C.; Keske, J. M.; Warncke, K.; Farid, R. S.; Dutton, P. L. *Nature* **1992**, *355*, 796 and references cited therein. (b) Farid, R. S.; Moser, C. C.; Dutton, P. L. *Curr. Opin. Struct. Biol.* **1993**, *3*, 225 and references cited therein.
9. (a) Varadarajan, R.; Szabo, A.; Boxer, S. G. *Proc. Natl. Acad. Sci. USA* **1985**, *82*, 5681. (b) Varadarajan, R. Ph.D. Thesis, Stanford University, Palo Alto, CA, 1989.
10. (a) Hubbard, S. R.; Hendrickson, W. A.; Lambright, D. G.; Boxer, S. G. *J. Mol. Biol.* **1990**, *213*, 215. (b) Hubbard, S. R.; Hendrickson, W. A.; Lambright, D. G.; Boxer, S. G., unpublished results.

11. Dayhoff, M. O. *Atlas of Protein Sequence and Structure, Volume 5, Supplement 3*; National Biomedical Research Foundation: Silver Spring, MD, 1978; pp. 236-238.
12. Takano, T. *J. Mol. Biol.* **1977**, *110*, 537.
13. Zewert, T. E. Ph.D. Thesis, California Institue of Technology, Pasadena, CA, 1990.
14. Wong, L.-L.; Winkler, J. R.; Gray, H. B., unpublished results.
15. Hanahan, D.; Jessee, J.; Bloom, F. R. *Methods Enzymol.* **1991**, *204*, 63.
16. (a) Kunkel, T. A. *Proc. Natl. Acad. Sci. USA* **1985**, *82*, 488. (b) Kunkel, T. A.; Bebenek, K.; McClary, J. *Methods Enzymol.* **1991**, *204*, 125.
17. Instruction Manual, *In vitro*-Mutagenesis System, Oligonucleotide-directed version 2.1 (Cat. No. RPN.1523), Amersham Corporation, Arlington Heights, IL.
18. Maniatis, T.; Fritsch, E. F.; Sambrook, J. *Molecular Cloning: A Laboratory Manual*; Cold Spring Harbor Laboratory: Cold Spring Harbor, New York, 1982.
19. Sanger, F.; Nicklen, S.; Coulson, A. R. *Proc. Natl. Acad. Sci. USA* **1977**, *74*, 5463.
20. (a) Dower, W. J.; Miller, J. F.; Ragsdale, C. W. *Nucl. Acids Res.* **1988**, *16*, 6127. (b) Instruction Manual, Pulse Controller Apparatus (Literature Index 1433), Bio-Rad, Richmond, CA.
21. Garfin, D. E. *Methods Enzymol.* **1990**, *182*, 425.
22. (a) Teale, F. W. J. *Biochim. Biophys. Acta* **1959**, *35*, 543. (b) Yonetani, T. *J. Biol. Chem.* **1967**, *242*, 5008.
23. Nagai, K.; Thøgersen, H. C. *Nature* **1984**, *309*, 810.
24. Connors, K. A. *Chemical Kinetics: Study of Reaction Rates in Solution*; VCH: New York, New York; pp. 66-70.
25. Chang, I.-J.; Wong, L.-L., Winkler, J. R.; Gray, H. B., unpublished results.
26. Beratan, D. N.; Betts, J. N.; Onuchic, J. N. *Science* **1991**, *252*, 1285.

Figure 2.1. Superposition of the main chain atoms of human (bold line) and sperm whale (thin) metmyoglobin structures (r.m.s. difference of 0.78 Å). Shown are the hemes and the proximal histidine ligands; the water ligands were omitted.

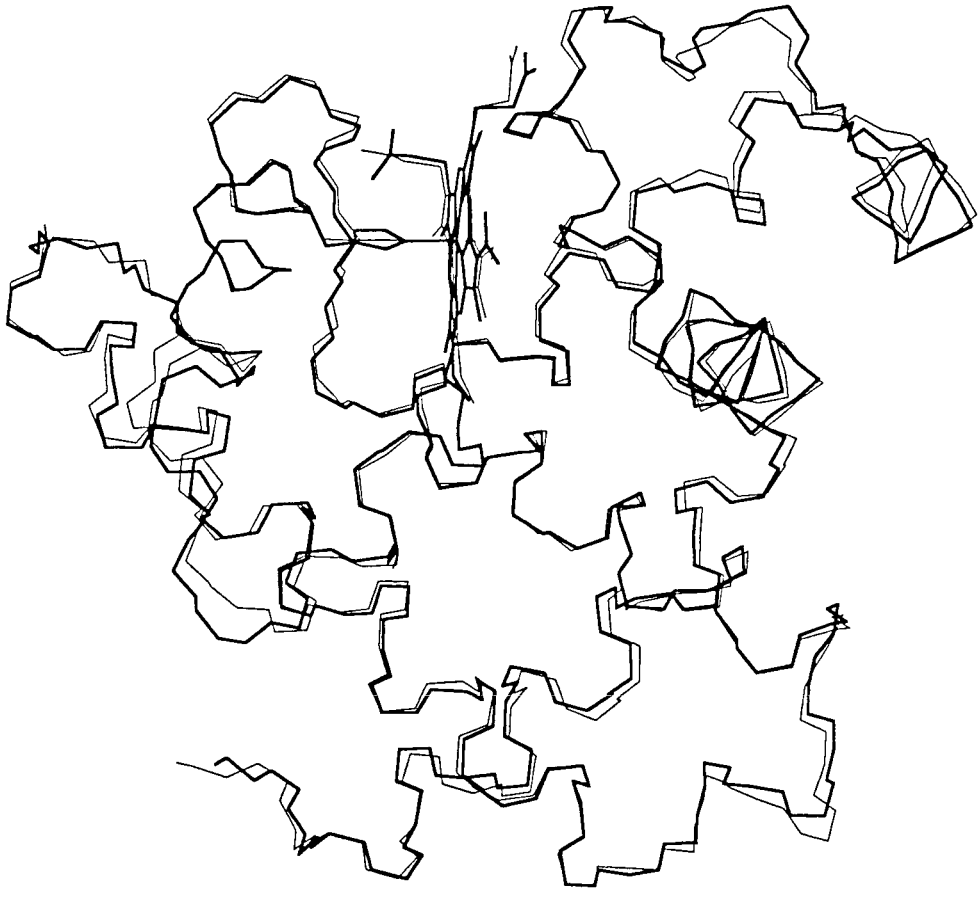

Figure 2.2. Computer-generated models of four Ru-modified histidines (His70 and His83 are genetically introduced; His48 and His81 are naturally occurring) of human myoglobin. ET kinetics in a_5Ru(His48)- and a_5Ru(His81)HuMb have been previously examined. The a_5Ru(His) moieties were modeled into the crystal structure of human myoglobin; the potential energies (van der Waals, electrostatic) of 400 conformers generated by rotating side-chain χ_1 and χ_2 dihedral angles were analyzed (using DREIDING force-field parameters which is part of the BIOGRAF modeling software). Distances represent the edge-to-edge separations based on the closest low-energy approach of the a_5Ru(HisX) group to the heme.

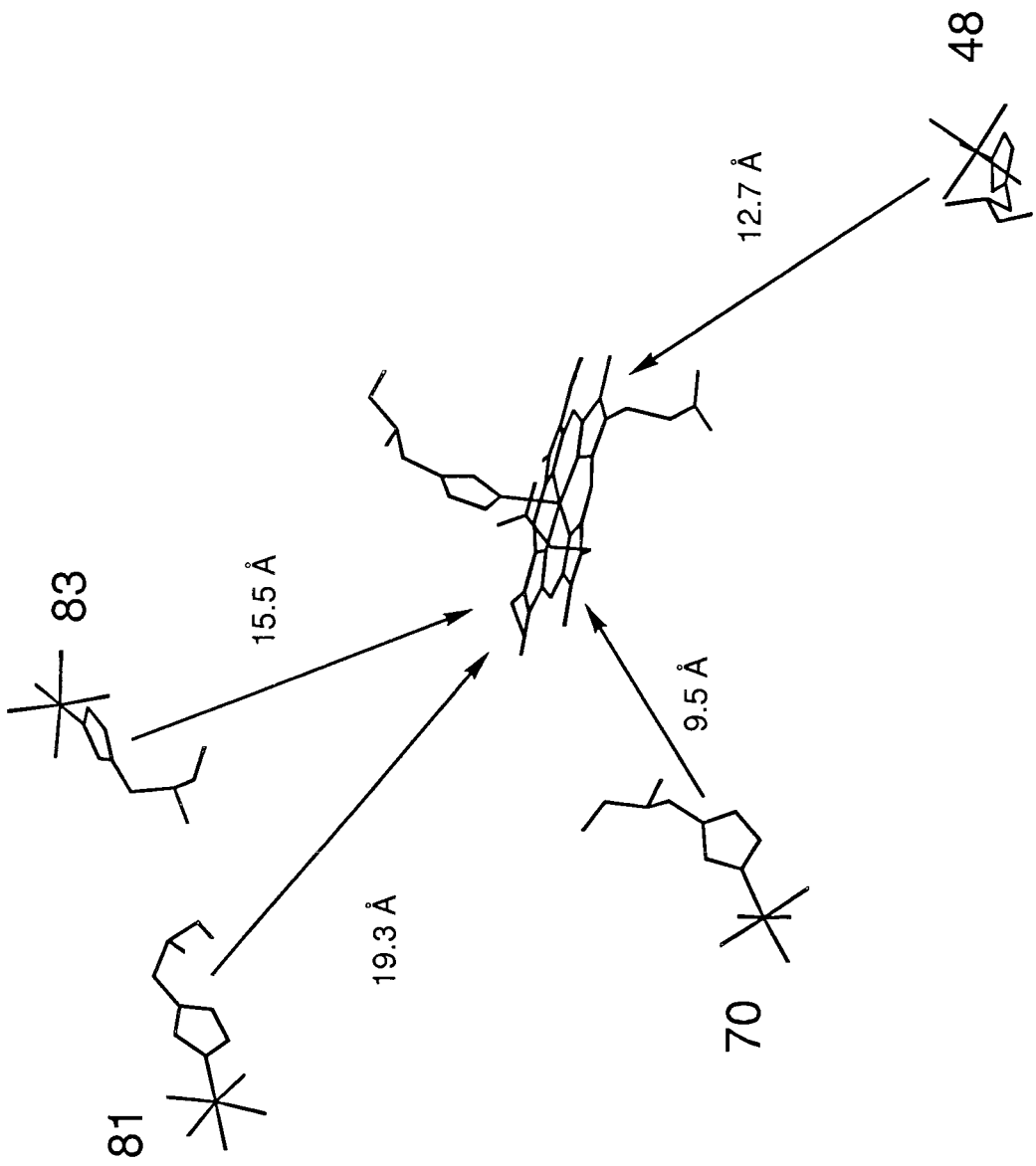
83
15.5 Å
81
19.3 Å
70
9.5 Å
48
12.7 Å

Figure 2.3. Construction of the M13mp19 plasmid containing the His48→Gln/His81→Gln/Cys110→Ala HuMb gene. The 243-bp *Bam*HI-*Afl*II fragment of pLcIIFXHuMb-H48Q/C110A and 505-bp *Afl*II-*Hin*dIII fragment of pLcIIFXHuMb-H48Q/C110A were cloned into the polylinker site of M13mp19.

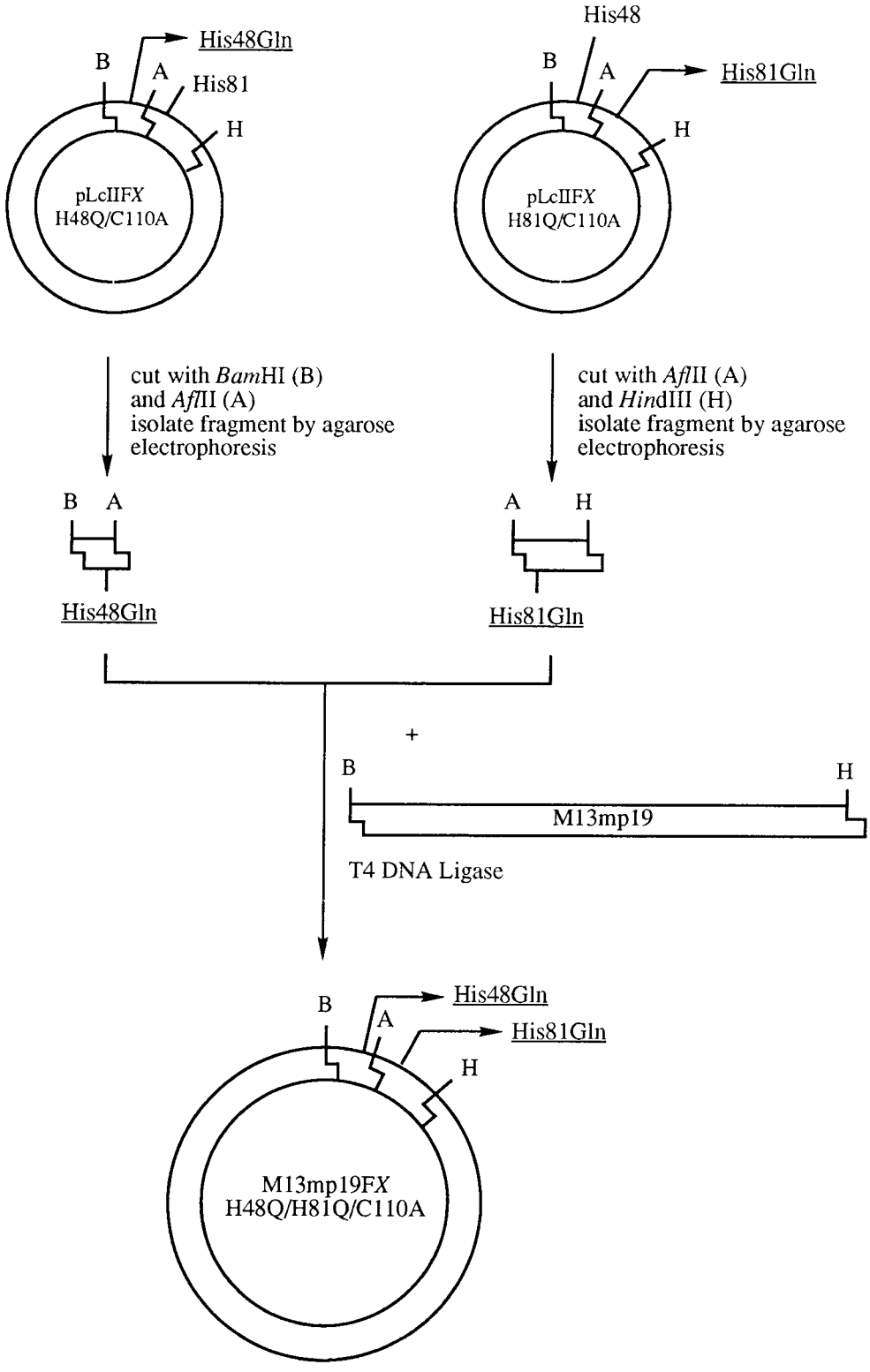
His48Gln
B
A
His81
H
pLcIIFX
H48Q/C110A
His48
B
A
His81Gln
H
pLcIIFX
H81Q/C110A
cut with BamHI (B)
and AflII (A)
isolate fragment by agarose
electrophoresis
cut with AflII (A)
and HindIII (H)
isolate fragment by agarose
electrophoresis
B A
His48Gln
A H
His81Gln
+
B
H
M13mp19
T4 DNA Ligase
B
His48Gln
A
His81Gln
H
M13mp19FX
H48Q/H81Q/C110A

Figure 2.4. Nucleotide sequence of the sense strand for the His70 HuMb gene. Shown are the mutations at and the regions around codons 48, 70, and 81. The presence of Cys110Ala mutation (not shown) was likewise confirmed.

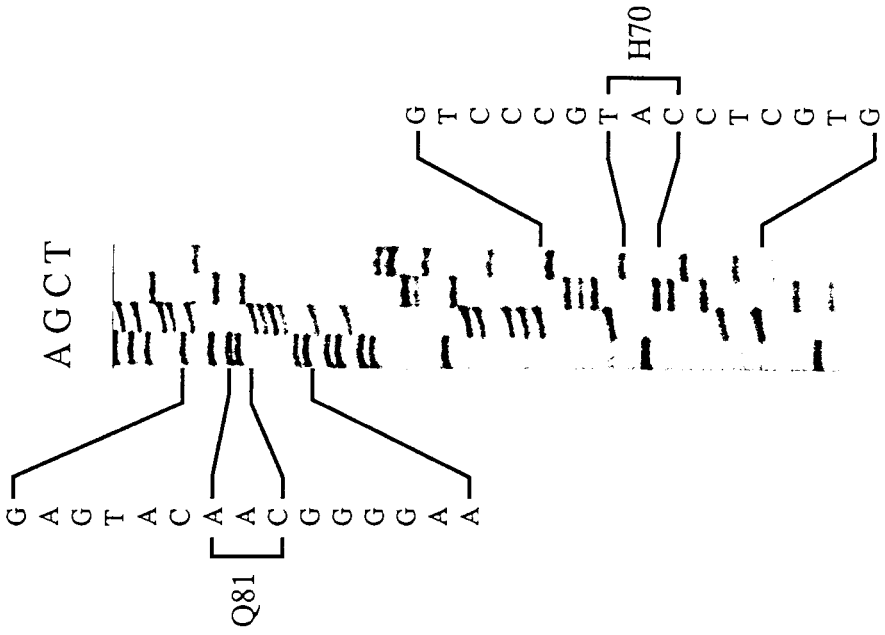
A G C T
G A G T A C A A C G G G G A A
Q81
G T C C C G T A C C T C G T G
H70

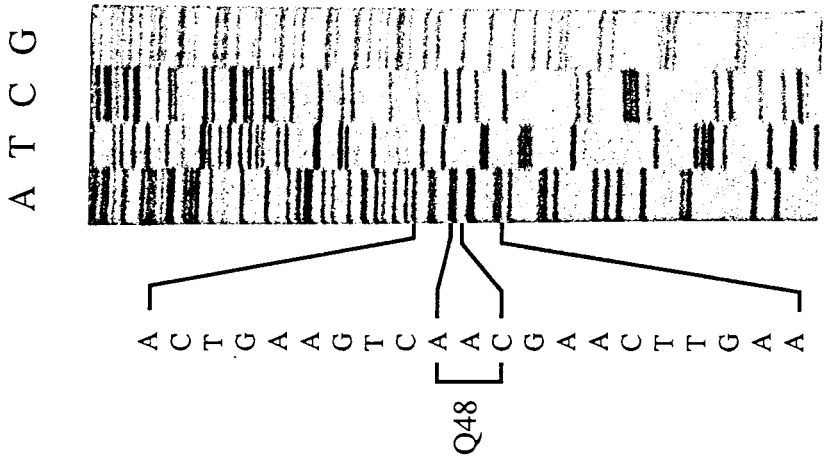
A T C G
A C T G A A G T C A A C G A A C T T G A A
Q48

Figure 2.5. System for human myoglobin expression. (**A**) Circular map of the pLcIIF*X*HuMb shuttle vector. By raising the incubation temperature to 42 °C, the plasmid directs the expression of a 21-kDa fusion protein consisting of 31 amino-terminal residues of λ *c*II, the factor X_a recognition site (F*X*), and HuMb. (**B**) PAGE-SDS gel of HuMb gene products. Lane 1, MW standards; lane 2, sperm whale myoglobin (Sigma); lane 3, total cellular proteins of *E. coli* harboring pLcIIF*X*-H70HuMb after temperature induction; lane 4, mature His70 HuMb protein after heme reconstitution and limited tryptic digestion; and lane 5, mature His83 HuMb holoprotein.

A

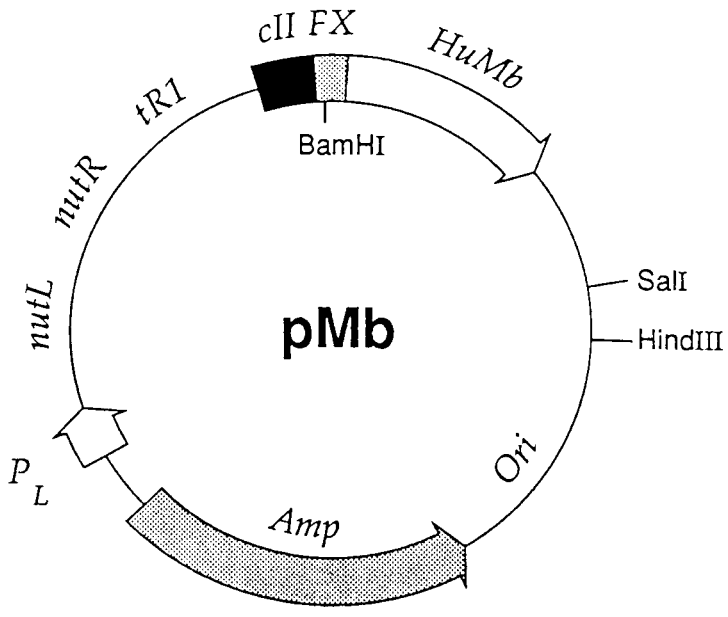
cII FX
HuMb
tR1
nutR
nutL
BamHI
SalI
HindIII
pMb
P_L
Amp
Ori

B

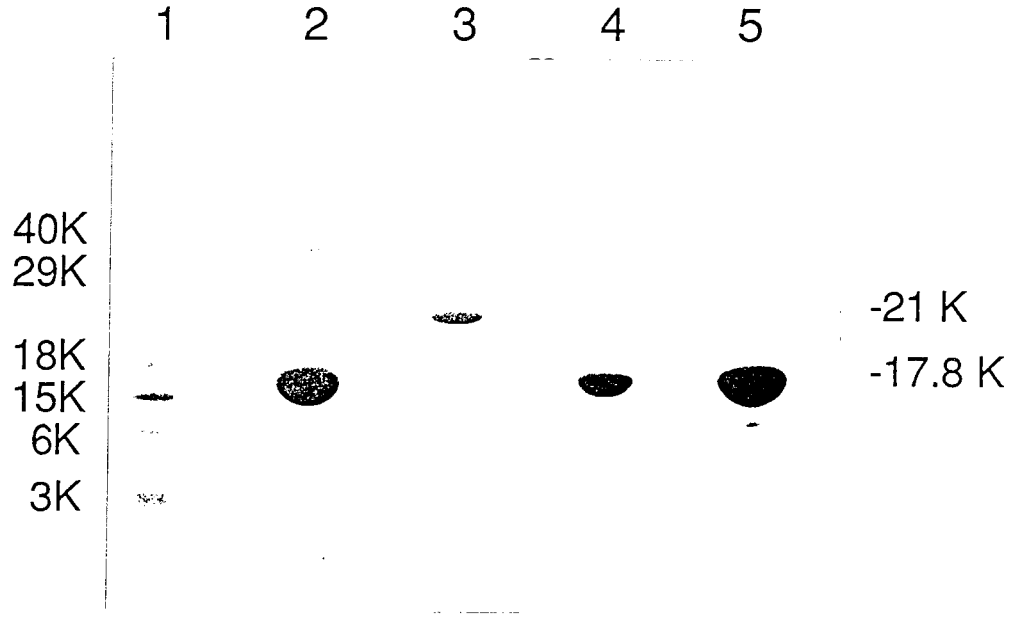
1
2
3
4
5
40K
29K
18K
15K
6K
3K
-21 K
-17.8 K

Figure 2.6. Cation-exchange chromatograms (Mono-S HR 10/10, Pharmacia FPLC) of the reaction products of mutant myoglobins with a_5Ru^{3+}: (**A**) His70; (**B**) His83 HuMb. In both cases, the unreacted mutant proteins elute close to the void volume, whereas the more positively charged 1:1 Ru:Fe products are retained on the column with varying degrees.

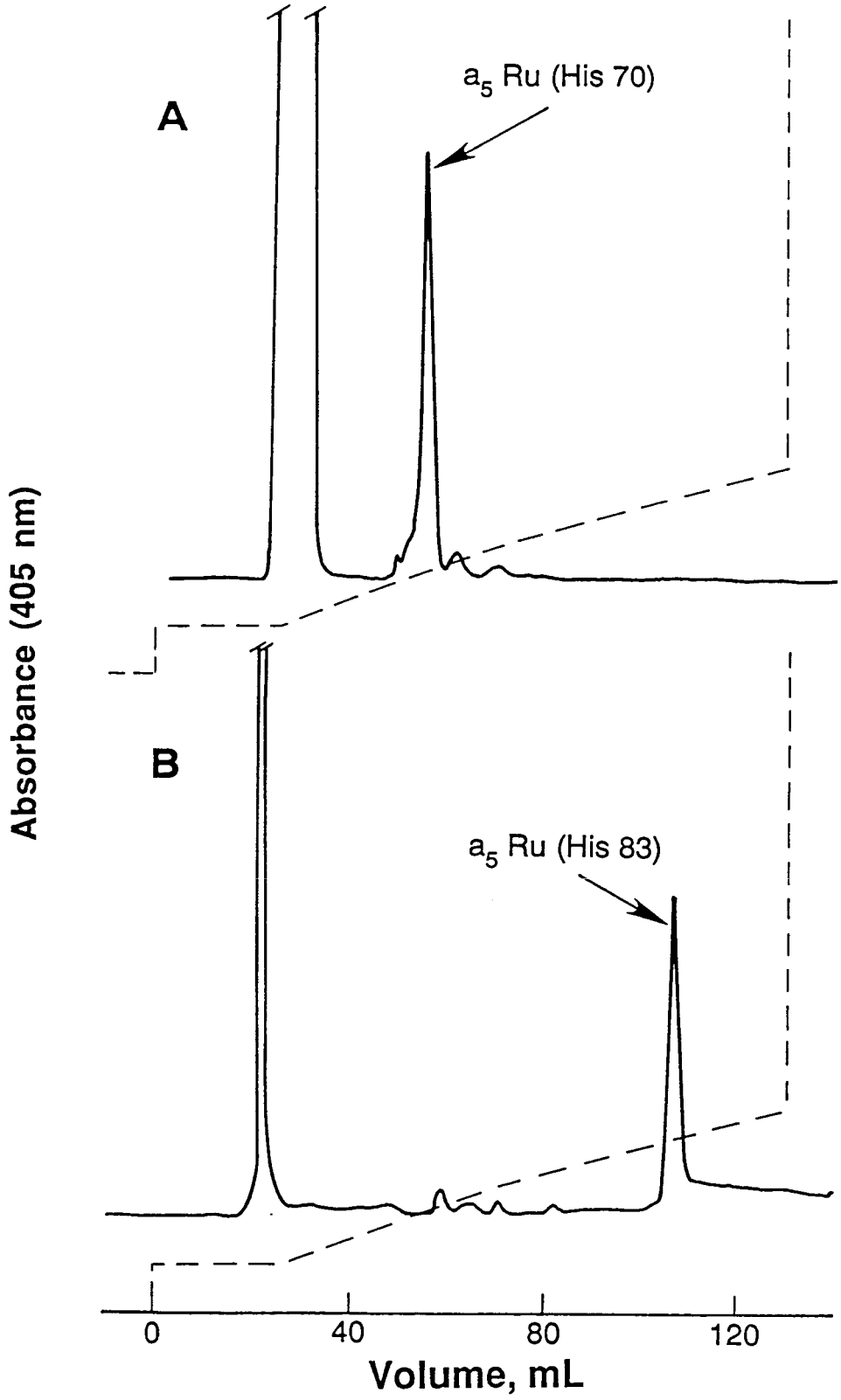
A
a_5 Ru (His 70)
B
a_5 Ru (His 83)
Absorbance (405 nm)
0
40
80
120
Volume, mL

Figure 2.7. Scheme for measuring intramolecular ET rates in a_5Ru/ZnP-modified myoglobins. The porphyrin is excited to a singlet state that decays efficiently by intersystem crossing (ic) to a lower-lying triplet state. Two pathways for ^{3}ZnP* deactivation are possible: a radiative process (k_d = 50 s^{-1}) and intramolecular ET to surface Ru^{3+} group. The latter is followed by a return to ground state *via* thermal charge recombination.

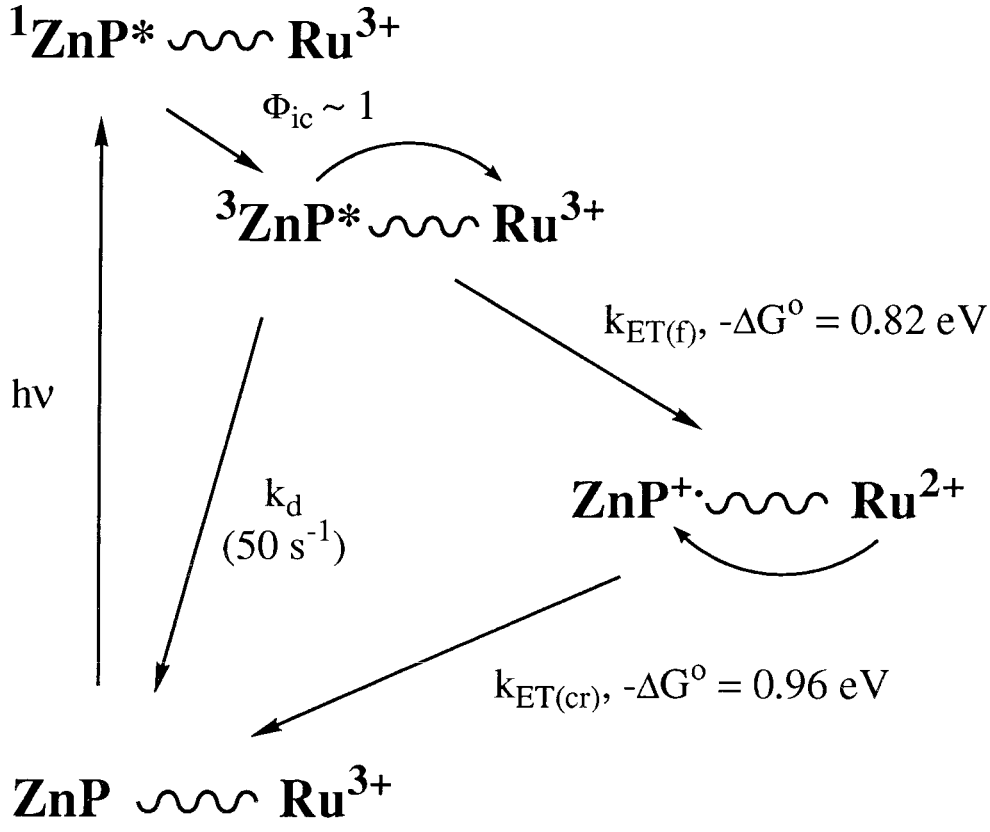
^{1}ZnP* ~~ Ru^{3+}
$\Phi_{ic} \sim 1$
^{3}ZnP* ~~ Ru^{3+}
$k_{ET(f)}$, $-\Delta G^o = 0.82$ eV
hν
k_d
(50 s^{-1})
ZnP$^{+\cdot}$ ~~ Ru^{2+}
$k_{ET(cr)}$, $-\Delta G^o = 0.96$ eV
ZnP ~~ Ru^{3+}

Figure 2.8. Transient absorbances at 450 nm (**A**) and 380 nm (**B**) of 5 μM a_5Ru(His70)/ZnP HuMb following a 10-ns, 532-nm excitation pulse. Smooth lines represent single-exponential fits to the data: (**A**) $\Delta A_{450} = -1.2 \times 10^{-3} + 1.8 \times 10^{-1} \exp(-1.6 \times 10^{7}\ s^{-1}\ t)$; (**B**) $\Delta A_{380} = -1.4 \times 10^{-3} + 1.1 \times 10^{-1} \exp(-1.6 \times 10^{7}\ s^{-1}\ t)$. The residuals are shown on top of each figure. The fast build-up component ($k_{ET(cr)}$) in **B** cannot be deconvoluted from the instrument response.

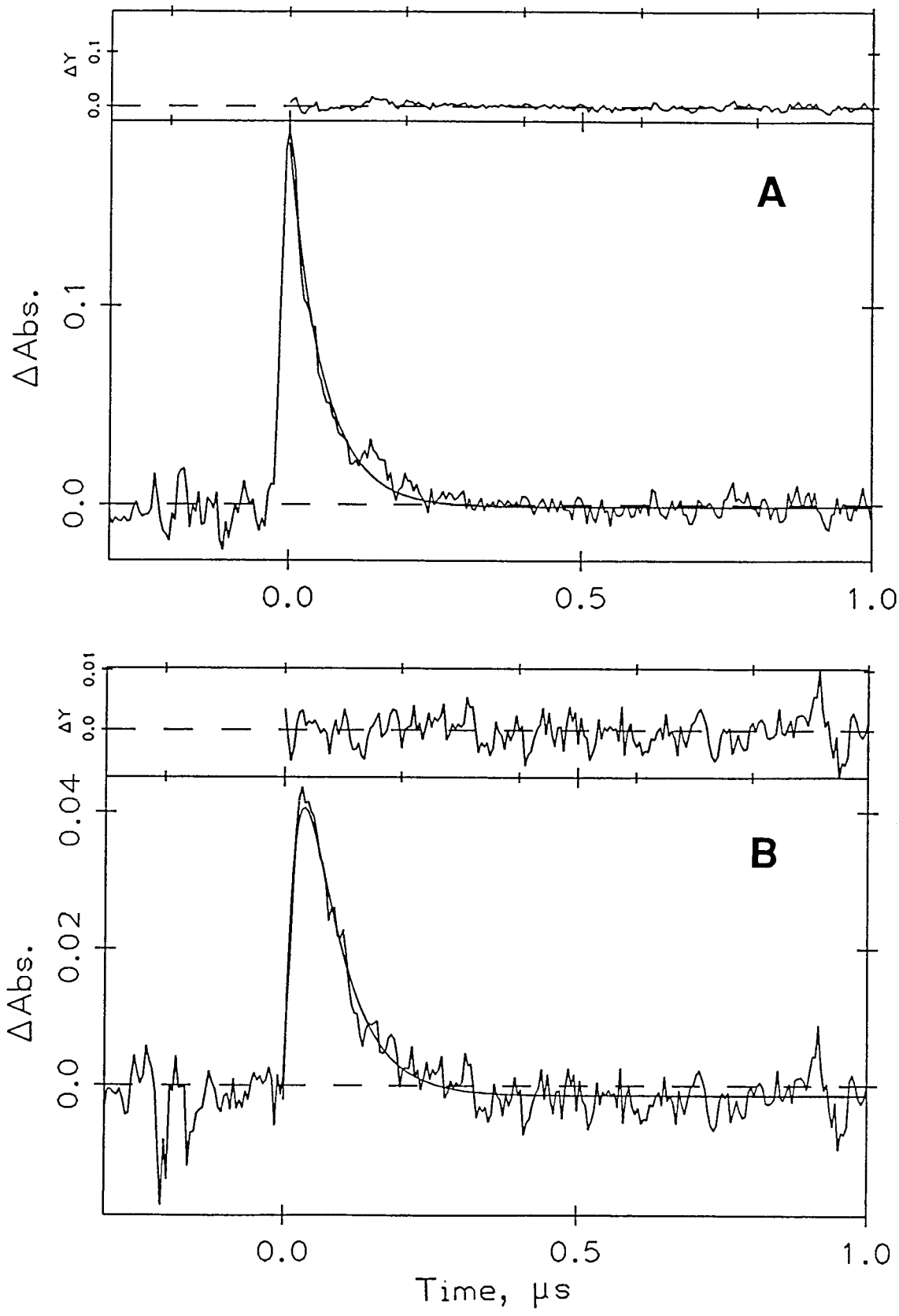
ΔY
0.1
0.0
A
ΔAbs.
0.1
0.0
0.0
0.5
1.0
ΔY
0.01
0.0
B
0.04
0.02
ΔAbs.
0.0
0.0
0.5
1.0
Time, μs

Figure 2.9. Transient absorbances at 450 nm (**A**) and 380 nm (**B**) of 2 μM a_5Ru(His83)/ZnP HuMb following a 10-ns, 532-nm excitation pulse. Smooth lines represent exponential fits to the data: (**A**) $\Delta A_{450} = 1.0 \times 10^{-3} + 2.6 \times 10^{-2} \exp(-4.5 \times 10^{2}\ s^{-1}\ t)$; (**B**) $\Delta A_{380} = 7.2 \times 10^{-4} + 3.5 \times 10^{-2} \exp(-4.5 \times 10^{2}\ s^{-1}\ t) - 3.2 \times 10^{-2} \exp(-7.3 \times 10^{2}\ s^{-1}\ t)$. The significance of the rate constant for each component in the trace is indicated.

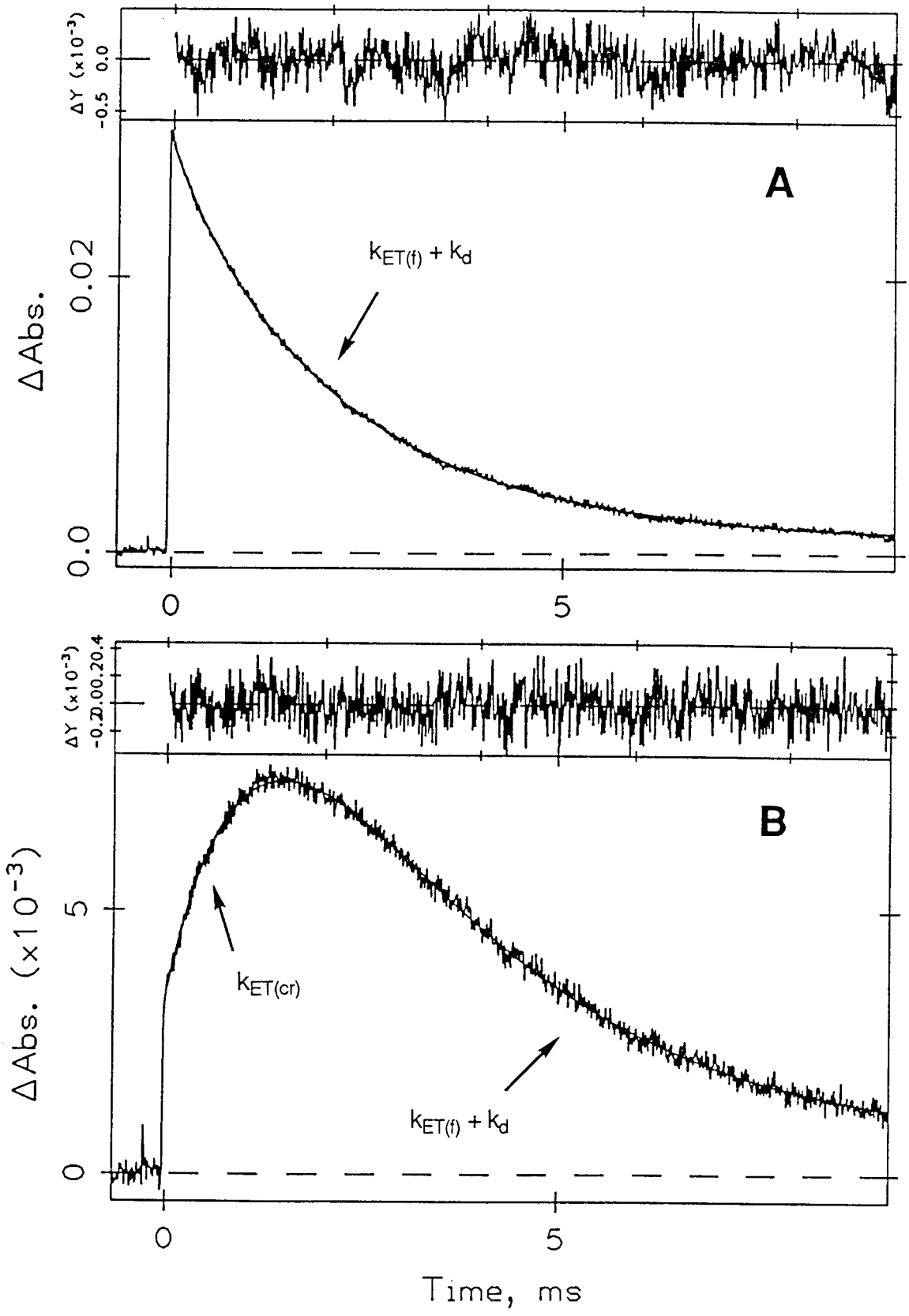
ΔY (x10⁻³)
-0.5 0.0
A
$k_{ET(f)} + k_d$
ΔAbs.
0.02
0.0
0
5
ΔY (x10⁻³)
-0.2 0.0 0.2 0.4
B
$k_{ET(cr)}$
$k_{ET(f)} + k_d$
ΔAbs. (x10⁻³)
5
0
0
5
Time, ms

Figure 2.10. Log k_{max} *vs.* edge-to-edge distance for the HuMb (Δ) and sperm whale (O) myoglobin systems. The solid lines are least-square fits to the different data sets.

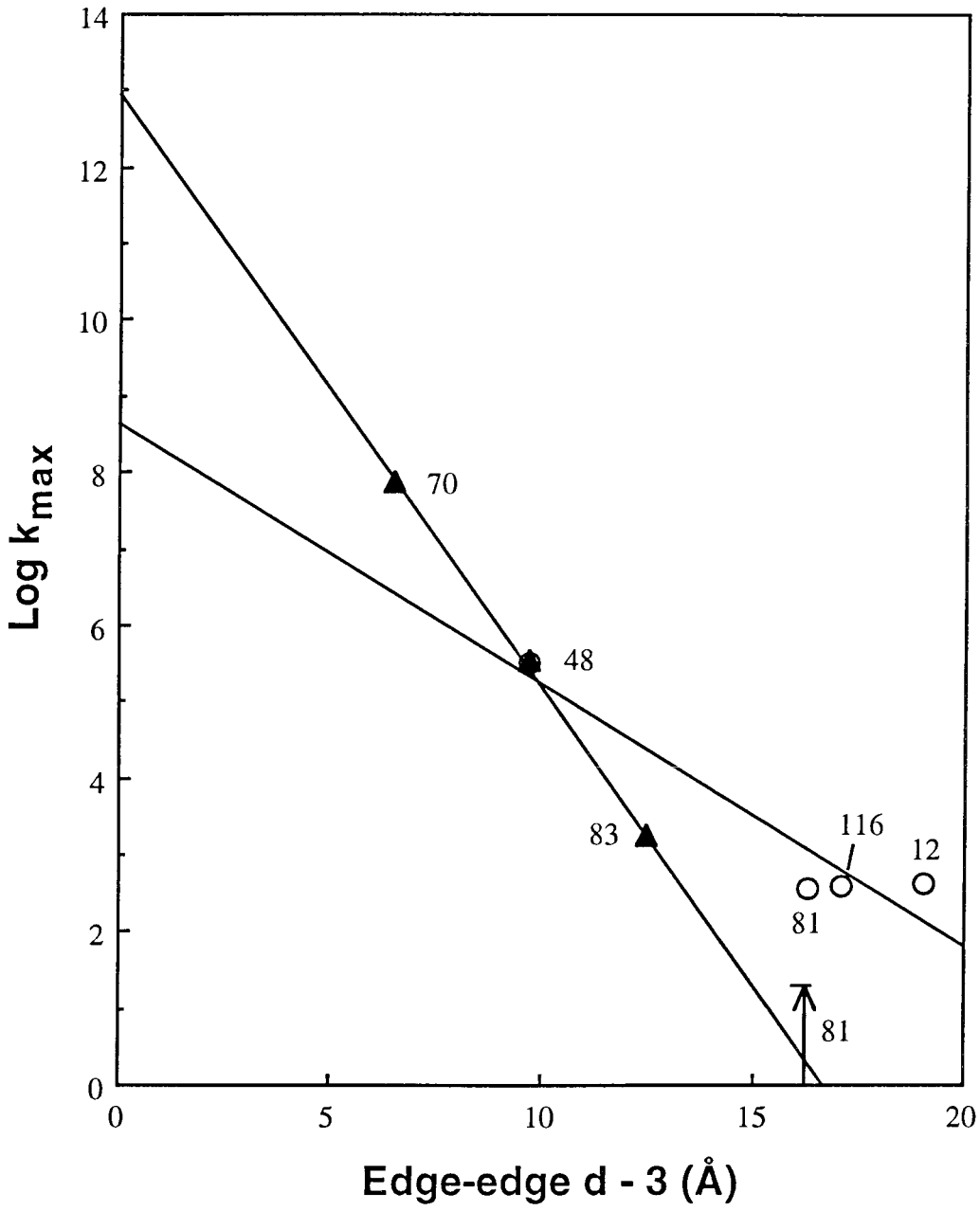
14
12
10
8
6
4
2
0
0
5
10
15
20
Log k_{max}
Edge-edge d - 3 (Å)
70
48
83
116
12
81
81

Chapter 3

Defining the Role of Aromatic Residues in Mediating Biological Electron Transfer. I: Construction, Characterization, and Electron-Transfer Studies of Ruthenium-Modified Recombinant Yeast Iso-1-cytochromes *c*.

[Part of the work described here is currently in press in the *J. Phys. Chem.* issue honoring Professor Gerhard L. Closs]

INTRODUCTION

In the previous chapter, we have studied a series of photoinduced ET reactions in myoglobin, a heme protein whose primary function is as an oxygen carrier in vertebrates. This chapter will focus on similar intramolecular reactions in a true ET protein, class I cytochrome *c* (cyt *c*).[1] The aim of the present work is to examine the distant electronic couplings in these two classes of metalloproteins in the hope of understanding the properties of an efficient ET system. Class I cytochromes *c* are small, monomeric, nuclear-encoded heme proteins (103-113 amino acids) that shuttle electron in the mitochondrial matrix.[1] The heme is covalently attached to the polypeptide chain *via* two thioether linkages to cysteine side chains (Cys14 and Cys17); this post-translational modification is catalyzed by a heme lyase upon mitochondrial translocation. Both oxidation states of the heme are characterized by a His/Met axial ligation to the iron. Because of their size and stability, mitochondrial cytochromes *c* represent one of the most widely studied electron-transfer proteins; they have been the benchmark for studies of cellular biosynthesis,[2] protein folding,[3] and protein electron transfer.[4-6]

Cyt *c* has been widely used for studying intramolecular ET reactions to and from synthetic redox groups attached to the surface of the protein.[4,5,6a-c] Our group has studied ET reactions between photoexcitable metal-substituted porphyrins and Ru ammine complexes at three different surface histidines of cyt *c* (His33 of horse heart cyt *c*; His39 of *Candida krusei* cyt *c*; genetically engineered His62 of yeast cyt *c*).[4a-c] The extracted donor-acceptor (D-A) couplings in these systems do not correlate with the predictions of a homogeneous barrier model. Several theories[7-10] have been developed to address how the heterogeneous character of a bridging medium may influence the electronic coupling between a donor and an acceptor site. In one such model, Beratan, Betts, and Onuchic[7] have invoked a σ-tunneling mechanism wherein structural units in the bridge such as H-bonds, σ bonds, and van der Waals contacts mediate ET. It is interesting that the rates for

Ru-modified cytochromes correlate remarkably well with a model that invokes bonding interactions of σ symmetry only.[4a,7] This raises the question of whether the presence of extended π system such as that of an aromatic side chain would affect the electronic coupling through the medium to a significant extent.

The issue of π-orbital participation in ET has been the subject of numerous experimental[11-13] and theoretical studies.[10,14] To address this matter, Ru-modified cytochromes will have to be constructed in which aromatic side chains (phe, tyr, trp) are along the path between the heme and the surface Ru; comparison with systems involving intervening aliphatic side chains should reveal any differential effects due to aromatic side chains. Our studies focus on iso-1-cytochrome *c* from *Saccharomyces cerevisiae*. This 103-amino acid protein is one of two isozymes of cytochrome *c* produced in yeast; intracellular levels of this protein is *ca.* 20-fold higher than that of isozyme-2. We have selected iso-1-cytochrome *c* for several reasons. First, the gene for iso-1-cytochrome *c* has been cloned and expressed at reasonable levels in *S. cerevisiae*.[15] Secondly, there now exists a wealth of biochemical and structural studies on the native protein as well as numerous genetic variants.[1b,16] Crystal structures of reduced[17a] and oxidized[17b] yeast iso-1-cytochrome *c* have been solved and refined to high resolution by Brayer *et al.*; the yeast protein exhibits a polypeptide fold typical of other class I cytochromes *c* (Figure 3.1).

In this chapter, I will discuss the construction of site-directed mutants of yeast iso-1-cytochromes *c* where in each case, a histidine is engineered at one of two surface positions (58 and 66). The paths to the heme from His66 and His58 contain Tyr67 and Trp59, respectively. Another site-directed mutant was constructed wherein the intervening Tyr67 in the His66 mutant was replaced with a phenylalanine. Each of these mutants was modified with two photoexcitable Ru polypyridine complexes to examine the rates of ET at different driving forces; ET reactions between the Ru complex and the

protein center were examined using a laser flash-quench strategy.[18a] While a_5Ru/ZnP (a = NH_3, ZnP = zinc porphyrin) modification of these cytochrome mutants would be ideal for direct comparison with the modified myoglobins presented in the previous chapter, protocols for ZnP substitution in yeast cytochrome *c* have led to extremely poor yields and are therefore impractical.

Yeast iso-1-cytochrome *c* has three naturally occurring non-heme-ligand histidines - His26, His33, and His39. The ET reactions between the heme and Ru complexes bound to His39 were examined. Based on the crystal structure, the path to the heme from this histidine consists of aliphatic side chains. Comparisons will also be drawn with other cytochromes that have been previously modified with the same Ru polypyridine complexes and whose ET reactions have been examined.[18]

MATERIALS AND METHODS

Design of Histidine Mutants

The crystal coordinates of reduced iso-1-cytochrome *c* and the Tyr67→Phe variant were kindly provided by Albert M. Berghuis and Gary D. Brayer (University of British Columbia). The structures were displayed and analyzed on an Evans and Sutherland PS390 terminal using BIOGRAF software (Molecular Simulations, Inc.). The aim of the search is to determine appropriate sites on the protein surface to incorporate a Ru-modifiable histidine for which the bridging medium to the heme contains an aromatic side chain. The first part of the search is to select an interior aromatic side that will satisfy the following criteria: low thermal motion and high sequence variability. The former is to minimize physical fluctuations in the bridge and prevent the possibility of 'conformationally gated' ET reaction. Information regarding thermal flexibility are derived from crystallographic temperature factors and NMR peak characteristics. The second part of the search is to determine a nearby surface site for which the aromatic side

chain is in the direct line-of-flight of the electron to the heme. Whether the surface residue can tolerate a histidine mutation is evaluated on the basis of sequence variability in the phylogenetic series and previous mutational studies. Analysis of the structure suggests two possible sites for histidine incorporation - positions 58 and 66. In the case of His58 mutant, a tryptophan (at position 59) is in the ET path. The bridging tyrosine (position 67) in the His66 variant also is replaced with a phylogenetically allowed phenylalanine.[1]

Preparation of Uracil-containing Template

A 2.5-kb *Bam*HI/*Hin*dIII fragment containing the Cys102→Ser/His39→Gln iso-1-cytochrome *c* gene (*CYC1*, see Appendix B for complete sequence) was cloned into M13mp18 plasmid in the following manner. 12 μg of 9.7-kb M13mp8*CYC1*-C102S/H39Q vector constructed previously by S. L. Mayo[19] were digested with *Bam*HI (4 μl 10 units/μL) and *Hin*dIII (4 μl 10 units/μL) in 80 μL 1 × B (low magnesium) buffer (Boehringer Mannheim), 4 h, 37 °C. The restriction enzymes were extracted 3× from the solution with TE-equilibrated (TE = 10 mM Tris, 1 mM EDTA, pH 8.0) 1:1 $CHCl_3$:phenol. Dissolved organic solvents were extracted from the DNA solution with diethyl ether. The DNA digests were then precipitated by (1) adding 1/10 volume 3 M sodium acetate, pH 5.2, and two volumes of ice-cold ethanol, (2) incubating at -20 °C overnight (at least 6 h), and (3) microcentrifugation for 30 mins at 4 °C. The supernatant was discarded and the pellet redissolved in 120 μL TE (DNA concentration ~ 0.1 μg/μL). 12 μg M13mp18 double-stranded or replicative form (RF) were digested in the same manner.

Ligation of the 2.5-kb *Bam*HI/*Hin*dIII fragment containing the Cys102→Ser/His39→Gln *CYC1* into M13mp18 RF were performed at 16 °C for 16 h and with a 5:1 insert-to-plasmid molar ratio: 6 μL, M13mp8*CYC1*-C102S/H39Q digests; 1 μL, M13mp18 RF digests; 1 μL, ligase (1 unit/μL); 2 μL, 10 × ligase buffer; and ddH_2O to

make 20 μL solution. At the completion of the reaction, the mixture was heated to 55 °C for 2 min to inactivate the enzyme and diluted with 80 μL of 1/10 TE to give a final concentration of ~80 ng/μL. 300 μL of competent *E. coli* MK303 strain (prepared following a modified Hanahan protocol[20]) were transformed with varying amounts of the ligation mixture (1, 5, and 15 μL). The MK303 strain selects only for M13mp18-derived plasmid; M13mp8 contains an amber mutation[21] that impairs its ability to propagate in the non-suppressor MK303 strain. The cells were plated on IPTG/Xgal-supplemented H medium; the recombinant clones were identified as clear plaques, whereas the nonrecombinant plaques were stained blue. Large-scale preparation of the replicative form from a positive clone was performed by transfecting 200 mL log-phase *E. coli* MK303 with the phage particles. The DNA was purified by equilibrium centrifugation in CsCl. The insert was confirmed by digestion with *Bam*HI and *Hin*dIII and fragment analysis by agarose gel electrophoresis.

A uracil-containing copy of this hybrid vector was prepared following the procedure described in pp. 48-49. The *dut⁻ ung⁻ E. coli* strain used for this experiment was BW313 (*dut ung thi-1 relA spoT1* F' (*lysA*)); it differs from CJ236 in that it lacks the F'-localized chloramphenicol marker. Thus, all growth media did not contain the antibiotic.

Oligonucleotide-directed Mutagenesis

Site-directed mutagenesis experiments followed the method developed by Kunkel and which was described in great details in pp. 49-50. The mutagenic oligonucleotides employed for these experiments are 18-23 base long and are listed below.

Leu58→His	5'- T T T C G T C C C A G* T* G* C A C G T T T T T C -3'
Glu66→His	5'- T A G T C A A G T A G* T G* T G A C A T G T T A -3'
Tyr67→Phe (Glu66→His)	5'- T A G T C A A G A* A G T G T G A C A -3'

The target codons are underlined; the mismatched bases are marked with asterisks. The Tyr67→Phe oligonucleotide was annealed unto a template containing the Glu66→His mutation in *CYC1*. Complete DNA sequences of the mutated *CYC1* genes in the single-stranded templates were determined by Sanger dideoxy method.[22]

Gene Expression

The M13mp18*CYC1* RF DNAs were isolated from 200 mL of infected TG1 (or MV1190) and purified by CsCl ultracentrifugation.[23] The 2.5-kb *Bam*HI/*Hin*dIII *CYC1*-containing fragment was cloned into tetracycline gene of YEp213 (*amp*^{r} *tet*^{r} *leu2*$^+$) in the same manner as the fragment was originally cloned into M13mp18. Recipe for ligation reaction (16 h, 16 °C) was as follows: 6.6 μL 0.1 μg/μL M13mp18*CYC1* RF digests; 1.4 μL 0.1 μg/μL YEp213 digests; 2 μL 10 × ligase buffer; 1 μL ligase (1 unit/μL); and ddH_2O to make 20 μL. 300 μL of chemically prepared competent HB101 (F$^-$ *hsdS20* (r_B^-, m_B^-) *recA13 ara-14 proA2 lacY1 galK2 rpsL20* (Sm^r) *xyl-5 mtl-1 supE44* λ^-) were transformed with varying amounts of the ligation mixture. Positive clones were selected by replica plating for ampicillin resistance and tetracycline sensitivity. Large-scale preparation of the YEp213*CYC1* plasmid from a mutant clone was performed by alkaline lysis method and equilibrium ultracentrifugation in CsCl. The insert was verified by restriction analysis.

There are several methods for yeast transformation, but the electroporation protocol described by Guarente proved to be most reliable.[24] 100 mL of *S. cerevisiae* GM3C2 (α *leu2-3 leu2-112 trp1-1 his4-519 cyc1-1 cyp3-1*) in YPD (10 g/L yeast extract, 20 g/L Bacto-peptone, 20 g/L dextrose) were grown at 30 °C to an OD_{600} of 1.3. The cells were spun down (GSA rotor, 250-mL bottle, 4 °C, 5.5k rpm, 5 min) and the supernate discarded. The cells were resuspended in 100 mL ice-cold ddH_2O with gentle pipetting motion and spun down as before. The cells were resuspended in 50 mL of ice-cold ddH_2O and spun down (SS34 rotor, 2.5 rpm, 5 min, 4 °C). The supernate was

discarded and cells were resuspended in 8 mL ice-cold 1 M sorbitol. They were transferred into a 50-mL disposable sterile tube and were spun down in Beckman TJ-6 benchtop centrifuge (2.5k rpm, 4 °C, 5 min). The supernate was discarded and the cells were resuspended in 0.2 mL 1 M ice-cold sorbitol. 40 μL of the cell suspension, 1-10 μg of YEp213*CYC1* plasmid were added (in no more than 3 μL TE solution) and the suspension were dispensed into 0.2-cm electroporation cuvettes. Each cuvette was transferred into the chamber of a Bio-Rad Gene Pulser apparatus and a short electrical pulse was applied (1.5 kV, 25 μF, 200 Ω). A time constant of 4.5 or higher must be obtained for optimum efficiency. 1 mL ice-cold 1 M sorbitol was immediately added to each suspension and the suspension was plated on SD medium (1 M sorbitol, 6.8 g/L Bacto-yeast nitrogen base, 20 g/L dextrose, 20 g/L Bacto-agar, 60 mg/L each of L-tryptophan and L-histidine). Sorbitol is added to the plate media to serve as an osmotic stabilizer. The plates were incubated at 30 °C for 5-7 days. The colonies were replated on YPG (10 g/L yeast extract, 20 g/L Bacto-peptone, 30 mL/L glycerol) to test for iso-1-cytochrome *c* expression.

Protein Purification

The proteins were prepared from 170-L fermentation of the yeast hosts in YPG (supplemented with 50 μg/mL ampicillin to prevent bacterial contamination) as described by Smith and coworkers.[15b] The proteins were extracted by stirring the cells in 1:1 v/w of 1 M NaCl and 0.5:1 v/w ethyl acetate for 36 h at 4 °C. The suspension was centrifuged (GSA rotor, 5k rpm, 40 min, 4 °C) and the pellet was discarded. The supernate was brought to 50% saturation with $(NH_4)_2SO_4$ (314 g/L of supernate). The resulting precipitate was pelleted by centrifugation. The supernate was filtered through a fritted-disc funnel (coarse porosity) and dialyzed at least 3× against 10 volumes of 12.5 mM NaP_i, 1 mM EDTA, 2 mM 2-mercaptoethanol, pH 7.0. The contents of the dialysis bags were pooled and to it were added 500 mL of Fast-flow CM52 Sepharose resin

(Pharmacia) prewashed with 50 mM NaP_i, pH 7.0, 1mM EDTA. The protein was made to bind to the resin by stirring the suspension at 4 °C for at least 2 h. The pink-colored resin was loaded into a 5.0 cm I.D. × 30 cm Econo-column (Bio-Rad) and washed with at least 1 column volume of 50 mM NaP_i, pH 7.0, 1mM EDTA. The protein was eluted with 2 column volumes of 0-1 M NaCl gradient in 50 mM NaP_i, pH 7.0, 1mM EDTA. The proteins were oxidized by adding Na[Co(EDTA)] or $[Co(phen)_3]Cl_3$ (phen = 1,10-phenanthroline). Final purification was achieved by cation-exchange chromatography on a Mono-S HR 16/10 column fitted to a Pharmacia FPLC system. The cytochromes were loaded in μ 50 mM NaP_i, pH 7.0, and eluted with 1.0 M NaCl in the same buffer using a programmed gradient. The mutant cytochromes eluted between 0.3 and 0.4 M NaCl. The purity of the each mutant protein was analyzed by SDS/PAGE.

Spectroscopic Characterization

UV/vis spectra of the purified mutant proteins in μ 100 mM NaP_i, pH 7.0, were taken using a Cary 14 spectrophotometer (Olis). Using a Jasco J600 polarimeter, circular dichroism (CD) spectra in the far-UV region (200-250 nm) were collected of ~100 μM ferricytochrome solutions (in μ 100 mM NaP_i, pH 7.0) in a 0.01-cm cell. An average of 10 scans was taken for each spectrum. In separate experiments, the mid-point melting temperatures of the mutant ferricytochromes were determined by monitoring the loss of the protein ellipticity at 222 nm with increasing temperature. 10 μM protein solutions in μ 100 mM NaP_i, pH 7.0, were employed for these experiments. Readings were collected in the time mode of J600 version 2.0 programmer as the temperature of the 0.10-cm water-jacketed cell containing the protein solution was adjusted from 25 to 80 °C with a Lauda 2KR thermostat (Brinkman Instruments). The data collected over this temperature range were analyzed in terms of a two-state transition model.[25]

Electrochemical Measurements

Direct electrochemistry of 0.4-0.6 mM protein solutions in μ 100 mM NaP_i, pH 7.0, was performed using an 8-mm gold disk electrode (Pine Instruments) modified with 4,4'-dipyridyl disulfide (Aldrich).[26] Before use, the electrode was dipped in a saturated solution of the promoter for 2 min and washed extensively with water. Cyclic voltammetry was carried out at 25 °C with a Ag/AgCl/KCl(saturated) reference electrode (Ingold Products) and a platinum counter electrode. The potential was controlled by a Princeton Applied Research potentiostat and the current output was recorded on a Houston Instruments X-Y recorder. A potential range of 50-400 mV (vs. NHE) was swept at 5 mV/s.

Ruthenium Modification

Covalent attachment of bis(2,2'-bipyridine)imidazoleruthenium(II) ($Ru(bpy)_2(im)^{2+}$) or bis(4,4'-dimethyl-2,2'-bipyridine)imidazoleruthenium(II) ($Ru(dmbpy)_2(im)^{2+}$) complex to the surface histidine was performed with minor modifications of a published procedure.[6b] All preparations and manipulations of the modified proteins were conducted with the exclusion of room light. $Ru(bpy)_2(CO_3)$ or $Ru(dmbpy)_2(CO_3)$ (courtesy of I-Jy Chang and Morten Bjerrum) was added in ten-fold excess to 0.2 mM protein solutions in μ 100 mM NaP_i, pH 7.0, and the reactions were carried out under an argon atmosphere. Subsequent reactions with imidazole involved passing the protein through Sephadex G-25 pre-equilibrated with 0.7 M imidazole, pH 7.8, eluting the proteins with the same imidazole buffer, and leaving the protein solutions under argon for 36 h at 25 °C. Excess imidazole was removed by gel-filtration chromatography. The samples were then loaded onto a Mono-S HR 16/10 column and the proteins were eluted with a slow 0-1M NaCl gradient in μ 50 mM NaP_i, pH 7.0. A 1:1 ruthenium:protein adduct was indicated by a 2:3 ratio of the 290- (largely bipyridine $\pi \rightarrow \pi^*$) to 410-nm (Soret) absorbance.[6b] Fractions containing the 1:1 Ru:Fe products

were collected, pooled, and run repeatedly using the same ion-exchange separation procedure until the bands were completely resolved.

Tryptic Analyses

The native and modified proteins were concentrated to 2 mg/mL in 0.1 M NH_4HCO_3, pH 8.0. A 2 mg/mL stock solution of trypsin was prepared in 1 mM HCl. 20 μL of the trypsin solution were initially added for every 1 mL of the protein solution and the reaction was carried out at 25 °C. Another 20 μL of trypsin (type XIII, Sigma) were added after 6 h and the reaction was allowed to proceed for another 14 h. The reactions were quenched by flash-freezing the solution in ethanol/dry ice and lyophilizing the samples. The lyophilized tryptic fragments were dissolved in 0.1% aqueous solution of TFA and loaded in two portions onto a reversed-phase PepRPC HR 5/5 column (Pharmacia) fitted to a Pharmacia FPLC system. The fragments were eluted with 0.1% TFA in acetonitrile using a linear gradient up to 40% v/v of the eluent. For the first run, the fragments were monitored with a 280-nm wavelength filter; for the second run, a 405-nm detector was used instead. The spectrum resulting from the latter should shed light on the extent of tryptic digestion; complete digestion is suggested by the presence of only one heme-containing band. The tryptic fragment containing the ruthenium label was collected and the purity of the fraction was confirmed by capillary zone electrophoresis (Applied Biosystems Model 270A) with 2.5 mM NaP_i buffer, pH 2.5, as the eluent and with 30 kV of applied voltage. The peptides were sequenced via automated Edman degradation[27] on an Applied Biosystems 473A sequencer; 1-3 nmol of the peptide were typically required for analysis.

Spectroscopic Characterization

The far-UV CD and UV/vis absorption spectra of the Ru-modified proteins were recorded as before. 0.2 mM protein solutions in a 0.10-cm cell were employed to obtain

the near-UV CD spectra (250-350 nm). Electronic emission spectra of the modified proteins were recorded on an in-house emission spectrometer; samples were excited with the 436 line of Hanovia 200 watt Hg/Xe lamp. Sample emission perpendicular to the excitation light was collected into a SPEX spectrometer and digitally recorded using an in-house software.

Electrochemical Measurements

The heme potentials of the Ru-modified proteins were determined following the same protocol as that for the unmodified proteins. The cyclic voltammetric scans were also extended to the high potential range in order to determine the $Ru^{3+/2+}$ potentials; however, the only signal detected was that arising from solvent oxidation. It becomes apparent that we need to resort to more sensitive pulse techniques and higher protein concentrations.

Because large-scale preparations of the Ru derivatives of all recombinant proteins is at this stage prohibitive, we have decided to focus our efforts on three representative systems that are most readily accessible. They are: (1) $(Ru(bpy)_2(im)(His66Phe67)$cyt *c* (yeast); (2) $Ru(bpy)_2(im)(His33)$cyt *c* (horse heart); and (3) $Ru(dmbpy)_2(im)(His33)$cyt *c* (horse heart). 10-30 mg of each of these modified proteins were prepared and purified following standard protocols. The protein solutions were concentrated to 1-3 mM in μ 100 mM NaP_i, pH 7.0 (*ca.* 1 mL solution). For the electrochemical studies, a non-isothermal configuration was used. The sample compartment is soaked in a variable-temperature bath; a salt bridge provides electrical contact between this compartment and a SCE reference electrode immersed in a saturated KCl room-temperature bath. A 5-mm pyrolytic edge-plane graphite electrode (PGE) and a platinum counter electrode were immersed in the protein solution. The $Ru^{3+/2+}$ potentials were determined by Osteryoung square wave voltammetry.[28] With the use of BAS-100 analyzer, a potential range of 0.3-

1.0 V vs. SCE was scanned with a step height of 2 mV, a square wave amplitude of 25 mV, and a frequency of 5 Hz (Figure 3.2).

ET Rate Measurements[18a]

The Ru-modified proteins were reduced with excess dithionite and desalted through Sephadex G-25. 20 μM solutions of reduced proteins in μ 100 mM NaP_i, pH 7.0, 7 mM hexaammineruthenium(III), were prepared, deoxygenated, and equilibrated under argon in vacuum cells with 1-cm fluorescence cuvette side arms. In the case methylviologen is employed as the oxidative quencher, the protein and quencher were prepared to concentrations of 6-12 μM and 10 mM, respectively. The samples were excited with 2 mJ, 20-ns pulses (480 nm) generated by a XeCl excimer-pumped dye laser (Lambda Physik LPX 210i, FL-3002). Sample emission was recorded at 670 nm and transient absorptions at 306, 400, 504, and 550 nm were collected. Kinetic traces represent an average of at least 1000 laser shots. The kinetic data were analyzed using DECON and/or KINFIT software, depending on the reaction time scale. UV/vis spectra of the samples were taken before and after the kinetics measurements to test for protein degradation.

RESULTS AND DISCUSSION

Design of D-A Systems

Yeast iso-1-cytochrome *c* contains 4 phenylalanines, 5 tyrosines, and a tryptophan. Of these, mobility (ring flip rates) is low for Phe10, Tyr46, Tyr48, Tyr67, Tyr97 and Trp59.[29] Among these, only Tyr46, Tyr48, Tyr67, and Trp59 are sufficiently buried in the protein in order to form part of ET bridges to the heme. Trp59 provides a suitable bridge for ET to or from the heme; the indole NH group is hydrogen-bonded to a heme propionate. In order to probe ET reaction through Trp59, Leu58 has to be replaced

with a histidine. Position 58 has a high sequence variability as 10 other amino acids (lys, gln, glu, asn, asp, thr, ile, val, ala, and gly) are found in other cytochromes and hence the protein should be able to tolerate a histidine substitution without affecting the polypeptide fold and structural stability. The distance between a Ru-modified His58 and the heme edge is 13.2 Å (Figure 3.3).

Of the three remaining candidate bridging residues, Tyr67 has been selected for several reasons. First, this residue interacts with the heme via a hydrogen bond between its hydroxy group and the Met80 ligand. Secondly, a phenylalanine substitution is not only phylogenetically allowed but also has previously been shown in horse heart[30] and rat cyt *c*[31] to be structurally nonperturbative. Position 66 provides a suitable surface site for probing ET through Tyr67. While a Glu66→His mutation has not been reported, there are several facts that attest to its feasibility. Six other amino acids (ala, val, gln, glu, asp, and lys) are found in the cytochrome *c* family. Glu66 of yeast iso-1-cytochrome *c* also has been mutated to other amino acids (leu, ser, gln, lys, tyr, and trp) and *in vivo* levels of the mutants are comparable to that of the wild-type protein.[32] The edge-to-edge distance between a Ru-modified His66 and the heme is 13.3 Å (Figure 3.3).

Site-directed Mutagenesis

Yeast iso-1-cytochrome *c* has three non-heme-ligand histidines - His 26, His33, and His39. Of these, His39 has been shown in related cytochromes to bind ruthenium complexes most readily under non-denaturing conditions,[4c,33] with His33 being only slightly reactive[4b,18a] and His26 being inert. The relative reactivities of these histidines correlate with their degrees of surface exposure and the high structural homologies among mitochondrial cytochromes *c* suggest that a similar trend can be expected in iso-1-cytochrome *c*. Thus, in order to optimize Ru-modification of a histidine engineered on the surface of iso-1-cytochrome *c*, at least His39 should be mutated to a non-reactive residue. Other amino acids found at this position in the phylogenetic family are lysine

(59), glutamine (28), alanine (1), valine (1), and threonine (3). Of these, glutamine has been selected because it closely mimics the wild-type histidine in terms of charge and H-bonding properties. All mutants were also constructed with a cysteine to serine mutation at 102;[19] this mutation prevents oxidative dimerization at the site of a surface sulfhydryl group.[34] The Cys102→Ser mutant has been shown to be isostructural and isofunctional to the wild-type protein[19]; others have also found that replacing Cys102 stabilizes the protein against autoreduction.[15b,25]

Site-directed mutagenesis experiments were carried out following the method of Kunkel.[30] The 2.5-kb fragment containing the Cys102→Ser/His39→Gln iso-1-cytochrome *c* gene was cloned into the M13mp18. Unlike the M13mp8 shuttle vector used in the past for cyt *c* mutagenesis, M13mp18 does not have any amber mutation, thus making it appropriate for transfection of the non-suppressor *dut⁻ ung⁻* strain. A uracil-containing single-stranded DNA copy of the M13mp18*CYC1*-C102S/H39Q plasmid was produced in the transfected *dut⁻ ung⁻ E. coli* strain, isolated, and employed as the template for oligonucleotide-directed mutagenesis. The mutagenic oligonucleotides were 18-23 bases long and biased yeast codons were used. They anneal to the wild-type template with a melting temperature > 37 °C (the extension temperature).

The clones were screened initially by blot hybridization of the single-stranded DNA copies with a P^{32}-labelled oligonucleotide containing the mutation.[36] This oligonucleotide could be the same as that used for mutagenesis or a shorter oligonucleotide that will allow discrimination between wild-type and mutant sequences at temperatures close to ambient. At this point, we shall refer to each mutant protein in terms of those replacements in addition to the Cys102→Ser and His39→Gln mutations; the adapted nomenclature is summarized in Table 3.1. Figures 3.4-3.5 show the DNA sequences of pertinent regions in the genes for His66, His58, and His66Phe67 cyt *c*. No secondary or unwanted mutations were found in these genes.

The mutant genes were cloned into the tetracycline gene of YEp213 (*tet*^{r} *amp*^{r} *leu2*$^+$)[15,37] and the hybrid plasmid amplified in *E. coli*. A recombinant *E. coli* clone was identified on the basis of its resistance to ampicillin and sensitivity to tetracycline. The hybrid plasmid was isolated from the bacteria and used to transform *S. cerevisiae* GM3C2 (strain deficient in both isozymes of cytochrome *c* as well as in histidine, leucine, and tryptophan biosynthesis) by electroporation. The plasmid was selected by plating on a minimal medium supplemented with L-tryptophan and L-histidine; the *leu2*$^+$ gene in the plasmid complements the deleterious mutation in the host strain.

In the YEp213-based construct, the cytochrome *c* gene is under the control of its natural promoter region (Figure 3.6).[2b] It consists of two upstream activation sequences (UAS1, UAS2) and the obligatory TATA box. Transcription of the gene from the TATA box is activated by the binding of protein factors (*HAP1* and *HAP2/3/4*) to the upstream activation sequences (UAS1 and UAS2, respectively). The binding of *HAP1* and *HAP2/3/4* to the respective DNA sequences is, in turn, promoted by intracellular heme and a shift to a nonfermentable carbon source (lactate or glycerol), respectively. Because several heme biosynthetic enzymes are oxygenases, the oxygen level determines the intracellular concentration of heme. Thus, full derepression of *CYC1* gene expression is achieved by growing the cells aerobically and on a nonfermentable carbon medium. It should also be noted that, under such conditions, a functional cyt *c* is required for obligatory respiration. For this reason, the *CYC1* gene has been conveniently used as a selection marker for the plasmid.

The mutants were isolated and purified using established protocols.[15] The yields of mutant cytochromes are typically 1-2 mg/L of cultures for small-scale batches (~10-20 L). The percentage yields were found to decrease with increasing fermentation volume (for 170-L batch, 0.5-0.8 mg/L), owing to poorer aeration. It has been suggested that protein yields also can be improved by plating the clones on minimal/trp/his medium

prior to cyt *c* induction. The plasmid localized *leu2*$^+$ is a very weak complementation marker that high copy numbers of the plasmid are necessary for cell viability.[38] Thus, this procedure ensures a high copy number of *CYC1* prior to transfer to nonfermentable carbon medium and high levels of protein production.

Spectroscopic Characterization

With the exception of His66Phe67 cyt *c*, the UV/vis spectra of reduced and oxidized forms of the mutants are identical to those of the wild-type protein. In the case of His66Phe67 cyt *c*, the Soret band (Figure 3.7, thin line) is blue-shifted by 2 nm relative to those of the wild-type and other mutant proteins. This is not surprising in view of the fact that Tyr67 is a heme pocket residue. The observed shift, however, contrasts that of the Tyr67→Phe mutant of rat cyt c[31] wherein the Soret is at 412 nm. All mutant ferricytochromes exhibit the 695-nm absorption band, diagnostic of the Fe^{3+}-Met ligation.[1b] The molar ellipticities at 222 nm of the mutants are within 4% of that of the wild-type protein suggesting comparable helical content.

Thermal Stabilities

While the room-temperature spectroscopic measurements tend to suggest minimal mutational effects on the structure, these experiments do not fully describe the thermodynamic effects of the mutations on the protein. The structure must be perturbed from that at ambient conditions to reveal any underlying effects especially those on the stability of the protein. For this purpose, the CD at 222 nm of the ferricytochromes was monitored with increasing temperature. Figure 3.8A shows the thermal denaturation profiles for the Gln39 base protein and His66Phe67 mutant. Each curve is adequately described by a two-state transition. The validity of this simple model is substantiated by the presence of an isochroic point (206 nm) in the far-UV spectra over the same range of

temperatures (Figure 3.8B). T_m (temperature at which the protein is half unfolded) of mutants are all within 4 °C of that of the pseudo-wild-type Ser102 protein.

Heme Potentials

Figure 3.9 illustrates cyclic voltammograms of the proteins at ambient conditions. The reactions of the mutant proteins with the modified gold electrode are quite reversible (peak separations of 65-75 mV). With the exception of His66Phe67 cyt *c*, the heme potentials are within 15 mV of that of the Cys102→Ser mutant, indicating minimal perturbation of the heme pocket by the surface mutations. Incorporation of the Tyr67→Phe mutation into the His66 cyt *c* lowers the heme potential by 48 mV (258(5) to 210(5) mV vs. NHE). This shift is consistent with a crystallographically observed water molecule in place of the tyrosine hydroxyl group;[39] this internal water can orient its dipole in order to stabilize the positively charged ferriheme (net charge of +1). Similar effects were observed when the same mutation (Tyr67→Phe) was incorporated into rat cyt *c* ($\Delta E_{1/2}$ = -35 mV),[31] horse heart cyt *c* ($\Delta E_{1/2}$ = -37 mV),[30] and the Cys102→Thr variant of iso-1-cytochrome *c* ($\Delta E_{1/2}$ = -55 mV).[17b]

Ruthenium Modification

Four proteins, namely, Ser102, His66, His58, and His66Phe67 cytochromes *c*, were each modified with two different Ru complexes ($Ru(bpy)_2(im)^{2+}$, **1**, and $Ru(dmbpy)_2(im)^{2+}$, **2**). All four mutants contain the wild-type His33 and His26. In addition to these residues, the Ser102 variant contains the native His39 whereas the others have His39 replaced with a glutamine and new histidines introduced at different surface positions. The reaction products of the mutant ferricytochromes with $Ru(bpy)_2(im)^{2+}$ were separated and purified by cation-exchange chromatography (Figure 3.10). Each band in the chromatogram was analyzed spectroscopically. A 1:1 Ru:protein adduct is characterized by a $A_{290}/A_{410} \sim 2/3$. In the case of His66, His66Phe67, and

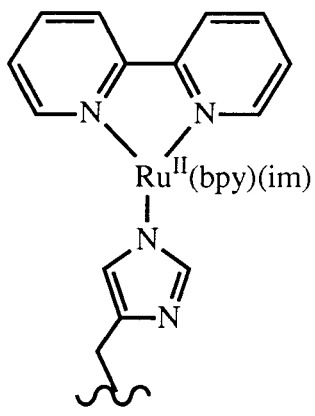

1

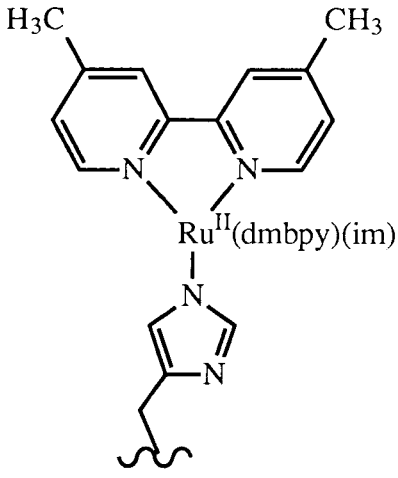

2

His58 cyt *c*, more than one band exhibited this spectral feature, but careful analysis of these products shows that only one has the MLCT band (~492 nm) characteristic of the histidine-bound $Ru(bpy)_2(im)^{2+}$ complex (Figure 3.7, thick line).[27] It appears that the ruthenium complex also binds to protein functionalities other than the histidines. As will be indicated later, the putative 1:1 products do correspond to those arising from the covalent attachment to the engineered histidines; there was no observable modification of the native His33. In the case of the Ser102 mutant, two bands possess the spectral features characteristic of the $Ru(bpy)_2(im)(His)^{2+}$ moiety. One of the bands is in large excess and as will be indicated later, is shown to have a His39-bound Ru complex.

The mutants were also modified with $Ru(dmbpy)_2(im)^{2+}$ and with few exceptions, the chromatograms were similar to those in Figure 3.10.

Spectroscopic Characterization

The UV/vis absorption spectra of both unmodified and Ru-modified proteins were determined. The difference spectrum is virtually identical to that of the model compound ($Ru(bpy)_2(im)^{2+}$), suggesting that the electronic structures of both sites are not perturbed when they are placed in proximity of each other (Figure 3.7). All Ru-modified proteins contain the characteristic 695-nm band. The $bpy^{-}\rightarrow Ru^{3+}$ emission band of the protein-

bound complex is also identical to that of the model compound (Figure 3.7, inset). This is not surprising since solvation around the protein-bound complex is expected to be comparable to that of the free complex.

Ru modification had no significant effects on the secondary structure of the protein as deduced from far-UV CD measurements. Difference CD spectra between the modified and unmodified proteins in the near-UV region (250-350 nm) reveal positive Cotton effects, indicating a slight preference for the right-handed isomer of the $Ru(bpy)_2(im)(His)^{2+}$ complex.[40]

Tryptic Analyses

To directly determine the site of Ru attachment on the protein, the modified proteins were digested completely with trypsin and the resulting fragments were separated by reverse-phase chromatography. Figure 3.11 shows the chromatograms of the tryptic digests for unmodified and modified His66Phe67 cyt *c* as monitored with a 280-nm filter. In Figure 3.11A, the major band corresponds to the heme fragment and the second largest band represents the peptide (56-73) containing the only other strong chromophore (Trp59) in the molecule. For the modified protein (Figure 3.11B), the latter band is displaced to higher percentage of eluent and identified spectroscopically to have a bound Ru complex. Amino-acid sequencing of this peptide corroborates its identity (Asn_{56}ValLeuTrpAspGluAsnAsnMetSer$His_{66}Phe_{67}$LeuThrAsnProXLys, X = ε-*N*-trimethyllysine). The eleventh cleavage cycle (position 66) shows a His in a very low yield, suggesting that the label is on this residue.

Sequence analyses of the Ru-containing tryptic fragments of His66 and His58 cyt *c* (not shown) indicate the same 56-73 peptide, suggesting in each case that the Ru complex is attached to the engineered histidine. These peptide sequences also confirm the mutations introduced at positions 58, 66, and/or 67 at the protein level. The site of modification in the Ru derivative of Ser102 cyt *c* was identified to be His39. Limited N-

terminal analysis of the Ru-containing fragment revealed a sequence of HisSerGlyGlnAlaGluGlyTyr... that corresponded to the 39-54 fragment. The yield of phenylthiohydantoin-histidine product at the first cycle was low relative to the succeeding residues in the sequence, indicating that the label is on this amino acid.

Electrochemical Measurements

To examine the effect of Ru attachment on the heme center, direct electrochemistry of the modified proteins was carried out. The heme potentials in the $Ru(bpy)_2(im)(His)^{2+}$-modified cytochromes are no more than 20 mV from the respective parent molecule (Figure 3.9). These shifts are well within the changes that normally accompany the introduction of point charges on the surface of a metalloprotein.[41]

That both protein-bound complex and free complex have identical absorption and emission properties implies that the electrochemical properties of the complex are likewise unperturbed upon attachment of the protein.[42] To corroborate this, the $Ru^{3+/2+}$ potential of the protein-bound $Ru(bpy)_2(im)(His)$ was determined by Osteryoung square wave voltammetry (OSWV). An OSWV scan of $Ru(bpy)_2(im)$(His33)cyt *c* at potentials above 0.5 mV vs. NHE (Figure 3.12A) revealed two peaks (a major peak at 1.06(1) and a minor one at 0.83(1) V vs. NHE). The major band is only 60 mV higher than that of the model compound ($Ru(bpy)_2(im)_2^{+2}$) in the same buffer and hence must be that of the $Ru(bpy)_2(im)$(His33) moiety. Repeated sweeps with the same electrode showed dramatic drop in both signals as the protein slowly adsorbed on the electrode surface (Figure 3.12B). When the working electrode was rinsed with ddH_2O and immersed in buffer, only the low-potential signal was observed (Figure 3.12C). When the electrode was polished and immersed in the protein solution, the same two-peak profile was seen.

Changing the Ru complex on horse heart cyt *c* to $Ru(dmbpy)_2(im)(His)$ causes *ca.* 110-mV shifts in both peaks (0.95(1) and 0.71(1) V vs. NHE), indicating that these signals correspond to the bound Ru (Figure 3.13). The major peak is only 70 mV higher

than that of $Ru(dmbpy)_2(im)_2^{+2}$ and hence should correspond to $Ru(dmbpy)_2(im)(His33)^{+2}$ moiety on horse heart cyt *c*. It is very likely that the lower-potential signals seen for both preparations arise from the unreacted aquo derivatives (i.e., $Ru(bpy)_2(H_2O)(His)$ or $Ru(dmbpy)_2(H_2O)(His)$). The crystal structure of horse heart cyt *c* indicates that His33 is only partially accessible on the protein surface and reaction of $Ru(bpy)_2(H_2O)(His)$ with imidazole may be hindered. Support for this hypothesis comes from an OSWV scan of $Ru(bpy)_2(im)$(His66Phe67)cyt *c* (Figure 3.14). His66 is a more reactive residue to Ru modification than His33 and indeed, a smaller signal size was observed for the low-potential species. Interestingly, Isied and coworkers have reported a $Ru(bpy)_2(im)(His33)^{3+/2+}$ potential equal to that of the low-potential species.[43] We note, however, that their measurements were performed by differential pulse polarography, a procedure that typically involves much slower sweep rates (1-2 mV/s). It is likely that the electrode was already passive by the time the $Ru^{3+/2+}$ region was reached and only the $Ru(bpy)_2(H_2O)(His)$ could be detected, as seen with our repeated scans.

Figure 3.15 summarizes the $Ru^{3+/2+}$ potentials for all three systems. As indicated earlier, the $Ru(bpy)_2(im)(His)^{3+/2+}$ and $Ru(dmbpy)_2(im)(His)^{3+/2+}$ potentials on horse heart cyt *c* are 60 and 70 mV higher than those of $Ru(bpy)_2(im)_2^{3+/2+}$ and $Ru(dmbpy)_2(im)(His)^{3+/2+}$, respectively. The $Ru(bpy)_2(im)(His)^{3+/2+}$ potential in His66Phe67 cyt *c* (0.99(1) V vs. NHE) is virtually identical to that of the model compound.

Table 3.2 summarizes all the structural and electrochemical properties of the mutant cytochromes.

ET Rate Measurements

ET kinetics were measured using a flash-quench procedure:[18a]

$$Ru^{2+}\text{-}Fe^{2+}\text{-cyt } c \xrightarrow{h\upsilon} {}^{*}Ru^{2+}\text{-}Fe^{2+}\text{-cyt } c \quad (1)$$

$${}^{*}Ru^{2+}\text{-}Fe^{2+}\text{-cyt } c + Q \longrightarrow Ru^{3+}\text{-}Fe^{2+}\text{-cyt } c + Q^{-} \quad (2)$$

$$Ru^{3+}\text{-}Fe^{2+}\text{-cyt } c \longrightarrow Ru^{2+}\text{-}Fe^{3+}\text{-cyt } c \quad (3)$$

$$Ru^{2+}\text{-}Fe^{3+}\text{-cyt } c + Q^{-} \longrightarrow Ru^{2+}\text{-}Fe^{2+}\text{-cyt } c + Q \quad (4)$$

The histidine-bound Ru complex is excited with a laser pulse (eq 1), generating an excited state that, in the absence of ET quenching processes, decays with a lifetime of 70 ns. In the presence of a quencher (Q = $Ru(NH_3)_6^{3+}$, 5-10 mM, or methylviologen, 10 mM), a fraction of the excited Ru complexes decay by a bimolecular ET route (eq 2) forming transient Ru^{3+}-Fe^{2+}-cyt *c* in less than 100 ns. The intramolecular ET reaction (eq 3) is monitored by transient absorption spectroscopy at wavelengths characteristic of the heme (550 nm) and Ru (306, 504 nm) oxidation states. The low-driving-force bimolecular recombination between the reduced quencher and the ferriheme (eq 4) proceeds on a timescale of several seconds to regenerate the original reactants.

Flash-quench transient-absorption kinetics at 550 nm (Figures 3.16A, 3.17A, 3.18A, 3.19A) for the $Ru(bpy)_2(im)$(His)-modified yeast cytochromes exhibit first-order decays and are found to be independent of protein concentration (5-20 μM). The ET kinetics were also monitored at wavelengths isosbestic for the heme (306, 504, or 339 nm) in order to follow the reaction at the Ru center (Figures 3.16B, 3.17B, 3.18B, 3.19B). The traces observed at these wavelengths are characterized by two exponential-decay components. One component corresponds to the excited-state decay as the Ru^{2+*} excited state absorbs at these wavelengths; the second component represents the $Ru^{3+} \rightarrow Ru^{2+}$ conversion. Data recorded at these wavelengths demonstrate that the bound Ru^{3+} is reduced at the same rate that the ferroheme is oxidized. Results of the fits to the kinetic traces are listed in Table 3.3.

Figure 3.20 shows the flash-quench transient-absorption kinetics for the Ru(dmbpy)$_2$(im)(His) derivatives. The $Fe^{2+}\rightarrow Ru^{3+}$ ET kinetics in these derivatives are 2-3 fold slower than in the corresponding Ru(bpy)$_2$(im)(His) derivatives. This trend is consistent with the lower driving force for these reactions. Table 3.3 lists the results of the fits for the Ru(dmbpy)$_2$(im)(His) derivatives.

Ru-Heme Electronic Couplings

In order to extract H_{AB}s for the Ru-modified cytochromes, the nuclear term must be factored from the experimental rate constants; this entails knowledge of the reaction driving forces and the reorganization free energy (λ). From the self-exchange parameters of cytochrome *c* and the closely related $Ru(bpy)_3^{3+}$, the Marcus cross relation predicts λ to be approximately 0.8 eV for the ET reactions in Ru-modified cytochromes.[9] This value was recently confirmed by a study of ET reactions in four different Ru polypyridine derivatives of His33 horse heart cyt *c*.[44] For each mutant protein, we have reported the intramolecular rates of $Fe^{2+}\rightarrow Ru^{3+}$ ET at two different driving forces; in principle, λ and H_{AB} can be determined analytically from each data pair. Figure 3.21 shows fits of Ru(His66Phe67)cyt *c* data to the Marcus equation (Chapter 2, eq 5) in which λ is either allowed to float or fixed at the same value as that of horse heart cyt *c* (0.8 eV). It is apparent that while λs for these fits vary by as much as 0.07 eV, the estimated k_{max}s are very close.[45] This is a consequence of the ET reactions being very close to the top of the parabola. The k_{max} and H_{AB} values for each modifiable histidine site have been calculated and are listed in Table 3.4.

The next chapter addresses the implications of the experimentally extracted Ru-heme electronic couplings on the role of intervening protein matrix especially aromatic residues in mediating intersite electron exchange.

SUMMARY

We have constructed site-directed mutants of yeast iso-1-cytochrome *c* aimed at addressing whether intervening aromatic residues can affect the rates of intersite ET to a significant extent. The mutants incorporate surface histidines (His66, His58) for ruthenium labelling that will allow us to probe ET through aromatic side chains (Tyr67 and Phe67 for His66; Trp59 for His58). Genetic, spectroscopic, and electrochemical analyses of these mutants and their Ru derivatives indicate that (1) the mutants are isostructural to the wild-type protein, and (2) attachment of Ru complexes to the protein resulted in minimal perturbations of both redox sites. The $Fe^{2+} \rightarrow Ru^{3+}$ ET reactions in the modified proteins were examined at two different driving forces. The kinetic traces are monoexponential, confirming the unimolecular nature of these reactions; examination of the reaction kinetics at different wavelengths suggests that no intermediate is formed in the course of exchange.

REFERENCES AND NOTES

1. (a) Pettigrew, G. W.; Moore, G. R. *Cytochromes c: Biological Aspects*; Springer-Verlag: New York, 1987. (b) Moore, G. R.; Pettigrew, G. W. *Cytochromes c: Evolutionary, Structural and Physicochemical Aspects*; Springer-Verlag, New York, 1990.
2. (a) Sherman, F. *Genetics* **1990**, *125*, 9. (b) Forsburg, S. L.; Guarente, L. *Ann. Rev. Cell. Biol.* **1989**, *5*, 153.
3. (a) Elöve, G. A.; Roder, H. In *Protein Refolding,* G. Georgiou and E. Bernardez-Clark, Eds. (ACS Symposium Series 470, American Chemical Society, Washington, D. C., 1991), pp. 50-63. (b) Roder, H.; Elöve, G. A.; Englander, S. W. *Nature* **1988**, *335*, 700.
4. (a) J . R. Winkler and H. B. Gray, *Chem. Rev.* **92**, 369 (1992). (b) Meade, T. J.; Gray, H. B.; Winkler, J. R. *J. Am. Chem. Soc.* **1989**, *111*, 4353. (c) Therien, M. J.; Selman, M. A.; Gray, H. B.; Chang, I.-J.; Winkler, J. R. *J. Am. Chem. Soc.* **1990**, *112*, 2420. (d) Bowler, B. E.; Meade, T. J.; Mayo, S. L.; Richards, J. H.; Gray, H. B. *J. Am. Chem. Soc.* **1989**, *111*, 8757. (d) Winkler, J. R.; Nocera, D. G.; Yocom, K. M.; Bordignon, E.; Gray, H. B. *J. Am. Chem. Soc.* **1982**, *104*, 5798. (e) Elias, H.; Chou, M. H.; Winkler, J. R. *J. Am. Chem. Soc.* **1988**, *110*, 429.
5. Conrad, D. W.; Zhang, H.; Stewart, D. E.; Scott, R. A. *J. Am. Chem. Soc.* **1992**, *114*, 9909.
6. (a) Durham, B.; Pan, L. P.; Long, J. E.; Millett, F. *Biochemistry* **1989**, *28*, 8659. (b) Durham, B. D.; Pan, L. P.; Hahm, S.; Long, J.; Millett, F. *ACS Advances in Chemistry Series*; Johnson, M. K., King, R. B., Kurtz, D. M., Kutal, C., Norton, M. L., Scott, R. A., Eds.; American Chemical Society: Washington, DC, 1990; Vol. 226, pp. 180-193. (c) Scott, J. R.; Willie, A.; McLean, M.; Stayton, P. S.; Sligar, S. G.; Durham, B.; Millett, F. *J. Am. Chem. Soc.* **1993**, *115*, 6820. (d) Geren, L.; Hahm, S.;

Durham, B.; Millett, F. *Biochemistry* **1992**, *30*, 9450. (e) Willie, A.; Stayton, P. S.; Sligar, S. G.; Durham, B.; Millett, F. *Biochemistry* **1992**, *31*, 7237. (f) Hahm, S.; Durham, B.; Millett, F. *Biochemistry* **1992**, *31*, 3472. (g) Pelletier, H.; Kraut, J. *Science* **1992**, *258*, 1748. (h) Eltis, L. D.; Herbert, R. G.; Barker, P. D.; Mauk, A. G.; Northrup, S. H. *Biochemistry* **1991**, 30, 3663.

7. (a) Onuchic, J. N.; Beratan, D. N.; Winkler, J. R.; Gray, H. B. *Annu. Rev. Biophys. Biomol. Struct.* **1992**, *21*, 349. (b) Beratan, D. N.; Betts, J. N.; Onuchic, J. N. *Science* **1991**, *252*, 1285. (c) Betts, J. N.; Beratan, D. N.; Onuchic J. N. *J. Am. Chem. Soc.* **1992**, *114*, 4043.
8. (a) Siddarth, P.; Marcus, R. A. *J. Phys. Chem.* **1990**, *94*, 8430. (b) Siddarth, P.; Marcus, R. A. *J. Phys. Chem.* **1992**, *96*, 3213. (c) Siddarth, P.; Marcus, R. A. *J. Phys. Chem.* **1993**, *97*, 2400.
9. (a) Kuki, A.; Wolynes, P. G. *Science* **1987**, *236*, 1647. (b) Gruschus, J. M.; Kuki, A. *J. Phys. Chem.* **1993**, *97*, 5583.
10. Broo, A.; Larsson, S. *J. Phys. Chem.* **1991**, *95*, 4925.
11. (a) Farver, O.; Pecht, I. *J. Am. Chem. Soc.* **1992**, *114*, 5764. (b) Farver, O.; Skov, L. K.; Pascher, T.; Karlsson, B. G.; Nordling, M.; Lundberg, L. G.; Vänngard, T.; Pecht, I. *Biochemistry* **1993**, 32, 7317. (c) Canters, G. W.; van de Kamp, M. *Curr. Opin. Struct. Biol.* **1992**, *2*, 859. (d) Farid, R. S.; Moser, C. C.; Dutton, P. L. *Curr. Opin. Struct. Biol.* **1993**, *3*, 225. (e) Wuttke, D. S.; Gray, H. B. *Curr. Opin. Struct. Biol.* **1993**, in press.
12. (a) Sykes, A. G. *Metal Ions in Biological Systems*; Sigel, H., Sigel, A., Eds.; Marcel Dekker: New York, 1991; Vol. 27, pp. 291-321. (b) Lloyd, E.; Tomkinson, N. P.; Sykes, A. G. *J. Chem. Soc. Dalton Trans.* **1992**, 753. (c) Govindaraju, K.; Christensen, H. E. M.; Lloyd, E.; Olsen, M.; Salmon, G. A.; Tomkinson, N. P.; Sykes, A. G. *Inorg. Chem.* **1993**, *32*, 40.

13. (a) Hazzard, J. T.; Mauk, A. G.; Tollin, G. *Arch. Biochem. Biophys.* **1992**, *298*, 91. (b) Everest, A. M.; Wallin, S. A.; Stemp, E. D. A.; Nocek, J. M.; Mauk, A. G.; Hoffman, B. M. *J. Am. Chem. Soc.* **1991**, *113*, 4337. (c) Bowler, B. E.; Meade, T. J.; Mayo, S. L.; Richards, J. H.; Gray, H. B. *J. Am. Chem. Soc.* **1989**, *111*, 8757. (d) Davies, M.; Sligar, S. G. *Biochemistry* **1992**, *31*, 11383.

14. (a) Christensen, H. E. M.; Conrad, L. S.; Hammerstad-Pedersen, J. M.; Ulstrup, J. *FEBS Lett.* **1992**, *296*, 141. (b) Christensen, H. E. M.; Conrad, L. S.; Mikkelsen, K. V.; Nielsen, M. K.; Ulstrup, J. *Inorg. Chem.* **1990**, *29*, 2808. (c) Christensen, H. E. M.; Conrad, L. S.; Mikkelsen, K. V.; Ulstrup, J. *J. Phys. Chem.* **1992**, *96*, 4451.

15. (a) Smith, M.; Leung, D. W.; Gillam, S.; Astell, C. R.; Montgomery, D. L.; Hall, B. D. *Cell* **1979**, *16*, 753. (b) Cutler, R. L.; Pielak, G. J.; Mauk, A. G.; Smith, M. *Prot. Eng.* **1987**, *1*, 95. (c) Pielak, G. J.; Mauk, A. G.; Smith, M. *Nature* **1985**, *313*, 152.

16. Mauk, A. G. *Structure and Bonding* **1991**, *75*, 131.

17. (a) Louie, G. V.; Brayer, G. D. *J. Mol. Biol.* **1990**, *214*, 527. (b) Berghuis, A. M.; Brayer, G. D. *J. Mol. Biol.* **1992**, *223*, 959. (c) Bushnell, G. W.; Louie, G. V.; Brayer, G. D. *J. Mol. Biol.* **1990**, *214*, 585.

18. (a) Chang, I.-J.; Gray, H. B.; Winkler, J. R. *J. Am. Chem. Soc.* **1991**, *113*, 7056. (b) Wuttke, D. S.; Bjerrum, M. J.; Winkler, J. R.; Gray, H. B. *Science* **1992**, *256*, 1007. (c) Wuttke, D. S.; Bjerrum, M. J.; Chang, I.-J.; Winkler, J. R.; Gray, H. B. *Biochim. Biophys. Acta* **1992**, *1101*, 168.

19. Mayo, S. L. Ph.D. Thesis, California Institute of Technology, 1988.

20. Hanahan, D.; Jessee, J.; Bloom, F. R. *Methods Enzymol.* **1991**, *204*, 63.

21. (a) Messing, J. *Methods Enzymol.* **1983**, *101*, 20. (b) Messing, J.; Vieira, J. *Gene* **1982**, *19*, 263.

22. Sanger, F.; Nicklen, S.; Coulson, A. R. *Proc. Natl. Acad. Sci. USA* **1977**, *74*, 5463.

23. Maniatis, T.; Fritsch, E. F.; Sambrook, J. *Molecular Cloning: A Laboratory Manual*; Cold Spring Harbor Laboratory: Cold Spring Harbor, New York, 1982.

24. (a) Becker, D. M.; Guarente, L. *Methods Enzymol.* **1991**, *194*, 182. (b) Instruction Manual, Pulse Controller Apparatus (Literature Index 1433), Bio-Rad, Richmond, CA.

25. Hickey, D. R.; Berghuis, A. M.; Lafond, G.; Jaeger, J. A.; Cardillo, T. S.; McLendon, D.; Das, G.; Sherman, F.; Brayer, G. D.; McLendon, G. *J. Biol. Chem.* **1991**, *266*, 11686.

26. (a) Allen, P. M.; Hill, H. A. O.; Walton, N. J. *J. Electroanal. Chem.* **1984**, *178*, 69. (b) Rafferty, S. P.; Pearce, L. L.; Barker, P. D.; Guillemente, J. G.; Kay, C. M.; Smith, M.; Mauk, A. G. *Biochemistry* **1990**, *29*, 9365.

27. Matsudaira, P. *Methods Enzymol.* **1990**, *182*, 602.

28. Osteryoung, J.; O'Dea, J. J. *Electroanal. Chem.* **1986**, *14*, 209.

29. Williams, R. J. P. *Z. Phys. Chimie* **1988**, *269*, 387.

30. Wallace, C. J. A.; Mascagni, P.; Chait, B. T.; Collawn, J. F.; Paterson, Y.; Proudfoot, A. E. I.; Kent, S. B. H. *J. Biol. Chem.* **1989**, *264*, 15199.

31. Luntz, T. L.; Schejter, A.; Garber, E. A. E.; Margoliash, E. *Proc. Natl. Acad. Sci. USA* **1989**, *86*, 3524.

32. Stewart, J. W.; Sherman, F. *J. Mol. Biol.* **1973**, *78*, 169.

33. Selman, M. A. Ph.D. Thesis, California Institute of Technology, 1989.

34. Zuniga, E. H.; Nall, B. T. *Biochemistry* **1983**, *22*, 1430.

35. (a) Kunkel, T. A. *Proc. Natl. Acad. Sci. USA* **1985**, *82*, 488. (b) Instruction Manual, Muta-Gene *in vitro* Mutagenesis Kit (Cat. No. 170-3571), Bio-Rad, Richmond, CA

36. Instruction Manual, *In vitro*-Mutagenesis System, Oligonucleotide-directed version 2.1 (Cat. No. RPN.1523), Amersham Corporation, Arlington Heights, IL.

37. Hicks, J. B.; Strathern, J. N.; Klar, A. J. S.; Dellaporta, S. L. *Genetic Engineering* **1982**, *4*, 219.

38. Knowlton, R. G. in *Maximizing Gene Expression*; Reznikoff, W., Gold, L., Eds.; Butterworths: Boston, 1986; pp. 171-194.

39. McLendon, G.; Hickey, D.; Berghuis, A.; Sherman, F.; Brayer, G. *ACS Advances in Chemistry Series*; Bolton, J. R., Mataga, N., McLendon, G., Eds.; American Chemical Society: Washington, DC, 1991; Vol. 228, pp. 179-190.

40. Mason, S. F. *Inorg. Chim. Acta Rev.* **1968**, *2*, 89.

41. Leitch, F. A.; Moore, G. R.; Pettigrew, G. W. *Biochemistry* **1984**, *23*, 1831.

42. Dodsworth, E. S.; Lever, A. B. P. *Chem. Phys. Lett.* **1986**, *124*, 152.

43. Cho, M.-Y. P. Ph.D. Thesis, Rutgers The State University of New Jersey - New Brunswick, 1989.

44. Bjerrum, M. J.; Chang, I.-J.; Winkler, J. R.; Gray, H. B., unpublished results.

45. We note, however, that when the λ is allowed to float, the calculated values for all the yeast cytochrome *c* systems are higher (from 0.07 to 0.2 eV) than that derived (0.8 eV) for the horse heart protein. This is supported by the fact that the rate for $Ru(dmbpy)_2(im)$ derivative of horse heart cyt *c* is only 20% (2.0×10^6 s^{-1}) lower than the rate for the $Ru(bpy)_2(im)$ derivative (2.5×10^6 s^{-1}), whereas the observed shifts in the yeast proteins are more significant. In view of a less extensive set of data for each yeast mutant compared to that used to obtain λ for His33 horse heart cyt *c*, the reported k_{max}in Table 3.5 represents an average of the values derived when λ is fixed and when it is a variable.

Table 3.1. Nomenclature and Description of the Mutant Yeast Iso-1-cytochromes *c*.

Mutant	Mutations	Histidines[a]
Ser102	Cys102→Ser	His26, His33, His39
Gln39	Cys102→Ser, His39→Gln	His26, His33
His58	Cys102→Ser, His39→Gln, Leu58→His	His26, His33, His58
His66	Cys102→Ser, His39→Gln, Glu66→His	His26, His33, His66
His66Phe67	Cys102→Ser, His39→Gln, Tyr67→Phe	His26, His33, His66

[a]Other than His18 heme ligand.

Table 3.2. Properties of Mutant Cytochromes *c*.[a]

Mutant	T_m, °C[b]	$E_{1/2}$, mV[c]	
		HisX	Ru(HisX)
Ser102	57(1)	272(5)[d]	–[e]
Gln39	57(1)	260(5)	–[e]
His58	54(1)	272(5)	290(5)
His66	53(1)	258(5)	255(5)
His66Phe67	55(1)	210(5)	215(5)

[a]Numbers in parentheses reflect uncertainties in preceding digit.
[b]Midpoint melting temperatures for the mutant ferricytochromes.
[c]Heme potentials (vs. NHE). HisX and Ru(HisX) refer to unmodified and $Ru(bpy)_2(im)^{2+}$-modified proteins, respectively.
[d]Reference 19.
[e]Not measured.

Table 3.3. Intramolecular $Fe^{2+} \rightarrow Ru^{3+}$ ET Rates in Ru(HisX)-modified Yeast Cytochromes *c*.[a]

HisX	$-\Delta G^{o}$, eV	k_{ET}, s^{-1}
His39	0.73(6)	$2.0(2) \times 10^{6}$
	0.61(7)	$9.6(9) \times 10^{5}$
His58	0.71(6)	$5.2(5) \times 10^{4}$
	0.59(7)	$2.6(3) \times 10^{4}$
His66	0.74(6)	$1.0(1) \times 10^{6}$
	0.62(7)	$4.4(4) \times 10^{5}$
His66Phe67	0.78(1)	$3.0(3) \times 10^{6}$
	0.66(2)	$2.0(2) \times 10^{6}$

[a]The first entry corresponds to surface histidine with $Ru(bpy)_2(im)^{2+}$ whereas the second pertains to the same residue modified with $Ru(dmbpy)_2(im)^{2+}$. Uncertainty in the preceding digit is enclosed in parentheses.

Table 3.4. Maximum $Fe^{2+} \rightarrow Ru^{3+}$ ET Rates in Ru(HisX)-modified Yeast Iso-1-cytcohrome *c* Mutants.

X	d(edge-edge), Å	k_{max},[a] s^{-1}
39	12.3	$2.7(9) \times 10^6$
58	13.2	$6.7(9) \times 10^4$
66	13.3	$1.4(5) \times 10^6$
66(Phe67)	13.3	$3.0(3) \times 10^6$

[a]Reference 45. Uncertainty in the preceding digit is enclosed in parenthesis.

Figure 3.1. Superposition of yeast iso-1-cytochrome *c* (solid line)[17a] and horse heart cytochrome *c*[17c] (thin lines). Based on the sequence alignment, the yeast protein has five extra N-terminal residues and one less amino acid compared to horse heart cytochrome *c*. The structural alignment based on the overlapping main chain atoms gave an r.m.s. difference of 0.51 Å.

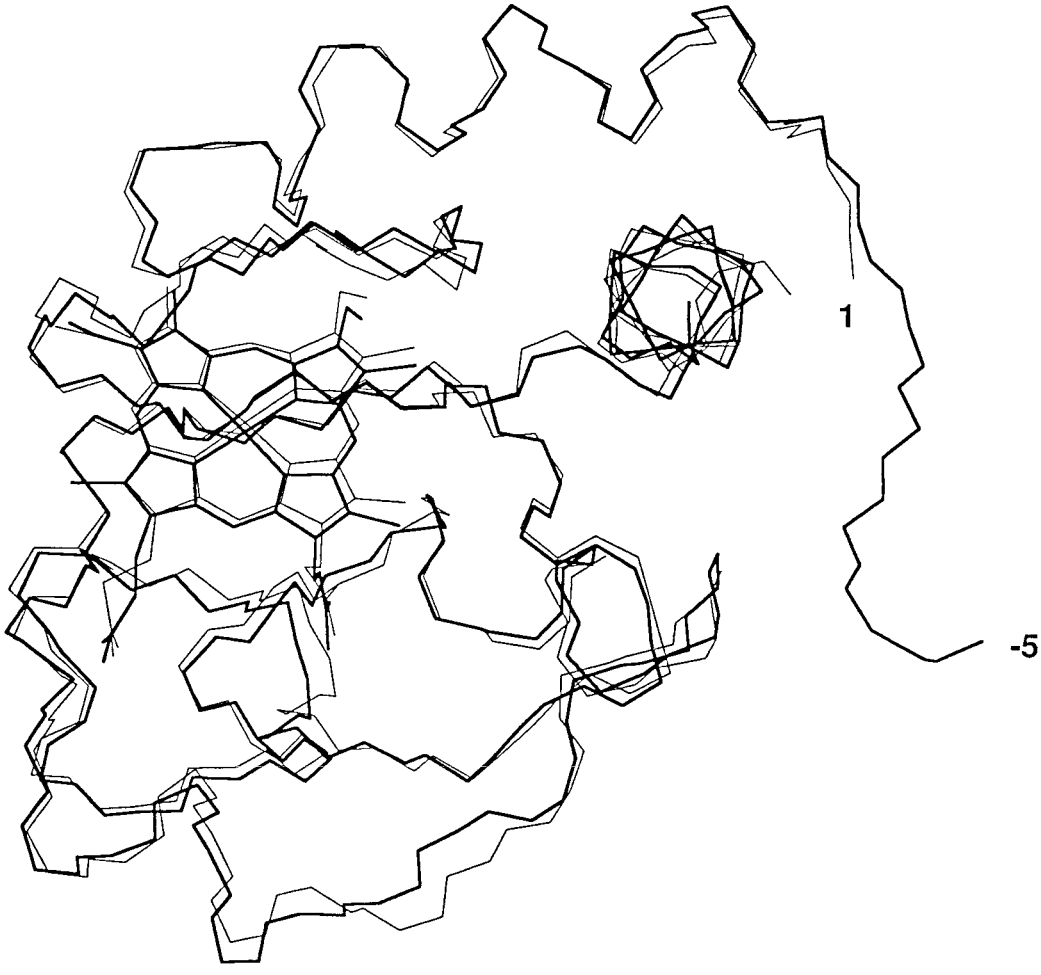
1
-5

Figure 3.2. Potential waveform for an Osteryoung square wave voltammetric scan.

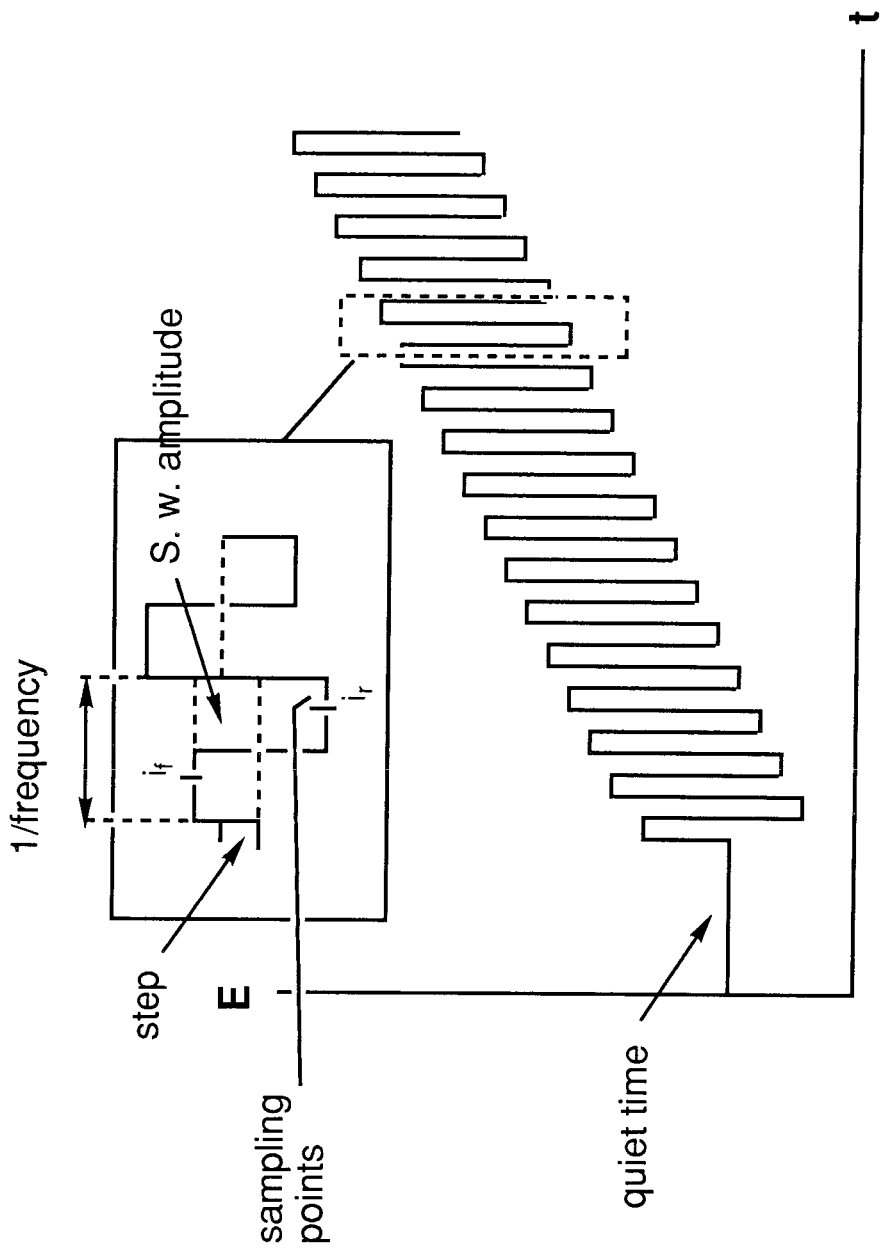
t
1/frequency
S. w. amplitude
i_f
i_r
step
E
sampling points
quiet time

Figure 3.3. Computer models of the proposed yeast cyt *c* mutants showing the surface histidines and the intervening aromatic side chains.

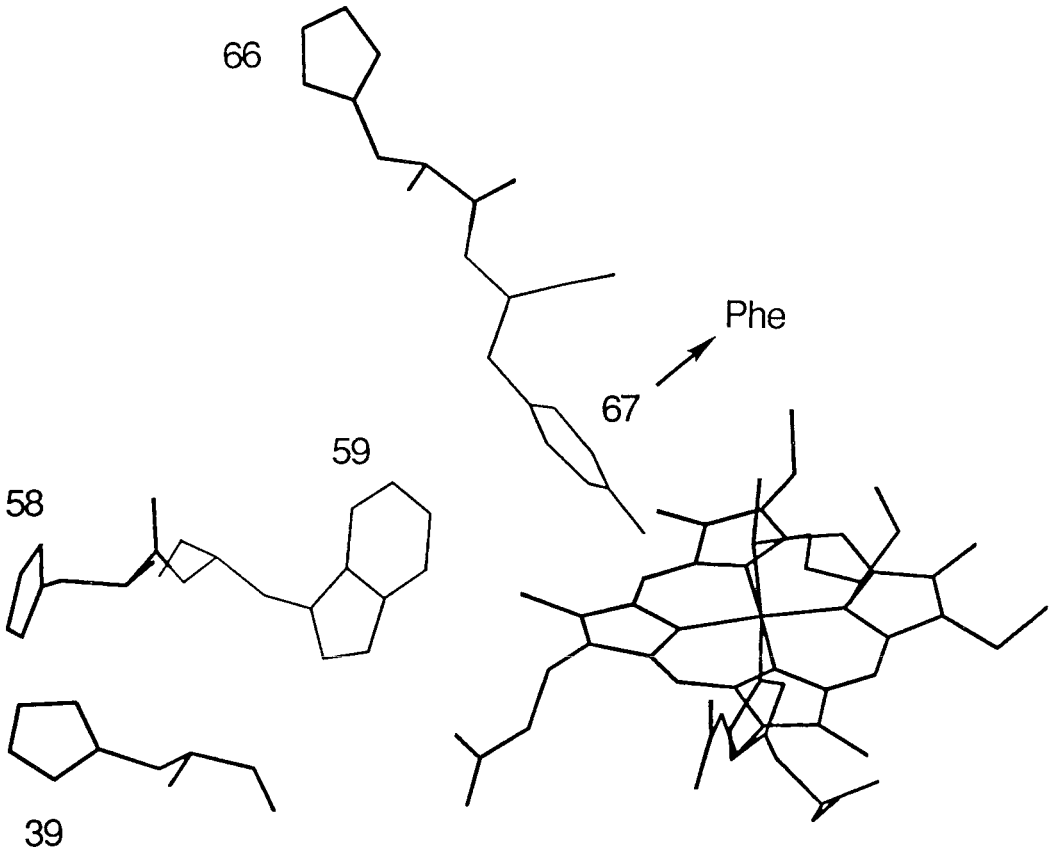
66
Phe
67
59
58
39

Figure 3.4. Sequence of the antisense strand for the Glu66→His/Tyr67→Phe yeast iso-1-cytochrome *c* determined using a single-stranded M13mp18 template. Shown are the mutations at position 67 and 66 as well as those in the gene for the base protein (H39Q, C102S).

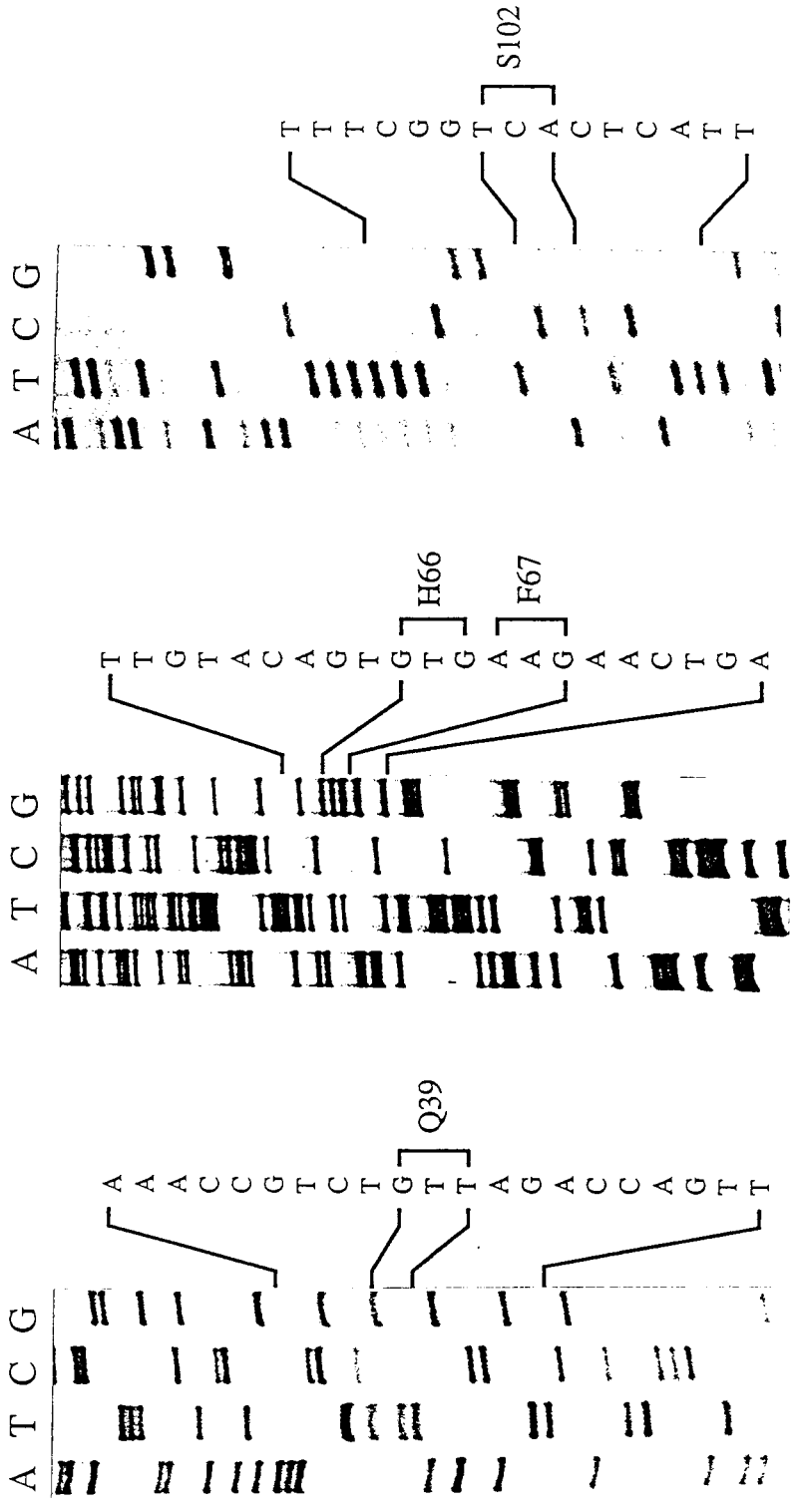
S102
T T T C G G T C A C T C A T T
H66
F67
T T G T A C A G T G T G A A G A A C T G A
Q39
A A A C C G T C T G T T A G A C C A G T T
A T C G

Figure 3.5. Sequences of the antisense strands for Leu58→His (left) and Glu66→His yeast iso-1-cytochromes *c* (right).

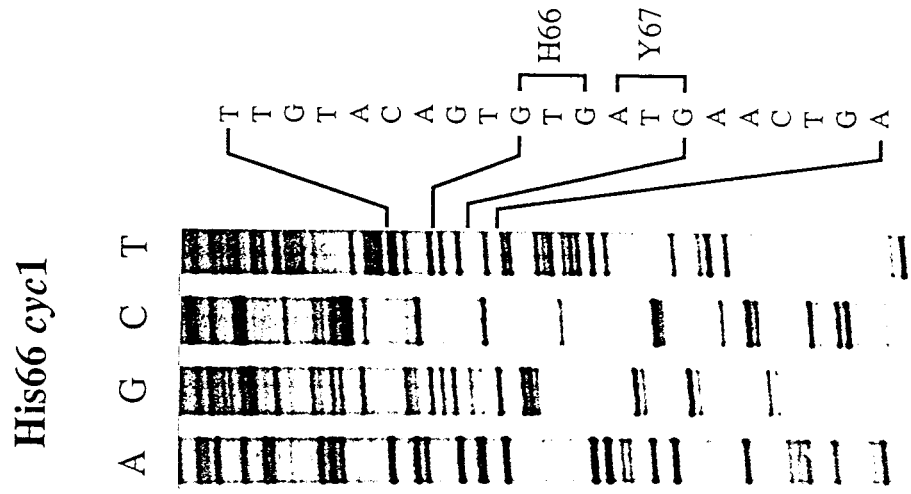
His66 cyc1
T
C
G
A
T T G T A C A G T G T G A T G A A C T G A
H66
Y67

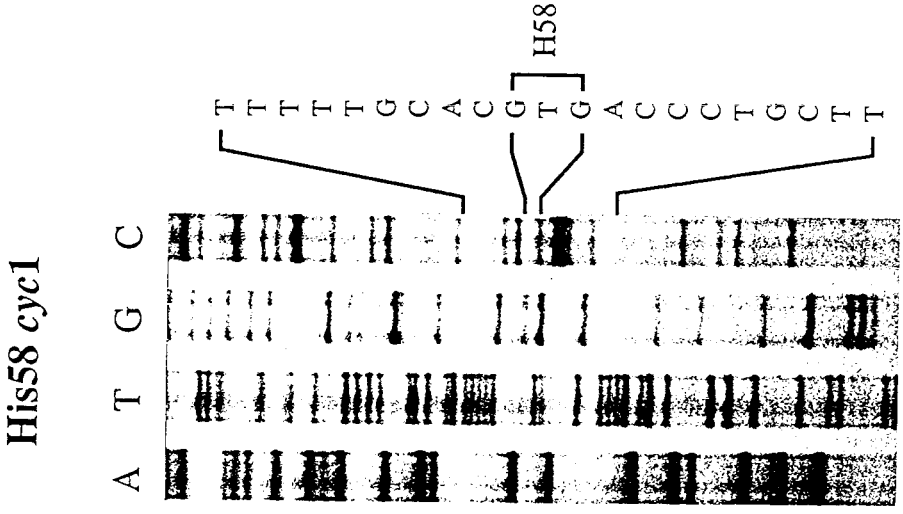
His58 cyc1
C
G
T
A
T T T T G C A C G T G A C C C T G C T T
H58

Figure 3.6. The high-copy-number YEp213 plasmid for *CYC1* expression in *S. cerevisiae*. The start of the *CYC1* gene is designated as 1.

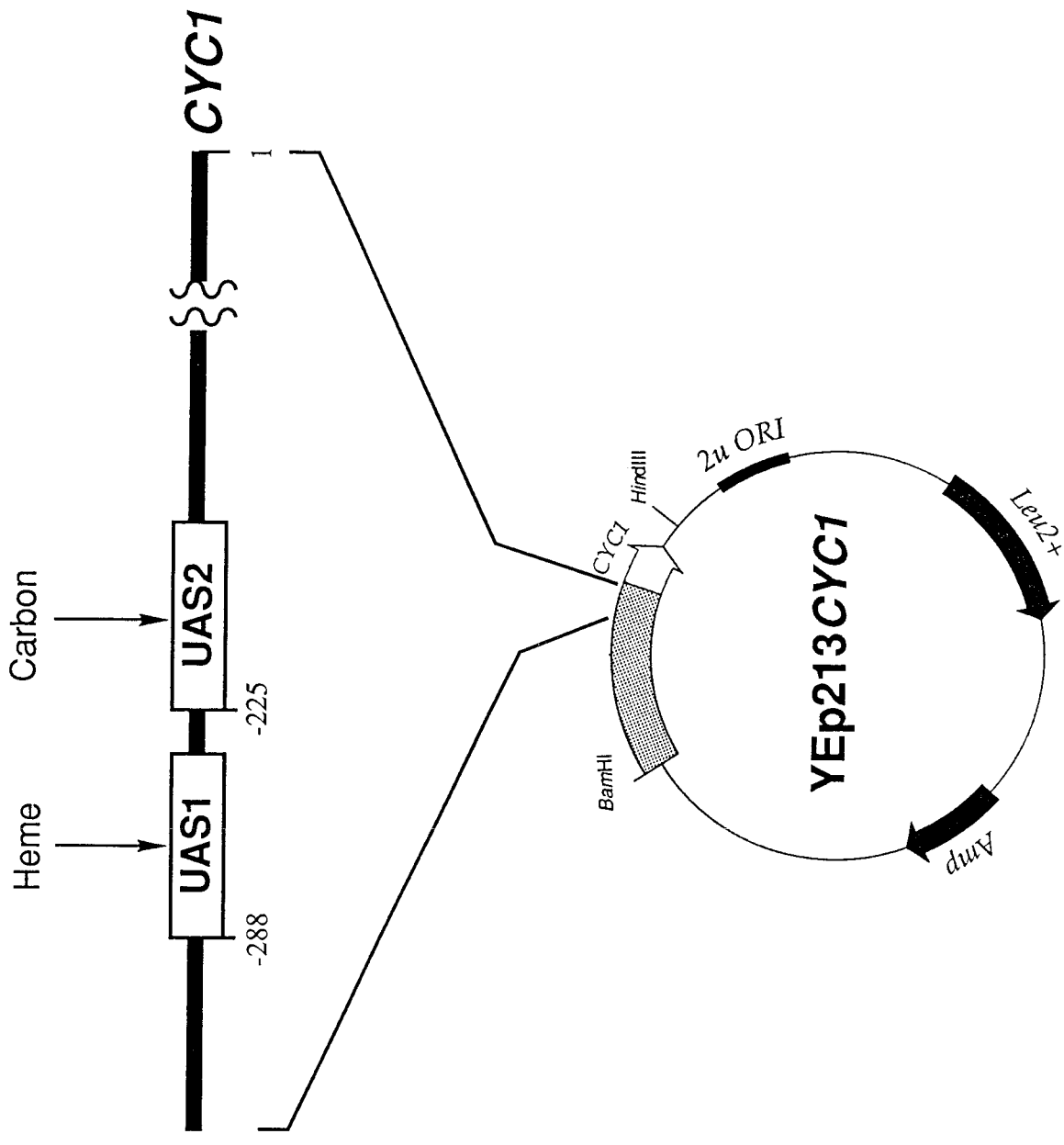
CYC1
1
Carbon
UAS2
-225
Heme
UAS1
-288
CYC1
HindIII
2u ORI
Leu2+
YEp213CYC1
BamHI
Amp

Figure 3.7. The UV/vis absorption spectra of (His66Phe67)- (thin line) and $Ru(bpy)_2(im)$(His66Phe67)cyt *c* (thick line). The difference spectrum is shown with dashed line. The inset shows the uncorrected emission spectra of $Ru(bpy)_2(im)$(His66Phe67)cyt *c* (solid line) and $Ru(bpy)_2(im)_2^{2+}$ (dashed line). All solutions are in μ 100 mM NaP_i, pH 7.0, 22 °C.

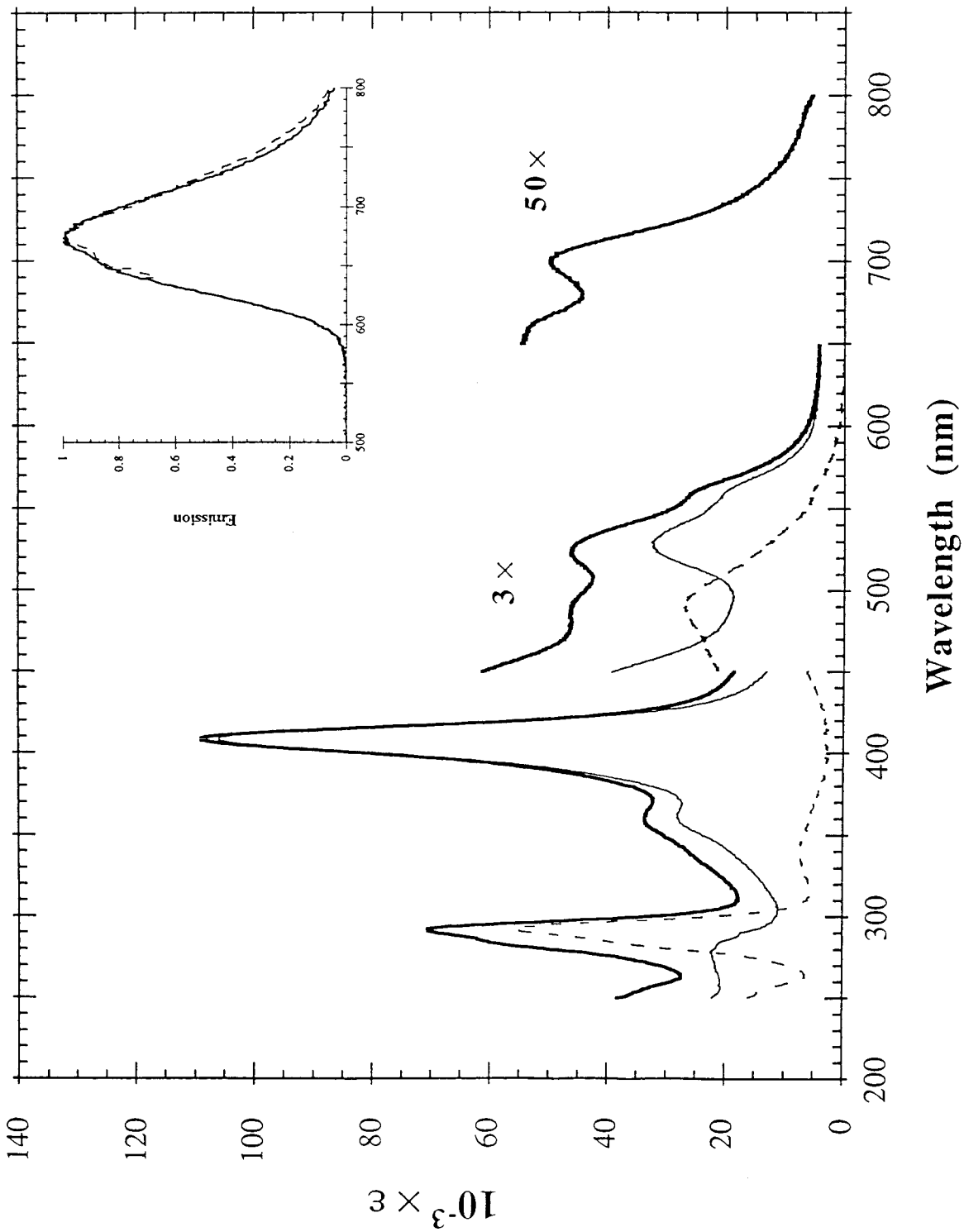
10-3 × ε
140
120
100
80
60
40
20
0
200
300
400
500
600
700
800
Wavelength (nm)
3 ×
50 ×
Emission
1
0.8
0.6
0.4
0.2
0
500
600
700
800

Figure 3.8. Thermal unfolding of representative yeast cyt *c* mutants. (**A**) Thermal denaturation profiles for the oxidized forms of Gln39 (open circle) and His66Phe67 (triangle) cyt *c* in μ 100 mM NaP_i, pH 7.0. (**B**) Thermally induced changes in the far-UV CD spectrum of Gln39 cyt *c*. Arrows indicate the directions of the shifts with increasing temperature.

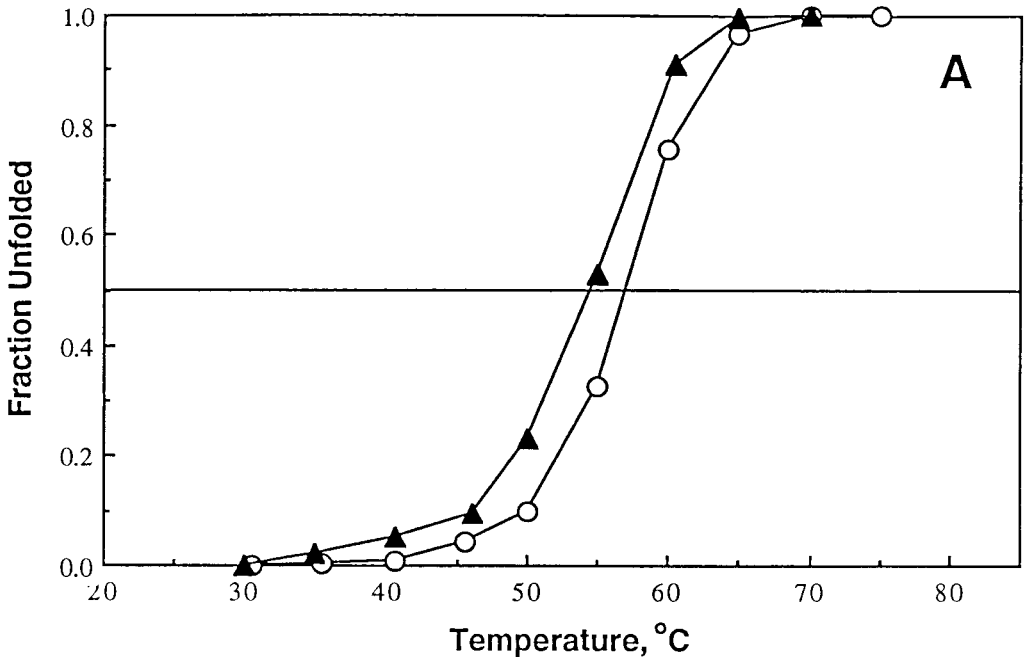
A
Fraction Unfolded
1.0
0.8
0.6
0.4
0.2
0.0
20
30
40
50
60
70
80
Temperature, °C

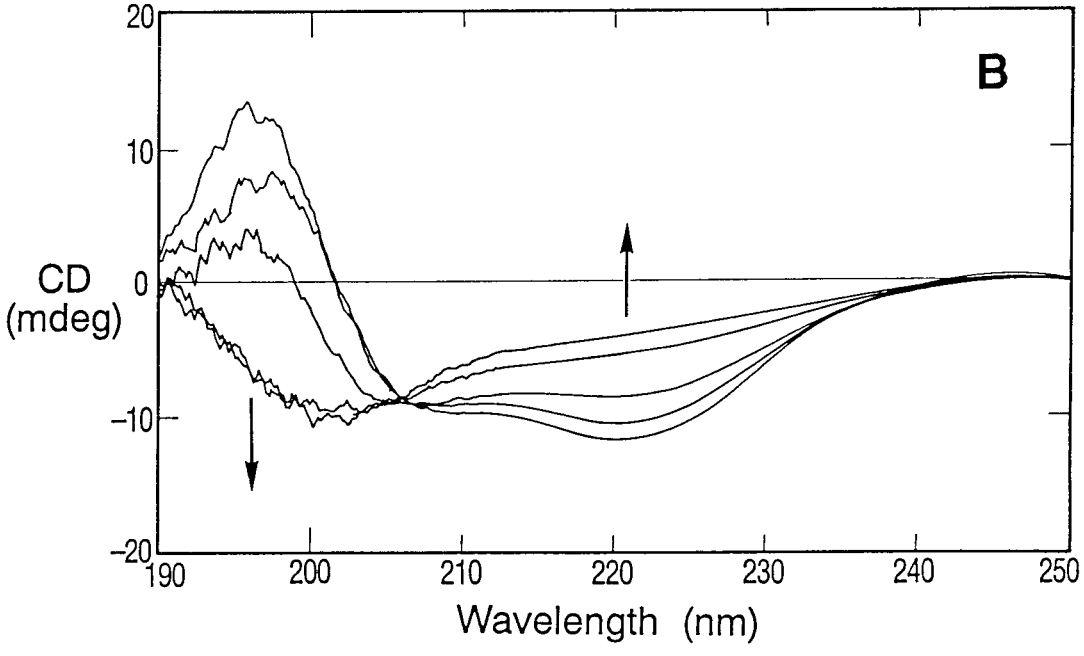
B
CD
(mdeg)
20
10
0
-10
-20
190
200
210
220
230
240
250
Wavelength (nm)

Figure 3.9. Cyclic voltammograms of unmodified (---) and $Ru(bpy)_2(im)$-modified yeast iso-1-cytochromes *c* (—) in μ 100 mM NaP_i, pH 7.0, 22 °C. Shown are the signal currents for Gln39 (A: peak separation ΔE of 75 mV; midpoint potential $E_{1/2}$ of 260 mV vs. NHE; scan rate V of 5 mV/s), His66 (dashed line, B: ΔE = 70 mV; $E_{1/2}$ = 258 mV vs. NHE; V = 5 mV/s), $Ru(bpy)_2(im)$(His66)- (solid line, B: ΔE = 115 mV; $E_{1/2}$ = 255 mV vs. NHE; V = 5 mV/s), His58 (dashed line, C: ΔE = 65 mV; $E_{1/2}$ = 272 mV vs. NHE; V = 5 mV/s), and $Ru(bpy)_2(im)$(His58)cyt *c* (solid line, C: ΔE = 110 mV; $E_{1/2}$ = 290 mV vs. NHE; V = 1 mV/s).

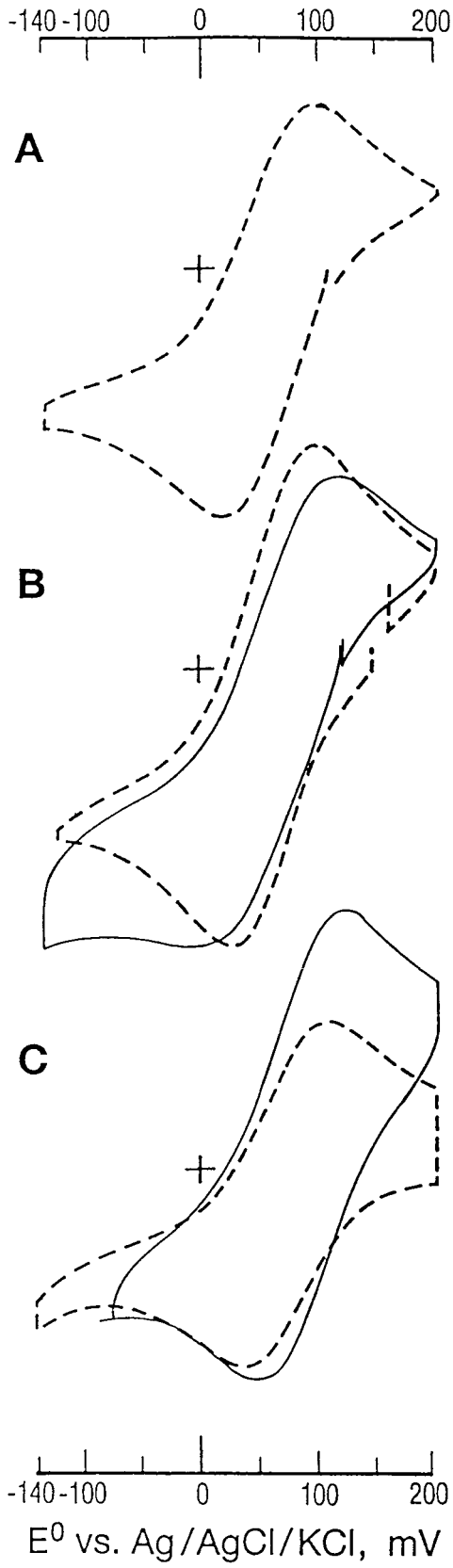
-140 -100 0 100 200
A
B
C
-140 -100 0 100 200
E⁰ vs. Ag/AgCl/KCl, mV

Figure 3.10. Cation-exchange chromatograms of the reaction products of $Ru(bpy)_2(im)^{2+}$ with the cyt *c* mutants: Ser102 (**A**); His58 (**B**); His66 (**C**); and His66Phe67 cyt *c* (**D**). The Ru:Fe contents of the protein bands are determined by the A_{290}/A_{410} ratio (~ 2/3 for 1Ru:1Fe) and are indicated beside the bands. Also marked are the desired 1:1 Ru(HisX) products whose sites of complexation (HisX) have been verified by tryptic analyses. The Ru reagent was also found to bind to protein functionalities other than a histidine (1:1(-)); these products do not have the characteristic 492-nm MLCT band.

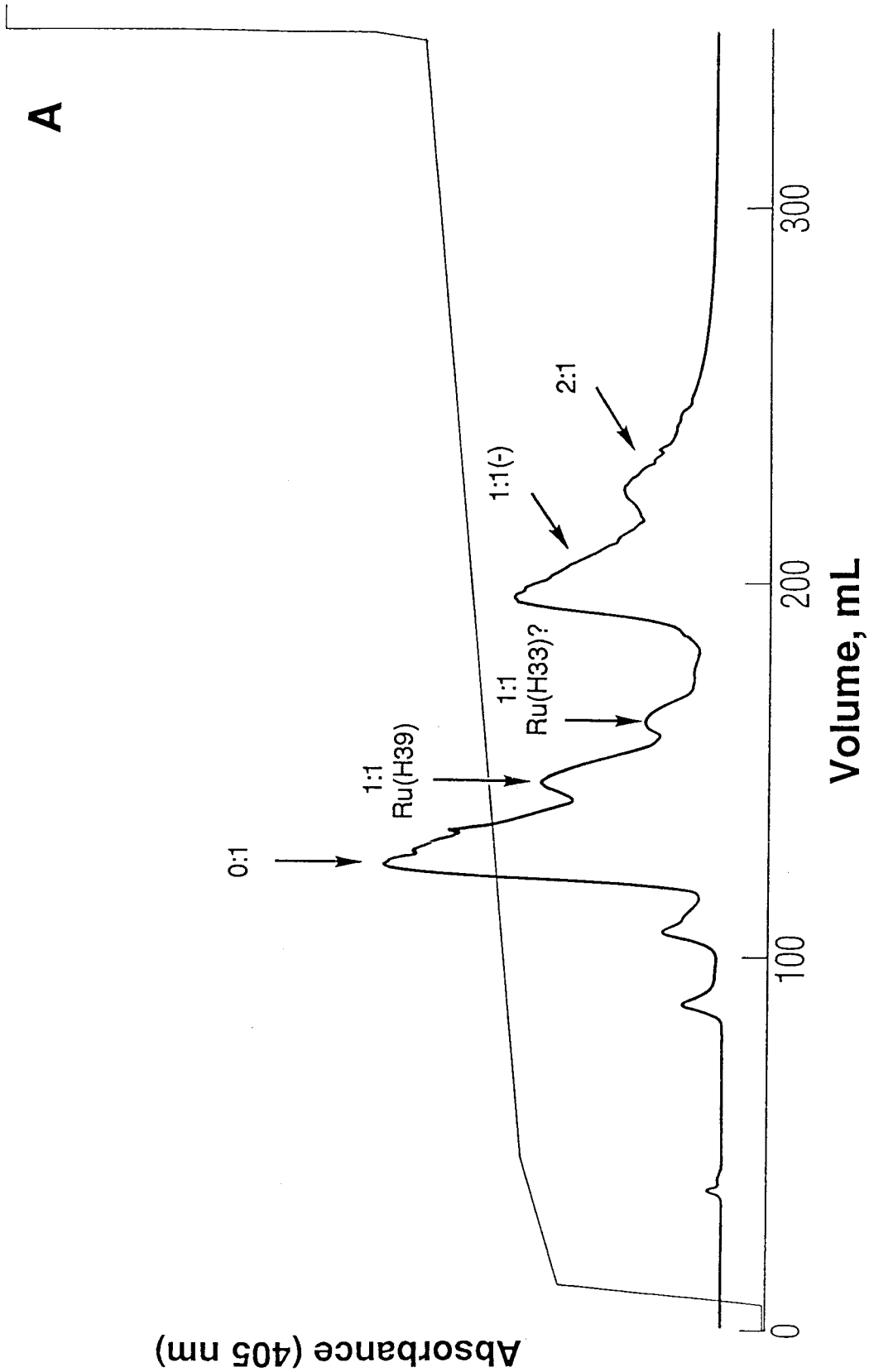
A
Absorbance (405 nm)
Volume, mL
0
100
200
300
0:1
1:1
Ru(H39)
1:1
Ru(H33)?
1:1(-)
2:1

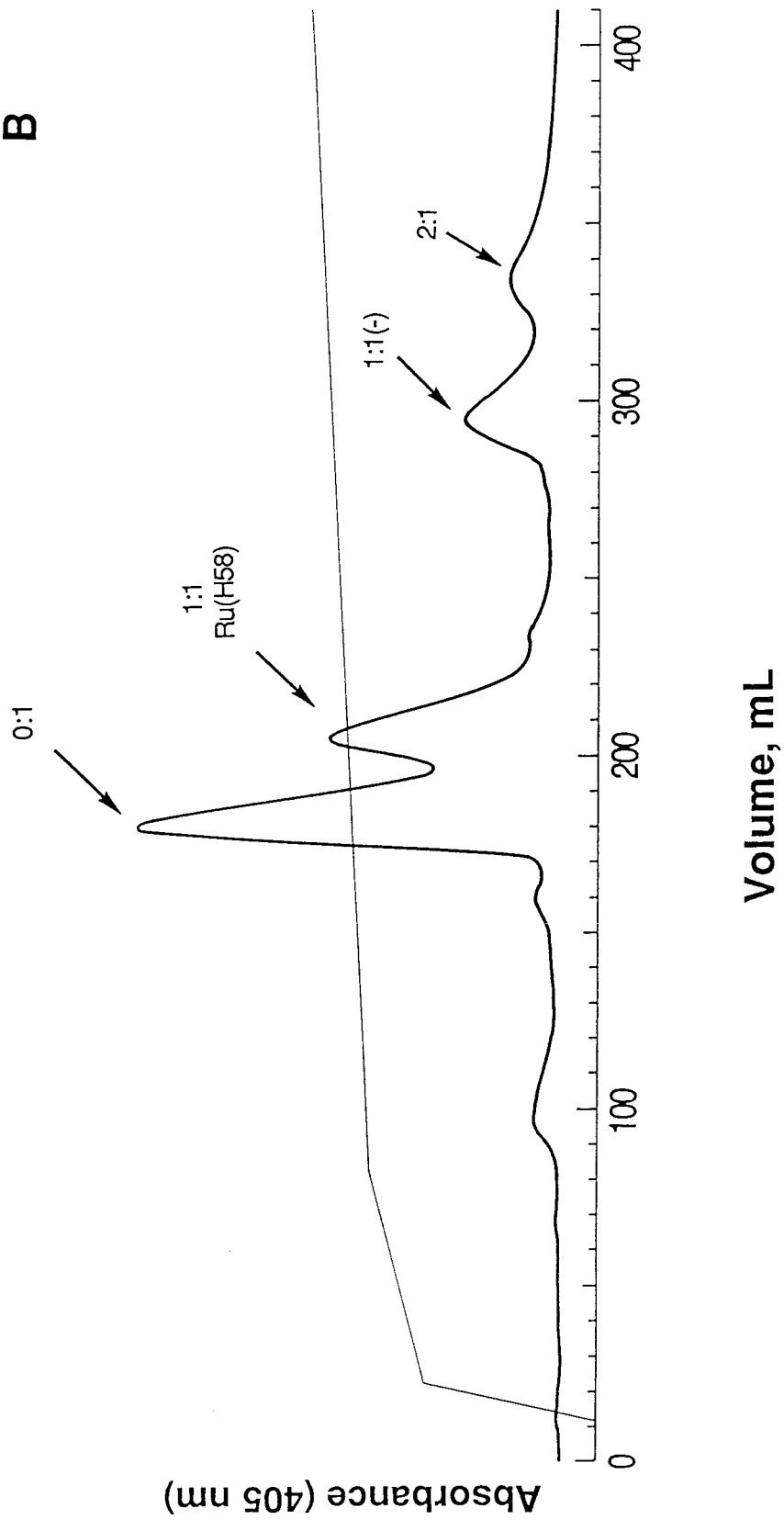
B
0:1
1:1
Ru(H58)
1:1(-)
2:1
0
100
200
300
400
Volume, mL
Absorbance (405 nm)

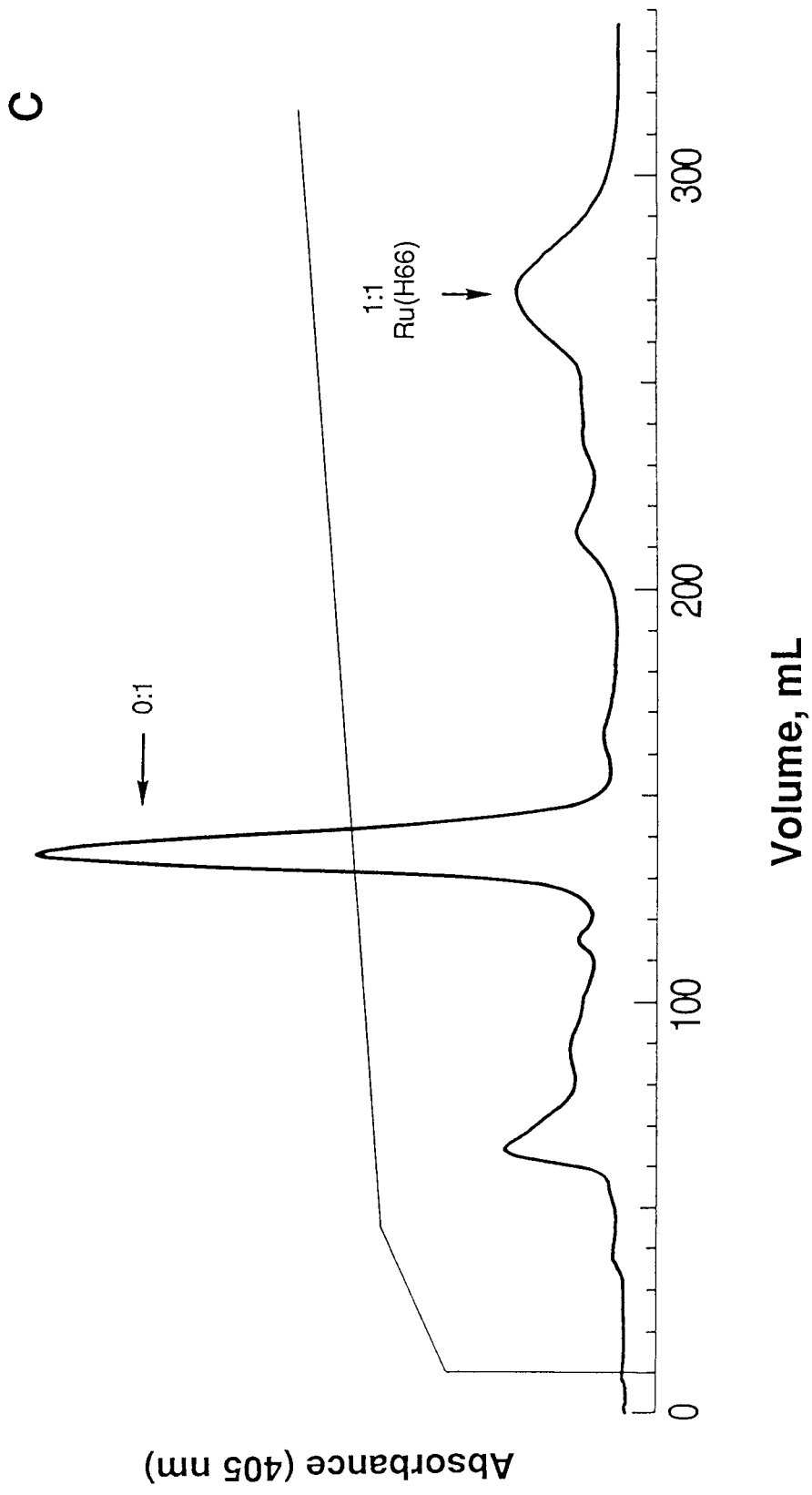
C
Absorbance (405 nm)
Volume, mL
0
100
200
300
0:1
1:1
Ru(H66)

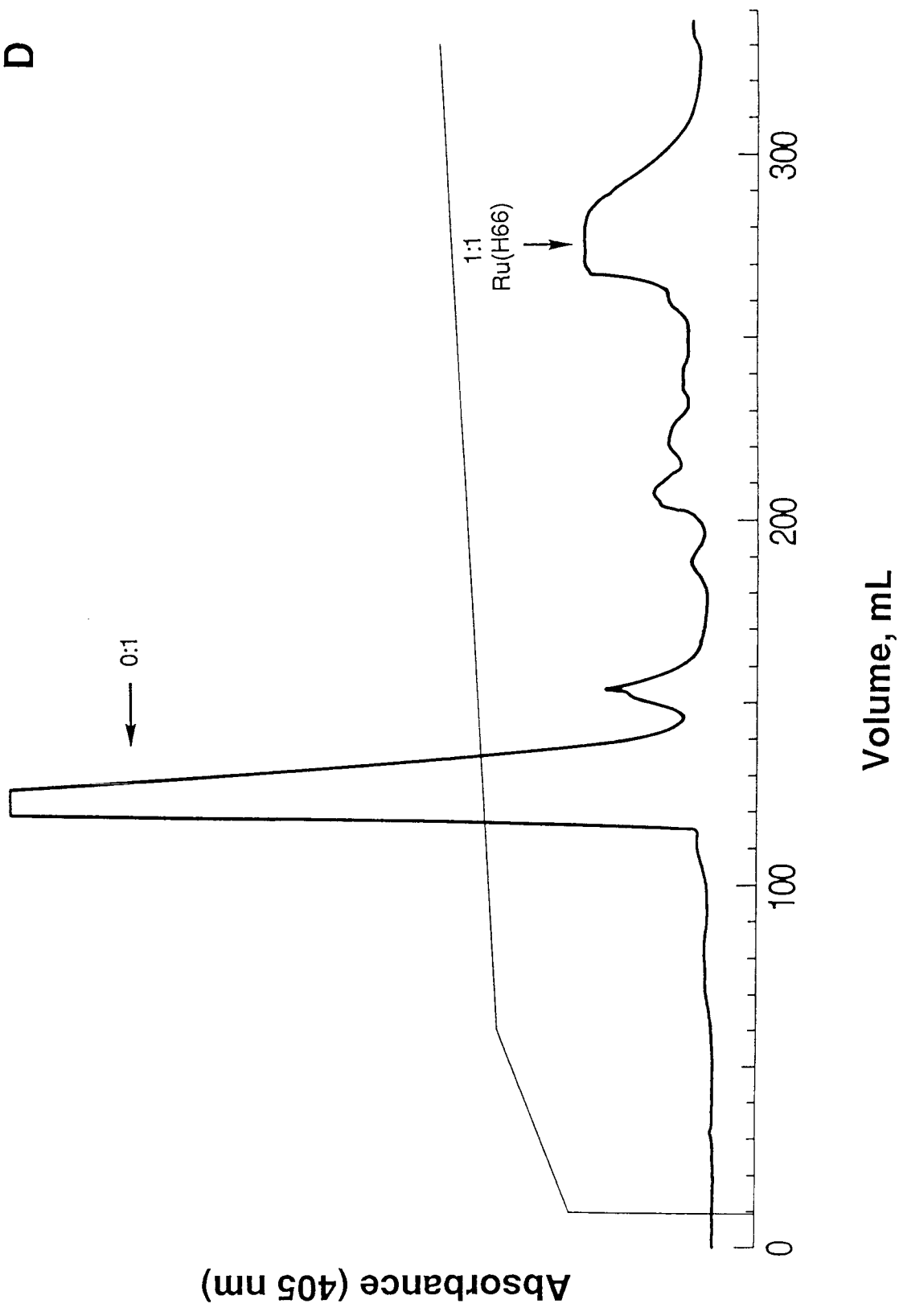
D
Absorbance (405 nm)
Volume, mL
0
100
200
300
0:1
1:1
Ru(H66)

Figure 3.11. Reverse-phase chromatograms of tryptic digests of His66Phe67 cyt *c* (**A**) and $Ru(bpy)_2(im)$(His66Phe67)cyt *c* (**B**) as monitored with a 280-nm filter. In **C**, an identical sample as in **B** was run using a 405-nm filter. Buffer A: 0.1% trifluoroacetic acid (TFA) in ddH_2O; buffer B, 0.1% TFA in acetonitrile. A resolving gradient was developed to 40% B over 100 mL of eluent. The tryptic fragments are identified by the number of the first and last residues in the sequence; the pendant metal centers are indicated as well.

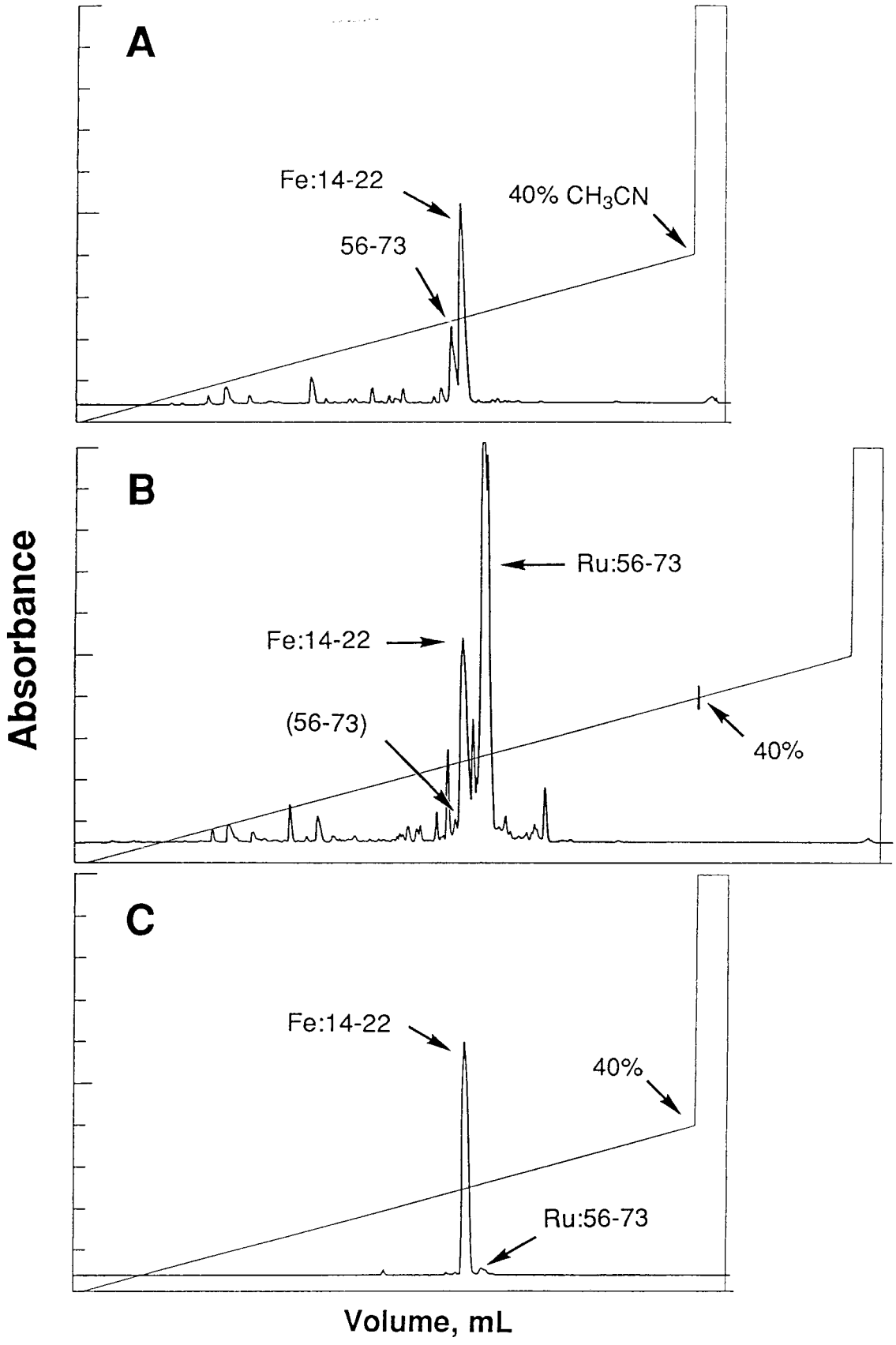
A
Fe:14-22
56-73
40% CH3CN
B
Ru:56-73
Fe:14-22
(56-73)
40%
C
Fe:14-22
40%
Ru:56-73
Absorbance
Volume, mL

Figure 3.12. Osteryoung square wave voltammograms of $Ru(bpy)_2(im)(His33)$cyt *c*. (**A**) First scan of the protein solution (*ca.* 1 mM in μ 100 mM NaP_i, pH 7.0, 22 °C). (**B**) Successive scan with the same electrode. (**C**) The working electrode rinsed after use with ddH_2O and immersed in phosphate buffer. OSWV of aqueous solutions of the model compound, $Ru(bpy)_2(im)_2Cl_2$, (**D**) and $Ru(bpy)_2(OH_2)(His33)$cyt *c* (c*a.* 0.6 mM) (**E**) were likewise collected.

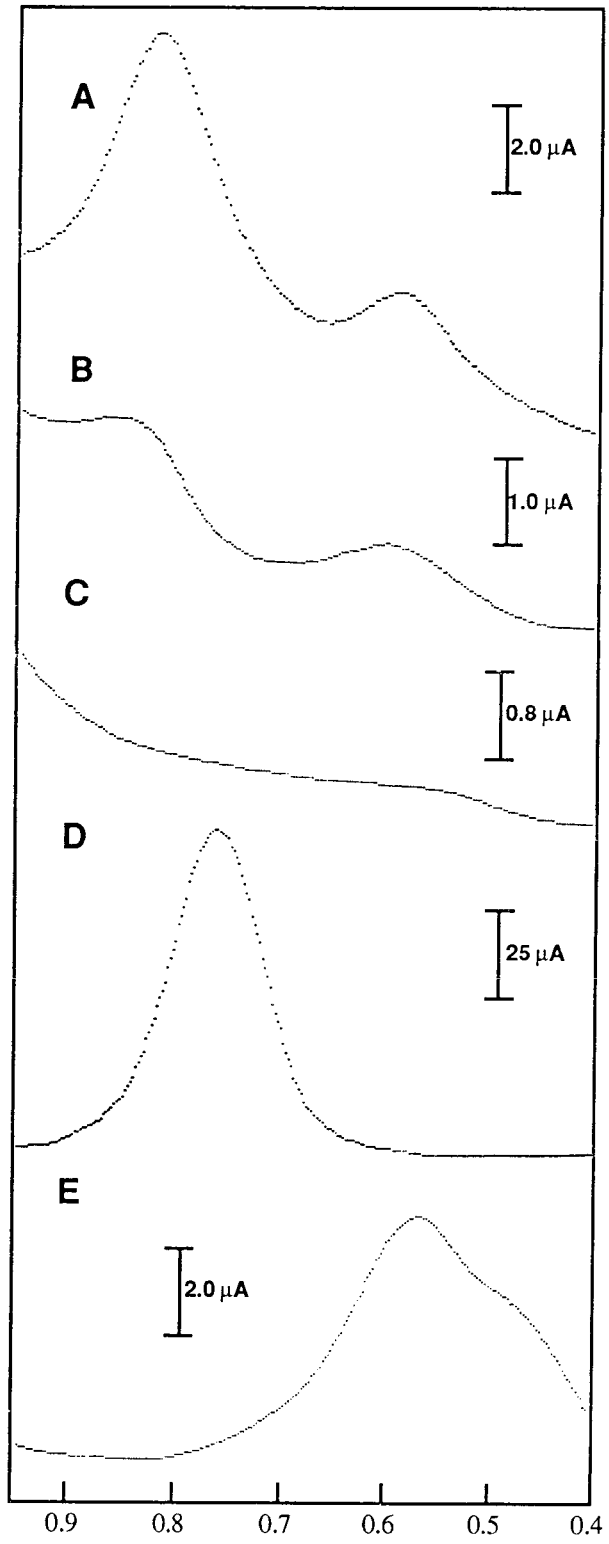
A
2.0 μA
B
1.0 μA
C
0.8 μA
D
25 μA
E
2.0 μA
0.9
0.8
0.7
0.6
0.5
0.4
E° vs. SCE, V

Figure 3.13. Osteryoung square wave voltammograms of $Ru(dmbpy)_2(im)(His33)$cyt *c*. (**A**) First scan of the protein solution at 22 °C (*ca.* 1 mM, μ 100 mM NaP_i, pH 7.0). (**B**) Successive scan with the same electrode. (**C**) The working electrode rinsed with ddH_2O and immersed in phosphate buffer. The model compound, $Ru(dmbpy)_2(im)_2Cl_2$, has a reduction potential of 0.878(5) mV vs. NHE (**D**). The shoulder in (**D**) is due to trace amounts of $Ru(bpy)_2(im)_2^{2+}$ left on the electrode between measurements.

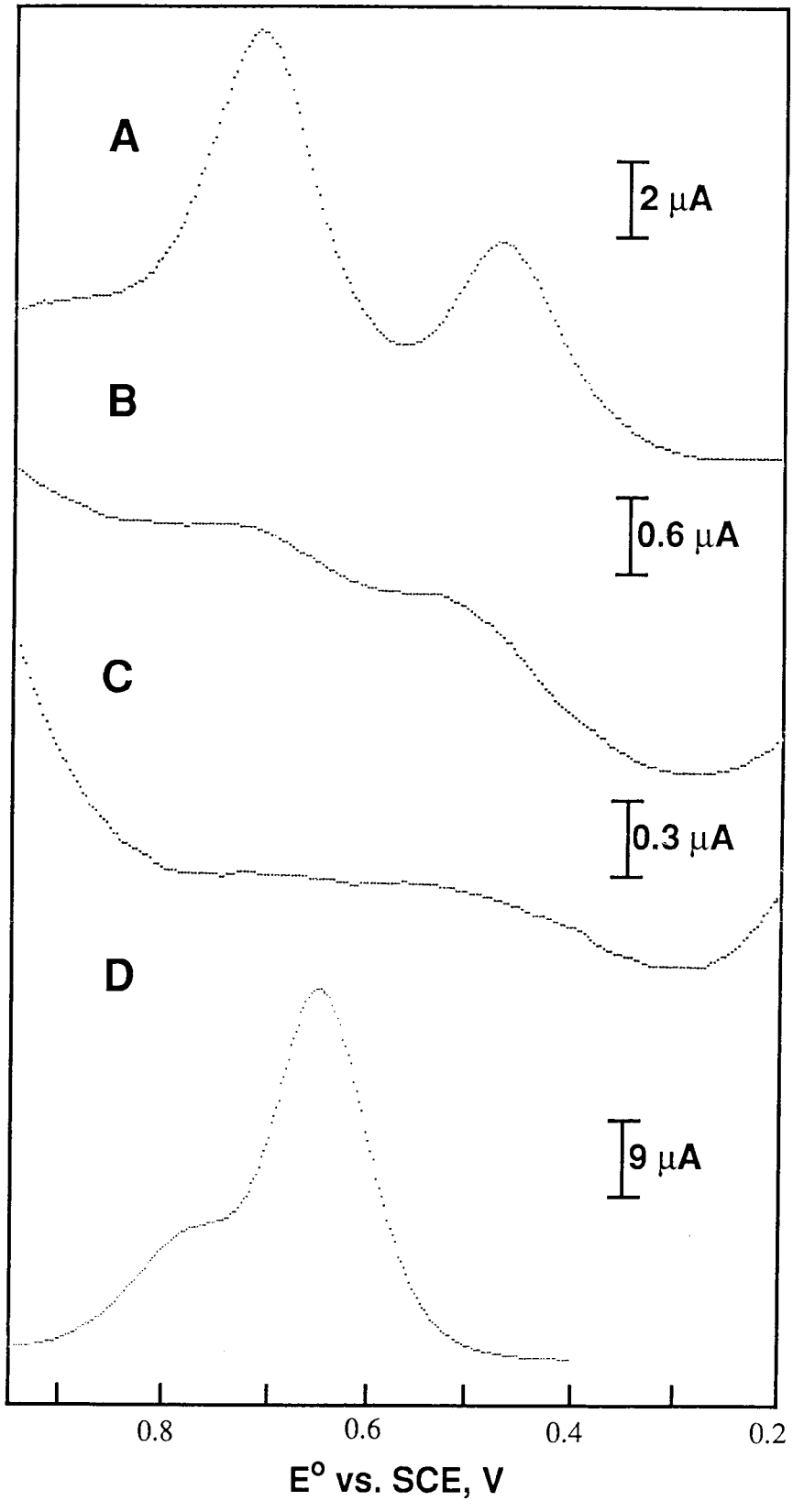
A
2 μA
B
0.6 μA
C
0.3 μA
D
9 μA
0.8
0.6
0.4
0.2
E° vs. SCE, V

Figure 3.14. Osteryoung square wave voltammograms of $Ru(bpy)_2(im)$(His66Phe67)cyt *c*. (**A**) First scan of the protein solution (*ca.* 1 mM in μ 100 mM NaP_i, pH 7.0, 22 °C). (**B**) Successive scan with the same electrode. (**C**) The working electrode rinsed with ddH_2O and immersed in phosphate buffer.

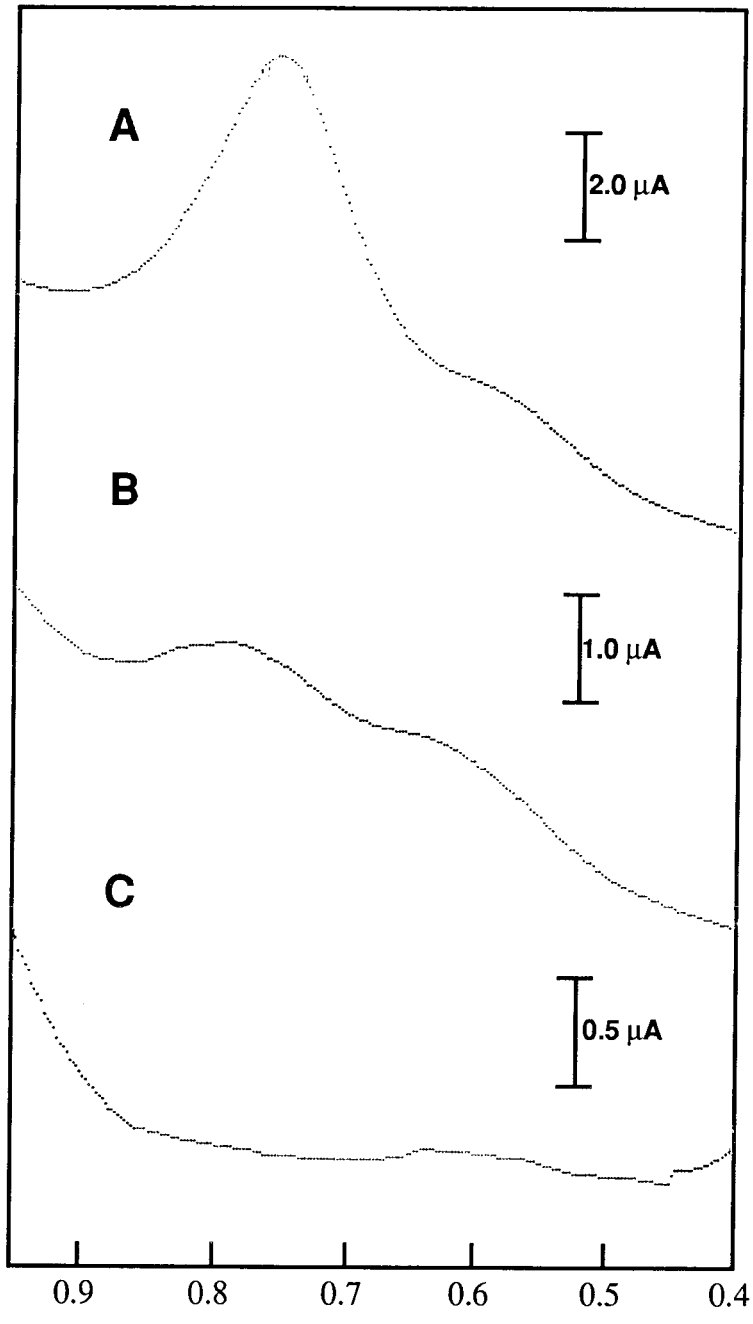
A
2.0 μA
B
1.0 μA
C
0.5 μA
0.9
0.8
0.7
0.6
0.5
0.4
E° vs. SCE, V

Figure 3.15. Comparison of OSWV scans for $Ru(bpy)_2(im)$(His66Phe67)cyt *c* (**A**), $Ru(bpy)_2(im)$(His33)cyt *c* (**B**), and $Ru(dmbpy)_2(im)$(His33)cyt *c* (**C**). Taken from the previous figures.

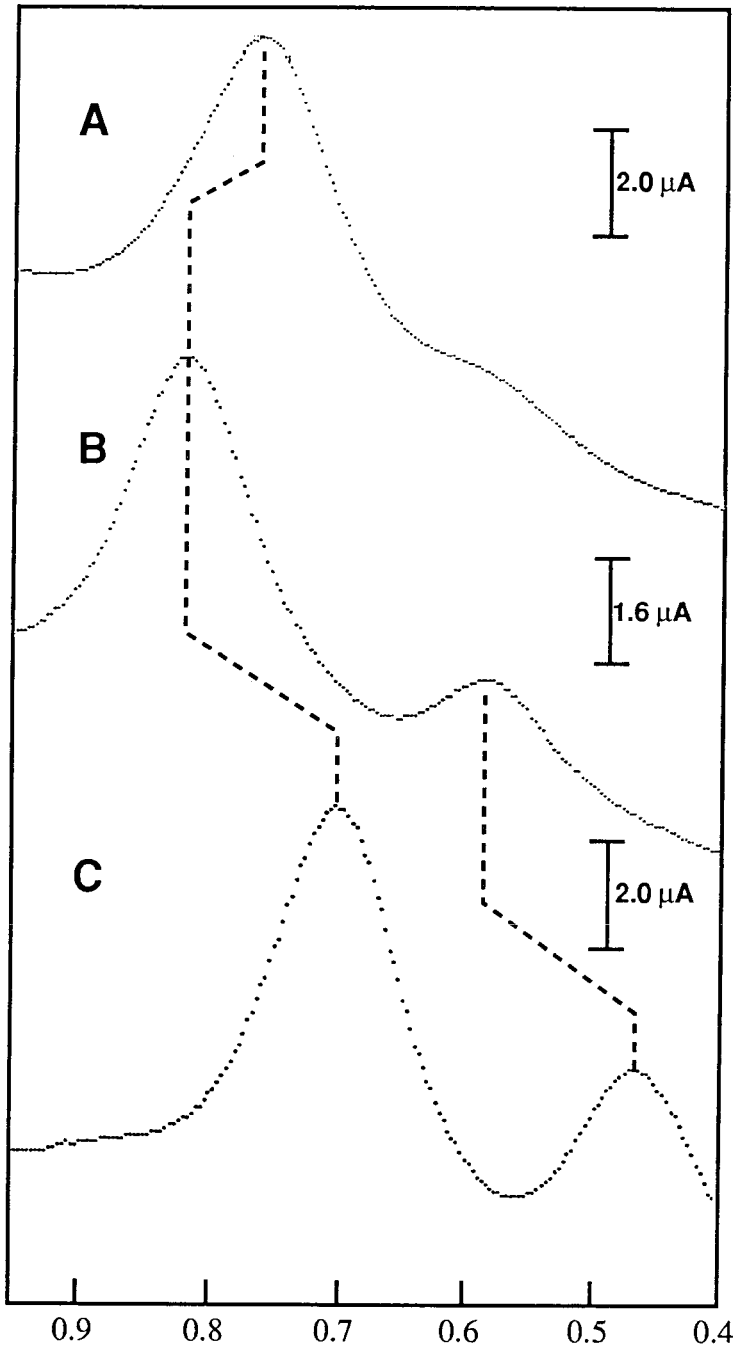
A
2.0 μA
B
1.6 μA
C
2.0 μA
0.9
0.8
0.7
0.6
0.5
0.4
E° vs. SCE, V

Figure 3.16. Transient absorbances at 550 nm (**A**) and 339 nm (**B**) of a solution of $Ru(bpy)_2(im)(His39)$cyt *c* (30 μM) and $Ru(NH_3)_6^{3+}$ (7 mM) following a 20-ns 480-nm excitation pulse (μ 100 mM NaP_i, pH 7.0, 22 °C).

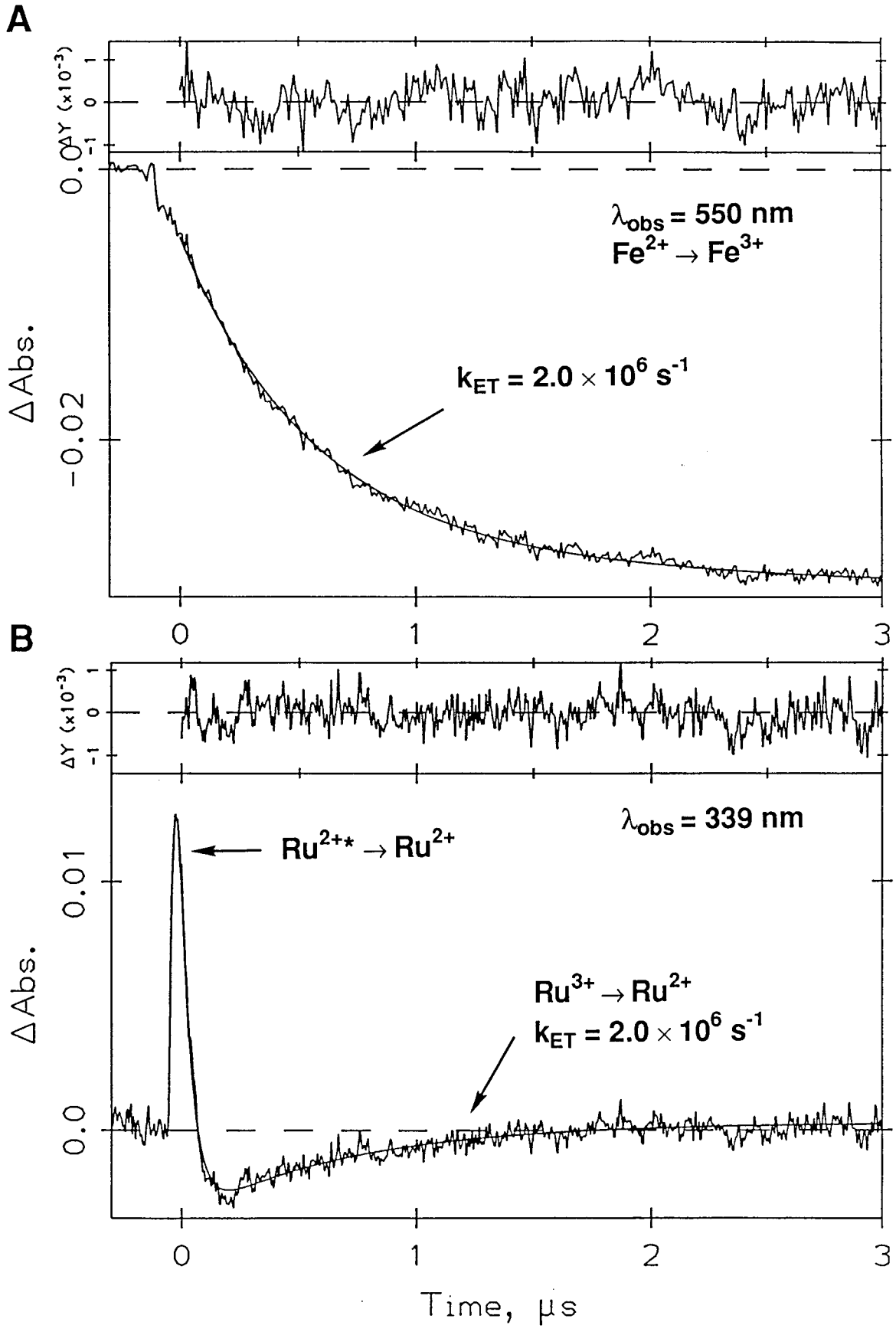
A
ΔY (x10⁻³)
1
0
-1
0.0
λobs = 550 nm
Fe2+ → Fe3+
kET = 2.0 × 10⁶ s⁻¹
ΔAbs.
-0.02
0
1
2
3
B
ΔY (x10⁻³)
1
0
-1
λobs = 339 nm
Ru2+* → Ru2+
0.01
Ru3+ → Ru2+
kET = 2.0 × 10⁶ s⁻¹
ΔAbs.
0.0
0
1
2
3
Time, μs

Figure 3.17. Transient absorbances at 550 nm (**A**) and 504 nm (**B**) of a solution of $Ru(bpy)_2(im)(His58)$cyt *c* (15 μM) and $Ru(NH_3)_6^{3+}$ (7 mM) following a 20-ns 480-nm excitation pulse (μ 100 mM NaP_i, pH 7.0, 22 °C).

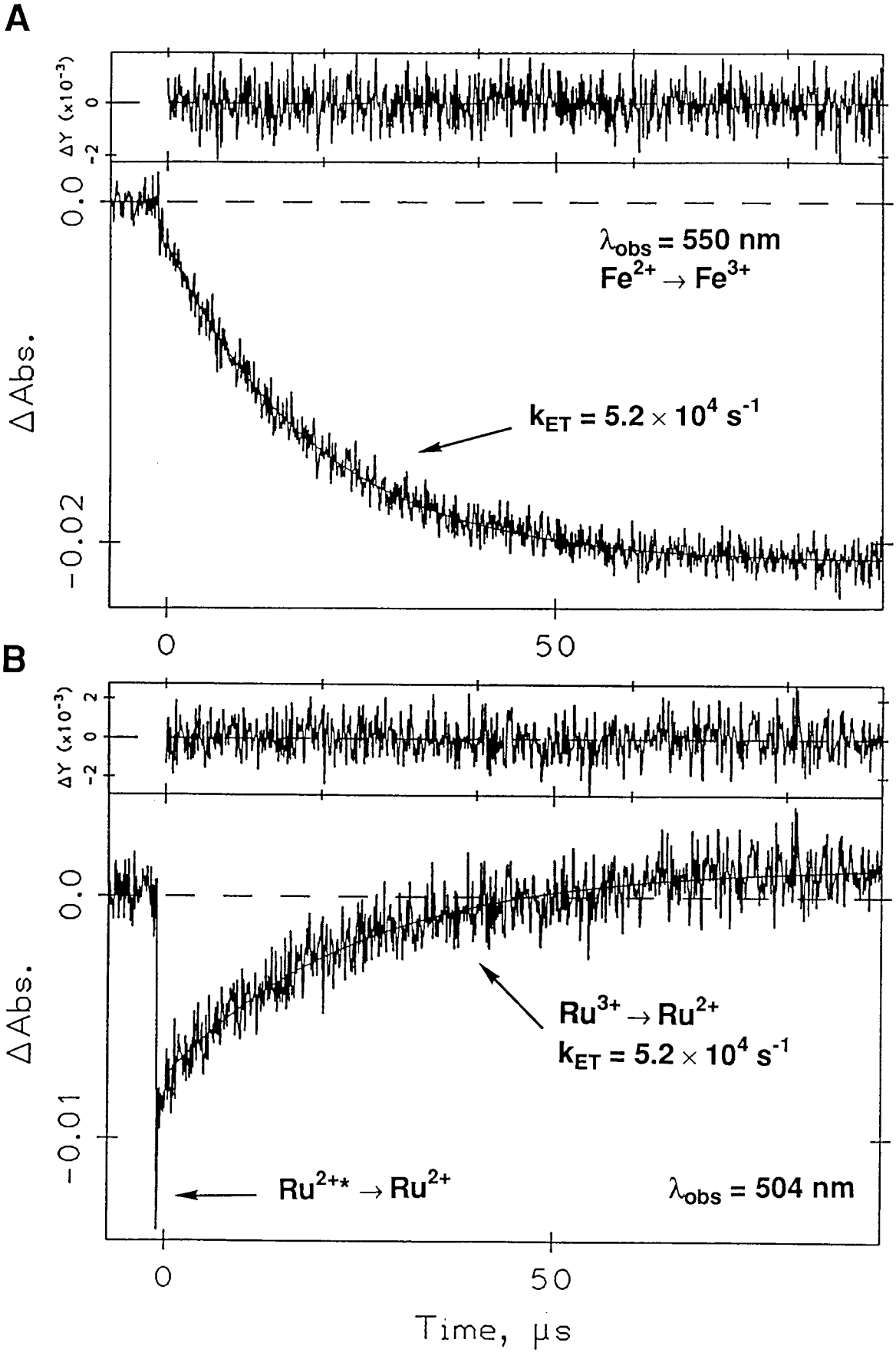
A
ΔY (x10⁻³)
0
-2
0.0
λobs = 550 nm
Fe2+ → Fe3+
ΔAbs.
kET = 5.2 × 10⁴ s⁻¹
-0.02
0
50
B
ΔY (x10⁻³)
2
0
-2
0.0
Ru3+ → Ru2+
kET = 5.2 × 10⁴ s⁻¹
ΔAbs.
-0.01
Ru2+* → Ru2+
λobs = 504 nm
0
50
Time, μs

Figure 3.18. Transient absorbances at 550 nm (**A**) and 339 nm (**B**) of a solution of $Ru(bpy)_2(im)(His66)cyt\ c$ (20 mM) and $Ru(NH_3)_6^{3+}$ (6 mM) following a 20-ns 480-nm excitation pulse (μ 100 mM NaP_i, pH 7.0, 22 °C).

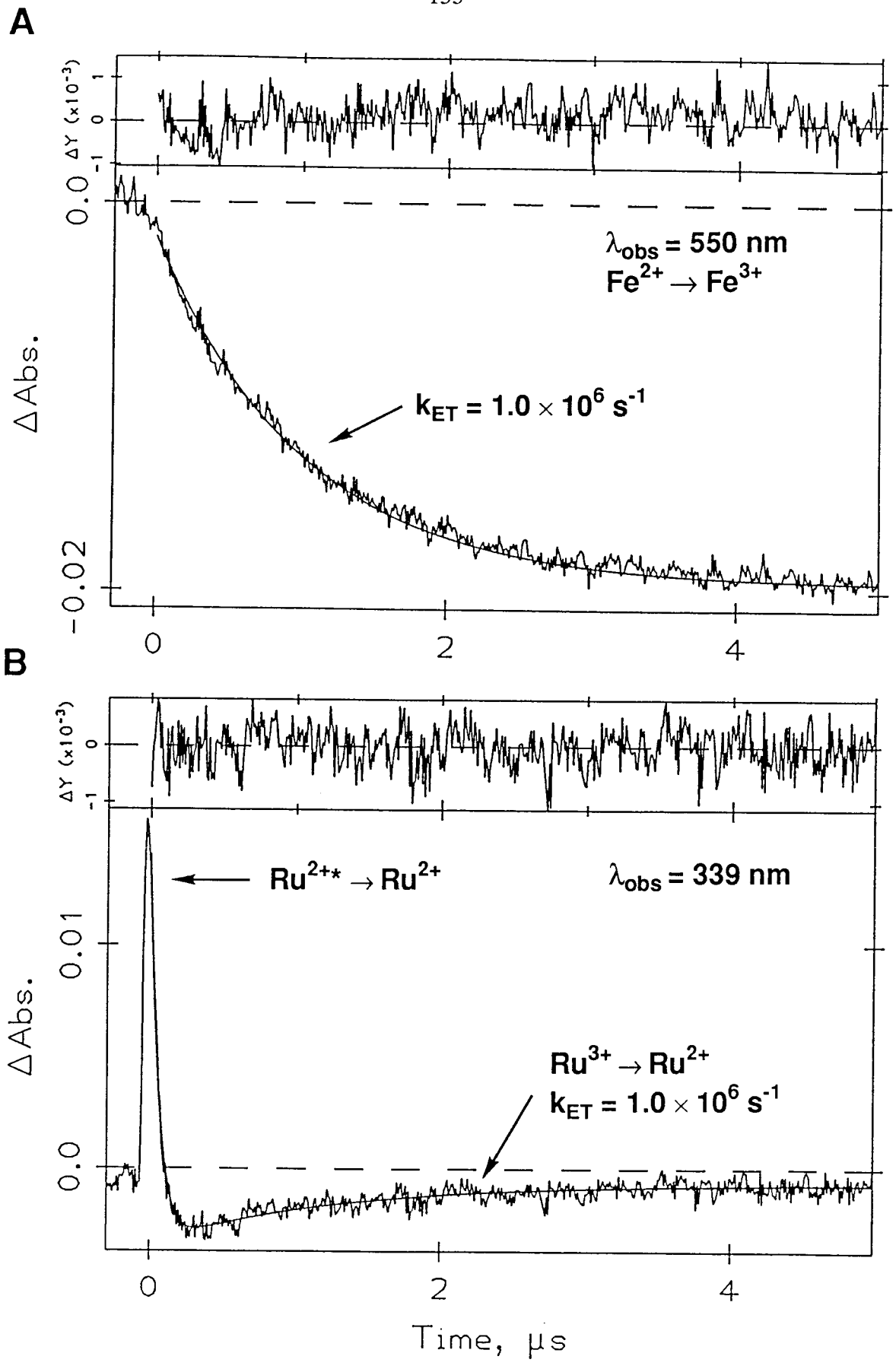
A
ΔY (x10⁻³)
1
0
-1
0.0
λobs = 550 nm
Fe2+ → Fe3+
ΔAbs.
kET = 1.0 × 10⁶ s⁻¹
-0.02
0
2
4
B
ΔY (x10⁻³)
0
-1
Ru2+* → Ru2+
λobs = 339 nm
0.01
ΔAbs.
Ru3+ → Ru2+
kET = 1.0 × 10⁶ s⁻¹
0.0
0
2
4
Time, μs

Figure 3.19. Transient absorbances at 550 nm (**A**) and 504 nm (**B**) of a solution of $Ru(bpy)_2(im)$(His66Phe67)cyt *c* (12 μM) and $Ru(NH_3)_6^{3+}$ (5 mM) following a 20-ns, 480-nm excitation pulse (μ 100 mM NaP_i, pH 7.0, 22 °C). The Ru signal does not return to the zero point at this time scale because of traces in the starting material of oxidized protein that gives an ET-inactive Ru^{3+}-Fe^{3+} complex.

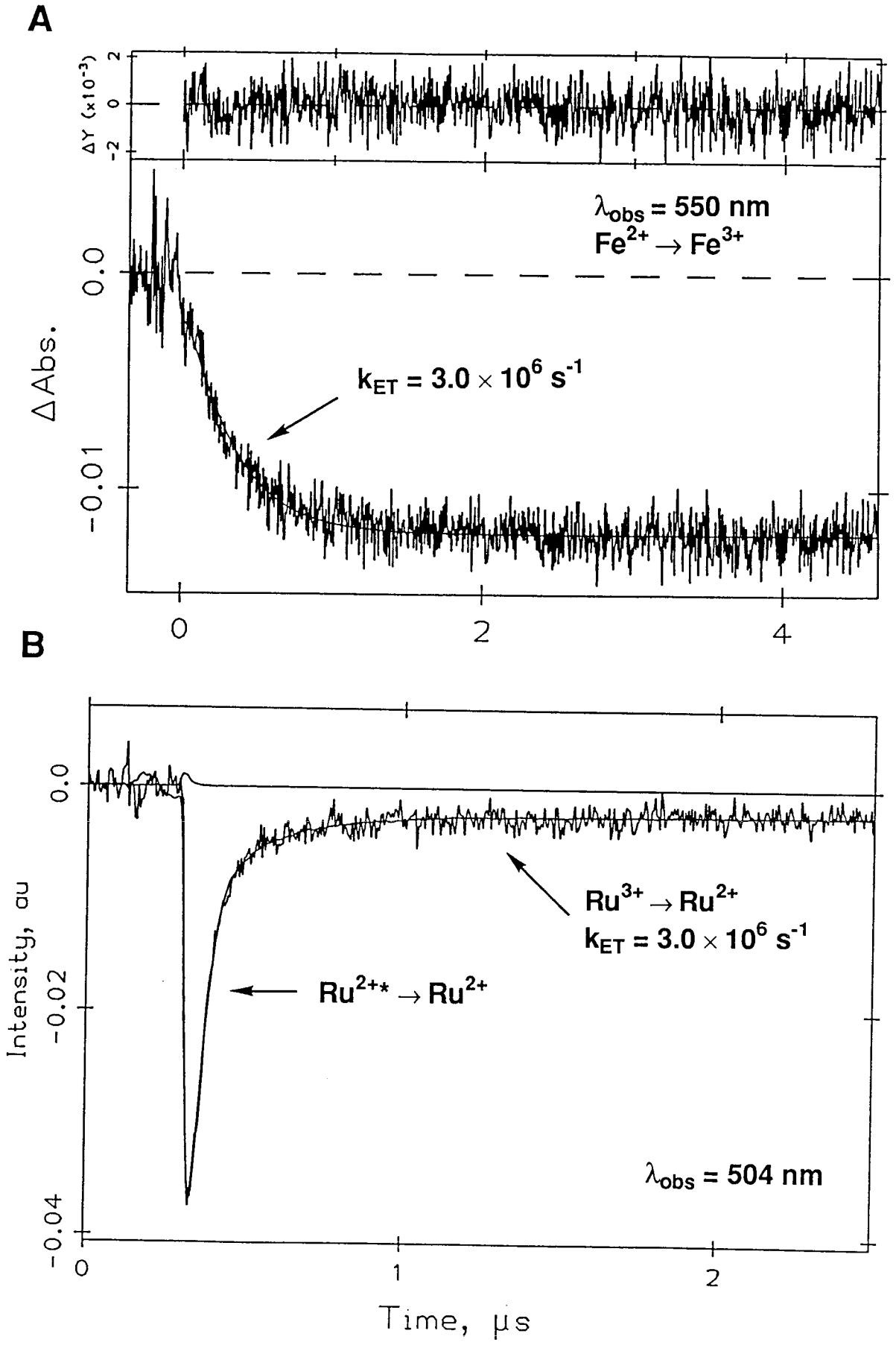
A
ΔY (x10⁻³)
2
0
-2
λobs = 550 nm
Fe2+ → Fe3+
0.0
ΔAbs.
kET = 3.0 × 10⁶ s⁻¹
-0.01
0
2
4
B
0.0
Intensity, au
Ru3+ → Ru2+
kET = 3.0 × 10⁶ s⁻¹
Ru2+* → Ru2+
-0.02
λobs = 504 nm
-0.04
0
1
2
Time, μs

Figure 3.20. Flash-quench transient-absorption traces (550 nm) for Ru(dmbpy)$_2$(im)(HisX)cytochromes *c*. (**A**) 14 μM Ru(dmbpy)$_2$(im)(His39)cyt *c* + 3 mM $Ru(NH_3)_6^{3+}$; (**B**) 10 μM Ru(dmbpy)$_2$(im)(His58)cyt *c* + 4 mM $Ru(NH_3)_6^{3+}$; (**C**) 20 μM Ru(dmbpy)$_2$(im)(His66)cyt *c* + 7 mM $Ru(NH_3)_6^{3+}$; and (**D**) 12 μM Ru(dmbpy)$_2$(im)(His66Phe67)cyt *c* + 10 mM methylviologen. All solutions are in μ 100 mM NaP_i, pH 7.0, 22 °C.

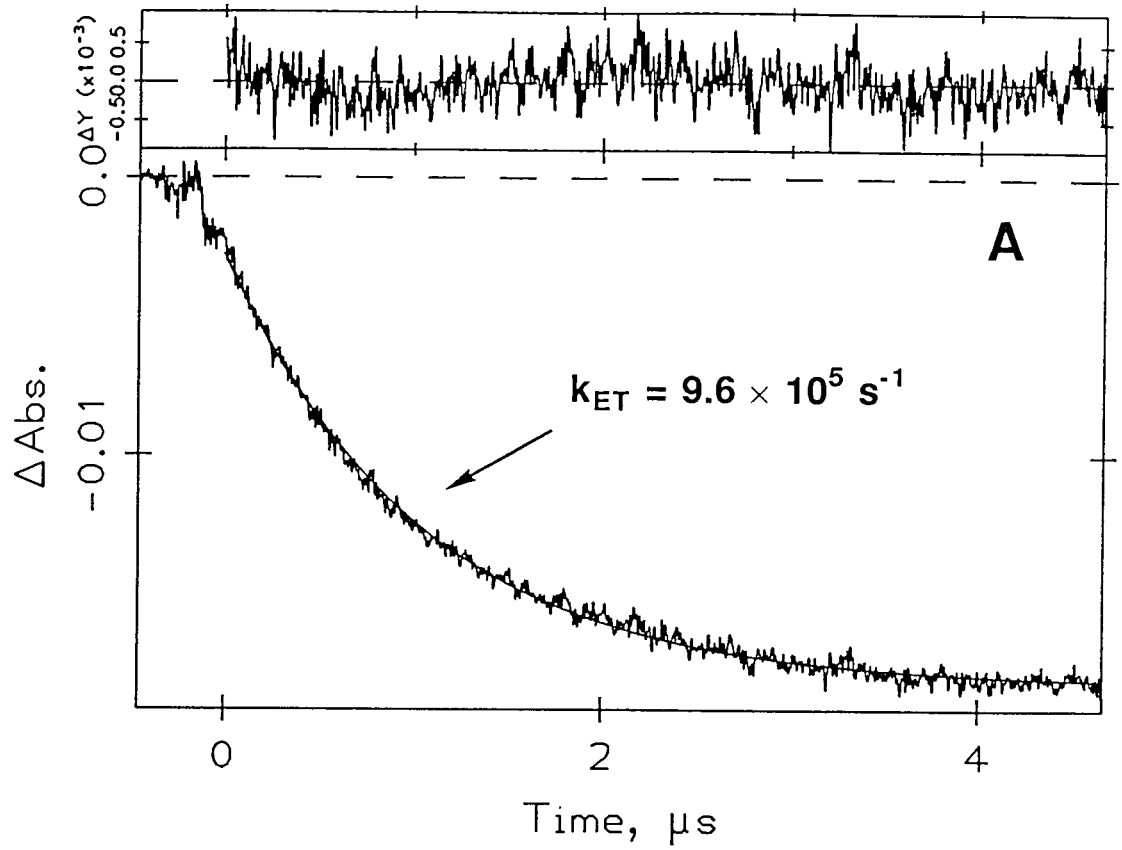
ΔY (x10⁻³)
0.0
-0.5 0.0 0.5
A
ΔAbs.
-0.01
$k_{ET} = 9.6 \times 10^5\ s^{-1}$
0
2
4
Time, μs

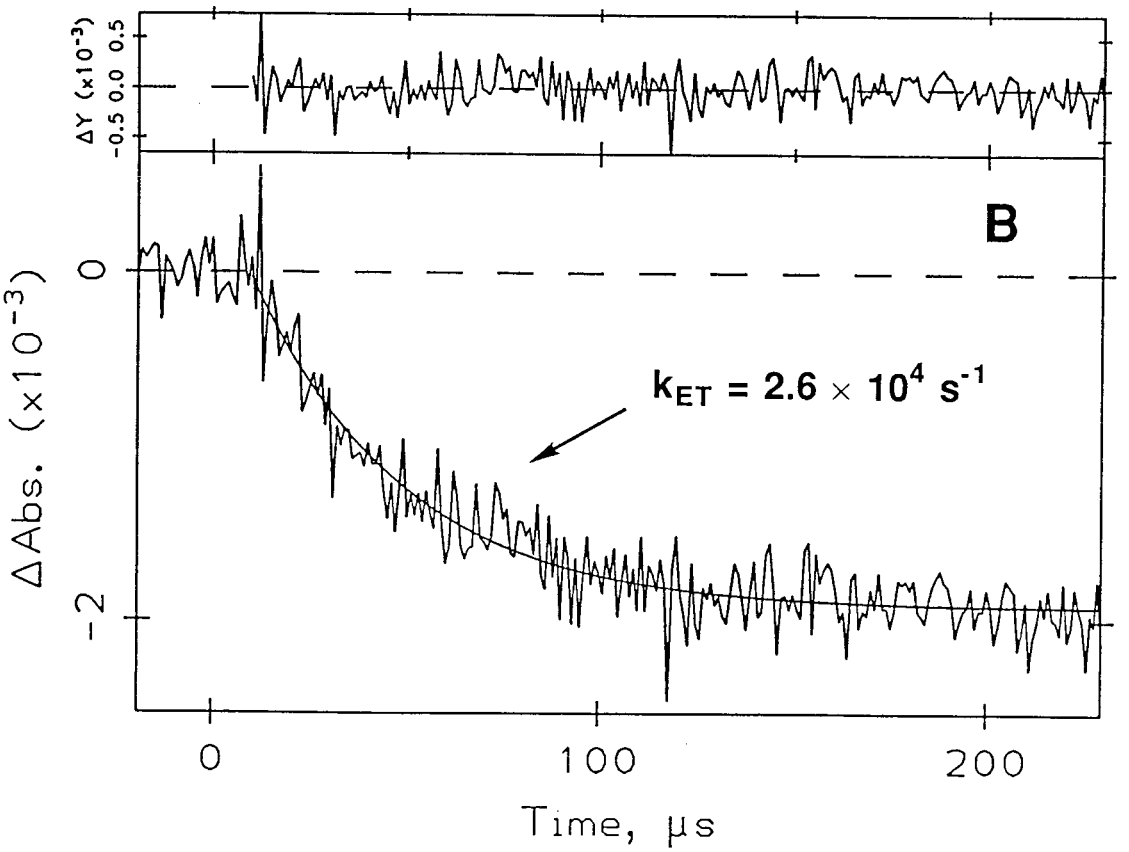
ΔY (x10⁻³)
-0.5 0.0 0.5
B
ΔAbs. (x10⁻³)
0
-2
$k_{ET} = 2.6 \times 10^4\ s^{-1}$
0
100
200
Time, μs

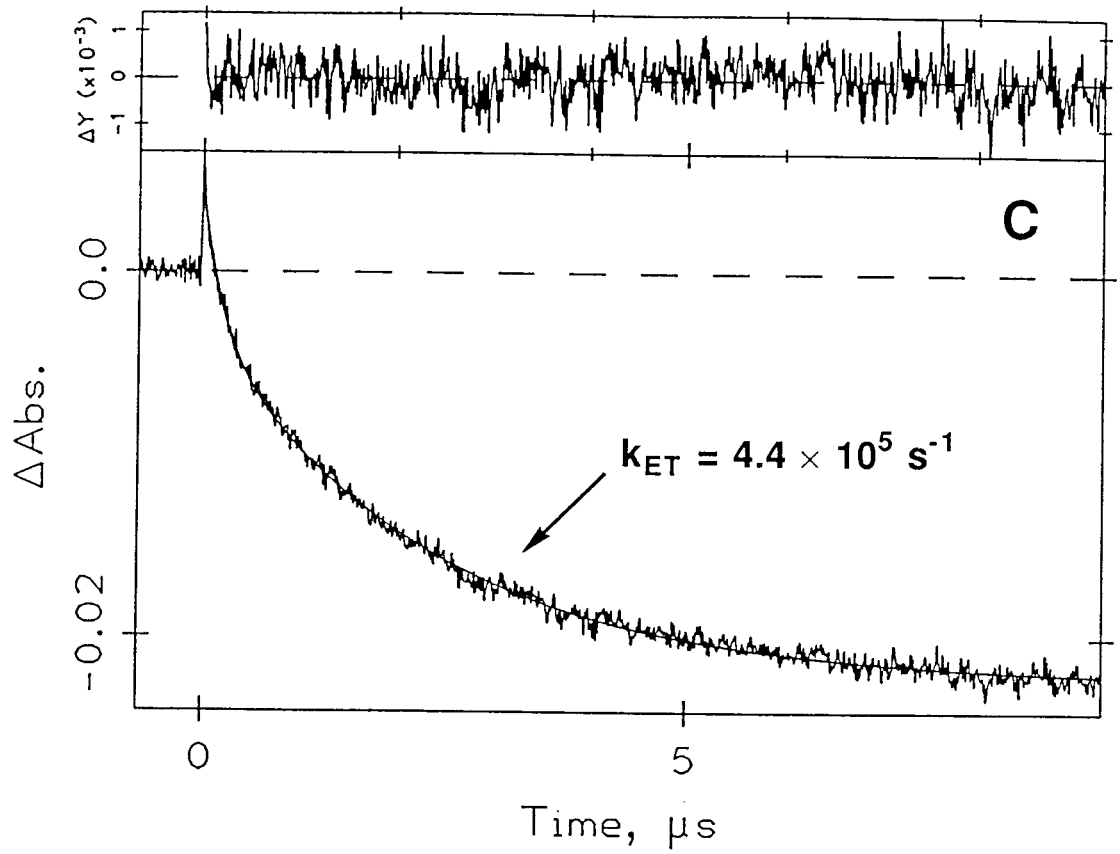
ΔY (x10⁻³)
1
0
-1
C
0.0
-0.02
ΔAbs.
$k_{ET} = 4.4 \times 10^5\ s^{-1}$
0
5
Time, μs

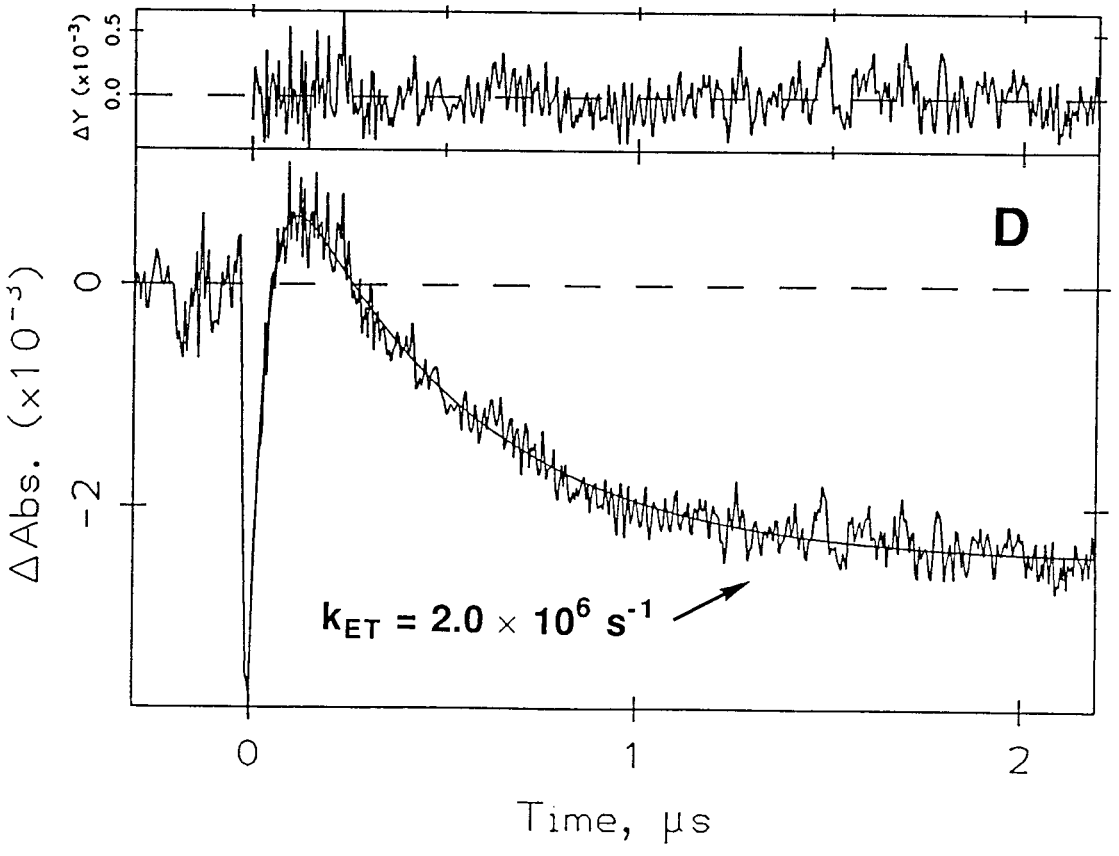
ΔY (x10⁻³)
0.5
0.0
D
0
-2
ΔAbs. (x10⁻³)
$k_{ET} = 2.0 \times 10^6\ s^{-1}$
0
1
2
Time, μs

Figure 3.21. Gaussian curves through the Ru(His66Phe67)cyt *c* data. In the analyses, λ is either held fixed at 0.8 eV (dashed line) or a variable (solid line). In the latter case, λ was determined to be 0.87 eV.

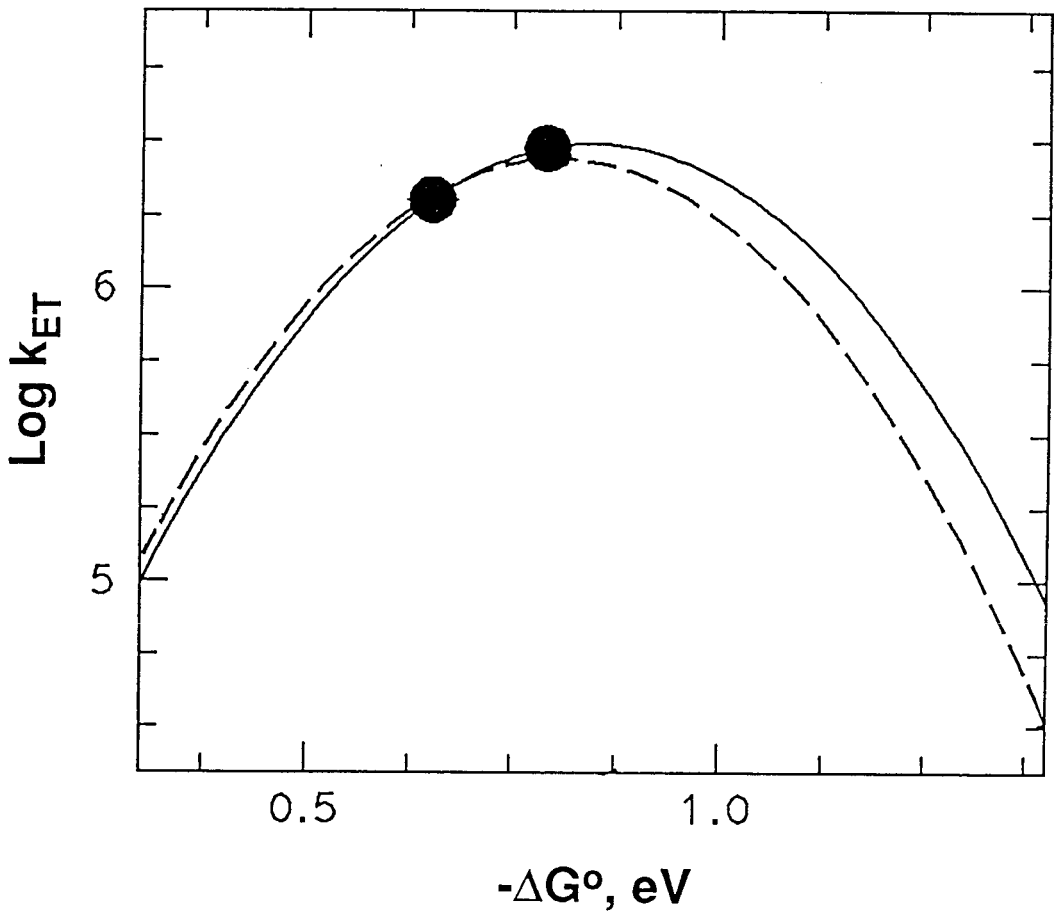
Log k_{ET}
6
5
0.5
1.0
-ΔG°, eV

Chapter 4

Donor-Acceptor Couplings in Ruthenium-Modified Human Myoglobins

Defining the Role of Aromatic Residues in Mediating Biological Electron Transfer. II: Donor-Acceptor Couplings in Ruthenium-Modified Yeast Iso-1-cytochromes *c*.

In the previous chapters, we have studied the intramolecular ET reactions in selected Ru-modified recombinant human myoglobins and cytochromes. In the following sections, we will examine the donor-acceptor (D-A) couplings in these systems in the context of current theoretical models so as to fully understand the mechanism of electron-exchange through a protein matrix.

SQUARE BARRIER MODEL

The concept of a one-dimensional square barrier is the oldest model ever formulated for quantum-mechanical tunneling,[1] but it is only in the recent year that there have been considerable experimental support for this model in ET reactions involving biological systems. In a major account, Dutton and coworkers[2] have analyzed the activationless ET rates for reactions involving bacterial photosynthetic reaction centers and in a number of chemically modified proteins; these systems represent a 20-Å distance spread and the rates cover 12 orders of magnitude. The rates were shown to follow an exponential dependence with intersite distance; the relationship is described by an ET rate of 10^{13} s^{-1} at van der Waals contact and a β of 1.4 s^{-1}, equivalent to a 10-fold drop in rate for every 1.7-Å increase in distance. The optimal rates for numerous covalently bridged D-A molecules were also analyzed collectively; β was found to be considerably smaller (0.7 $Å^{-1}$) and the rates extrapolated to a contact ET rate of ~10^{12} s^{-1}.

Computer models of the Ru-modified myoglobin and cytochrome *c* mutants were constructed using a rigid-body search procedure (Tables 4.1-4.2).[3] A logarithmic plot of k_{max} as a function of the edge-to-edge distances for these systems and other previously studied cytochromes[4] is shown in Figure 4.1A along with the line suggested by Dutton and coworkers. The k_{max} values for the Ru-modified heme proteins, however, fall below Dutton's line and do not correlate well with edge-to-edge separations. It is striking, for example, that Ru(His66)cyt *c* and Ru(His58)cyt *c* have roughly the same edge-to-edge

separation, yet the rates differ by 20-fold. Furthermore, both Ru(His66)- and Ru(His58)cyt *c* do not stand out from the rest of the systems, suggesting that the intervening aromatic side chains have no significant effect on the D-A couplings.

It is possible that the discrepancies between Dutton's analysis and the heme protein ET data arise from the use of the edge-to-edge distance scale. The implication of this distance scale is that, when the edges of the two redox sites are in van der Waals contact, the ET reaction will be adiabatic ($k_{max} = 10^{13}$ s^{-1}). Electronic structure calculations, however, suggest that the electron self-exchange reactions of $Ru(NH_3)_6^{3+/2+}$ and $Fe(OH_2)_6^{3+/2+}$, in which there is very little delocalization of donor and acceptor metal orbitals onto the ligands, are nonadiabatic.[5] If the $Fe^{2+} \rightarrow Ru^{3+}$ intramolecular ET reactions in the modified cytochromes involve primarily metal-localized donor and acceptor states, then metal-to-metal separations would be more appropriate in rate *vs.* distance correlations. For the reactions in ZnP-modified heme proteins, the donor wavefunction in $^3ZnP^*$ and acceptor wavefunction in $ZnP^{+\cdot}$ species are delocalized on the porphyrin ring;[6] hence it is reasonable to make use of a Ru-to-edge distance scale. Examination of Figure 4.1B, however, shows that a shift to a Ru-to-Fe distances for the modified cytochromes or Ru-to-edge scale for the modified myoglobins does not improve matters. In fact, the scatter of the data points becomes even more substantial. Our conclusion is that the ET rates in the modified myoglobins and cytochromes *c* cannot be accounted for by a homogeneous-barrier model. Indeed, the available evidence shows that the distant electronic couplings depend strongly on the details of the structure of the intervening medium.

HETEROGENEOUS BARRIER MODELS

Several theoretical models have been devised to explicitly account for the inhomogeneity of the polypeptide matrix. In the following sections, the ET rates in the

Ru-modified heme proteins will be analyzed in terms of two such models - the tunneling model (TP)[7] and the artificial intelligence-superexchange formalism (AI-EH).[8]

σ-Tunneling Pathway Model (TP)

Beratan, Betts, and Onuchic[7] have proposed that electron tunneling between two redox sites in a protein is mediated by specific bonded and nonbonded interactions in the intervening polypeptide. Tunneling is more efficient (coupling decays more slowly) through bonded orbitals (σ or hydrogen bonded) than through-space. This property of bonded interactions is evident from the extremely low β extracted for covalently bonded D-A molecules.[2] The novelty of the TP model, however, is in invoking participation of through-space contacts and hydrogen bonds in mediating ET; these weak interactions offer routes that would be less tortuous than completely covalent paths through the polypeptide chain.

A pathway search algorithm has been developed to extract electron-tunneling pathways between two given sites in a protein in the order of decreasing electronic coupling.[7c] The most rudimentary form of the tunneling model assumes H_{AB} to be a product of decay factors for each element in the *best* pathway (eq 1).

$$H_{AB} \propto \Pi_i \, \varepsilon_C(i) \, \Pi_j \, \varepsilon_H(j) \, \Pi_k \, \varepsilon_S(k) \qquad (1)$$

Values for the decay factors are determined based on eq 2; such parameterization was possible using ET data on synthetic D-A systems and semi-empirical calculations.

$$\varepsilon_C = \text{const.} \approx 0.6 \qquad (2a)$$

$$e_H = \varepsilon_C^2 \exp[-1.7(R - 2R_C)] \qquad (2b)$$

$$\varepsilon_S = \sigma_S \varepsilon_C \exp[-1.7(R-R_C)] \approx 0.5\varepsilon_C \exp[-1.7(R-R_C)] \qquad (2c)$$

Because these parameters are normalized, they take into account (in an average way) high-order contributions to the couplings, a distribution in bond energies and interactions, and local quantum interference effects.

Tunneling Pathways in Cytochromes

The crystal structures of yeast iso-1-cytochrome *c* in both oxidation states have been solved to high resolutions by Brayer and coworkers.[9] Certain oxidation-dependent changes involving residues in the heme pocket have been noted. Details regarding these differences warrant careful examination before performing any pathway search.

Ru(His66)cyt *c* probes the ET reaction to the heme through the internal Tyr67. Tyr67 is part of an elaborate H-bonding network to the Met80 ligand and the heme propionate. In the reduced form,[9a] the thermodynamically favored configuration has Tyr67(OH) serving as a H-bond donor to the Met80 S_δ (Figure 4.2A). It is argued that when the heme is oxidized, the Tyr67(OH)-Met80(S) H-bond is broken. Instead, the aromatic substituent interacts with a nearby internal water molecule, orienting it in such a way that the solvent dipole stabilizes the positively charged ferriheme (Figure 4.2B). This change is reflected in a longer Tyr67(O)-Met80(S) distance in the ferricytochrome structure. Given these alternative conformations of the Tyr767 OH group, one can obtain dramatically different tunneling pathways and predicted electronic couplings for Ru(His66)cyt *c*. This dilemma can be resolved by referring to the Marcus theory. It has been suggested that for reactions that are close to activationless such as those in the Ru-modified cytochromes, the transition state tends to resemble the reactant configuration (see Figure 1.5C). On the basis of this argument, the tunneling pathways were determined using the structure of the reduced cytochrome *c*. The best edge-to-edge pathway for Ru(His66)cyt *c* (Figure 4.3A) consists of 11 σ bonds and the 3.2-Å H-bond between Tyr67(OH) and Met80(S).

Trp59 likewise undergoes a crystallographically defined displacement on going from the reduced to the oxidized protein (Figure 4.4). Based on the reduced structure of the protein, the best pathway from a Ru-modified His58 to the heme (Figure 4.5A) involves 13 σ bonds and a 3.1-Å H-bond between indole nitrogen and a heme propionate group. As for Ru(His39)cyt *c*, the optimum pathway to the heme proceeds along the polypeptide chain to residue 41 and through a 3.2-Å H-bond between a backbone amide and the heme propionate (Figure 4.6A); in the oxidized form of the protein, this same hydrogen bond decreases in length to 2.6 Å.

The pathway for ET in Ru(His58)cyt *c* is two bonds longer than that of Ru(His66)cyt *c*, which is consistent with the smaller coupling constant for His58. σ-tunneling lengths (σl) are calculated by multiplying the effective number of bonds in a pathway (defined as the (nonintegral) number of covalent bonds that give same decay as the actual pathway) by an average bond length of 1.4 Å (Table 4.1). The current parameterization of the pathway model imposes a coupling-decay factor of 0.6 for each covalent bond.[8] This factor defines $\beta' = 0.73$ Å^{-1} in correlations of k_{max} with σl and implies that the intramolecular ET rate drops by two orders of magnitude for every 6.3-Å increase in the σ-tunneling length. In a linear fit with constrained β′, we find that the activationless rate constants for Ru(His58)-, Ru(His66)cyt *c*, and other modified cytochromes correlate reasonably well with the effective lengths of edge-to-edge σ-tunneling pathways (Figure 4.7A).

Though the edge-to-edge σ-tunneling model predicts the weaker coupling in Ru(His58)cyt *c* than in Ru(His66)cyt *c*, the maximum ET rate for Ru(His58)cyt *c* is slower than expected for its calculated tunneling length (Figure 4.7A). Part of the discrepancy again could be due to the edge-to-edge scale where it is implicitly assumed that the coupling involves donor and acceptor orbitals that are delocalized over the ligands. It has been shown that H_{AB} for two contacting metal complexes depends upon

the square of the metal-ligand orbital mixing coefficient.[5] If the metal-ligand mixings in Ru-modified cytochrome *c* are relatively small, then the σ tunnels should extend to the metal-atom redox centers rather than stopping at the ligands. A metal-to-metal pathway is in better accord with the coupling in Ru(His58)cyt *c*, since the pathway is extended by the σ bonds of the porphyrin ring. Figure 4.7B presents a plot of log k_{max} values versus the Ru-to-Fe tunneling lengths, i.e., adding σ bonds of the ligands and the metal-ligand bonds to the edge-to-edge paths. A constrained-β′ fit of log k_{max} *vs.* Ru-to-Fe σl shows only a marginally improved correlation over the edge-to-edge σl fit. The primary distinction between the two distance measures is found in the one-bond-limit ET rates: 2×10^{12} s^{-1} for the edge-to-edge scale and 4×10^{14} s^{-1} for the Ru-to-Fe scale (Figure 4.7B).[10]

While we find a reasonable correlation of maximum ET rates with σ-tunneling lengths, there are some discrepancies. For example, the electronic couplings between Ru(His58)- and Ru(His72)cyt *c* do not correlate with the respective tunneling lengths (Figure 4.7). While these systems were evaluated on the basis of a static crystal model, the dynamics of the residues in the ET pathways may contribute to the effective electronic couplings. In the case of Ru(His72)cyt *c*, this could manifest itself as shortening of the through-space gap in the proposed pathway that leads to a better donor-acceptor coupling.[4c]

Regardless of the model used to analyze the data, our results show that the electronic couplings for intramolecular ET reactions in Ru(His58)- and Ru(His66)cyt *c* are not enhanced by aromatic residues in the intervening media. Instead, the rates and the couplings can be described adequately by a model that involves only σ interactions.[7] The correlation of ET rates with σ-tunneling lengths does not preclude a coupling role for the π orbitals of the aromatic groups in the pathway, but it does indicate that, in the Ru-modified cytochromes that we have examined, they are no more efficient in mediating the

coupling than is the σ-bonded framework.[11] Hence, the presence of aromatic groups in the medium between redox sites does not necessarily result in faster ET than in a purely aliphatic medium.

The $Fe^{2+} \rightarrow Ru^{3+}$ ET rate to the surface Ru(His66) group exhibits a slight increase upon replacement of the intervening Tyr67 with a phenylalanine. This observation is surprising since the electronic coupling between Phe67 and Met80 would be expected to be weak, owing to the Phe67-Met80 space jump created in the σ-tunneling pathway. Crystallographic studies on the Phe67 mutant of iso-1-cytochrome *c*, however, show that a water molecule occupies the space vacated by the Tyr67 hydroxyl group (Figure 4.8).[12] Since the water molecule exhibits relatively high thermal factors in both oxidation states of the protein, ET could be coupled to the motions of this water molecule and other nearby groups in the heme pocket. In an effort to elucidate the effects of the motions in the heme pocket on intersite exchange in Ru(His66Phe67)cyt *c*, the ET rates were measured at elevated pressures (up to 1 kbar); no change was however observed (data not shown). It is possible that the packing in this section of heme pocket is tight enough not to respond to the applied pressure. Alternatively, the temperature dependence of the ET rate in Ru(His66Phe67)cyt *c* could provide valuable insights into the role of the intervening water molecule.

Tunneling Pathways in Myoglobins

The rates in the Ru/ZnP-modified human myoglobins exhibit a pronounced exponential dependence with distance, although the calculated β (1.7 $Å^{-1}$) is higher than that suggested by Dutton and coworkers. The tunneling pathways have been determined for these modified myoglobins based on the 1.6-Å resolution crystal structure of human myoglobin[13] (Figure 4.9A-C). The rates in the HuMb systems do not correlate with σl values. Furthermore, the HuMb points are systematically offset from the cyt *c* points; the rates are faster than those predicted by the single-pathway model. The pathway searches

reveal a significant distinction between HuMb and cytochrome *c*: a small number of paths dominates the coupling in cytochrome *c*, while a great many more nearly equivalent paths can be found in Mb. Tables 4.1-4.2 list the number of paths with couplings within a factor of ten of the best path for each of the Ru-modified proteins that have been studied. Fewer than 20 paths contribute in cytochromes *c*, while nearly ten times that number are found in some HuMb derivatives. If just the best route is used to calculate σl in HuMb, then several near-optimum routes will be neglected. Many tunneling pathways contributing to the D-A coupling should substantially increase the overall coupling. If a sufficiently large number of paths contributes to the total electronic coupling, the explicit nature of one path becomes unimportant and tunneling lengths should closely parallel edge-edge distances.

The large number of pathways obtained for HuMb compared to cytochrome *c* clearly demonstrates that in some systems the dominant pathway model must be modified to account for the contributions from nearly equivalent pathways.[14] Accordingly, we have calculated overall couplings as the sum of the couplings for the individual pathways in both Mb and cytochrome *c* (Tables 4.1-4.2). The multiple-pathway couplings were converted to edge-edge σ-tunneling lengths as was done for single pathways. The results of this analysis appear in Figure 4.10A. The solid line is drawn through the $Ru(bpy)_2(im)$cyt *c* systems and has the required distance decay of 0.73 $Å^{-1}$. The offset of the HuMb data has been reduced. It is important to note that electron transfers involving Zn-substituted cytochromes *c*[15,16] correlate well with the same $\beta' = 0.73$ $Å^{-1}$ line. The deviations of the HuMb data, then, are not likely the result of differences in ZnP and FeP ET reactions.

Figure 4.10B presents a plot of log k_{max} values *versus* the Ru-to-porphyrin edge tunneling lengths for the Ru/ZnP-modified myoglobins, *i.e.*, adding σ bonds of the ligands and the metal-ligand bonds to the edge-to-edge paths. Also shown are the

corresponding data for $Ru(bpy)_2(im)(His)$- and Ru/ZnP-cytochrome *c*. Inclusion of multiple pathways result in a marked improvement in correlation among the cytochrome *c* points, especially between Ru(His72)cyt *c* and Ru(His58)cyt *c*. Deviations of the HuMbs from the cyt *c* points are also less pronounced compared to the predictions of the multiple-pathway edge-edge tunneling lengths. The best constrained-β′ fit of log k_{max} *vs.* Ru-to-Fe σl for the cytochrome *c* data shows a marked difference in the calculated one-bond-limit ET rates: 5×10^{13} s^{-1} for the Ru-to-Fe scale and 2×10^{11} s^{-1} for the edge-to-edge scale.

Summary

A homogeneous-barrier model has been shown to describe a large number of ET systems, but fails to account for many of the results. A model that explicitly treats the inhomogeneities of the intervening medium is clearly called for, and the Beratan-Onuchic σ-tunneling pathway model is an important first step.[7] While we find reasonable correlation of the cytochrome *c* data with the predictions of the single-pathway formalism, it fails to describe adequately the electronic couplings in HuMb. This raises the possibility that alternative pathways through the protein matrix are involved and that a multiple-pathway formalism of the model presents a more appropriate approach to the general problem of D-A coupling in proteins. Whether the larger number of competing pathways is characteristic of non-ET proteins remains to be addressed. However, it is tempting to suppose that specific routes between redox sites offer no functional advantage for proteins whose primary functions are not to shuttle electrons. Although inclusion of multiple tunneling pathways does move the Ru-modified HuMb data points in the right direction, the correlation of k_{max} with σl is not completely satisfactory. Our analysis assumes only constructive interference among pathways. However, more sophisticated treatments of distant electronic couplings in model complexes and proteins could identify an important role for destructively interfering multiple pathways.[5,14] A particular

characteristic of myoglobin, the flexibility of the porphyrin in the heme pocket,[15] also may be a complicating factor. Pathway analyses are based on crystal-structure coordinates, but the dynamics of porphyrin motion could influence ET rates in HuMb.

Artificial Intelligence-Superexchange Model (AI-EH)

A hybrid approach to the electronic coupling problem in proteins has been introduced by Siddarth and Marcus.[8] In this method, an artificial intelligence (AI) search equivalent to the pathway search in the TP model is combined with extended Hückel calculations (EH) on a subset of amino acids in the proteins. In the AI search procedure, the amino acid residues important in mediating the electron transfer between the donor and acceptor are selected using a predefined evaluation function; this procedure reduces the complexity of the electronic structure problem. The selected residues are then used to form the basis set in an EH calculation of the electronic coupling matrix element H_{AB}. The method is not expected to produce highly accurate *absolute* values of H_{AB}, but is expected to describe *relative* values of this matrix element. The calculations take into account high-order effects such as interferences among competing pathways, stereoelectronic effects in the bridging medium and at the redox sites, as well as competition and crossovers between σ and π systems.[18,19]

Cytochromes[8c,20]

Figures 4.3B, 4.5B, and 4.6B show the amino acid residues proposed to mediate ET in Ru(His66)-, Ru(His58)-, and Ru(His39)cyt *c*, respectively. Both TP and AI-EH models find the same links between the heme and Ru(His66) and Ru(His58) groups (Figures 4.3B, 4.5B). For Ru(His39)cyt *c*, the AI-EH model does not attribute any role for Ser40 and invokes instead the participation of asparagines 52 and 56 (Figure 4.6B). Site-directed mutagenesis of the these residues to less bulkier or non-H-bonding side chains should shed light on their role. Figure 4.11 shows the results of the AI-EH

analyses for all the Ru-modified cytochromes; the calculated k_{max}s are plotted relative to Ru(His33)cyt *c*. The correlation with experimentally derived k_{max}s is reasonable and as with the TP model, the analyses draw no special role for the intervening aromatic side chains in Ru(His66)-, Ru(His66Phe67)-, and Ru(His58)cyt *c*. The addition of more residues in the extended Hückel calculations (filled circles in Figure 4.11) results in a slight improvement in the correlation, most notably that between Ru(His72)cyt *c* and Ru(his58)cyt *c*.

Myoglobins[8d]

An AI-EH analysis of the a_5Ru/ZnP-modified human myoglobins has been recently reported and the authors found an improvement in correlation with the experimental data compared to the predictions of the multiple-pathway model (Figure 4.12). Figures 4.9D-F show the amino acid residues that are important in bridging the redox sites. In general, more amino acids are used in these calculations than those that comprise the dominant pathway routes. It is very encouraging that *both* the TP and AI-EH analyses suggest that multiple pathways are important in mediating the electronic coupling in myoglobin.

CONCLUSION

Regardless of the models (square and heterogenous barrier models) used to analyze the data, the results indicate that the intersite electronic couplings are not enhanced by aromatic side chains in the poplypeptide bridge. We do not preclude the participation of the π-systems of these groups in ET, but in order to couple to these systems from an initially σ-type bridge, severe penalties are normally imposed unto the overall coupling. As a result, these π-systems are no more efficient in mediating the intersite exchange than the σ framework.

Many complex issues are involved in understanding electronic coupling in long-range electron transfer. The elegance of the single-pathway model for ET in proteins is in its simplicity, but from it come its shortcomings. We find that contributions of alternative pathways (that may bring about either interference or constructive effects) and stereoelectronic effects (in the bridge and at the boundaries of the redox sites) to the distant electronic couplings can be quite significant. This is clearly evident when the correlation with experimental data improves after adapting a multiple-pathway formalism and even more if a more wholistic approach (such as the AI-EH model) is applied.

REFERENCES AND NOTES

1. (a) Gamow, G. *Z. Phys.* **1928**, *51*, 204. (b) Hopfield, J. J. *Proc. Natl. Acad. Sci. USA* **1974**, *71*, 3640. (c) Jortner, J. *J. Chem. Phys.* **1976**, *64*, 4860.
2. Moser, C. C.; Keske, J. M.; Warncke, K.; Farid, R. S.; Dutton, P. L. *Nature* **1992**, *355*, 796.
3. A rigid-geometry search on the Ru-modified histidine was performed by successively rotating the two side-chain dihedral angles by 18° from 0 to 360° (Shih, H. H.-L.; Brady, J.; Karplus, M. *Proc. Natl. Acad. Sci. USA* **1985**, *82*, 1695). The most stable 20 conformers were examined for any unfavorable van der Waals ($d < 3$ Å) contacts. Because interconversions among different conformers are expected to be extremely rapid (Brooks III, C. L.; Karplus, M.; Pettitt, B. M. *Adv. Chem. Phys.* **1988**, *71*, 95), the shortest donor-acceptor distances are given for the modified proteins.
4. (a) Chang, I.-J.; Gray, H. B.; Winkler, J. R. *J. Am. Chem. Soc.* **1991**, *113*, 7056. (b) Bjerrum, M. J.; Chang, I.-J.; Winkler, J. R.; Gray, H. B., unpublished kinetic results on four different Ru polypyridine derivatives of His33 horse heart cytochrome *c*. (c) Wuttke, D. S.; Bjerrum, M. J.; Winkler, J. R.; Gray, H. B. *Science* **1992**, *256*, 1007. (d) Wuttke, D. S.; Bjerrum, M. J.; Chang, I.-J.; Winkler, J. R.; Gray, H. B. *Biochim. Biophys. Acta* **1992**, *1101*, 168.
5. Newton, M. D. *J. Phys. Chem.* **1988**, *92*, 3049.
6. (a) Barkigia, K. M.; Chantranupong, L.; Smith, K. M.; Fajer, J. *J. Am. Chem. Soc.* **1988**, *110*, 7566. (b) Fajer, J.; Borg, D. C.; Forman, A.; Felton, R. H.; Vegh, L.; Dolphin, D. *Ann. N. Y. Acad. Sci.* **1973**, *206*, 349. (c) Fajer, J.; Borg, D. C.; Forman, A.; Dolphin, D.; Felton, R. H. J. *Am. Chem. Soc.* **1970**, *92*, 3451. (d) Fajer, J.; Bielski, B. H. J.; Felton, R. H. *J. Phys. Chem.* **1968**, *72*, 1201.

7. (a) Onuchic, J. N.; Beratan, D. N.; Winkler, J. R.; Gray, H. B. *Annu. Rev. Biophys. Biomol. Struct.* **1992**, *21*, 349. (b) Beratan, D. N.; Betts, J. N.; Onuchic, J. N. *Science* **1991**, *252*, 1285. (c) Betts, J. N.; Beratan, D. N.; Onuchic J. N. *J. Am. Chem. Soc.* **1992**, *114*, 4043.

8. (a) Siddarth, P.; Marcus, R. A. *J. Phys. Chem.* **1990**, *94*, 8430. (b) Siddarth, P.; Marcus, R. A. *J. Phys. Chem.* **1992**, *96*, 3213. (c) Siddarth, P.; Marcus, R. A. *J. Phys. Chem.* **1993**, *97*, 2400. (d) Siddarth, P.; Marcus, R. A. *J. Phys. Chem.* **1993**, *97*, 6111.

9. (a) Louie, G. V.; Brayer, G. D. *J. Mol. Biol.* **1990**, *214*, 527. (b) Berghuis, A. M.; Brayer, G. D. *J. Mol. Biol.* **1992**, *223*, 959.

10. The edge-to-edge limiting ET rate (σl = 1.4 Å) of 2×10^{12} s^{-1} is reasonably close to the limiting rates ($> 5 \times 10^{12}$ s^{-1}) extracted from studies of synthetic donor-acceptor complexes (Appendix C). The one-bond limit in the metal-to-metal scale corresponds to a hypothetical Ru-Fe dimer; given the strong coupling expected for such a complex, it is difficult to evaluate the significance of the extrapolated ET rate. It is of interest to note that Barbara and coworkers have observed ET rates near 10^{13} s^{-1} in CN-bridged Ru dimers (Tominaga, K.; Kliner, D. A. V.; Johnson, A. E.; Barbara, P. F. *J. Chem. Phys.* **1993**, *98*, 1228).

11. Theoretical analyses of long-range ET in proteins suggest that in certain cases aromatic residues between donors and acceptors can enhance rates *via* improved coupling *and* lower activation barriers (Christensen, H. E. M.; Conrad, L. S.; Hammerstad-Pedersen, J. M.; Ulstrup, J. *FEBS Lett.* **1992**, *296*, 141).

12. McLendon, G.; Hickey, D.; Berghuis, A.; Sherman, F.; Brayer, G. *ACS Advances in Chemistry Series*; Bolton, J. R., Mataga, N., McLendon, G., Eds.; American Chemical Society: Washington, DC, 1991; Vol. 228, pp. 179-190.

13. (a) Hubbard, S. R.; Hendrickson, W. A.; Lambright, D. G.; Boxer, S. G. *J. Mol. Biol.* **1990**, *213*, 215. (b) Hubbard, S. R.; Hendrickson, W. A.; Lambright, D. G.; Boxer, S. G., unpublished results.
14. Onuchic, J. N.; Andrade, P. C. P.; Beratan, D. N. *J. Chem. Phys.* **1991**, *95*, 1131.
15. Meade, T. J.; Gray, H. B.; Winkler, J. R. *J. Am. Chem. Soc.* **1989**, *111*, 4343.
16. Therien, M. J.; Selman, M. A.; Gray, H. B.; Chang, I.-J.; Winkler, J. R.; *J. Am. Chem. Soc.* **1990**, *112*, 2420.
17. La Mar, G. N.; Haukson, J. B.; Dugad, L. B.; Lidell, P. A.; Venkataramana, N.; Smith, K. M. *J. Am. Chem. Soc.* **1991**, *113*, 1544.
18. Liang, C.; Newton, M. D. *J. Phys. Chem.* **1992**, *96*, 2855.
19. Gruschus, J. M.; Kuki, A. *J. Phys. Chem.* **1993**, *97*, 5583.
20. Siddarth, P.; Marcus, R. A. *J. Phys. Chem.* **1993**, in press.

Table 4.1. ET Parameters for $Ru(bpy)_2(im)$-modified Cytochromes *c*.[a]

X	log k_{max}	d(edge-edge)	d(Ru-Fe)	Dominant Pathway		Multiple Pathway	
				σl(edge-edge)	σl(Ru-Fe)	σl(edge-edge)[b]	σl(Ru-Fe)
33[c]	6.4	11.1	17.9	19.5	27.9	16.1 (5)	24.5
39	6.4	12.3	20.3	19.6	28.0	19.6 (1)	28.0
66	6.1	13.3	18.9	19.6	25.2	17.9 (2)	23.5
72[d]	6.0	8.4	13.8	24.6	30.2	20.2 (11)	25.8
58	4.8	13.2	20.2	21.4	29.8	21.0 (4)	29.4
62[d]	4.0	14.5	20.2	28.8	37.2	22.5 (22)	30.9

[a]d and σl values are reported in Å.
[b]Numbers of paths with H_{AB} within an order of magnitude of the best pathway are enclosed in parentheses.
[c]Reference 4a-b.
[d]Reference 4c-d.

Table 4.2. ET Parameters for Ru/ZnP-modified Human Myoglobins.[a]

X	log k_{max}	d(edge-edge)	d(Ru-Fe)	Dominant Pathway		Multiple Pathway	
				σl(edge-edge)	σl(Ru-edge)	σl(edge-edge)[b]	σl(Ru-edge)
70	7.9	9.5	13.6	24.3	28.5	15.7 (106)	19.9
48	5.5	12.7	13.3	37.5	41.7	29.9 (79)	34.1
83	3.2	15.5	16.7	43.5	47.7	32.5 (186)	36.7

[a]d and σl values are reported in Å.
[b]Number of paths with H_{AB} within an order of magnitude of the best pathway is enclosed in parenthesis.

Figure 4.1. Activationless ET rates as a function of donor-acceptor separation distance (reference line, β = 1.4 Å^{-1}): (**A**) log k_{max} *vs.* edge-to-edge distance; and (**B**) log k_{max} *vs.* Ru-to-Fe distance for Ru(bpy)$_2$(im)(HisX)cytochromes *c* (filled circles) (X = 33, 39, 58, 62, 66, 72) and Ru-to-edge for Ru(HisX)/ZnP-modified myoglobins (boxes) (X = 48, 70, 83).

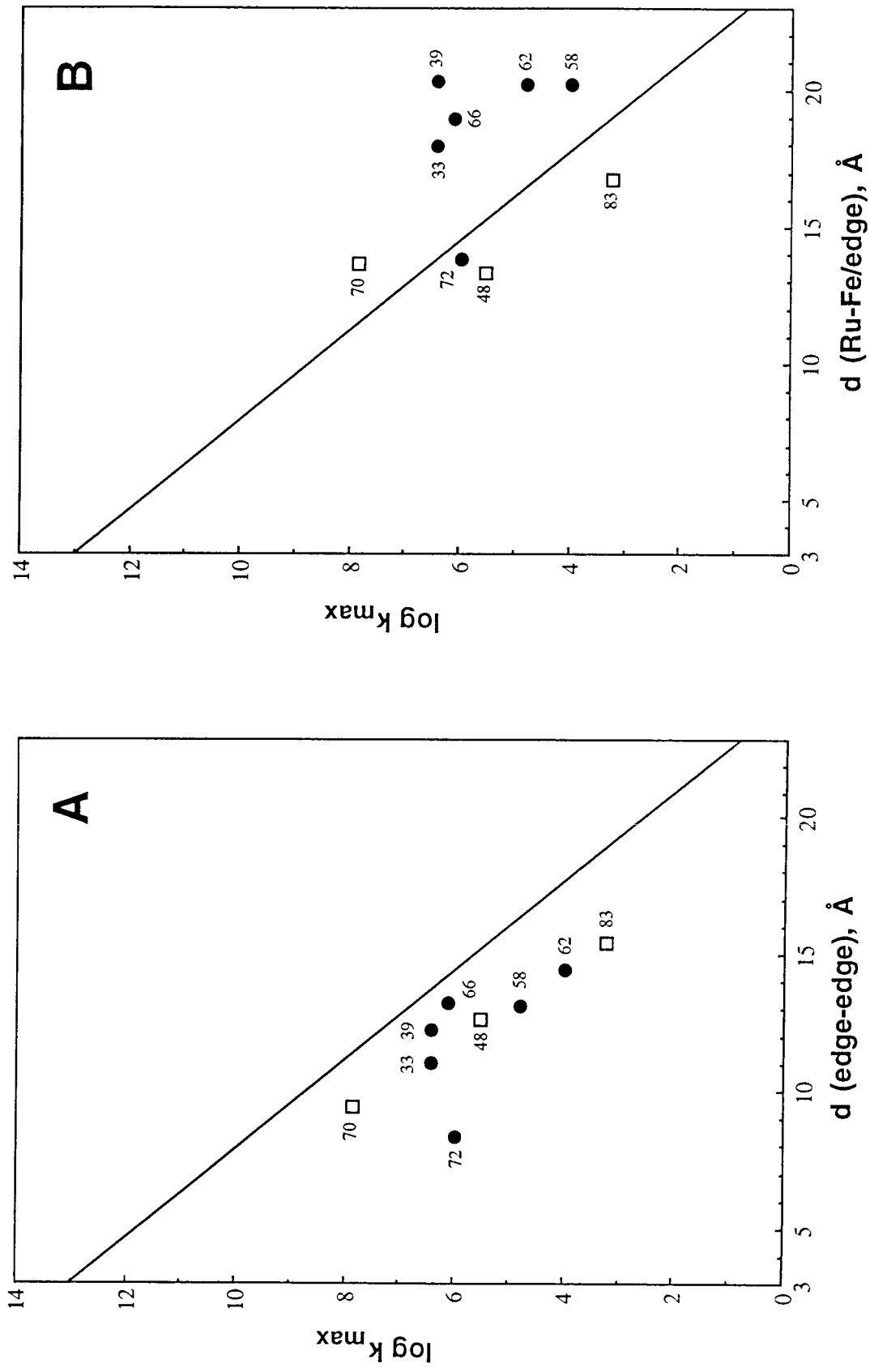
A
log k max
d (edge-edge), Å
0
2
4
6
8
10
12
14
3
5
10
15
20
70
72
33
39
48
66
58
62
83
B
log k max
d (Ru-Fe/edge), Å
0
2
4
6
8
10
12
14
3
5
10
15
20
70
72
33
39
48
66
58
62
83

Figure 4.2. Stereo-drawings of the region around Tyr67 in (**A**) reduced and (**B**) oxidized yeast iso-1-cytochrome *c*. Shown is the proposed placement of hydrogen bonds for the purpose of discerning the orientation of the Wat166 dipole; the hydrogens involved in bonding are indicated in thin lines and the bonds are shown using dashed lines. Adapted from reference 9b.

A

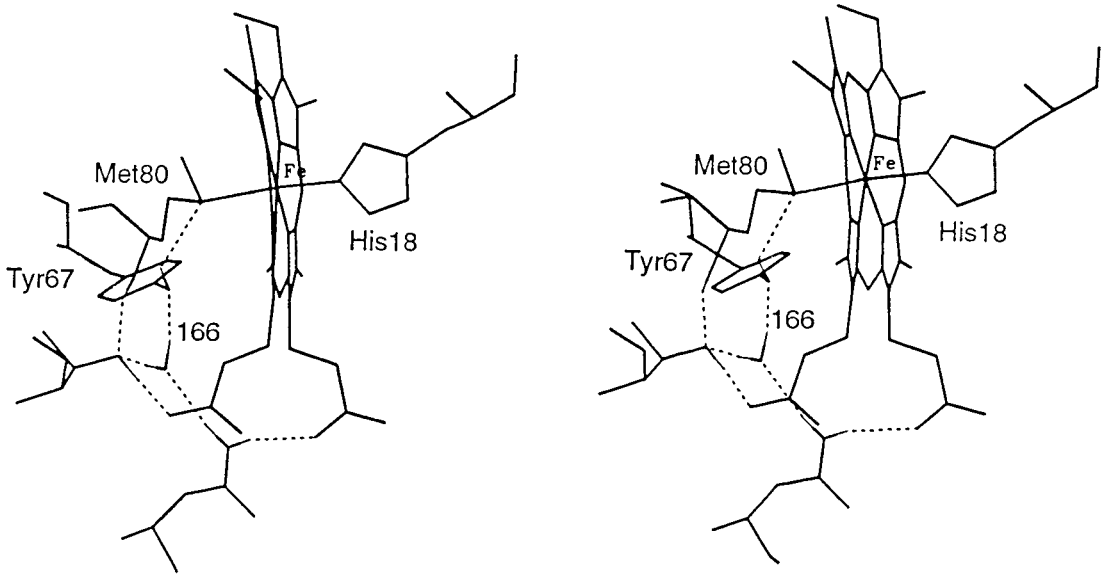
Met80
Fe
His18
Tyr67
166
Met80
Fe
His18
Tyr67
166

B

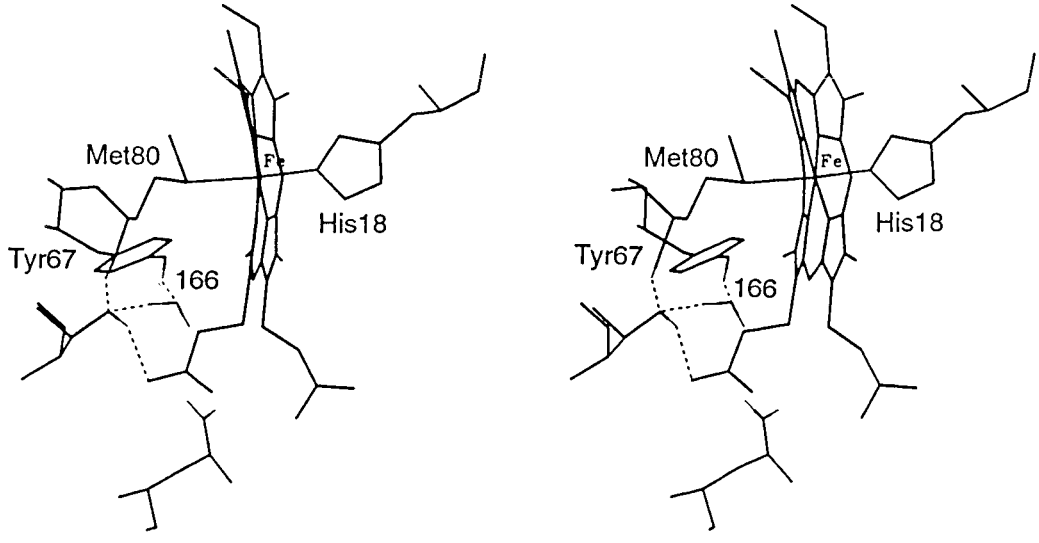
Met80
Fe
His18
Tyr67
166
Met80
Fe
His18
Tyr67
166

Figure 4.3. Proposed bridging residues for ET in $Ru(bpy)_2(im)(His66)$cyt *c*. (**A**) In bold is the σ-tunneling pathway through Tyr67. (**B**) In bold are the amino acids proposed by AI-EH model to be important in mediating the electron exchange.

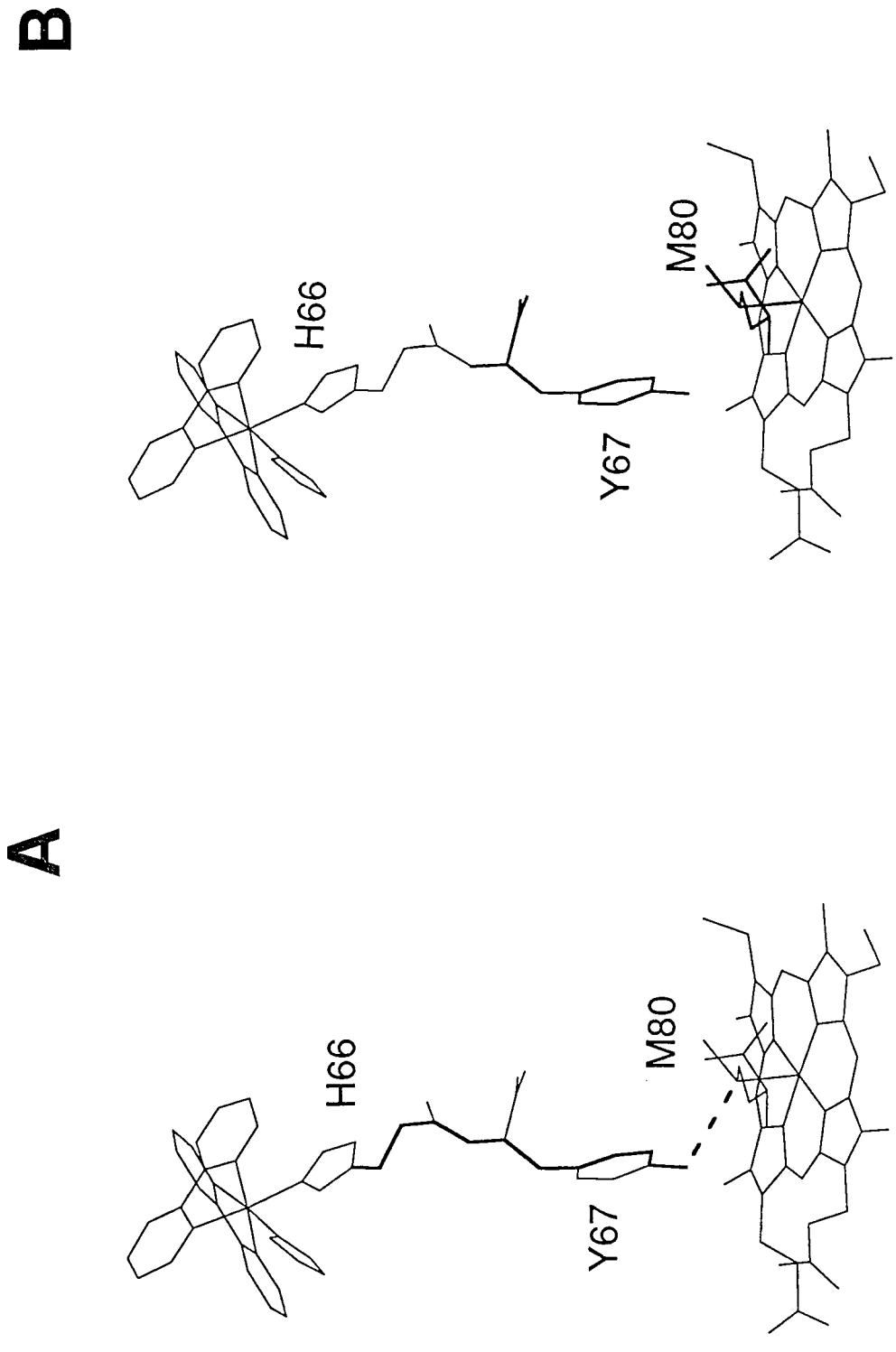
B
H66
Y67
M80
A
H66
Y67
M80

Figure 4.4. Stereo-drawing showing the positional shifts in the region of Trp59 on going from the oxidized (thick lines) to reduced (thin lines) protein. In the oxidized protein the hydrogen bond (dashed line) between the side chain of Trp59 and the nearby heme propionate (HP7) lengthens by 0.3 Å. Adapted from reference 9b.

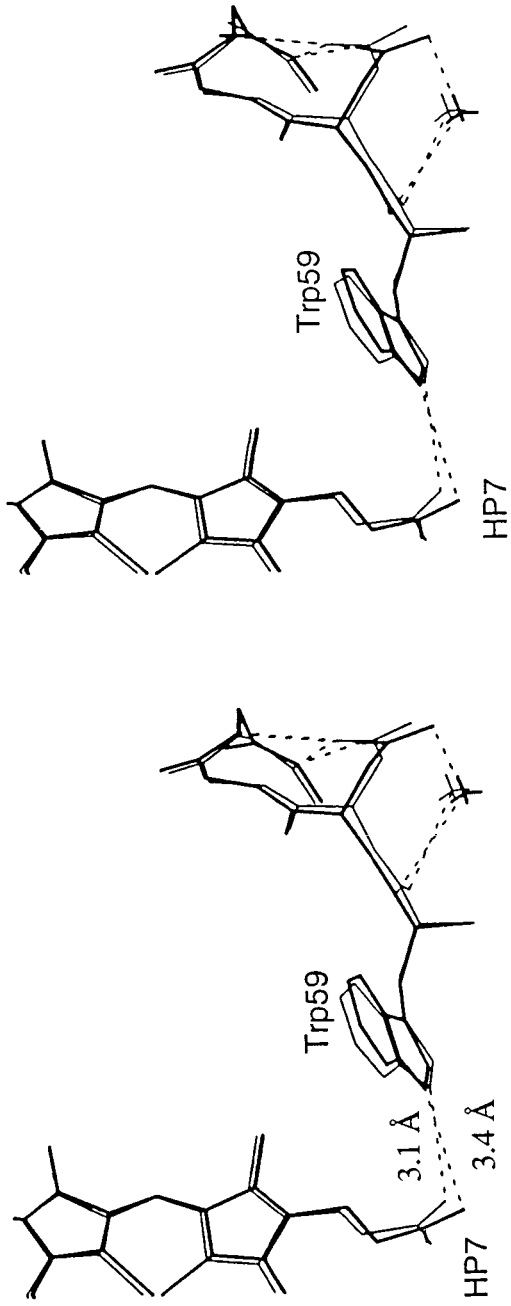
Trp59
HP7
Trp59
3.1 Å
3.4 Å
HP7

Figure 4.5. Proposed bridging residues for ET in $Ru(bpy)_2(im)(His58)$cyt *c*. (**A**) In bold is the σ-tunneling pathway through Trp59. (**B**) The same intervening residue is selected by the AI-EH model to be important in mediating the electron exchange.

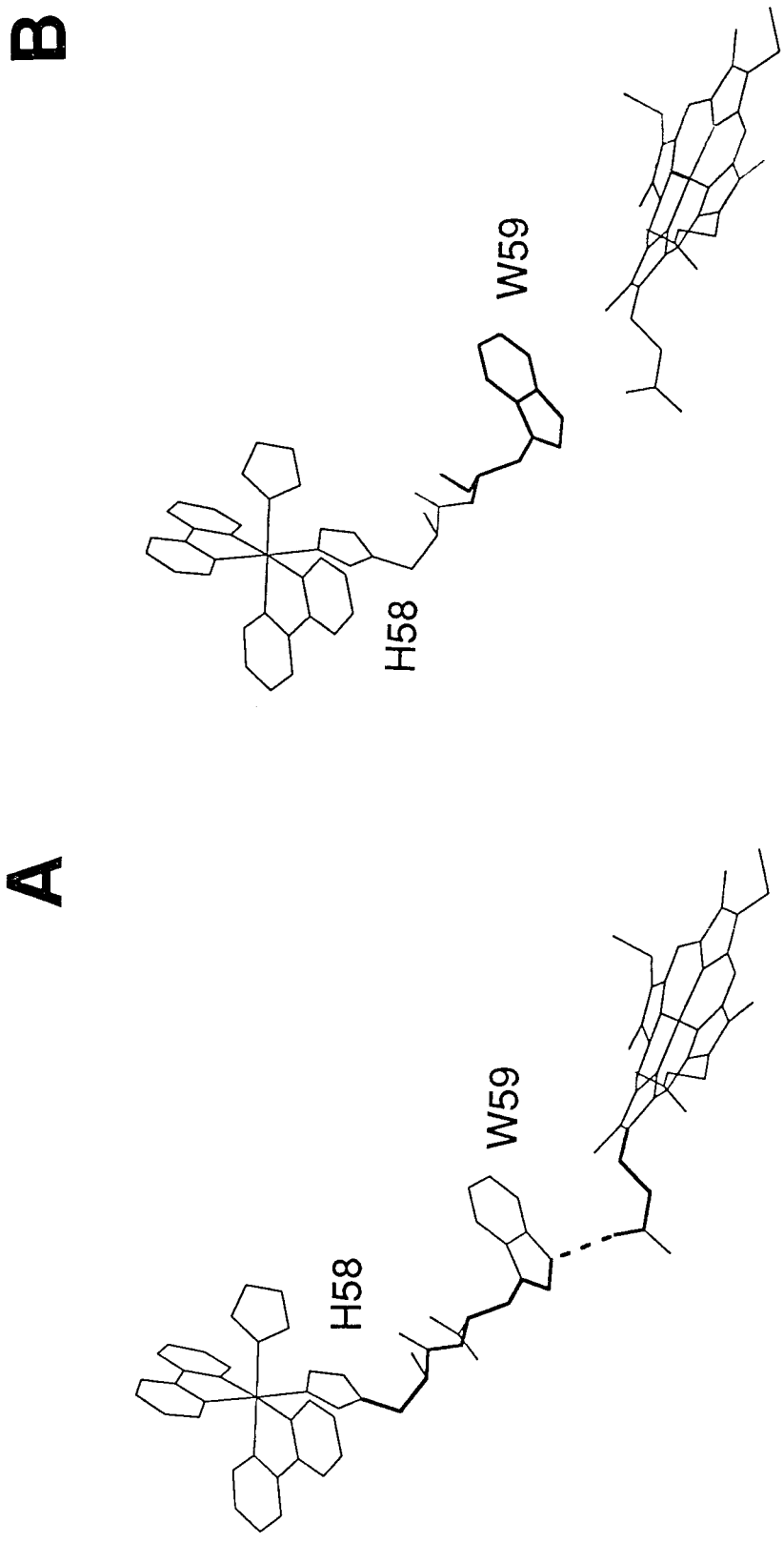
A
H58
W59
B
H58
W59

Figure 4.6. Proposed bridging residues for ET in $Ru(bpy)_2(im)(His39)$cyt *c*. (**A**) In bold is the σ-tunneling pathway along the protein backbone. (**B**) In bold are the amino acids proposed by AI-EH model to be important in mediating the electron exchange.

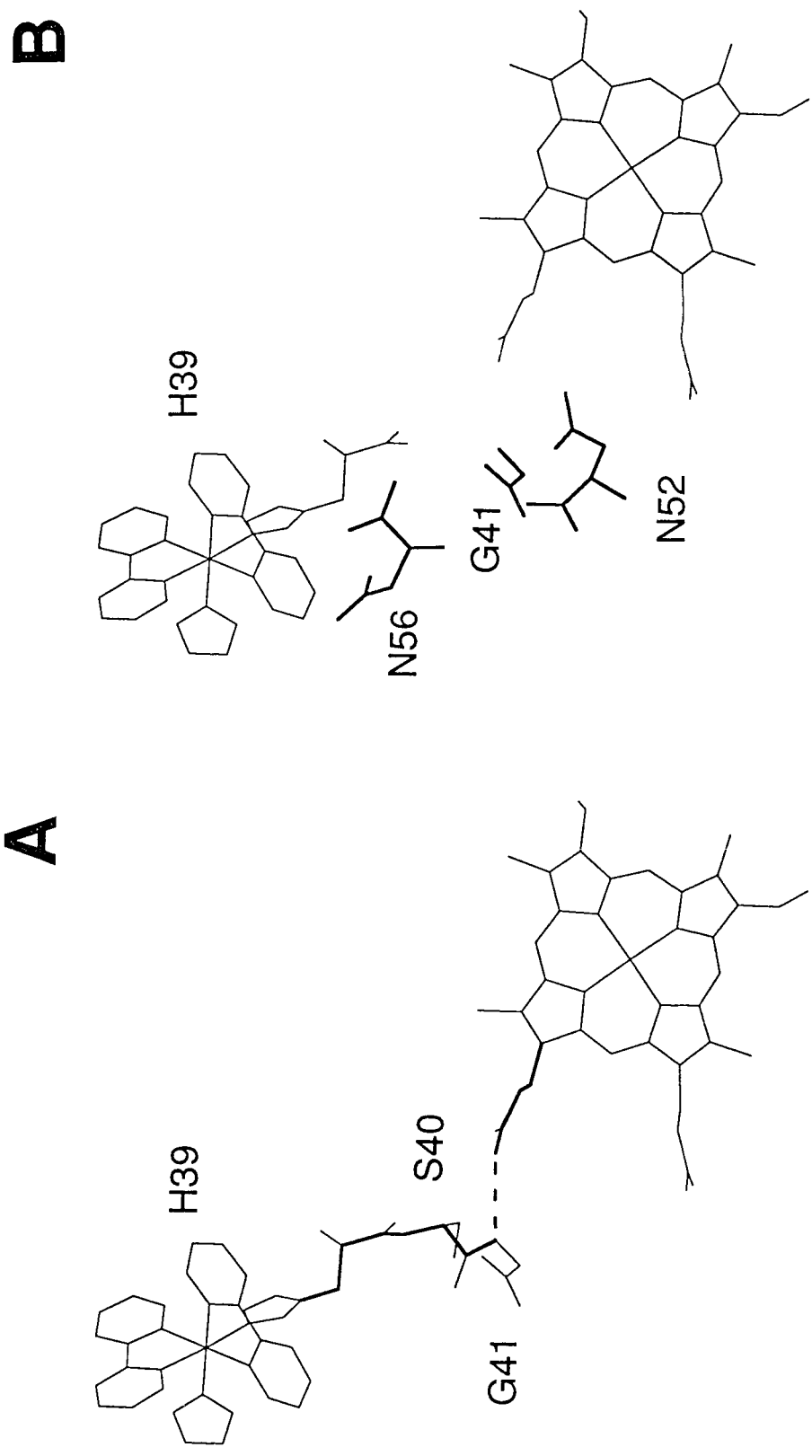
A
H39
S40
G41
B
H39
N56
G41
N52

Figure 4.7. Maximal ET rates in $Ru(bpy)_2(im)(HisX)$-modified cytochromes *c* (X = 33, 39, 59, 62, 66, 72) as functions of (**A**) edge-to-edge and (**B**) metal-to-metal σ-tunneling lengths. Solid lines are constrained linear fits ($\beta' = 0.73$ Å^{-1}) to the data and are described as follows: **A**, $\log k_{max} = -0.32\sigma l + 12.7$; and **B**, $\log k_{max} = -0.32\sigma l + 15.0$.

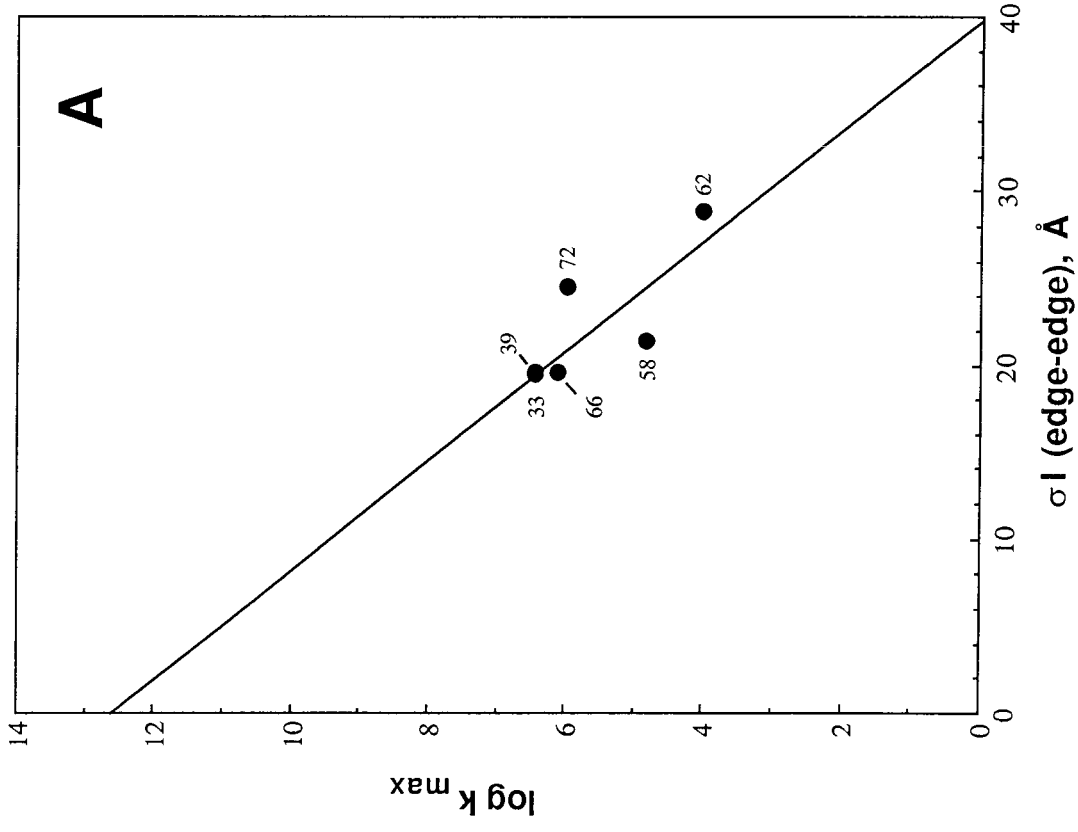
A
log k max
σ l (edge-edge), Å
0
2
4
6
8
10
12
14
0
10
20
30
40
39
33
66
72
58
62

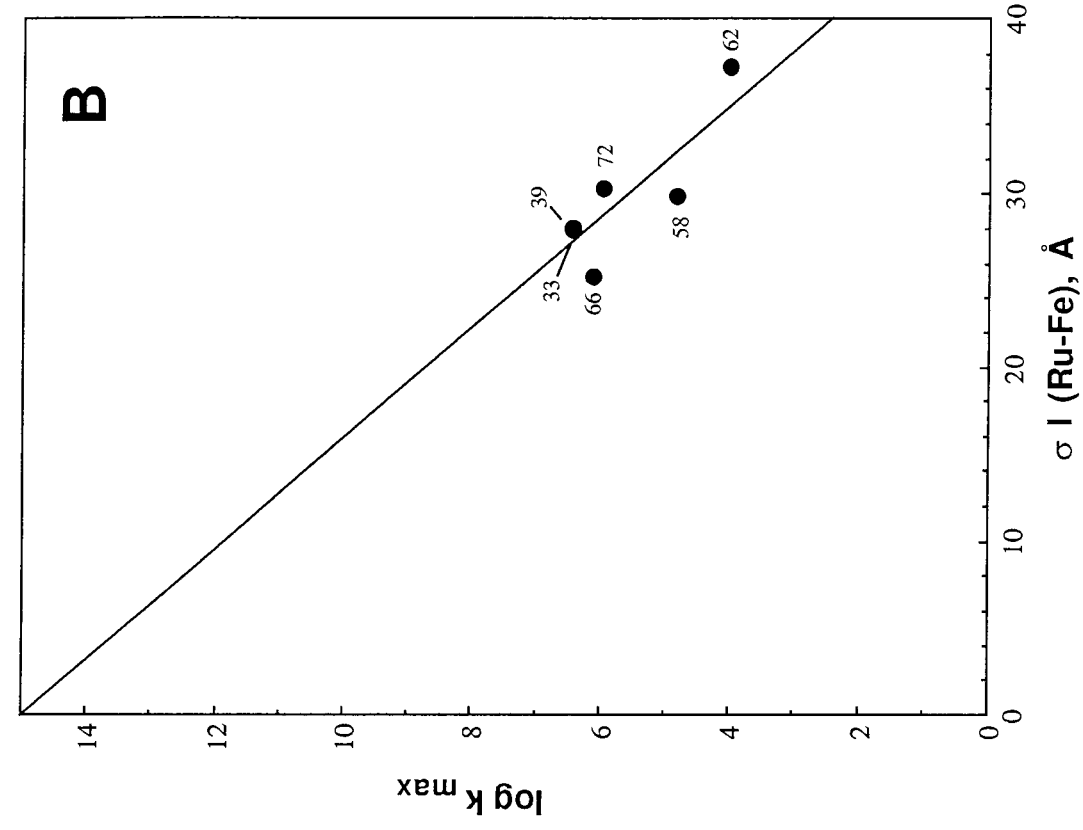
B
log k max
σ l (Ru-Fe), Å
0
2
4
6
8
10
12
14
0
10
20
30
40
39
33
66
72
58
62

Figure 4.8. The heme pocket of the Tyr67→Phe yeast iso-1-cytochrome *c* mutant. Figure is made courtesy of Berghuis and Brayer.

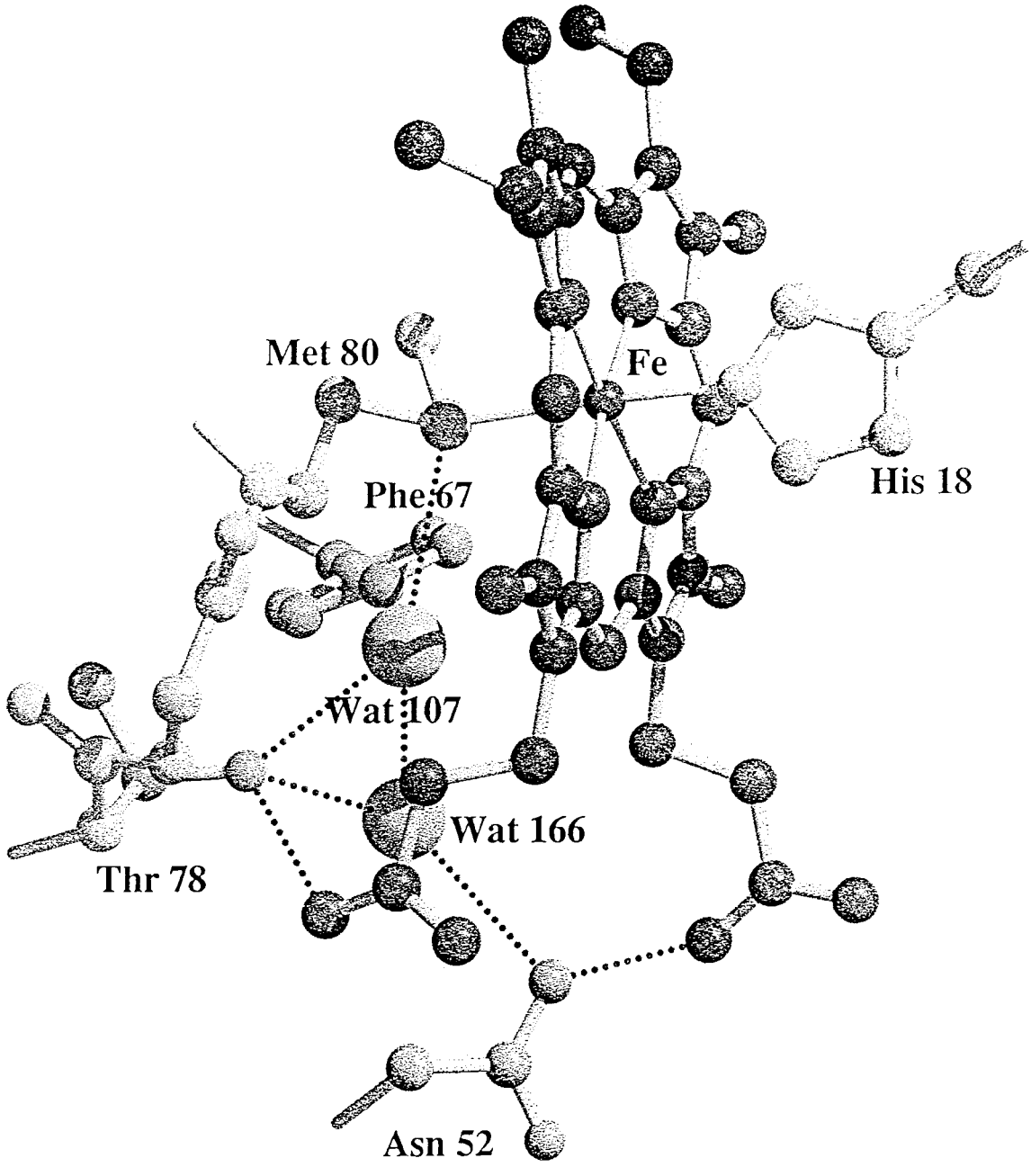
Met 80
Fe
His 18
Phe 67
Wat 107
Wat 166
Thr 78
Asn 52

Figure 4.9. Proposed bridges for ET in a_5Ru(HisX)/ZnP-modified human myoglobins (X = 48, 70, 83). **A-C**, dominant σ-tunneling pathways. **D-F**, amino acids proposed by AI-EH model for bridging the redox sites.

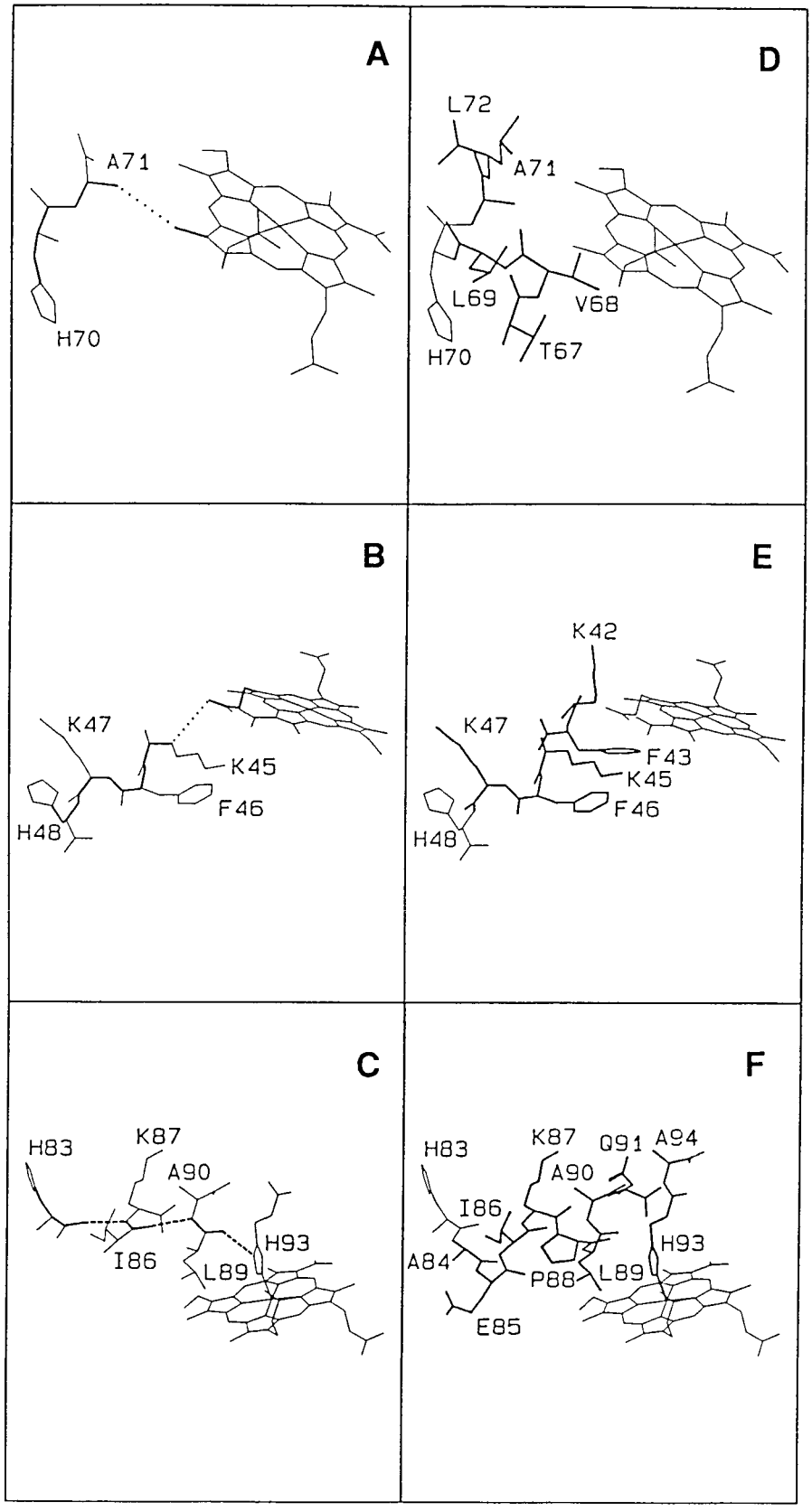
A
A71
H70
D
L72
A71
L69
V68
H70
T67
B
K47
K45
F46
H48
E
K42
K47
F43
K45
F46
H48
C
H83
K87
A90
I86
L89
H93
F
H83
K87
Q91
A94
A90
I86
H93
A84
P88
L89
E85

Figure 4.10. Maximal ET rates as functions of (**A**) the edge-to-edge and (**B**) Ru-to-Fe for $Ru(bpy)_2(im)(HisX)$cytochromes *c* (filled circles) (X = 33, 39, 58, 62, 66, 72) or Ru-to-edge multiple-pathway σ-tunneling lengths for Ru(HisX)/ZnP-modified myoglobins (open boxes) (X = 48, 70, 83) and cytochromes (open circles) (X = 33, 39, 62). The smaller boxes mark the dominant tunneling lengths for the myoglobin data. The solid lines are constrained-β′ fits to the six $Ru(bpy)_2(im)(HisX)$cyt *c* points and are described by the following equations: **A**, $\log k_{max} = -0.32\sigma l + 11.8$; and **B**, $\log k_{max} = -0.32\sigma l + 14.2$.

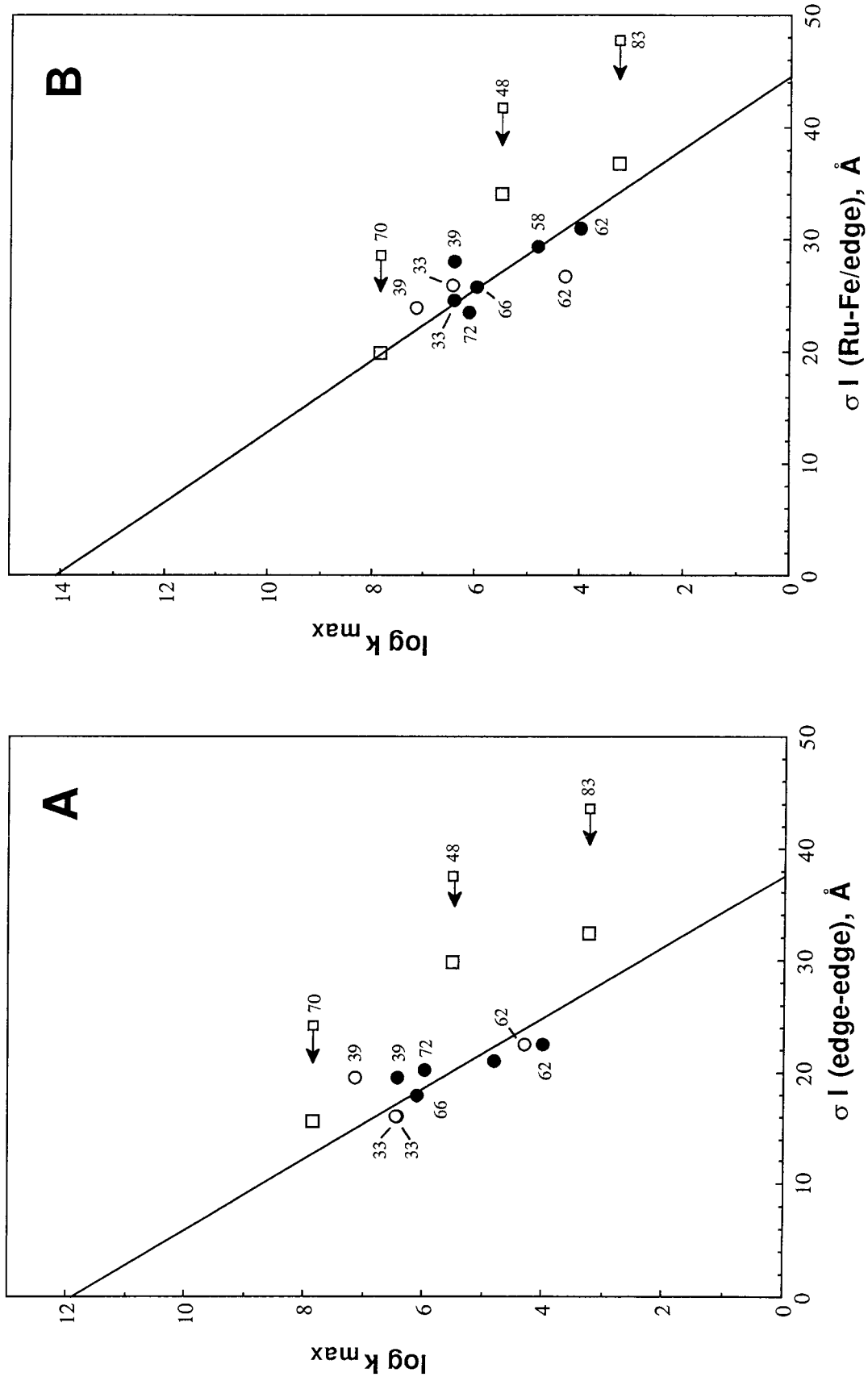
A
B
log k max
σ I (edge-edge), Å
σ I (Ru-Fe/edge), Å
0
2
4
6
8
10
12
14
0
10
20
30
40
50
70
39
39
72
66
33
33
48
62
62
83
70
39
33
33
72
66
39
58
62
62
48
83

Figure 4.11. Correlation of experimental and AI-EH-derived rate constants for $Ru(bpy)_2(im)$-modified cytochromes. Open circles are predictions based on the best paths (Figures 4.3B, 4.5B, and 4.6B) and the filled circles represent the predictions using extended basis sets.[8c,20] The points were scaled relative to the predicted coupling in Ru(His33)cyt *c*.

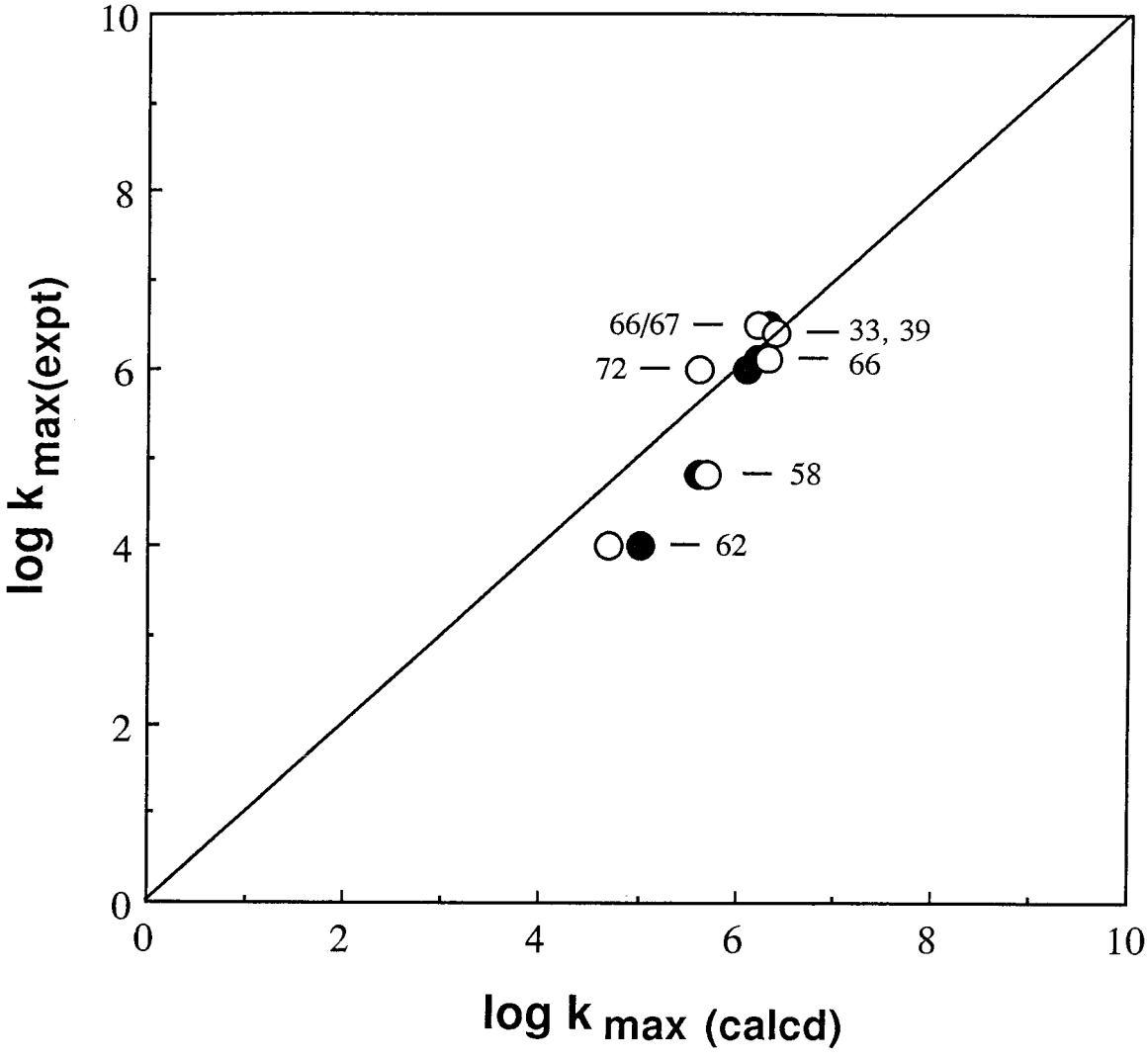
10
8
6
4
2
0
0
2
4
6
8
10
log k max(expt)
log k max (calcd)
66/67
33, 39
72
66
58
62

Figure 4.12. Correlation of experimental and calculated rate constants for Ru/ZnP-modified human myoglobins. Triangles represent the predictions of the multiple-path TP model, whereas the circles correspond to those of the AI-EH model.[8d]

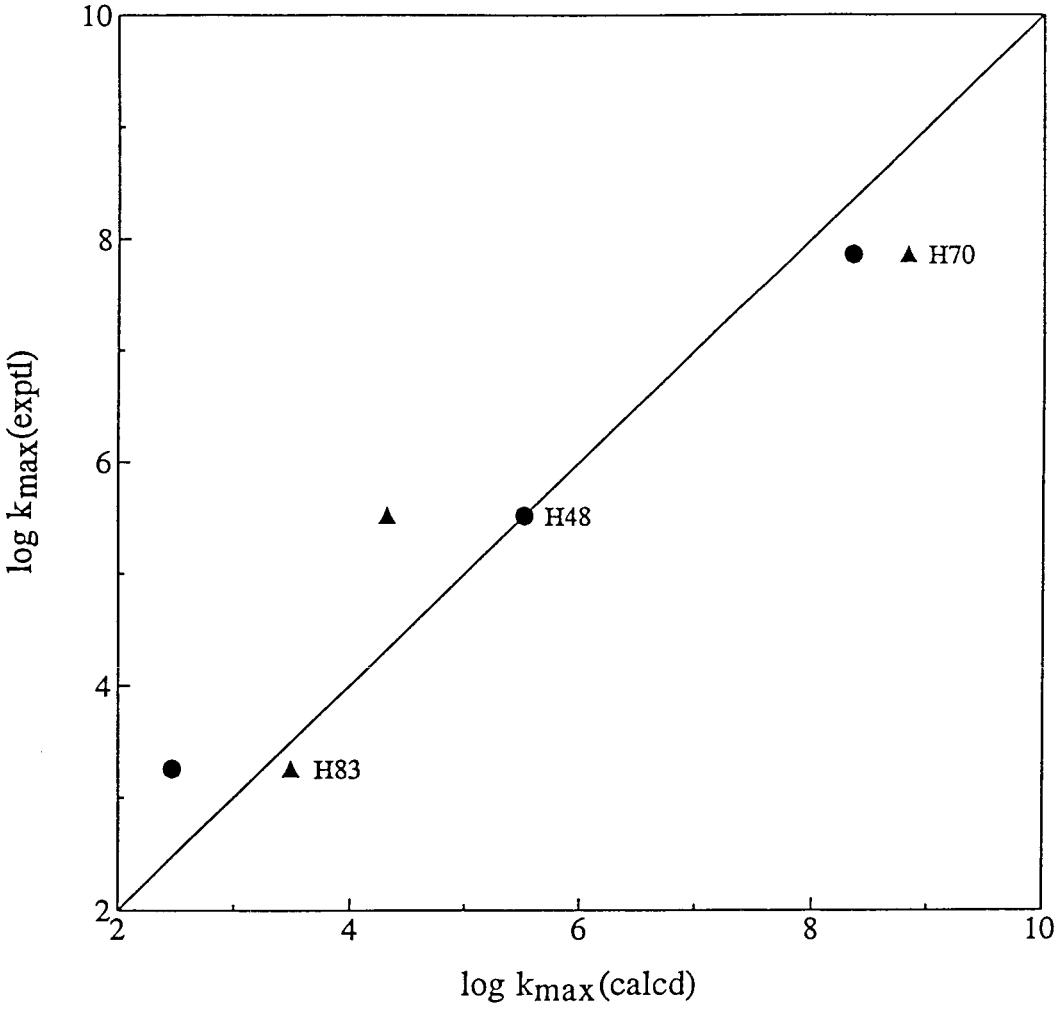
10
8
6
4
2
2
4
6
8
10
log k_{max}(exptl)
log k_{max}(calcd)
H70
H48
H83

Chapter 5

Ruthenium(II)-Mediated Protein Crosslinking and Stabilization

[This work is described in A. Muheim, R. J. Todd, D. R. Casimiro, H. B. Gray, & F. H. Arnold, *J. Am. Chem. Soc.*, **1993**, *115*, 5312.]

INTRODUCTION

Proteins play a central role in biology. They catalyze a variety of chemical transformations that would otherwise proceed at least 10^6-fold slower. The advent of recombinant DNA methodologies and computer-aided modeling techniques have greatly facilitated the construction of structural variants of natural enzymes with combinatorial catalytic properties.[1] Research in catalytic antibody generation[2] has further expanded the realm of protein-catalyzed processes to unnatural reactions. For these reasons, enzymes have become widely used for medical and commercial applications. Despite the overwhelmingly large body of chemical transformations mediated by proteins, enzymes are active only over narrow ranges of pH, temperature, ionic strength, and solvent compositions. Their reactivities depend on the integrity of the active sites and the global polypeptide fold. In view of this, the development of general strategies to increase the stability of the folded form has been the focus of numerous research endeavors.

Studies show that the folded form of a protein is only 5-15 kcal mol^{-1} more stable than the denatured state.[3] Thus, an approach that will stabilize a protein by a comparable degree is much desired. The presence of disulfide bridges in the structures of some proteins as revealed by x-ray crystallography provides the first clue as to how the folded, active form is assembled and stabilized. For some proteins, disulfides are a major source of stability of the folded form. For example, ribonuclease A unfolds completely when all four disulfide bonds are broken.[4] Bovine pancreatic trypsin inhibitor (BPTI) has a melting temperature around 95 °C, but loss of three native disulfides results in complete unfolding, and breaking the crosslink between residues 5 and 15 or 14 and 38 lowers the melting temperature (T_m) by 50 °C.[5]

It became apparent that introduction of new disulfides by genetic engineering into a protein offers promising possibilities in enhancing its stability and utility. However, as more studies emerges, the approach is met with mixed results. Introduction of multiple

disulfides in T4 lysozyme resulted in as much as 31 °C increase in T_m, and the stabilizing effects of multiple disulfides approximate the sum of the contributions from the individual crosslinks.[6] Subtilisin BPN' was stabilized 5.8 °C by crosslinking residues 22 and 87.[7] On the other hand, Wells and coworkers have prepared five other single disulfide mutants of subtilisin BPN' but none showed any substantial stability over the wild-type protein.[8] The stabilizing effects are generally less than expected and are difficult to characterize.

Certain complications can be seen in engineering disulfides into a protein. First, the criteria for designing disulfides in a protein are poorly defined. Because the bridge involves two short side chains, they often have to be introduced between buried residues and as such, their design requires considerable structural information. A new disulfide could introduce unfavorable strain into the folded structure and disrupt the internal hydrophobic packing. While an alternative design strategy is to base the choice of cysteine replacement on naturally occurring disulfides of homologous proteins, success is determined by the degree of homology in regions around the disulfides. The introduction of disulfides Cys29-Cys119 and Cys148-Cys243 in subtilisin which are analogous to those found in protease K was not stabilizing to the protein.[8] Yeast iso-1-cytochrome *c* was even destabilized by 1.2 kcal mol^{-1} upon introducing a Cys20-Cys102 disulfide, modeled on that of bullfrog cytochrome *c*.[9] Secondly, disulfide groups are sensitive to reducing environments, thereby limiting their utility.

As an alternative to introducing disulfides, other groups have utilized artificial bifunctional agents[10] to create intrachain crosslinks between nitrogenous groups or strong oxidants to generate reactive groups for esterification of side chain carboxylates.[11] In recent years, there has been growing interest in the engineering of metal-chelating sites on surfaces of proteins to effect enzymatic regulation,[12] facilitate separation of recombinant proteins through immobilized metal-affinity chromatography,[13] and

determine local secondary structures.[14] There also are some examples of how this technique may be used to stabilize the folded structures of proteins. Handel and DeGrado have introduced a Zn^{2+}-binding site on the surface of a four-helix bundle which, in the absence of the metal ion, has the properties of a molten globule.[15] Arnold and coworkers have shown that binding of exchange-labile Cu^{2+} to novel di-histidine sites on cytochrome *c* can stabilize the protein against both temperature and guanidine-hydrochloride-induced denaturation.[16]

Modeling studies suggest several motifs that will chelate metals.[17] They are listed in Table 5.1. Because these motifs depend on the nature of the local secondary structure, the design of chelating sites is possible with minimal structural information.[18] Another advantage of metal chelation concerns the ability to fine tune the stability of the bridge by varying the metal ion and its ligands. Given that the metal chelating sites are designed on the basis of the structure of the folded state, it is conceivable that exchange-labile metal ions bind preferentially to the folded structure. In the denatured state, the metal is no longer chelated to the sites and may be coordinated to solvent molecules or to remote sites on the denatured protein. Because of the uncertainty concerning the interactions of the metal ions with the unfolded protein, the effects of exchange-labile ions can be rather difficult to predict. In contrast, substitution-inert metal ions are expected to be bound to chelating site in both folded and unfolded form. Thus, this can be likened to a disulfide bridge or any other covalent crosslink. The effect is generally attributed to lowering the entropy of the unfolded state.

To our knowledge, there has been only one example of the use of inert metal ions to stabilize the folded state. Ghadiri and coworkers have used tetraammineruthenium(III) complex to bind to a His-X_3-His site on a peptide and induce the formation of an α-helical structure.[19] The metal ion stabilizes the folded structure by no more than 1 kcal mol^{-1}. Extension of this approach to a protein has yet to be demonstrated.

This chapter focuses on the modification of di-histidine mutants of cytochrome *c* with Ru complexes. Arnold and coworkers have previously prepared two mutants of *Saccharomyces cerevisiae* iso-1-cytochrome *c* each having two spatially adjacent surface histidines (Figure 5.1). In one case, a His-X_3-His site (positions 4 and 8) was incorporated into the 11-amino acid N-terminal helix of cytochrome *c* (cyt *c*).[13a] The second mutant incorporates a Leu58→His mutation which creates a metal-chelating site across a short segment of antiparallel β-sheet with the native His39.[16b,20] Both mutants have been shown by immobilized metal-affinity chromatography and Cu(II)IDA-PEG (polyethylene glycol substituted with iminodiacetate and metallated with Cu^{2+}) partitioning to chelate metal ions. The mutants and their Ru derivatives were characterized by absorption spectroscopy (UV/vis and CD) and direct electrochemical measurements. The stabilizing effects of Ru-mediated crosslinking towards thermal denaturation were examined and will be presented here.

MATERIALS AND METHODS

Cytochrome *c* Mutants

S. cerevisiae GM3C2 (defective in both isozymes of cytochrome *c*) strains harboring the His39His58 and His4His8 cyt *c* genes were kindly provided by Dr. Robert J. Todd and Professor Frances H. Arnold (Chemical Engineering, Caltech). The cell strains were grown in 10-L of YPG (10 g/L yeast extract, 20 g/L Bacto-peptone, 30 mL/L glycerol) at 30 °C. Once saturated (~3 days), the cells were pelleted by centrifugation in GSA rotor at 5k rpm, 4°C. The mutant proteins were isolated following standard procedures[21] with a few minor modifications. All solutions contained 1 mM EDTA to prevent metal binding to the chelating site. As a final purification step, the proteins were oxidized overnight with excess $Co(EDTA)^-$. Excess oxidant was removed by passing the protein solution through Sephadex G-25 resin (10 volumes) and washing with μ 50 mM

NaP_i, 1 mM EDTA, pH 7.0. The protein solutions were loaded unto a Mono-S 16/10 column pre-equilibrated with μ 50 mM NaP_i, pH 7.0 and eluted with a 0-1 M NaCl gradient in 50 mM NaPi, pH 7.0. The proteins elute off the column between 0.3-0.4 M NaCl.

Ruthenium Modification

The ferricytochrome solutions were concentrated to 0.2 mM in μ 100 mM NaP_i, pH 7.0 and were transferred to a Shlenck flask. $Ru(bpy)_2CO_3 \cdot H_2O$ (bpy = 2,2'-bipyridine) was weighed out to give a 5-fold excess and dissolved in a small aliquot (< 200 μL) of the phosphate buffer. The Ru solution was then added to the protein solution and the flask was subjected to repeated vacuum/Ar pump cycles. The solution was stirred at ambient temperature. To monitor the extent of each reaction, 50 μL aliquots were taken at certain time intervals and passed through Pharmacia PD-10 (Sephadex G-25) to remove excess reagent. The UV/vis spectrum of the front protein band was taken. For cytochrome *c*, a 2:3 ratio of the 292- (aromatic side chain, heme, and bpy π-π^*) and 410-nm absorbances is representative of a 1:1 adduct. At this point, the reaction was quenched by loading the entire reaction mixture unto a Sephadex G-25 column and washing with μ 100 mM NaP_i, pH 7.

The solution was incubated in the NaP_i buffer at room temperature for 1-2 days. It was concentrated and passed through G-25 column to remove any weakly bound Ru complex. In the case of His39His58 cyt *c*, the protein solution was first loaded unto a 16/10 Mono S cation-exchange column and washed with a 0-1 M NaCl gradient in μ 50 mM NaP_i, pH 7.0. The band representing the modified His39His58 mutant were pooled, exchanged to low salt buffer, and concentrated. A 1-mL IDA column (HiTrap, Pharmacia) was charged with Cu^{2+} by loading 0.5 mL 0.1 M $CuSO_4$ solution and washing with ddH_2O. The Cu(II)IDA column was rinsed with at least 10 mL 1 mM imidazole, 50 mM NaP_i, 500 mM NaCl, pH 7. A 2-mL aliquot was loaded unto the

column (1-mL HiTrap, Pharmacia) with the same imidazole buffer and eluted with 20 mM imidazole, 50 mM NaP_i, 500 mM NaCl, pH 7, in 60 mL (1-2 mL/min flow rate). The 1:1 product was quickly diluted with 100 mM NaP_i, pH 7 and exchanged to the same buffer by ultrafiltration to avoid ligand substitution in the bound Ru complex by the exogenous imidazole.

In the case of His4His8 cyt *c*, the quenched reaction mixture was loaded directly to the Cu(II)IDA column and fractionated in the same manner as described above. The 1:1 adducts of His39His58 and His4His8 cyt *c* were further purified by running them a second time through Cu(II)IDA column.

Direct Electrochemistry

The heme reduction potentials of the unmodified and modified proteins were determined by cyclic voltammetry. 2 mL of 0.4-0.6 mM protein solution in μ 100 mM NaPi, pH 7 were prepared. A 8-mm gold electrode (Pine Instruments) was polished with alumina, sonicated in ddH_2O, and dipped in saturated solution of dithiodipyridine (Aldrich) in the NaP_i buffer for at least 5 mins.[22] The electrode surface was washed with ddH_2O and dipped in the protein solution along with a Pt mesh counter electrode and SCE reference electrode. The electrodes were connected to a Princeton Applied Research potentiostat and a potential range of -150 to 150 mV vs. SCE was scanned at a rate of 5 mV/s. The current through the solution at this applied potential range was recorded on a Houston Instruments X-Y recorder.

Tryptic Analysis

The Ru-modified His39His58 cyt *c* was concentrated to 2 mg/mL in 0.1 M NH_4HCO_3, pH 8.0. A 2 mg/mL stock solution of trypsin was prepared in 1 mM HCl. 20 microliters of the trypsin solution were initially added for every 1 mL of the protein solution and the reaction was carried out at 25 °C. Another 20 microliters of trypsin were

added after 6 h and the reaction was allowed to proceed for another 14 h. The reactions were quenched by flash-freezing the solution in ethanol/dry ice and lyophilizing the samples. The lyophilized tryptic fragments were dissolved in 0.1% aqueous solution of TFA and loaded onto reversed-phase column HR 5/5 fitted to a Pharmacia FPLC. The fragments were eluted with 0.1% TFA in acetonitrile using a linear gradient up to 30% v/v of the eluent and detected using a 280-nm wavelength filter. The tryptic band containing the ruthenium label was collected and sequenced via automated Edman degradation on an Applied Biosystems 473A sequencer.

Thermal Denaturation

Approximately 11 μM solutions of the unmodified and modified ferricytochromes in μ 100 mM NaP_i, pH 7 were transferred into 0.1-cm water-jacketed CD cells (Jasco). The ellipticity at 222 nm was monitored at temperatures beginning from 25 °C up to values when the protein has fully unfolded. Readings were collected in the time mode of J600 version 2.0 programmer as the temperature of the 0.10-cm water-jacketed cell containing the protein solution was adjusted from 25 to 80 °C with a Lauda 2KR thermostat (Brinkman Instruments). The data collected over this temperature range were analyzed in terms of a two-state transition model.

RESULTS AND DISCUSSION

Ruthenium Modification

Both cyt *c* mutants were modified with $Ru(bpy)_2CO_3$; a ruthenium polypyridine complex was selected for these studies because of their strong absorption properties which make protein modification easily tractable. Figure 5.2 shows the cation-exchange chromatogram for the reaction products of His39His58 cyt *c*. None of the bands represented a pure 1:1 product. Instead, the band marked 1 exhibited a Ru:protein ratio

of less than 1 indicating that it is a mixture of the 1:1 adduct and unreacted protein. This initial chromatographic step was not applicable for His4His8 cyt *c*. The 1:1 Ru:Fe products were strongly retained on the column that they required too high a salt concentration (0.7-0.8 M NaCl) for elution (data not shown). Resolution at this concentration range was very poor.

The band containing the 1:1 Ru-modified His39His58 cyt *c* was further fractionated by Cu(II)IDA chromatography (Figure 5.3). Because both His39 and His58 are no longer accessible to the immobilized metal ions, the 1:1 product with the chelated Ru eluted close to the void volume. The unmodified protein eluted with 15 mM imidazole. Figure 5.4 shows the corresponding Cu(II)IDA chromatogram for the reaction products of His4His8 cyt *c*. On the basis of their UV/vis spectra, the first band contained 2:1 Ru:protein products (which otherwise would have been separated by cation-exchange chromatography), the second band the desired 1:1 product, and the third band the unreacted material. His4His8 cyt *c* exhibits a lower affinity (11 mM imidazole for elution) for bound copper complexes than His39His58 cyt *c*. This difference cannot be attributed to more favorable column-protein ionic interactions in the region near His39 and His58 as both starting and elution buffers contain high salt concentrations (500 mM NaCl). It is possible that the rigidity of the helical turn that separates His4 and His8 constrains the interaction of this site with the immobilized metal ions whereas the His39His58 region is considerably more flexible to permit a favorable geometry.

That the Ru complex is bound to both His39 and His58 was also confirmed by tryptic analysis. The tryptic fragments were separated by reverse phase chromatography (Figure 5.5A). The Ru-containing band was isolated, its purity verified by capillary-zone electrophoresis, and its amino acid sequence determined by Edman degradation (Figure 5.5B). Because the Ru complex crosslinks two tryptic fragments (39-54, His_{39}SerGlyGlnAlaGluGlyTyrSerTyrThr-AspAlaAsnIleLys and 56-73,

AsnValHis$_{58}$TrpAspGluAsnAsnMetSerGluTyrLeuThrAsnPro-TMLLys, TML = ε-*N*-trimethyllysine), the expected mixture of amino acid at each cleavage cycle was observed.

Heme Potentials

The heme potentials of the Ru-modified proteins were determined by cyclic voltammetry and compared to those of the unmodified cytochromes. The voltammograms are shown in Figure 5.6. His39His58 cyt *c* has a heme potential of 290(5) mV vs. NHE which is higher than that of Ser102 mutant (272(5) mV vs. NHE). Crosslinking His39 and His58 causes the heme potential to approach that of Ser102 protein, indicating that the modification partially restores the heme environment to the wild-type configuration. In contrast, Ru modification of the His4His8 protein had little effect on the heme potential (257(5), Ru(bpy)$_2$(His4)(His8)cyt *c*; 254(5) mV vs. NHE, His4His8 cyt *c*). It is apparent that the electronic structure of the heme center is not perturbed by surface modification of the protein.

A consequence of the higher than normal heme potential of His39His58 cyt *c* is its instability towards autoreduction. After an overnight incubation of the oxidized protein in 100 mM NaP_i, pH 7, at 4 °C, >20% has autoreduced. This property also was noticeable in the reaction of oxidized His39His58 cyt *c* with $Ru(bpy)_2^{2+}$; the first band in Figure 5.2 was identified to have a reduced heme. In contrast, the oxidized form of the corresponding Ru-crosslinked protein is extremely stable and showed no spectral change for at least a week at 4 °C. Excess dithiothreitol is added for long-term storage of the unmodified protein. Stability of His4His8 cyt *c* towards autoreduction was not affected by modifying with $Ru(bpy)_2^{2+}$.

Thermal Stabilities

The thermal stabilities of the proteins were evaluated by monitoring the CD ellipticity at 222 nm of the protein solution as a function of temperature. The denaturation profiles are shown in Figure 5.7. The Ser102 mutant has a midpoint of melting temperature of 56.3 °C. Introduction of Leu58→His destabilizes the protein by ~7 °C. Crosslinking the di-histidine site with $Ru(bpy)_2^{2+}$ increases the melting temperature to 72.8 °C, a 23.2 °C over that of the unmodified protein, 16.5 °C over that of the pseudo-wild-type protein. Near-UV CD spectrum of the modified protein showed a very low optical activity around the bpy π-π^* band comparable to that observed in the unmodified protein. This indicates that the band contains a near equimolar mixture of His39His58 cyt *c* with Δ and Λ isomers of the $Ru(bpy)_2(His)_2^{2+}$ moiety. Because the denaturation curve shows a two-state transition over a wide range of temperature, the difference in protein stability between the two isomers is expected to be negligible.

His4His8 cyt *c* has a T_m of 51.1 °C. Crosslinking helical turn does not enhance the thermal stability of the protein; in fact, the protein is destabilized by 2.0 °C.

Comparison with Other Crosslinking Strategies

Ru modification of His39 and His58 effectively introduces a covalent bridge across a β-sheet in the molecule. It is widely believed that the effect of a covalent crosslink on protein stability is to lower the backbone entropy of the unfolded state and the magnitude of this effect is proportional to the size of the loop formed by the crosslink. To test this hypothesis, a Ru crosslink of a smaller loop size (five residues) is created between two histidines separated by a helical turn. The crosslink did not enhance the thermal stability of the protein; in fact, the protein has been destabilized by 2 °C. The resistance of each Ru-modified protein to guanidine hydrochloride-induced unfolding (GdnHCl) was also determined by monitoring the absorbance at 410 nm with increasing denaturant concentration (data not shown). Ru modification of His39His58 cyt *c*

increases the midpoint of GdnHCl-induced denaturation from 0.9 M to 2.27 M GdnHCl; in contrast, crosslinking His4 and His8 slightly lowers the GdnHCl concentration for half-denaturation by 1.3 M, from 2.27 to 0.96 M. From these data and by assuming a two-state transition process, $\Delta\Delta G_u$s (change in unfolding free energy) for crosslinking His39His58 and His4His8 cyt *c* have been calculated to be 5.5 and -0.8 kcal/mol, respectively.

Pace and coworkers have analyzed the stabilizing effects of natural disulfides in a select group of proteins and proposed that the entropic contribution of a crosslink is determined by the loop size, *n* (eq 1).

$$\Delta S = -2.1 - (3/2)R \ln n \qquad (1)$$

This expression predicts that a disulfide between residues 39 and 58 should contribute 3.3 kcal mol^{-1} (at 25 °C) to the stability of the protein which is considerably less than what is observed using a Ru bridge. It is very apparent that introduction of a surface Ru-mediated crosslink can dissipate any conformational strain much better than a disulfide bridge. Although direct experimental comparison with a disulfide bridge between positions 39 and 58 would be desirable, modeling studies indicate that such as a short crosslink can not be physically accomodated.

Table 5.2 lists the thermodynamic properties of larger set of protein crosslinks including natural and novel (genetically or chemically introduced) bridges, and it is clearly evident that the Ru crosslink in His39His58 cyt *c* exhibits one of the highest stabilizing effect on the basis of its loop size. The magnitude of its effect is comparable to removing the native Cys77-Cys95 bridge in human lysozyme; replacing both residues with alanine lowers T_m by 15 °C and $-\Delta G_u$ by 4.6 kcal mol^{-1}. In other cases, the same effect can only be achieved with a larger loop size (e.g., 35, crosslinked Lys7 and Lys41 in RNase A; 74, ester bond between Glu35 and oxindolealanine at 108 in hen lysozyme; 122, native Cys6-Cys127 bridge in hen lysozyme) or with multiple crosslinks (e.g., native

Cys2-Cys10/Cys6-Cys103 in RNase T1; new Cys9-Cys164/Cys21-Cys142 in T4 lysozyme).

CONCLUSION

We present the first application of substitution-inert metal complexes in enhancing the stability of proteins with surface chelating sites. The approach effectively introduces a covalent crosslink in the molecule that is analogous to a disulfide bridge. In here, we observed a dramatic thermal stabilization by crosslinking His39 and His58 of yeast cyt *c* with $Ru(bpy)_2^{2+}$. The histidines are located on opposite strands of an antiparallel β-sheet. The approach is very attractive for several reasons. First, the crosslinks are introduced on the surface where they are unlikely to perturb the internal packing of the protein. In contrast, disulfides are normally created between two buried residues and additional conformational strain can be introduced. Secondly, they can be used to stabilize proteins with β-sheets.

REFERENCES AND NOTES

1. Sandberg, W. S.; Terwilliger, T. C. *Proc. Natl. Acad. Sci. USA* **1993**, *90*, 8367 and references cited therein.
2. (a) Janda, K. D.; Shevlin, C. G.; Lerner, R. A. *Science* **1993**, *259*, 490. (b) Lerner, R. A.; Benkovic, S. J.; Schultz, P. G. *Science* **1991**, *252*, 659.
3. Pace, C. N. *Trends Biochem. Sci.* **1990**, *15*, 14.
4. Konishi, Y.; Ooi, T.; Scheraga, H. A. *Biochemistry* **1982**, *21*, 4741.
5. States, D. J.; Creighton, T. E.; Dobson, C. M.; Karplus, M. *J. Mol. Biol.* **1987**, *195*, 731-739.
6. Matsumura, M.; Signor, G.; Matthews, B. *Nature* **1989**, *342*, 291.
7. Pantoliano, M. W.; Ladner, R. C.; Bryan, P. N.; Rollence, M. L.; Wood, J. F.; Poulos, T. L. *Biochemistry* **1987**, *26*, 2077.
8. Mitchinson, C.; Wells, J. A. *Biochemistry* **1989**, *28*, 4807.
9. Betz, S. F.; Pielak, G. J. *Biochemistry* **1992**, *31*, 12337.
10. (a) Ueda, T.; Yamada, H.; Hirata, M.; Imoto, T. *Biochemistry* **1985**, *24*, 6316. (b) Lin, S. H.; Konishi, Y.; Denton, M. E.; Scheraga, H. A. *Biochemistry* **1984**, *23*, 5504. (c) Yamada, H.; Kuroki, R.; Hirata, M.; Imoto, T. *Biochemistry* **1983**, *22*, 4551. (d) Goldenberg, D. P.; Creighton, T. E. *J. Mol. Biol.* **1984**, *179*, 527. (e) Cuatrecasas, P.; Fuchs, S.; Anfinsen, C. B. *J. Biol. Chem.* **1969**, *244*, 406. (f) Hardman, J. K.; Hardman, D. F. *J. Biol. Chem.* **1971**, *246*, 6489. (g) Marfey, P. S.; Nowak, H.; Uziel, M.; Yphantis, D. A. *J. Biol. Chem.* **1965**, *240*, 3264.
11. (a) Imoto, T.; Hartdegen, F. J.; Rupley, J. A. *J. Mol. Biol.* **1973**, *80*, 637. (b) Beddell, C. R.; Blake, C. C. F.; Oatley, S. J. *J. Mol. Biol.* **1977**, *97*, 643.
12. (a) Higaki, J. N.; Haymore, B. L.; Chen, S.; Fleterrick, R. J.; Craik, C. S. *Biochemistry* **1990**, *29*, 8582. (b) Higaki, J. N.; Fletterick, R. J.; Craik, C. S. *Trends Biochem. Sci.* **1992**, *17*, 100.

13. (a) Todd, R. J.; Van Dam, M. E.; Casimiro, D.; Haymore, B. L.; Arnold, F. H. *Proteins, Struct. Funct. Genet.* **1991**, *10*, 156. (b) Brewer, S. J.; Haymore, B. L.; Hopp, T. P.; Sassenfeld, H. M. in *Purification and Analysis of Recombinant Proteins*; R. Seethram and S. Sharma, Eds.; Dekker: New York, 1991; pp.239-265.

14. (a) Suh, S.-S.; Haymore, B. L.; Arnold, F. H. *Protein Eng.* **1991**, *4*, 301. (b) Pessi, A.; Bianchi, E.; Crameri, A.; Venturini, S.; Tramontano, A.; Sollazo, M. *Nature* **1993**, *362*, 367.

15. Handel, T.; DeGrado, W. F. *J. Am. Chem. Soc.* **1990**, *112*, 6710.

16. (a) Kellis, J. T., Jr.; Todd, R. J.; Arnold, F. H. *Bio/Technology* **1991**, *6*, 994. (b) Umana, P.; Kellis, J. T., Jr.; Arnold, F. H. *ACS Symp. Ser.* **1993**, *516*, 102.

17. Arnold, F. H.; Haymore, B. L. *Science* **1991**, *252*, 1796.

18. Nishikawa, K.; Noguchi, T. *Methods Enzymol.* **1991**, *202*, 31.

19. Ghadiri, M. R.; Fernholz, A. K. *J. Am. Chem. Soc.* **1990**, *112*, 9633.

20. The sequences 37-40 and 57-59 form an imperfect antiparallel β-sheet called a β-bulge (Louie, G. V.; Brayer, G. D. *J. Mol. Biol.* **1990**, *214*, 527. Berghuis, A. M.; Brayer, G. D. *J. Mol. Biol.* **1992**, *223*, 959). However, residues 39 and 58 are on the portion of this structure that exhibits a regular β-sheet pattern.

21. Cutler, R. L.; Pielak, G. J.; Mauk, A. G.; Smith, M. *Protein Eng.* **1987**, *1*, 95.

22. Villafranca, J. E.; Howell, E. E.; Oatley, S. J.; Xuong, N.; Kraut, J. *Biochemistry* **1987**, *26*, 2182.

23. Eder, J.; Wilmanns, M. *Biochemistry* **1992**, *31*, 4437.

24. Radford, S. E.; Woolfson, D. N.; Martin, S. R.; Lowe, G.; Dobson, C. M. *Biochem. J.* **1991**, *273*, 211.

25. Pace, C. N.; Grimsley, G. R.; Thomson, J. A.; Barnett, B. J. *J. Biol. Chem.* **1988**, *263*, 11820.

26. Kuroki, R.; Inaka, K.; Taniyama, Y.; Kidokoro, S.; Matsushima, M.; Kikuchi, M.; Yutani, K. *Biochemistry* **1992**, *31*, 8323.

27. Goto, Y.; Tsunenaga, M.; Kawata, Y.; Hamaguchi, K. *J. Biochem. (Tokyo)* **1987**, *101*, 319.

28. (a) Matsudaira, P. *Methods Enzymol.* **1990**, *182*, 602. (b) User Bulletin, Protein Sequencer, Issue No. 14, Applied Biosystems, Inc., Nov. 18, 1985.

Table 5.1. Possible Metal-Chelation Sites in Secondary Structural Folds.[a]

Sequence	α helix	β strand	Reverse β Turn
HisHis	-	-	-
HisXHis	-	+	-
HisXXHis	-	-	+
HisXXXHis	+	-	-

[a]Biscoordination is either possible (+) or not (-).

Table 5.2. Thermodynamic Effects of Natural, Genetically and Chemically Introduced Crosslinks in Proteins.

Protein	Crosslink	Loop Size[a]	ΔTm, °C[b] ($\Delta\Delta G_u$, kcal mol^{-1})	Ref
New				
Chemical Crosslink				
Yeast Iso-1-cyt *c*	His39-His58	20	23.2(5.5)	this work
Hen Lysozyme	Glu35-Trp108	74	29.4(5.2)	11
	Lys1-His15	16	-[e] (2.3)	10a
RNase A	Lys7-Lys41	35	-[e] (4.9)	10b
Disulfide				
T4 Lysozyme	3-97/9-164/21-142	373	31.9 (-[e])	
	9-164/21-142	278	22.9 (-[e])	
	3-97/9-164	251	26 (-[e])	
	21-142	122	13.7 (-[e])	
	9-164	156	12.9 (-[e])	
	3-97	95	6.7 (-[e])	6
Subtilisin	22-87	66	5.8 (-[e])	7
DHFR[c]	39-85	37	-[e] (1.8)	22
PRAI[d]	27-212	186	-[e] (1)	23
Yeast Iso-1-cyt *c*	20-102	83	-1.8 (-1.2)	9
Natural Disulfide				
Hen Lysozyme	6-127	122	24 (-[e])	24
RNase T_1	2-10/6-103	107	22.1 (7.2)	
	2-10	9	6 (3.4)	25
Human Lysozyme	77-95	19	15 (4.6)	26
Immunoglobulin LC	26-86	61	-[e] (4.7)	27

[a]For mutiple crosslinks, the loop size is the sum of those of the individual crosslinks.
[b](+), for increasing T_m or ΔG_u upon crosslink formation. For natural disulfides, comparisons were made between oxidized and reduced (if disulfide(s) specified is(are) the only one(s) existing) or mutated/chemically blocked proteins.
[c]Dihydrofolate reductase.
[d]Yeast N-(5'-phosphoribosyl)anthranilate isomerase.
[e]Not determined.

Figure 5.1. Integral model of Ru-crosslinked di-histidine sites on the surface of the yeast iso1-cytochrome *c* mutants.

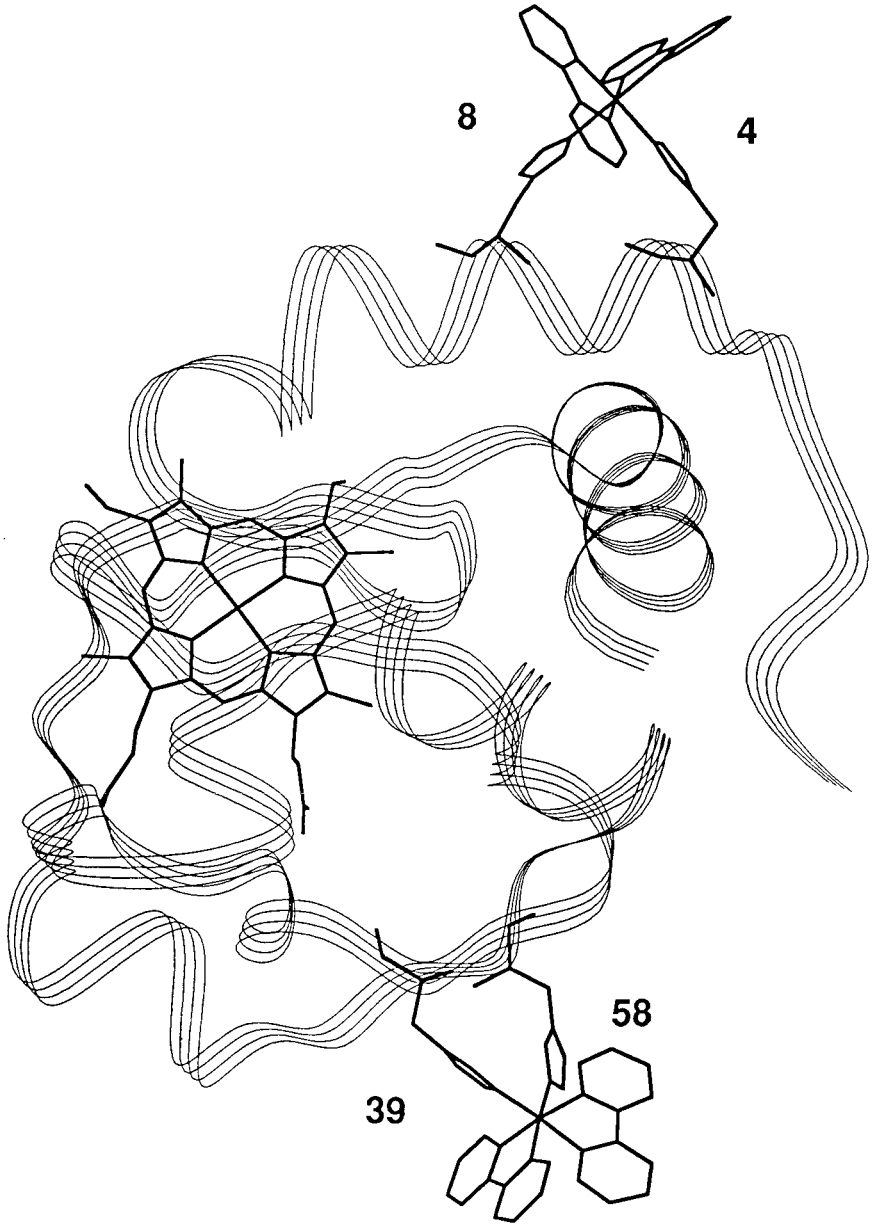
8
4
58
39

Figure 5.2. Cation-exchange chromatogram of the reaction products of His39His58 cyt *c* with $Ru(bpy)_2^{2+}$. The first band was unmodified cyt *c* (0:1 Ru:Fe) resulting from autoreduction. This was followed by a mixture of unmodified ferricytochrome and the 1:1 Ru:Fe product, which was further fractionated by metal-affinity chromatography.

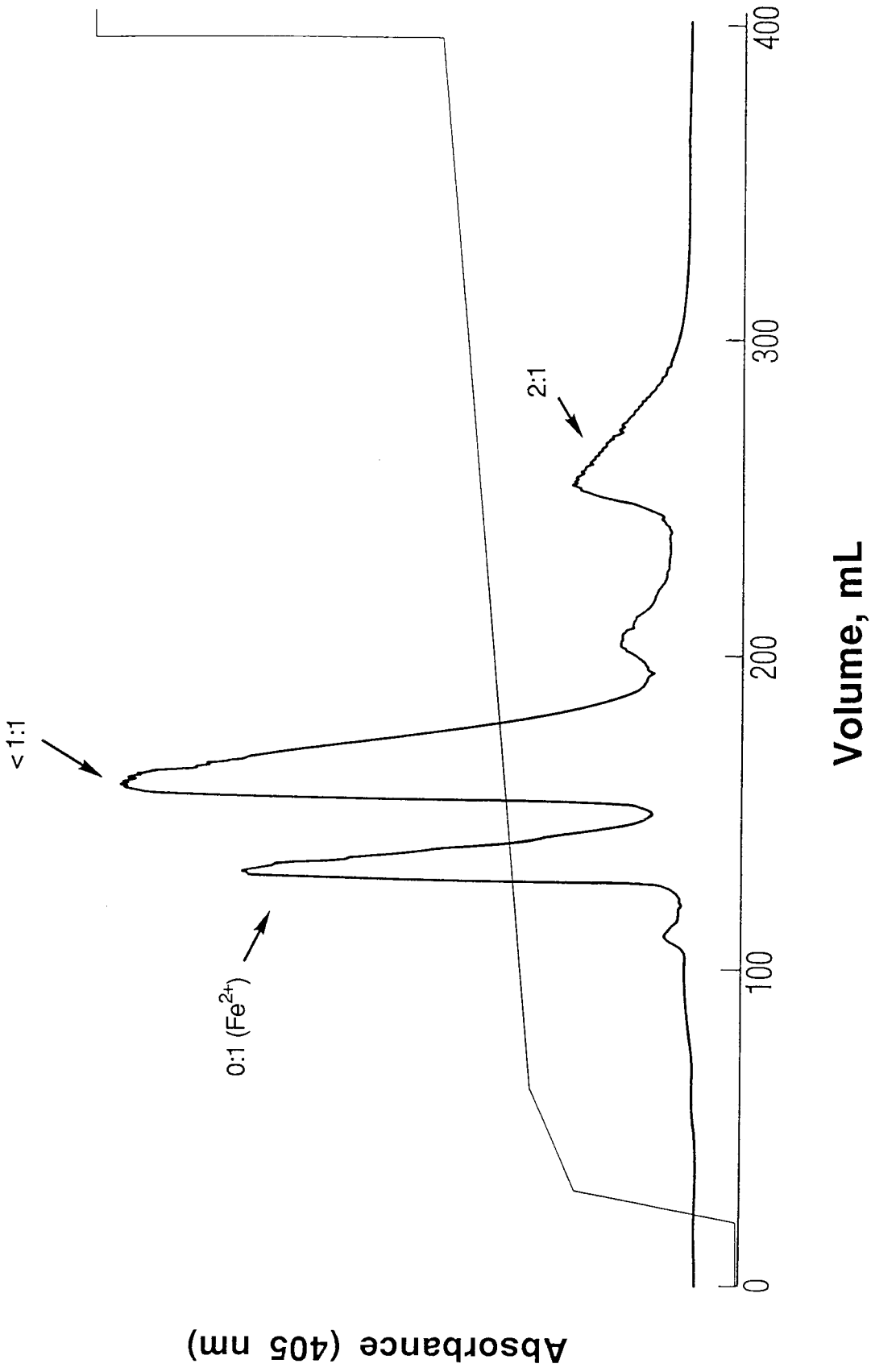
Absorbance (405 nm)
Volume, mL
0
100
200
300
400
< 1:1
0:1 (Fe^{2+})
2:1

Figure 5.3. Cu(II)IDA chromatogram of partially purified $Ru(bpy)_2$(His39)(His58)cyt *c*. A straight 1-20 mM gradient (in 50 mM NaP_i, 500 mM NaCl, pH 7.0) was developed over 55 mL of eluent at 1-2 mL/min flow rate. The retention property of $Ru(bpy)_2$(His39)(His58)cyt *c* (marked with an asterisk) is comparable to that of the His39Gln variant of iso-1-cytochrome (---). The unmodified His39His58 cyt *c* elutes at *ca.* 16 mM imidazole.

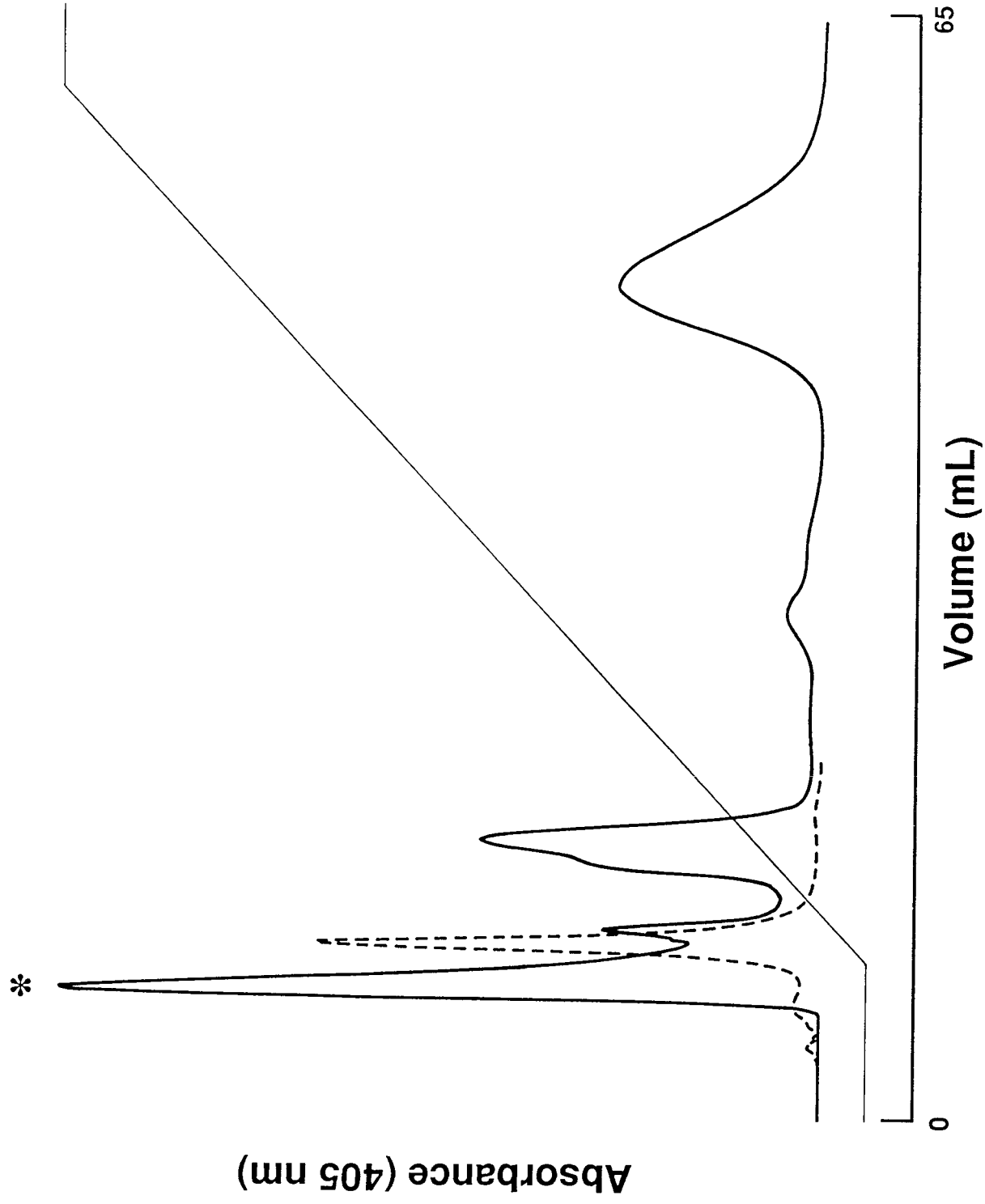
Absorbance (405 nm)
Volume (mL)
0
65
*

Figure 5.4. Cu(II)IDA chromatogram of $Ru(bpy)_2$(His4)(His8)cyt *c* reaction mixture. The correct 1:1 Ru:Fe product (∗) is preceded by 2:1 side products; the unmodified His4His8 cyt *c* is the last to elute at *ca.* 11 mM imidazole.

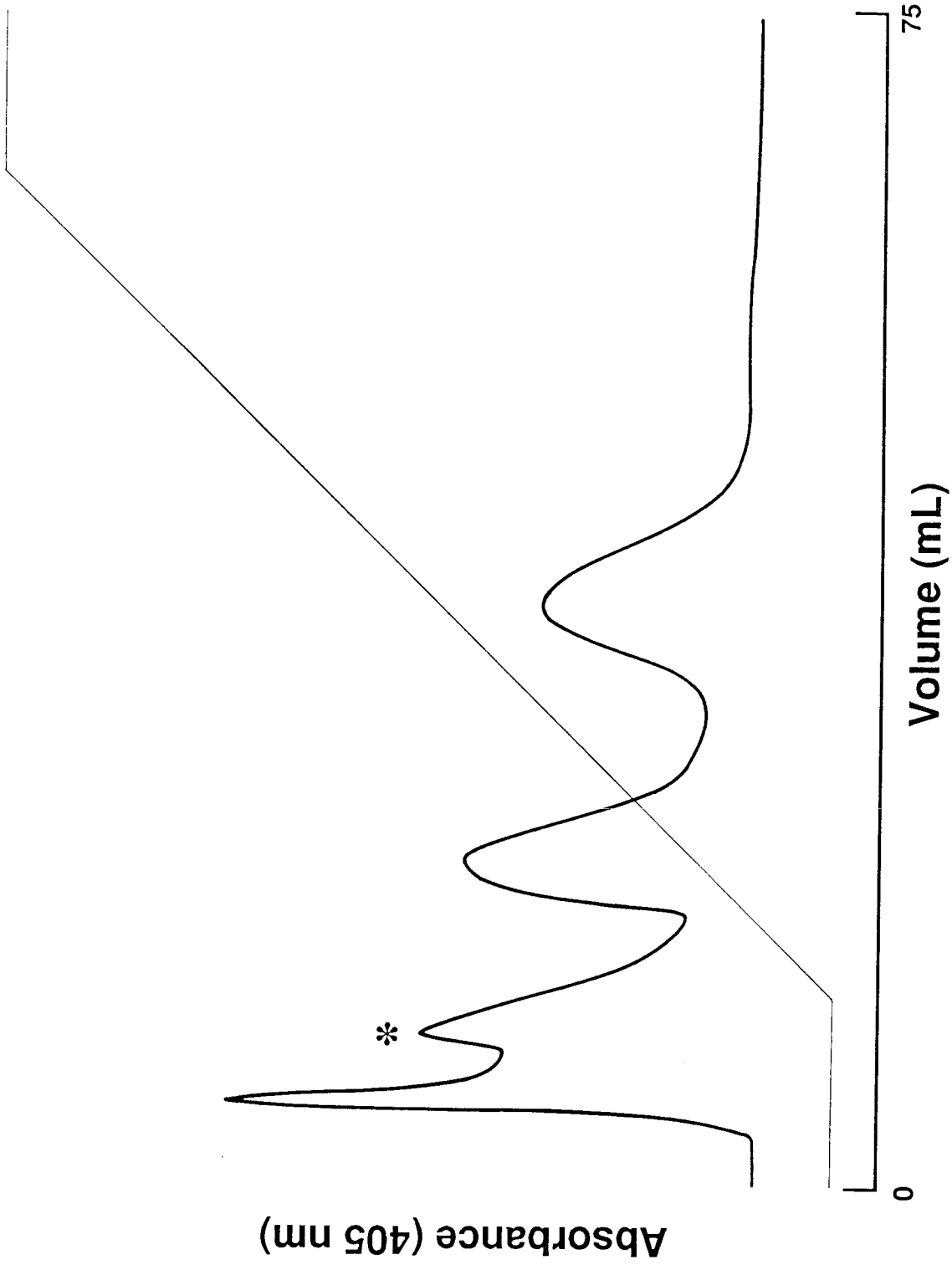
Absorbance (405 nm)
Volume (mL)
0
75
*

Figure 5.5. Isolation and sequence analysis of the Ru-containing tryptic fragment of $Ru(bpy)_2$(His39)(His58)cyt *c*. (**A**) Reverse-phase chromatography of tryptic digests of $Ru(bpy)_2$(His39)(His58)cyt *c* on a Pharmacia RPC HR5/5 column. (**B**) Yields of PTH-amino acid derivatives (PTH = phenylthiodantoin) observed at each cycle of cleavage of Ru-containing tryptic digest (*ca.* 1 nmol of starting material). The yields of PTH-His39 and PTH-His58 are notably low, suggesting that the label is attached to both residues. The low yields of PTH derivatives of ser, trp, and asp in the analyses are typically attributed to their degradation.[28]

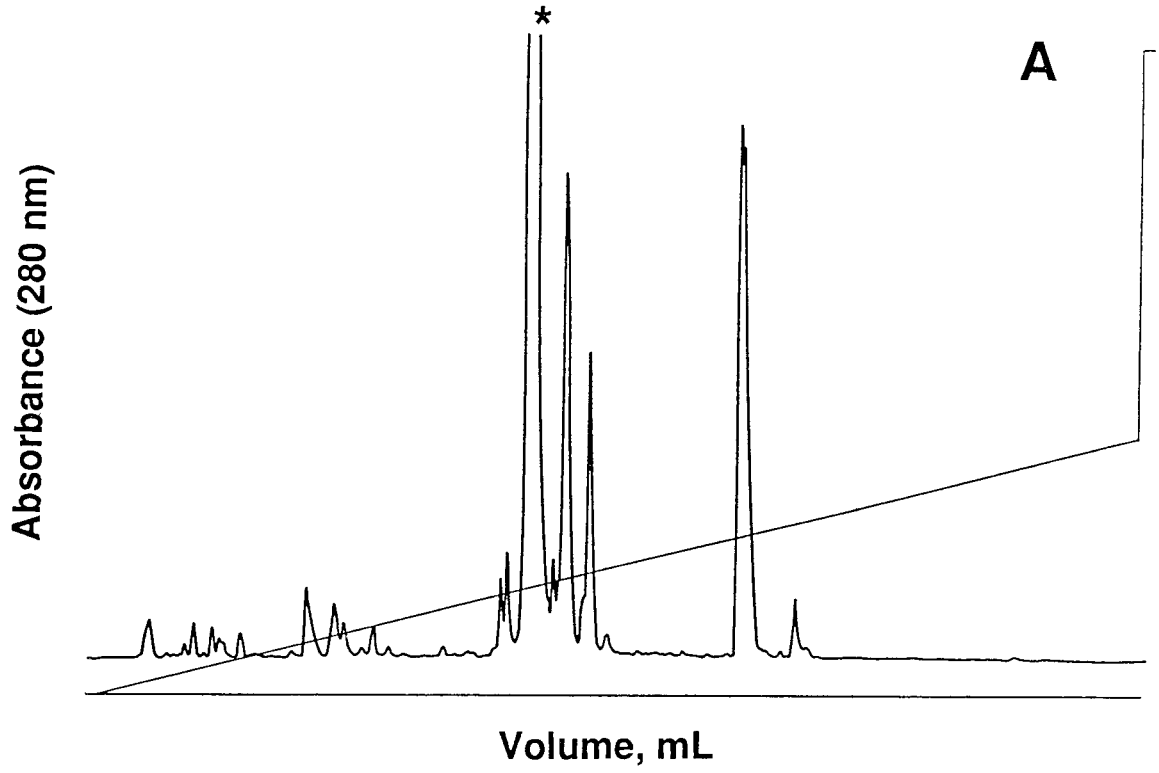
A
*
Absorbance (280 nm)
Volume, mL

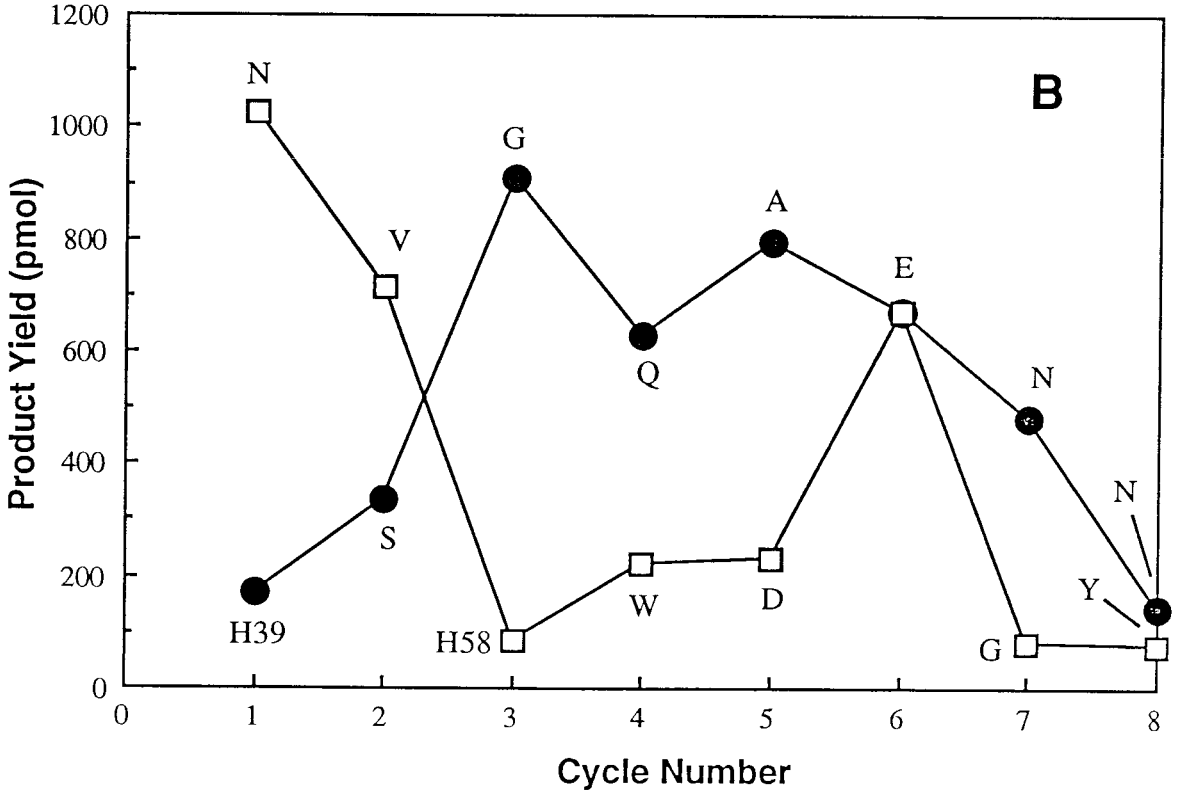
B
Product Yield (pmol)
Cycle Number
N
V
G
A
E
N
N
Y
G
Q
S
H39
H58
W
D
0
200
400
600
800
1000
1200
0
1
2
3
4
5
6
7
8

Figure 5.6. Cyclic voltammograms of unmodified (---) and Ru-modified (—) di-histidine mutants: (**A**) His4His8 cyt *c*; (**B**) His39His58 cyt *c*.

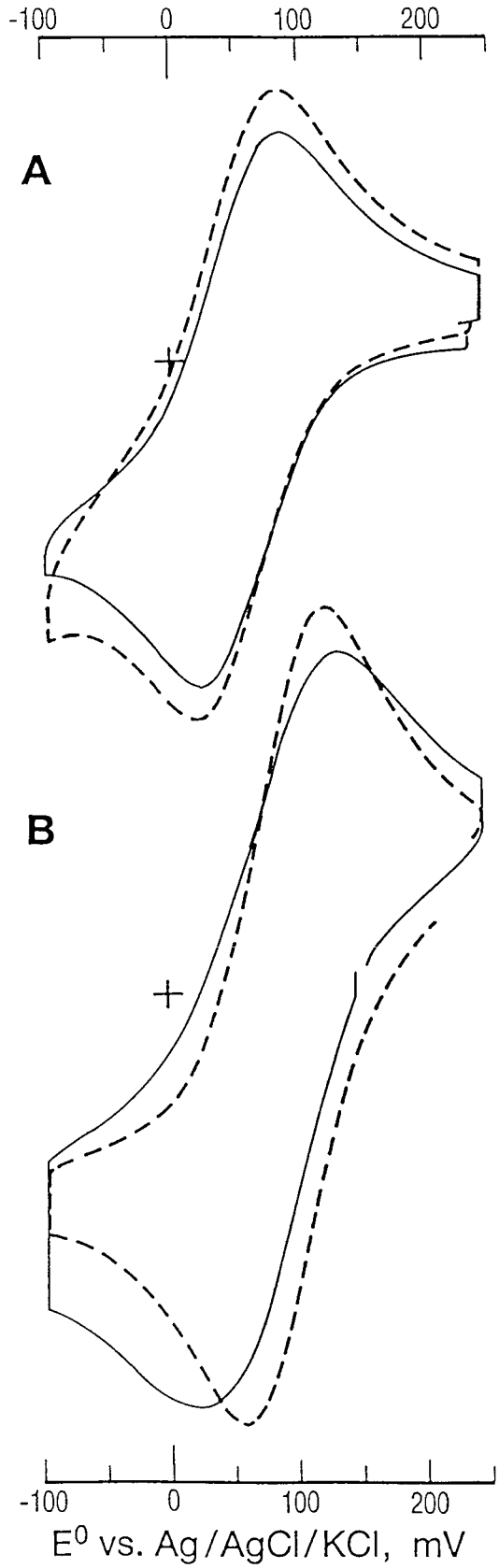
-100
0
100
200
A
B
-100
0
100
200
E⁰ vs. Ag/AgCl/KCl, mV

Figure 5.7. Thermal denaturation of unmodified (triangles) and Ru-crosslinked di-histidine mutants (boxes): (**A**) His39His58 cyt *c*; (**B**) His4His8 cyt *c*.

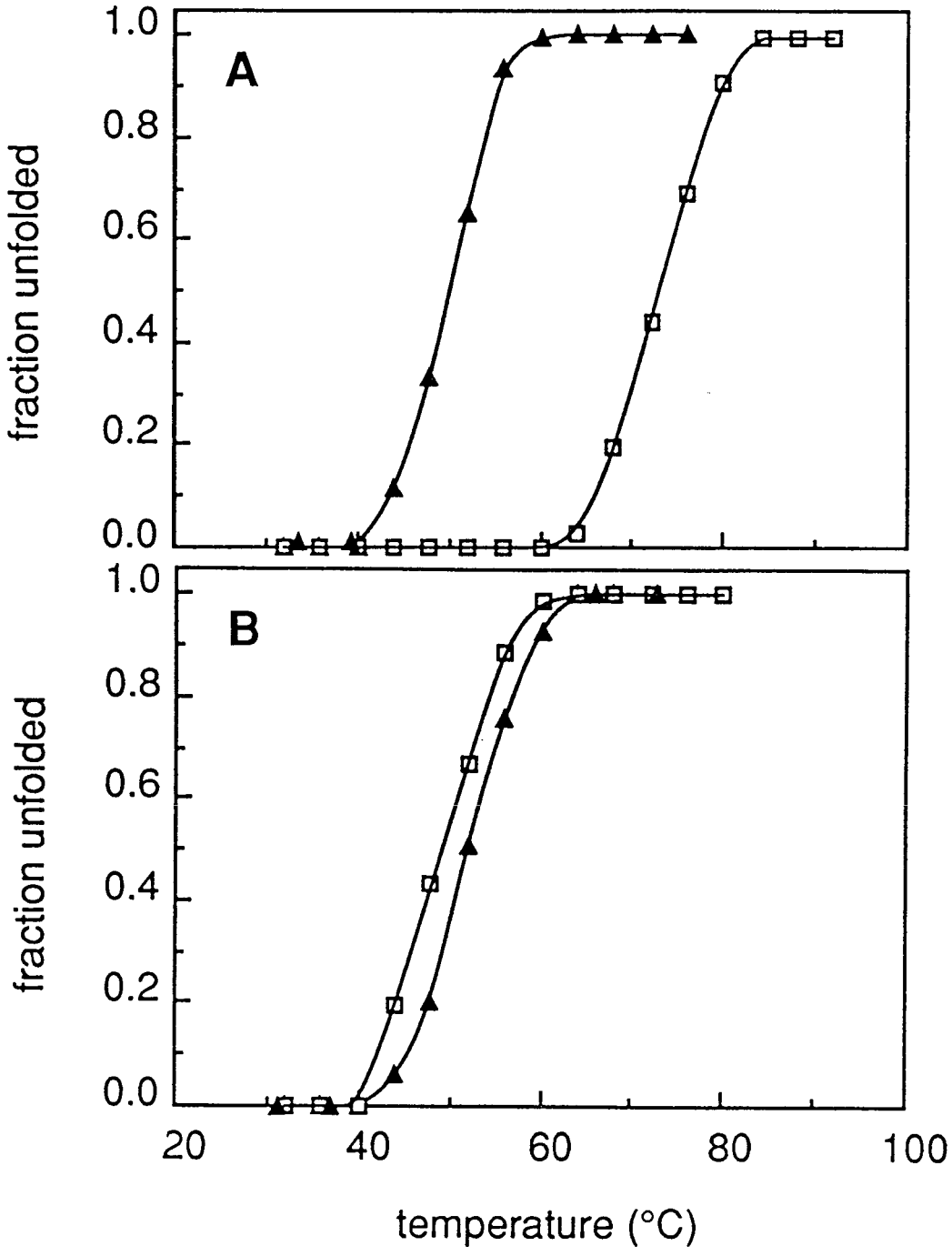
A
B
fraction unfolded
fraction unfolded
1.0
0.8
0.6
0.4
0.2
0.0
20
40
60
80
100
temperature (°C)

Chapter 6

Structurally Engineered Cytochromes with Novel Ligand-Binding Properties. Expression of *S. cerevisiae* Met80Ala iso-1-cytochrome *c*

[*Proc. Natl. Acad. Sci. USA*, **1993**, in press.]

Cytochrome *c* is a relatively small protein (MW ~ 12-13 kilodaltons) that shuttles electrons in the mitochondrial matrix.[1] It contains a heme prosthetic group that is covalently incorporated into the apoprotein by a membrane-bound lyase upon mitochondrial translocation. This system has long been a benchmark for studies of eukaryotic transcription,[2] protein folding and stability,[3] and long-range electron transfer (ET).[4] It also was one of the first proteins to be subjected to site-directed mutagenesis.[5] Because of the requirement of post-translational heme attachment, the expression (either homologous or heterologous) of mitochondrial cytochromes *c* has largely been limited to eukaryotic organisms, the most favored of which is baker's yeast (*S. cerevisiae*). Smith and coworkers[5] have utilized a multi-copy plasmid (YEp) for overexpressing yeast iso-1-cytochrome *c* under the control of its natural promoter. The host cells are grown in nonfermentable carbon media where cytochrome *c* expression is fully derepressed and a functional gene product is required for aerobic respiration. Other groups[6] have used integrative vectors that result in a single-copy gene of cytochrome *c*. Having a chromosomal gene copy allows expression of the protein either in a rich or in a lactate medium.

While a great many cytochrome *c* mutants have been generated by recombinant DNA techniques, only those variants that retain significant wild-type ET activity have been isolated in reasonable yields. With the exception of His18Arg yeast cytochrome *c*,[7] these exclude replacements of the axial ligands (His18 and Met80) or the cysteines (positions 14 and 17) that provide the covalent heme linkages.[8] While total synthesis of cytochrome *c* has been reported,[9] it is not at present a practical route to nonfunctional variants due to severe losses incurred during solid-phase synthesis, heme attachment, and refolding steps. Although cytochrome *c* can be manipulated by semisynthesis (cyanogen-bromide cleavage and fragment condensation),[10] the mutatable region is restricted to the C-terminal fragment (e.g., residues 66-104 of horse heart cytochrome *c*). Thus, the

development of a more general expression system for cytochrome *c* is of considerable interest; such a system would greatly expand the possible structural changes that could be incorporated into this paradigmatic protein.

Here, we report an expression system using a YEp vector bearing both the target nonfunctional variant as well as the functional cytochrome *c* gene to support the growth of the yeast cells in media containing a nonfermentable carbon source (Figure 6.1A). In order to facilitate the purification of the functional protein from the target nonfunctional mutant protein, a di-histidine chelating site (His39, Leu58His; Figure 6.1B) was engineered onto the surface of the functional protein[11] so that the two isoforms could be separated by immobilized metal-affinity chromatography. The initial target protein was chosen to be Met80Ala iso-1-cytochrome *c* for the following reasons. First, studies by Sherman *et al.* showed that yeast cells containing methionine-80 mutant proteins (Met80→Arg, Thr, Ile) maintain certain levels of holoproteins (~20% of native protein); and their *in vitro* levels of heme incorporation and mitochondrial transport also are similar to those of the native protein.[12] Although no mutants were isolated, a result that has been attributed to the instability of the proteins, the above experiments indicate that they can be made *in vivo*. Second, several semisynthetic Met80 mutant proteins of horse heart cytochrome *c* have been prepared and shown to be stable species.[13-16] Finally, replacing Met80 with an alanine creates a binding site for dioxygen,[15,16] which represents an important step in the engineering of artificial oxygenases.[17]

A 1.1-kb *Sma*I-*Hin*dIII fragment containing a functional gene (His39/Leu58His) was cloned into the *Hin*dIII site of YEp213/Met80Ala using a short *Hin*dIII linker (Figure 6.1A). In this construct, identical copies of the upstream control sequence direct independent expression of the two cytochrome *c* genes. Expression in a selective medium and cell lysis followed standard procedures.[18] Transformation of *S. cerevisiae* GM3C2[19] (strain deficient in both cytochrome *c* isozymes) with a YEp213 vector

containing the Met80Ala gene alone did not show any cell growth in the glycerol-based medium, whereas cells harboring the two-copy vector grew to saturation in three days. Cu(II)IDA (IDA = iminodiacetate) chromatography of the crude protein extract (Figure 6.1C) revealed three heme-containing bands, two of which were retained strongly on the column and later identified to be the chelating wild-type protein in different oxidation states ($Fe^{3+/2+}$). The third band bound weakly to the column and was further fractionated by cation-exchange chromatography. The UV/vis spectrum of purified Met80Ala iso-1-cytochrome *c* matches that of the oxy-ferrous form of the analogous horse heart mutant prepared by semisynthesis.[15,16] The protein constitutes 25-30% (0.5-0.6 mg/L) of the total cytochromes *c* (2 mg/L) purified from this system; it represents the first recombinant, nonfunctional axial-ligand mutant of cytochrome *c* produced in quantities that permit extensive biophysical characterization.

Sites of heme attachment (Cys14 and Cys17) and the mutation at position 80 were verified by NH_2-terminal sequencing of the holoprotein and the C-terminal cyanogen-bromide cleavage fragment, respectively.[20] The yeast Met80Ala iso-1-cytochrome *c* exhibits nearly all the properties of a heme protein with an available sixth ligation site. In the reduced form, the mutant can either have a vacant coordination site (deoxy form) or bind small exogenous ligands such as O_2 and CO (Figure 6.2A). The spectroscopic properties of the yeast protein are similar to those of the horse heart Met80Ala variant.[15,16] In a survey of derivatives of naturally occurring heme proteins, the closest resemblance can be drawn to horseradish peroxidase (HRP) (Figure 6.2B and Table 1). The observation that the electronic absorption bands of the various Met80Ala iso-1-cytochrome *c* species are slightly blue-shifted relative to those of their HRP analogues can be accounted for by the difference in π conjugation between *c* and *b* hemes (heme *b* having two extra vinyl substituents).[21]

At neutral pH, the UV/vis spectrum of the oxidized Met80Ala protein is analogous to that of the alkaline form of ferri-HRP, suggesting the presence of a hydroxyl ligand (Figure 6.3). Acid titration of the mutant produces similar spectral changes as in HRP and myoglobin, indicating direct protonation of the hydroxyl ligand to form the aquo-ferric derivative. Interestingly, the pK_a (~6.5) is lower than those of HRP (10.9) and horse myoglobin (8.9).[22] Addition of thiomethoxide (CH_3S^-) to the oxidized Met80Ala protein results in an absorption spectrum similar to that of the imidazole derivative of cytochrome P-450_{cam}, with slight blue shifts attributable to the different heme types (*c* vs. *b*); as expected, the spectrum of the Met80Ala(CH_3S^-) protein mimics closely that of semisynthetic Met80Cys horse heart cytochrome *c*.[14]

The approach based on the combined use of a two-copy expression vector and metal-affinity separation expands the possibilities of incorporating structural changes in regions of cytochrome *c* that are not accessible by either semisynthetic or previous recombinant DNA strategies.[23] Employing this methodology, we have successfully expressed and purified a cytochrome *c* derivative that possesses novel ligand-binding properties. These findings represent an important step toward the long-term goal of developing a deeper understanding of heme-mediated processes; with such an understanding, it should be possible to engineer useful catalytic functions into cytochrome *c* and related heme-containing molecules.

REFERENCES AND NOTES

1. (a) Pettigrew, G. W.; Moore, G. R. *Cytochromes c: Biological Aspects*; Springer-Verlag: New York, 1987. (b) Moore, G. R.; Pettigrew, G. W. *Cytochromes c: Evolutionary, Structural and Physicochemical Aspects*; Springer-Verlag: New York, 1990.
2. (a) Sherman, F. *Genetics* **1990**, *125*, 9. (b) Forsburg, S. L.; Guarente, L. *Ann. Rev. Cell. Biol.* **1989**, *5*, 153.
3. (a) Elöve, G. A.; Roder, H. in *Protein Refolding,* Georgiou, G., Bernardez-Clark, E., Eds.; ACS Symposium Series 470; American Chemical Society: Washington, D. C., 1991; pp. 50-63. (b) H. Roder, G. A. Elöve, S. W. Englander, *Nature* **1988**, *335*, 700.
4. Winkler, J . R.; Gray, H. B. *Chem. Rev.* **1992**, *92*, 369.
5. Pielak, G. J.; Mauk, A. G.; Smith, M. *Nature* **1985**, *313*, 152.
6. (a) Holzschu, D. *et al.*, *J. Biol. Chem.* **1987**, *262*, 7125. (b) Hilgen, S. E.; Pielak, G. J. *Protein Eng.* **1991**, *4*, 575.
7. With a nonfermentable carbon-based medium, the yield of this mutant was dramatically lower (< 100 μg per L fermentation) than that of the wild-type protein (Garcia, L. L.; Fredericks, Z.; Sorrell, T. N.; Pielak, G. J. *New J. Chem.* **1992**, *16*, 629. Sorrell, T. N.; Martin, P. K.; Bowden, E. F. *J. Am. Chem. Soc.* **1989**, *111*, 766).
8. Hampsey, D. M.; Das, G.; Sherman, F. *FEBS Lett.* **1988**, *231*, 275. The numbering scheme used here is based on mammalian sequences. Yeast iso-1-cytochrome *c* has five more amino-terminal residues than the mammalian analogues.
9. Di Bello, C.; Vita, C.; Gozzini, L. *Biochem. Biophys. Res. Commun.* **1992**, *183*, 258.
10. (a) Humphries, J.; Offord, R. E.; Smith, R. A. G. *Curr. Opin. Biotech.* **1991**, *2*, 539. (b) R. E. Offord, in *Protein Design and the Development of New Therapeutics and*

Vaccines, Hook, J. B., Poste, G., Eds.; Plenum: New York, 1990; pp. 253-282. (c) C. J. A. Wallace, *FASEB J.* **1993**, *7*, 505.

11. (a) Umana, P.; Kellis, J. T.; Arnold, F. H. in *Biocatalyst Design for Stability and Specificity*, Himmel, M. E.; Georgiou, G., Eds.; ACS Symposium Series 516, American Chemical Society: Washington, D. C., 1993; pp. 102-107. (b) Arnold, F. H.; Haymore, B. L. *Science* **1991**, *252*, 1796.
12. Dumont, M. E.; Ernst, J. F.; Sherman, F. *J. Biol. Chem.* **1988**, *263*, 15928.
13. Raphael, A. L.; Gray, H. B. *Proteins* **1989**, *6*, 338.
14. Raphael, A. L.; Gray, H. B. *J. Am. Chem. Soc.* **1991**, *113*, 1038.
15. Wallace, C. J. A.; Clark-Lewis, I. *J. Biol. Chem.* **1992**, *267*, 3852.
16. Bren, K. L.; Gray, H. B. *J. Inorg. Biochem.* **1993**, *51*, 111.
17. Wuttke, D. S.; Bjerrum, M. J.; Winkler, J. R.; Gray, H. B. *Science* **1992**, *256*, 1007.
18. Cutler, R. L.; Pielak, G. J.; Mauk, A. G.; Smith, M. *Protein Eng.* **1987**, *1*, 95.
19. Faye, G.; Leung, D. W.; Tatchell, K.; Hall, B. D.; Smith, M. *Proc. Natl. Acad. Sci. USA* **1981**, *78*, 2258.
20. Amino-terminal sequencing of the holoprotein showed no identifiable amino-acid residue at the cycles number 19 (residue 14 in the numbering scheme) and 22 (residue 17), suggesting that the cysteines at these positions are covalently attached to the prosthetic group. The holoprotein (0.7 mM solution in 70% formic acid) was cleaved with a 130-excess of cyanogen bromide for 46 h. The reaction mixture was exchanged by ultrafiltration to 100 mM NH_4HCO_3 (pH 8.0), lyophilized, and run through a Pharmacia ProRPC 5/10 column in order to isolate the 65-103 fragment. The amino-acid sequence of this peptide confirmed the alanine mutation at position 80.
21. Rux, J. J.; Dawson, J. H. *FEBS Lett.* **1991**, *290*, 49.

22. Antonini, E.; Brunori, M. *Hemoglobin and Myoglobin in Their Reactions with Ligands*; North-Holland: Amsterdam, 1971; pp. 47-48.

23. (a) We emphasize, however, that this method relies on the cellular machinery that assembles the holoprotein; mutations that interfere with heme reconstitution or render the protein susceptible to intracellular proteolysis may not give recoverable products. (b) Efforts are currently being directed at introducing mutations in the other heme ligand position (His18). A His18→Met substitution that would create a mimic of bacterioferritin[24] did not produce any isolable protein. Other potentially interesting mutations include arg,[7] gln, and glu; the latter is expected to raise the heme reduction potential and in conjunction with a Met80→Ala replacement, offers a route to novel oxygenases.

24. (a) Cheesman, M. R.; Thomson, A. J.; Greenwood, C.; Moore, G. R.; Kadir, F. *Nature (London)* **1990**, *346*, 771. (b) McKnight, J.; Cheesman, M. R.; Reed, C. A.; Orosz, R. D.; Thomson, A. J. *J. Chem. Soc. Dalton Trans.* **1991**, 1887.

Table 6.1. Electronic Absorption Data (λ_{max}, nm) for Selected Heme Proteins.

Protein	δ	Soret (γ)	visible (α, β)/near-IR			
Ferrous Derivatives						
M80A[a], deoxy	327(354,sh)	410(437,sh)	521(sh)	548	564(sh)	
HRP, deoxy	382	437	519(sh)	558	589(sh)	
Mb[b], deoxy		435		559		
M80A-O_2	351	408	537	570		
HRP-O_2	354	417	544	578		
Mb-O_2	348	417	544	580		
M80A-CO	345(394,sh)	414	531	554		
HRP-CO	350	423	542	572		
Mb-CO	346	423	540	579		
Ferric Derivatives						
M80A (pH 3.5)		398	494		624	
HRP		403	498		641	
Mb		408	505		633	
M80A (pH 7.0)	357	406	536	566	626	
HRP-alkaline		414	542	576	640	
Mb-alkaline	358	411	539	585		
M80A-SCH_3	355	416	535	566	648	763
Cyt P-450-Imidazole	358	425	542	574	638	753
M80C[c]	355	416	540	570	635	734

[a]Met80Ala-iso-1-cytochrome *c*.
[b]Horse myoglobin.
[c]Semisynthetic Met80Cys horse heart cytochrome *c* (reference 14).

Figure 6.1. (**A**) Vector construct for expression of Met80Ala (*cyc*1$^-$) and Leu58His (*cyc*1$^+$) cytochrome *c*. The shaded boxes contain the promoter and upstream activation sequences for *cyc*1 transcription. *Leu*$^+$ and ampicillin resistance markers also are present for plasmid selection in yeast and *E. coli*, respectively. Mutations in the *cyc*1 gene were introduced using standard oligonucleotide-directed mutagenesis protocols (Kunkel, T. A. *Proc. Natl. Acad. Sci. USA* **1985**, *82*, 488). (**B**) Molecular model of Leu58His cytochrome *c*, indicating the location of the surface di-histidine site for high-affinity binding to immobilized metal complexes. Energy-minimization calculations were performed on the 1.23-Å structure of yeast iso-1-cytochrome *c* (Louie, G. V.; Brayer, G. D. *J. Mol. Biol.* **1990**, *214*, 527) using BIOGRAF, version 3.0 (Molecular Simulations, Inc.). (C) Chromatogram showing the purification on a Cu(II)IDA column of homogenized protein extracts containing the nonfunctional Met80Ala and the functional His39/Leu58His proteins. About 50 mg of protein extracts were loaded onto a 5-mL HiTrap Chelating column (Pharmacia LKB) that was charged with 2 mL 100 mM $CuSO_4$. The proteins were eluted with a 1-20 mM imidazole gradient in 50 mM sodium phosphate and 500 mM NaCl, pH 7.0. Peak I contains the Met80Ala mutant and other proteins that bind weakly to the column and were subsequently purified to homogeneity by ion-exchange chromatography. Peaks II and III contain reduced and oxidized His39/Leu58His proteins, respectively. The purity and identity of the Met80Ala protein were established by SDS-PAGE and amino-acid sequencing.

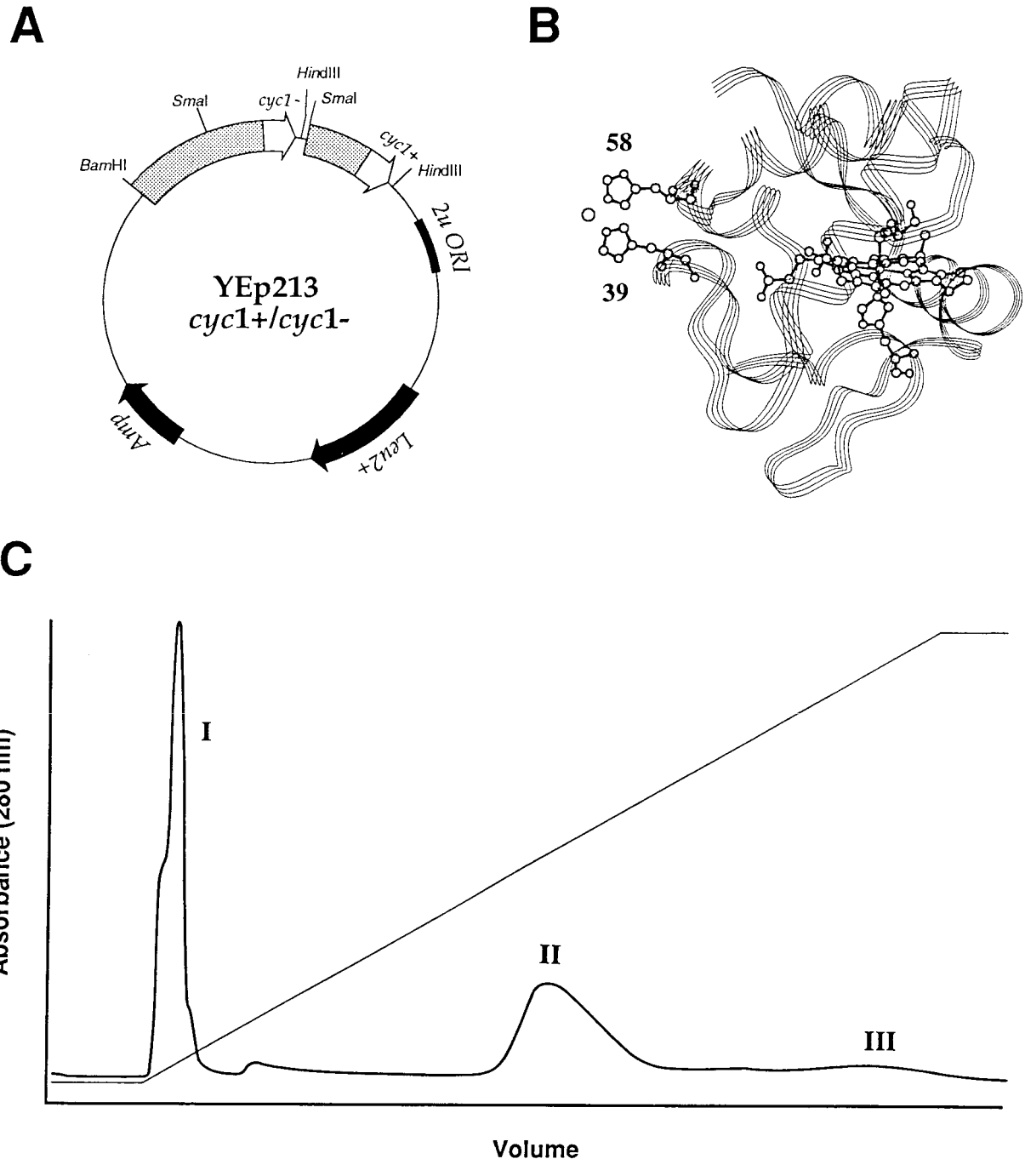
A
HindIII
SmaI
cyc1-
SmaI
cyc1+
BamHI
HindIII
2μ ORI
YEp213
cyc1+/cyc1-
Amp
Leu2+
B
58
39
C
Absorbance (280 nm)
I
II
III
Volume

Figure 6.2. Electronic absorption spectra of ferrous Met80Ala iso-1-cytochrome *c* derivatives (**A**) and analogous HRP species (**B**). The proteins were in μ 100 mM sodium phosphate buffer, pH 7.0. The deoxy derivatives of both proteins were prepared under a nitrogen atmosphere by adding excess $Na_2S_2O_4$ to the protein solutions and running the solution through a Sephadex-G25 column. Exposing the deoxy form of the Met80Ala protein to air results in the oxy form; and exposure of the oxy protein to CO yields the CO derivative. The oxy and CO forms of HRP were prepared according to D. Keilin and E. F. Hartree (*Biochem. J.* **1951**, *49*, 88).

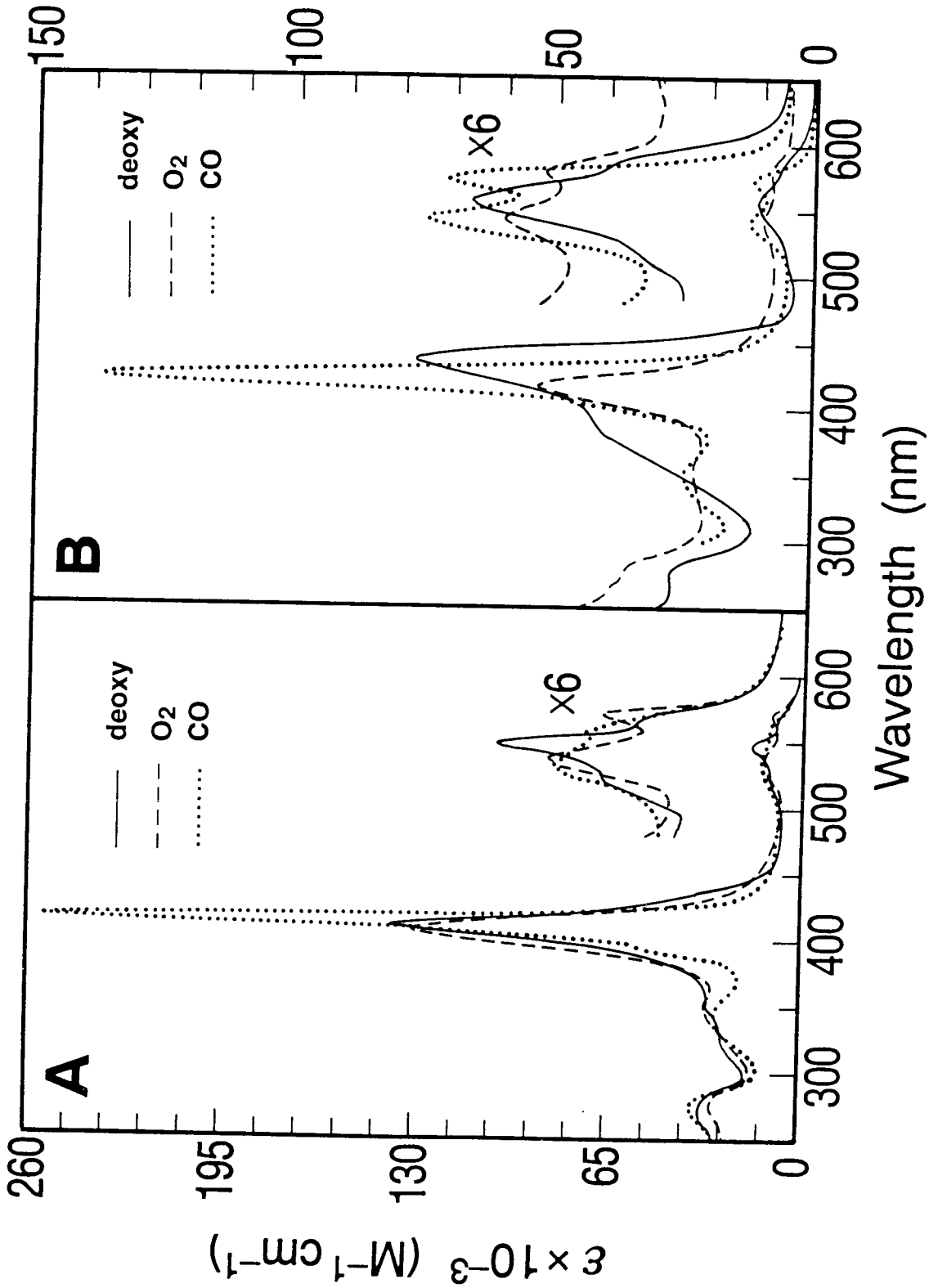
A
B
deoxy
O2
CO
×6
×6
260
195
130
65
0
150
100
50
0
300
400
500
600
300
400
500
600
Wavelength (nm)
ε × 10−3 (M−1 cm−1)

Figure 6.3. Electronic absorption spectra of ferric Met80Ala iso-1-cytochrome *c* derivatives (**A**) and analogous HRP and cytochrome P-450_{cam} (Cyt P-450_{cam}) species (**B**). All proteins were in μ 100 mM sodium phosphate buffer, pH 7.0, except for the alkaline form of HRP, which was prepared in 100 mM $NaHCO_3$, pH 11.4, and the imidazole (Im) derivative of Cyt P-450_{cam}, which was kept in 100 mM sodium phosphate, 88 mM imidazole, and 22 μM camphor (pH 7.0). The oxyferrous Met80Ala protein was reacted overnight under argon with $Co(phen)_3^{3+}$ to yield the oxidized mutant. The thiomethoxide derivative of the Met80Ala protein was prepared by adding a 500-fold excess of $NaSCH_3$ to a ferric-Met80Ala protein solution. The imidazole derivative of Cyt P-450_{cam} was prepared according to reference 21.

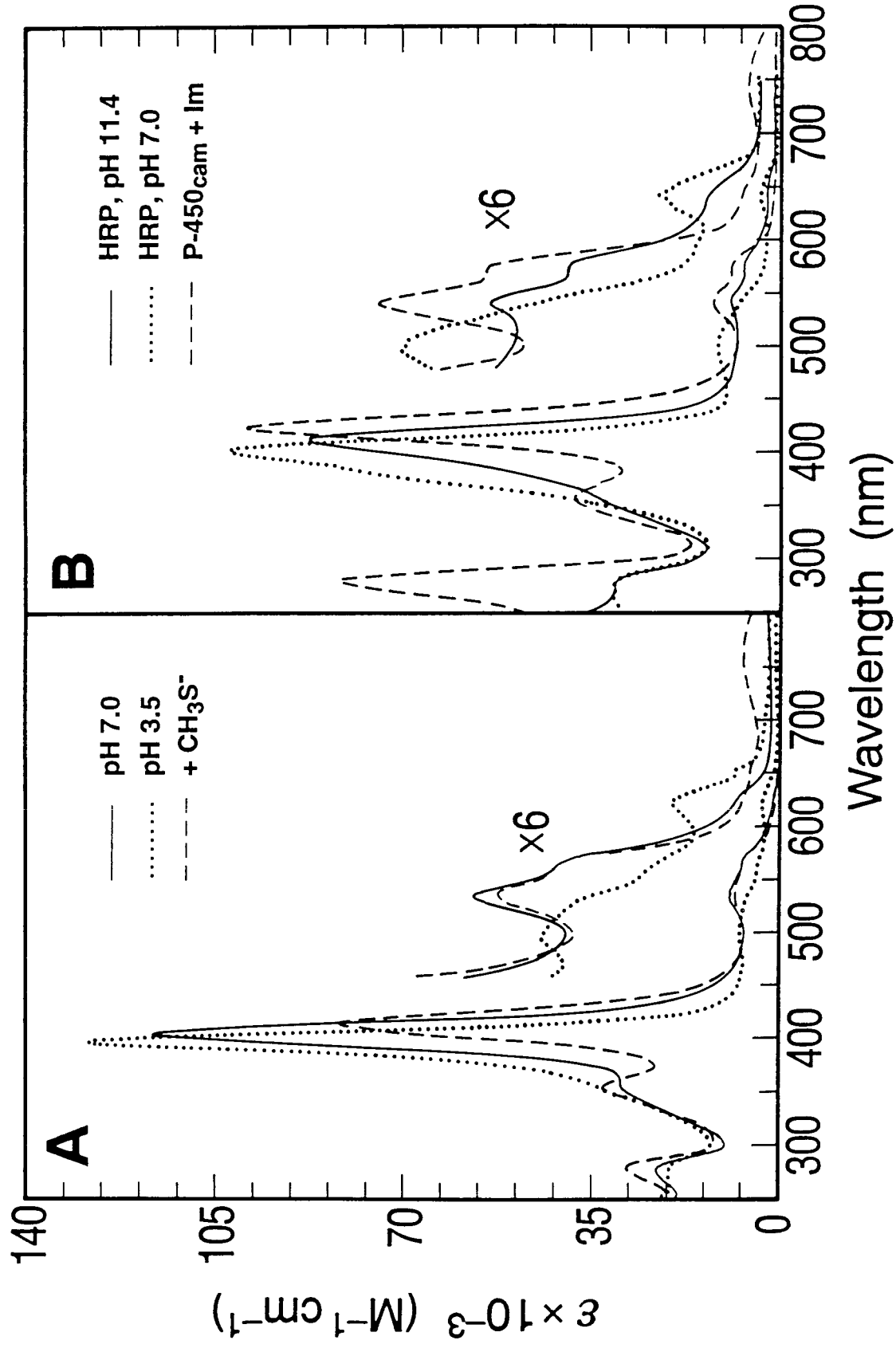
A
B
pH 7.0
pH 3.5
+ CH_3S^-
HRP, pH 11.4
HRP, pH 7.0
P-450cam + Im
×6
×6
140
105
70
35
0
300
400
500
600
700
800
Wavelength (nm)
$\varepsilon \times 10^{-3}$ (M^{-1} cm^{-1})

Appendix A.

Sequence of Human Myoglobin Gene

The bottom strand is the one incorporated in the M13mp19 single-stranded template.

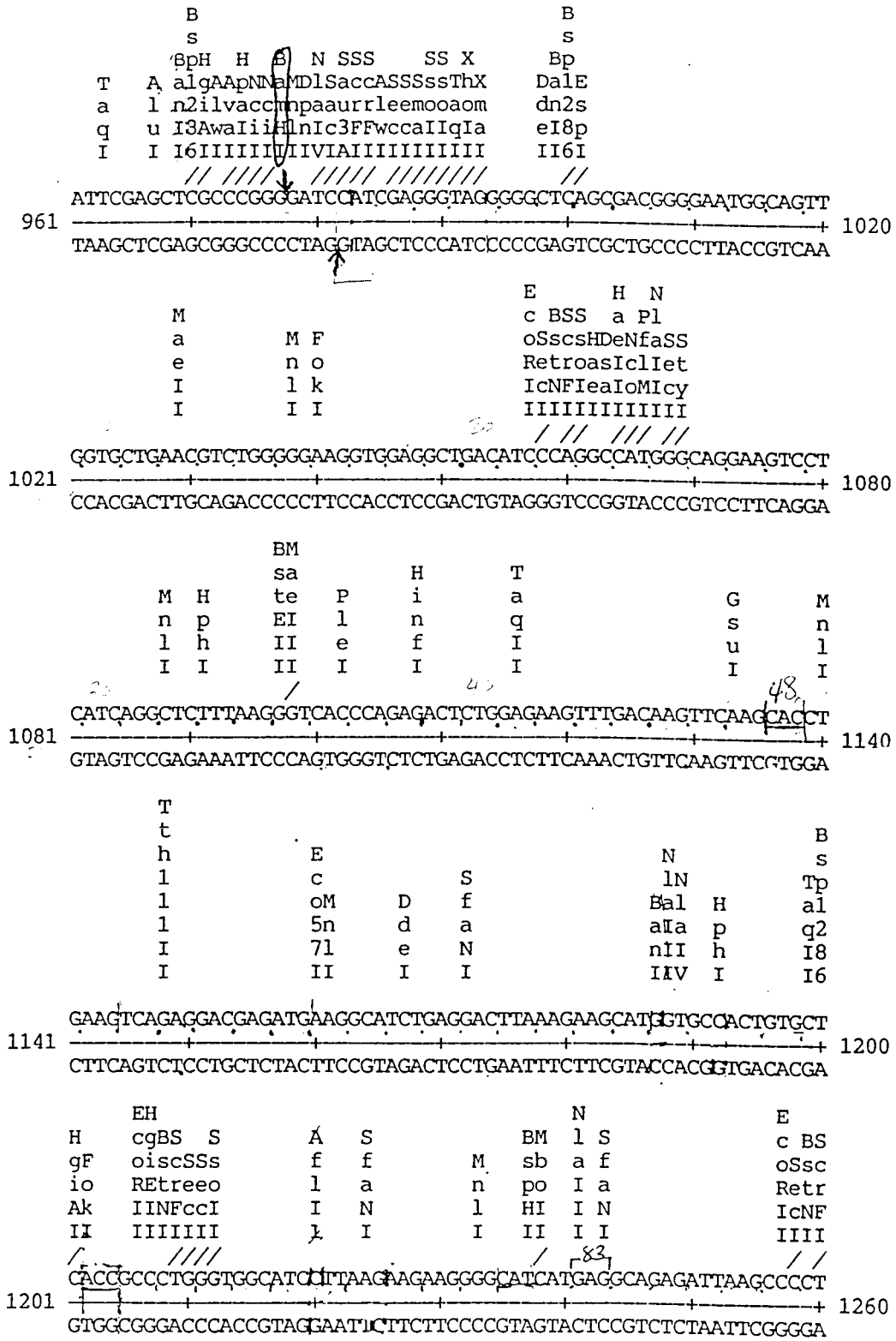

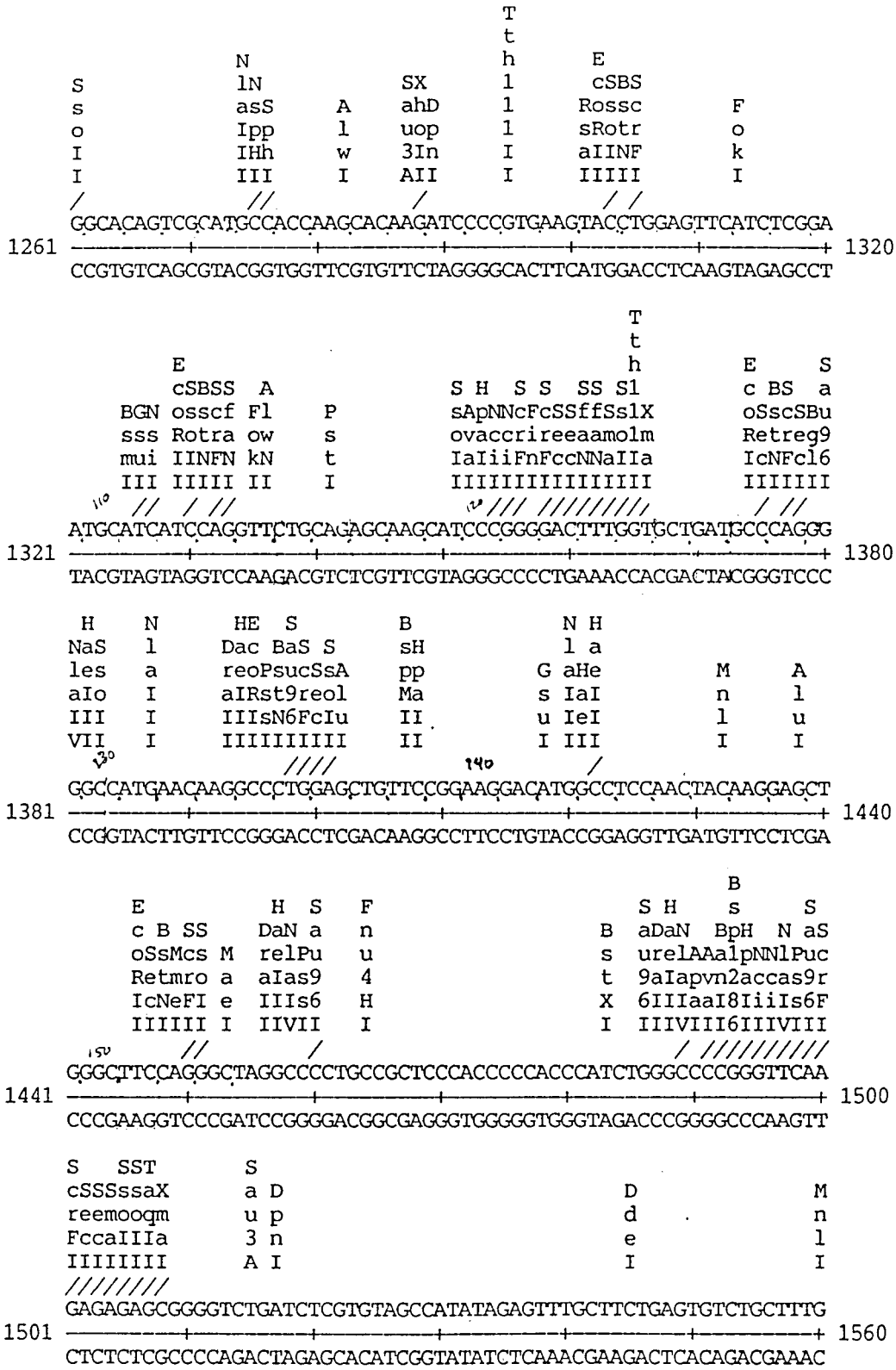

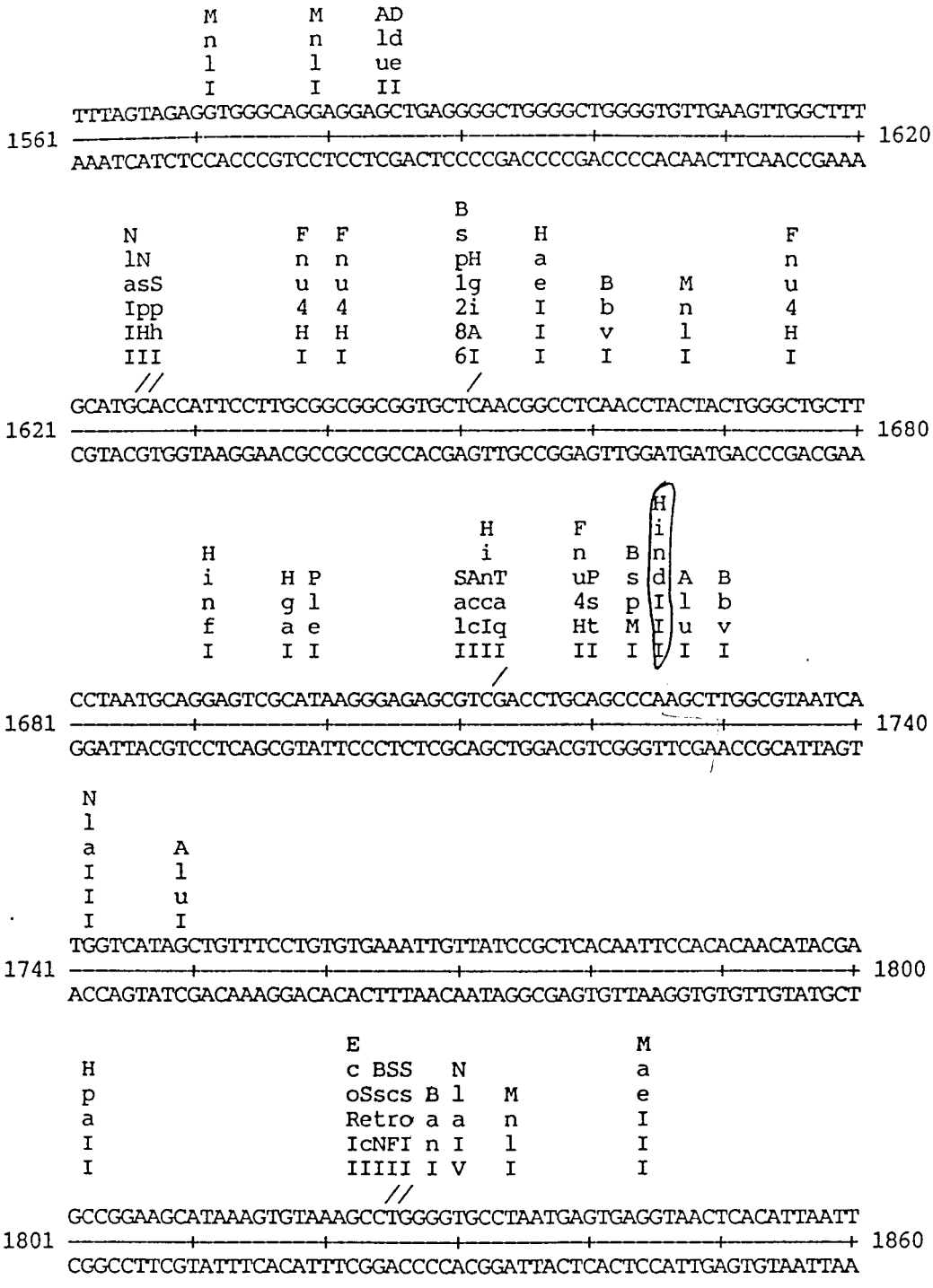
M M AD
n n ld
l l ue
I I II
TTTAGTAGAGGTGGGCAGGAGGAGCTGAGGGGCTGGGGCTGGGGTGTTGAAGTTGGCTTT
1561
1620
AAATCATCTCCACCCGTCCTCCTCGACTCCCCGACCCCGACCCCACAACTTCAACCGAAA
B
N F F s H F
lN n n pH a n
asS u u 1g e B M u
Ipp 4 4 2i I b n 4
IHh H H 8A I v l H
III I I 6I I I I I
GCATGCACCATTCCTTGCGGCGGCGGTGCTCAACGGCCTCAACCTACTACTGGGCTGCTT
1621
1680
CGTACGTGGTAAGGAACGCCGCCGCCACGAGTTGCCGGAGTTGGATGATGACCCGACGAA
H
i
n
H H F B d A B
i i n s I l b
n g l SAnT uP p I u v
f a e acca 4s M I I I
I I I lcIq Ht I I I I
IIII II
CCTAATGCAGGAGTCGCATAAGGGAGAGCGTCGACCTGCAGCCCAAGCTTGGCGTAATCA
1681
1740
GGATTACGTCCTCAGCGTATTCCCTCTCGCAGCTGGACGTCGGGTTCGAACCGCATTAGT
N
l
a A
I l
I u
I I
TGGTCATAGCTGTTTCCTGTGTGAAATTGTTATCCGCTCACAATTCCACACAACATACGA
1741
1800
ACCAGTATCGACAAAGGACACACTTTAACAATAGGCGAGTGTTAAGGTGTGTTGTATGCT
E M
H c BSS N a
p oSscs B l M e
a Retro a a n I
I IcNFI n I l I
I IIIII I V I I
GCCGGAAGCATAAAGTGTAAAGCCTGGGGTGCCTAATGAGTGAGGTAACTCACATTAATT
1801
1860
CGGCCTTCGTATTTCACATTTCGGACCCCACGGATTACTCACTCCATTGAGTGTAATTAA

Appendix B.

Sequence of 2.5-kb *CYC1*-containing Fragment

The top strand is the one incorporated in the M13mp18 single-stranded template.

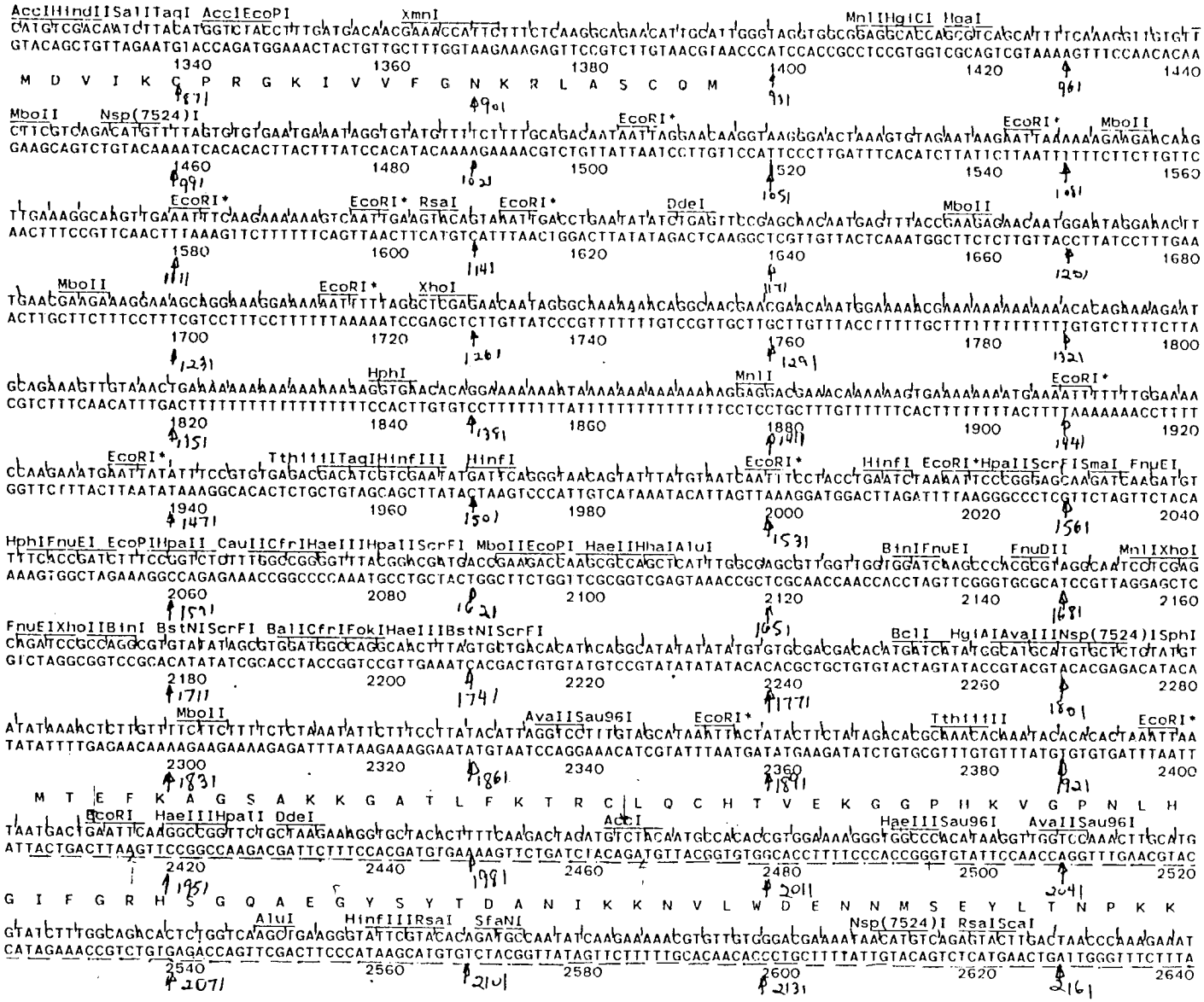
AccIHindIISalITaqI AccIEcoPI
XmnI
MnlIHgiCI HgaI
MboII Nsp(7524)I
EcoRI*
EcoRI* MboII
EcoRI* RsaI
EcoRI*
DdeI
MboII
MboII
EcoRI*
XhoI
HphI
MnlI
EcoRI*
EcoRI* Tth111ITaqIHinfIII HinfI
EcoRI*
HinfI EcoRI*HpaIIScrFISmaI FnuEI
HphIFnuEI EcoPIHpaII CauIICfrIHaeIIIHpaIIScrFI MboIIEcoPI HaeIIHhaIAluI
BtnIFnuEI FnuDII MnlIXhoI
FnuEIXhoIIBtnI BstNIScrFI BalICfrIFokIHaeIIIBstNIScrFI
BclI HgiAIAvaIIINsp(7524)ISphI
MboII
AvaIISau96I EcoRI*
Tth111II
EcoRI*
EcoRI HaeIIIHpaII DdeI
AccI
HaeIIISau96I AvaIISau96I
AluI HinfIIIRsaI SfaNI
Nsp(7524)I RsaISacI

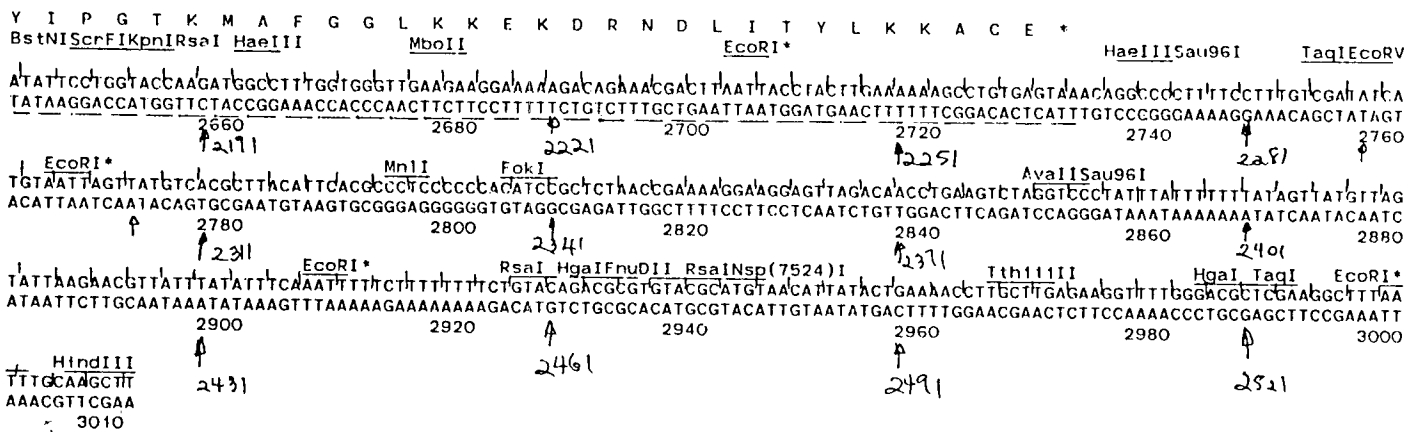
Y I P G T K M A F G G L K K E K D R N D L I T Y L K K A C E *
BstNI ScrFI KpnI RsaI HaeIII MboII EcoRI* HaeIII Sau96I TaqI EcoRV
2660 2680 2700 2720 2740 2760
2171 2221 2251 2281
EcoRI* MnlI FokI Sau96I
2780 2800 2820 2840 2860 2880
2231 2341 2371 2401
EcoRI* RsaI HgaI FnuDII RsaI Nsp(7524)I Tth111II HgaI TaqI EcoRI*
2900 2920 2940 2960 2980 3000
HindIII
2431 2461 2491 2521
3010

Appendix C.

Bond-Mediated Electron Transfer in Synthetic D-A Systems

Figure C1. Log k_{max} vs. number of bonds in various synthetic donor-linker-acceptor molecules. The line fit (slope, -0.35 per bond; y-intercept, 13.2) is drawn through the data for a series of porphyrin-spirocyclobutane-quinone systems[1] (O). The values for the slope and y-intercept translate to a β' of 0.81 per bond and a one-bond activationless rate of 7×10^{12} s^{-1}. 1, iridium-alkylphosphinite-pyridinium;[2] 2, rhenium-peptide-dimethylaniline;[3] 3, biphenyl-steroid-acceptor;[4] 4, rhenium-cyclohexane-thiafulvene;[5] 5, porphyrin-triptycene-quinone;[6] and 6, porphyrin-bicyclooctane-quinone systems.[7]

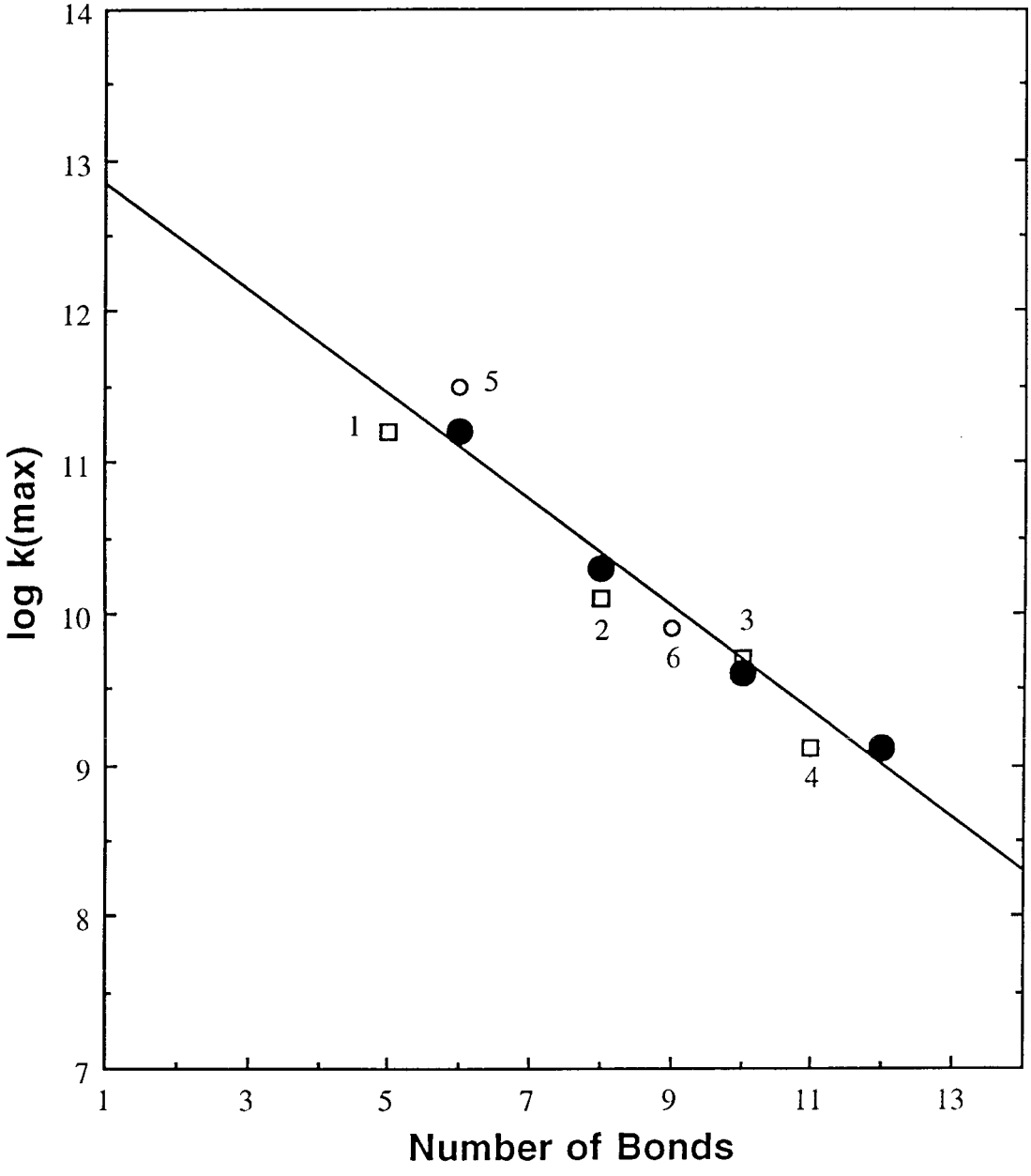
14
13
12
11
10
9
8
7
log k(max)
1
3
5
7
9
11
13
Number of Bonds
1
2
3
4
5
6

REFERENCES

1. Knapp, S.; Murali Dhar, T. G.; Albaneze, J.; Gentemann, S.; Potenza, J. A.; Holten, D.; Schugar, H. J. *J. Am. Chem. Soc.* **1991**, *113*, 4010.
2. Fox, L. S.; Kozik, M.; Winkler, J. R.; Gray, H. B. *Science* **1990**, *247*, 1069.
3. MacQueen, D. B.; Schanze, K. S. *J. Am. Chem. Soc.* **1991**, *113*, 7470.
4. Closs, G. L.; Miller, J. R. *Science* **1988**, *240*, 440.
5. Perkins, T. A.; Hauser, B. T.; Eyler, J. R.; Schanze, K. S. *J. Phys. Chem.* **1990**, *94*, 8745.
6. Wasielewski, M. R.; Niemczyk, M. P.; Svec, W. A.; Pewitt, E. B. *J. Am. Chem. Soc.* **1985**, *107*, 1080.
7. Joran. A. D.; Leland, B. A.; Felker, P. M.; Zewail, A. H.; Hopfield, J. J.; Dervan, P. B. *Nature* **1987**, *327*, 508.